EFFECTS OF REPULSIVE COUPLING IN ENSEMBLES OF EXCITABLE ELEMENTS

DISSERTATION

zur Erlangung des akademischen Grades
DOCTOR RERUM NATURALIUM
(Dr. rer. nat.)

im Fach Physik
Spezialisierung: Theoretische Physik

eingereicht an der
Mathematisch-Naturwissenschaftlichen Fakultät
der Humboldt-Universität zu Berlin

von
M. SC. ROBERT RONGE

Präsidentin der Humboldt-Universität zu Berlin:
Prof. Dr. Julia von Blumenthal

Dekanin der Mathematisch-Naturwissenschaftlichen Fakultät:
Prof. Dr. Caren Tischendorf

Gutachter:	PD Dr. Michael A. Zaks
	PD Dr. Serhiy Yanchuk
	Prof. Dr. Katharina Krischer
Eingereicht am:	18.05.2022
Tag der mündlichen Prüfung:	03.11.2022

ZUSAMMENFASSUNG

Die vorliegende Arbeit ist der kollektiven Dynamik identischer anregbarer Elemente gewidmet. Ein klassisches Beispiel für ein anregbares Element ist das Neuron: Nur ein ausreichend starker Stimulus veranlasst es zu einer Reaktion in Form eines Nervenimpulses bevor es zu seinem Ruhezustand zurückfindet; andernfalls verbleibt es im Ruhezustand. Anregbare Elemente der Klasse 1 können im Rahmen der nichtlinearen Dynamik als Systeme nahe einer Sattel-Knoten-Bifurkation auf einem invarianten Kreis beschrieben werden. Der Prototyp eines solchen Systems ist der Aktive Rotator. Der Fokus unserer Arbeit liegt auf dem Studium Aktiver Rotatoren.

In Teil eins der Arbeit motivieren wir zunächst das klassische Modell abstoßend gekoppelter Aktiver Rotatoren nach Shinomoto und Kuramoto und verallgemeinern es indem wir höhere Fourier-Moden in der internen Dynamik der einzelnen Rotatoren berücksichtigen. Wir führen außerdem das mathematische Rüstzeug auf dem unsere Arbeit beruht ein. Dazu gehören insbesondere die Theorie normal-hyperbolischer invarianter Mannigfaltigkeiten, die Averaging-Methode und Watanabe-Strogatz-Integrabilität die es ermöglicht, Systeme identischer Winkelvariablen durch Möbius-Transformationen zu beschreiben.

In Teil zwei untersuchen wir zunächst die Existenz und Stabilität periodischer Zwei-Cluster-Lösungen für verallgemeinerte Aktive Rotatoren und beweisen anschließend die Existenz eines Kontinuums periodischer Lösungen für eine Klasse von Watanabe-Strogatz-integrablen Systemen zu denen insbesondere auch das klassische Aktive-Rotatoren-Modell gehört und zeigen dass (i) dieses Kontinuum eine normal-anziehende invariante Mannigfaltigkeit bildet und (ii) eine der periodischen Lösungen des Kontinuums ein Splay State ist. Darauf aufbauend entwickeln wir eine Störungstheorie für solche Systeme die auf der Averaging-Methode beruht. Mit Hilfe dieser Methode können wir Rückschlüsse auf die asymptotische Dynamik des verallgemeinerten Aktive-Rotatoren-Modells auf Grundlage der entarteten Dynamik des klassischen Modells ziehen. Als Hauptergebnis stellen wir fest dass sowohl periodische Zwei-Cluster-Lösungen als auch Splay States robuste und potentiell stabile Lösungen für Systeme identischer Aktiver Rotatoren sind. Wir untersuchen außerdem einen “Stabilitätstransfer” zwischen diesen Lösungen durch sogenannte Broken-Symmetry States.

In Teil drei widmen wir uns Ensembles höherdimensionaler Klasse-I-anregbarer Elemente in Gestalt von Morris-Lecar-Neuronen. Wir stellen insbesondere fest, dass die asymptotische Dynamik solcher Systeme mit der der Aktiven Rotatoren vergleichbar ist. Dies legt nahe, dass unsere Ergebnisse aus Teil zwei ein qualitatives Bild für die Beschreibung komplizierterer und realistischerer Neuronenmodelle liefern.

ABSTRACT

This thesis is dedicated to the study of the collective dynamics of excitable elements. A classic example for an excitable element is the neuron: Only if it receives a sufficiently strong stimulus will it respond with an outgoing nerve impulse before returning to its state of rest; otherwise, it stays at rest. Class I excitable elements can be described within the theory of nonlinear dynamics as systems which are close to a saddle-node bifurcation on an invariant circle. The prototype for such a system is the so-called Active Rotator. Our work focuses on the study of Active Rotators.

In part one of this thesis, we motivate the classic model of repulsively coupled Active Rotators by Shinomoto and Kuramoto and generalize it by considering higher order Fourier modes in the on-site dynamics of the Rotators. We also introduce the arsenal of mathematical methods which our work relies on, namely the theory of normally attracting invariant manifolds, the method of averaging, and Watanabe-Strogatz integrability which allows to describe systems of identical angular variables in terms of Möbius transformations.

In part two, we investigate the existence and stability of periodic two-cluster states for generalized Active Rotators and afterwards prove the existence of a continuum of periodic orbits for a class of Watanabe-Strogatz integrable systems which includes, in particular, the classic Active Rotator model. We show (i) that this continuum constitutes a normally attracting invariant manifold and (ii) that one of its periodic solutions is a splay state. From this, we develop a perturbation theory for such systems, which builds on the method of averaging. By virtue of this method, we can deduce the asymptotic dynamics of the generalized Active Rotator model by means of the degenerate dynamics of the classic model. As a main result, we find that periodic two-cluster states as well as splay states are robust and potentially stable periodic solutions for systems of identical Active Rotators. We also investigate a "transfer of stability" between these solutions by means of so-called broken-symmetry states.

In part three, we study ensembles of higher dimensional class I excitable elements in form of Morris-Lecar neurons. We find that in particular, the asymptotic dynamics of such systems are similar to those of Active Rotators, which suggests that our results from part two yield a suitable qualitative description of more complicated and realistic neural models.

I've put in so many enigmas and puzzles that it will keep the professors busy for centuries arguing over what I meant, and that's the only way of insuring one's immortality.

— James Joyce

PUBLICATIONS

The results of this work constitute the content of the following three articles:

[RZ21a] R. Ronge and M. A. Zaks. “Emergence and stability of periodic two-cluster states for ensembles of excitable units.” In: *Physical Review E* 103.1 (2021), p. 012206.

[RZ21b] R. Ronge and M. A. Zaks. “Splay states and two-cluster states in ensembles of excitable units.” In: *The European Physical Journal Special Topics* 230.14 (2021), pp. 2717–2724.

[RZP] R. Ronge, M. A. Zaks, and T. Pereira. “Continua and hyperbolicity of periodic orbits in ensembles of oscillators.” (in preparation).

We look at the world through windows on which have been drawn grids (concepts). Different philosophies use different grids. A culture is a group of people with rather similar grids. Through a window we view chaos, and relate it to the points on our grid, and thereby understand it. The ORDER is in the GRID. That is the Aneristic Principle.

— Principia Discordia

ACKNOWLEDGMENTS

It is a commonplace that pursuing a PhD is as much an intellectually challenging and satisfying endeavor as it is arduous labor. It can keep you up all night because you finally found the solution for that one problem you were desperately trying to solve and are too excited to implement that solution the next day to fall asleep. It can also rob you of your sleep because no matter how hard you try, this very problem eludes all your efforts to solve it even though it seems so simple (or you wake up at night and just realize that what you thought would work turns out to be plain wrong). I had my fair share of all of these moments. It is therefore all the more important to have yourself surrounded with people that inspire (and sometimes press) you to keep working and who share their experience and knowledge with you.

I would therefore like to first and foremost thank my supervisor PD Dr. Michael A. Zaks for giving me the opportunity to work with him, his support and guidance through the last four and a half years, and his patience with me when I was not necessarily working on what I was supposed to. I am in great debt to him for allowing me to pursue my scientific ideas even when they seemed sketchy and crude at first. I would also like to thank Professor Tiago Pereira for welcoming me at USP in São Carlos and for his help to make those crude ideas rigorous. My stay in Brazil was a most fruitful and exciting experience, even if it lasted not as long as I hoped for, for circumstances that nobody could foresee. I would especially like to express my gratitude to both of them for the countless hours of discussions and explanations of concepts and ideas that would have otherwise completely eluded me.

Pursuing a PhD goes hand in hand with meeting new people and often making new friends. I therefore want to seize the opportunity to mention my friends and (former) colleagues in the IRTG and the HU: Adrian Pacheco-Pozo, Andreas Koher, Chris Gong, Fabian Baumann, Florian Stelzer, Frederik Wolf, Jörg Nötel, Lukas Ramlow, Nico Wunderling, Nicolai Friedhoff, Patrick Pöschke, Rico Berner, Sebastian Milster, Sebastian Vellmer, Sten Rüdiger, and Tommaso Rosati, to name a few. I think I also speak for all participants when I say that especially the Portuguese classes with Carlos Alberto Afonso were great fun for all of us. I would also like to thank David Hansmann for the administration of the IRTG 1740 and his help with organizational issues, as well as for our common lunch and coffee breaks.

During my way too short stay in Brazil, I fell in love with the country and with the city of São Carlos and this was all due to the wonderful friends, I made there. I want to especially thank Zheng Bian and Edmilson Roque Santos not only for sharing their superior knowledge and experience with me but also for the great time we had together. I am in great debt to them alone for the hours and hours of discussing my numerous mathematical problems and giving me advice on how to solve them.

My time in Brazil would not have been such a wonderful experience, if I hadn't met so many great people who generously welcomed me there. For this, I would like to thank Zheng and Edmilson as well as Asrat Belachew Mekonnen, Douglas Finamore, Fernando Cordeiro de Queiroz, Hans Muller Junho de Mendonça, Matheus Palmero Silva, Richard Javier Cubas Becerra, Thomas Kaue Dal Maso Peron, and Zeray Hagos Gebrezabher. A special thanks goes to Vander Luis de Souza Freitas and Edson Santos without whom I would probably still be stuck either at Guarulhos airport or the Tieté bus terminal and to Stefan Ruschel who, when I told him about my mathematical struggles, encouraged me to go to São Carlos in the first place because he knew that Tiago was just the right person to help me.

I also want to take this opportunity to thank Andreas, Edmilson, Frederik, Lukas, Rico, Thomas, and Zheng for proofreading this thesis as well as their many valuable comments and brazenly blame them for any typos that made it through.

Zum Schluss möchte ich meiner gesamten Familie und Ana Carolina de Carvalho Belmani für ihre Liebe und Unterstützung danken und dafür dass sie immer geduldig ein „Wenn sie fertig ist." als Antwort auf die Frage wann ich meine Doktorarbeit endlich einreiche akzeptiert haben. Ohne euch hätte ich es nicht bis hierher geschafft und eines Tages werde ich euch auch erklären worum es bei meiner Arbeit eigentlich ging.

This work has been financially supported by the IRTG 1740/TRP 2011/50151-0, funded by the DFG/FAPESP.

CONTENTS

LIST OF FIGURES

LIST OF SYMBOLS

ϕ, φ, θ, ϑ	Scalar angular variables
$\boldsymbol{x}$, $\boldsymbol{\phi}$, $\boldsymbol{\theta}$, ...	Vector variables
N	Ensemble size
$\mathbb{S}^1$	Circle $\mathbb{R}/2\pi\mathbb{Z}$
$\mathbb{T}^N$	N-dimensional torus $\mathbb{S}^1 \times \cdots \times \mathbb{S}^1$
$\mathbb{T}^N_{\text{ordered}}$	Ordered N-dimensional torus
$\mathbb{T}_p$	Two-cluster subspace
$\mathbb{D}_r$	Complex disk of radius r
$\mathbb{D}$	Complex unit disk $\mathbb{D}_1$
$\partial\mathbb{D}$	Complex unit circle
$\mathcal{M}$	Normally attracting invariant manifold
$\mathcal{M}_\epsilon$	Perturbed manifold
$\overline{A}$	Closure of the set A
α, ψ	Möbius group parameters
$G_{\alpha,\psi}$	Möbius transformation
$\mathcal{G}$	Möbius group
Z	Kuramoto order parameter
$\boldsymbol{\Lambda}(\boldsymbol{\theta})$, $\Lambda_{p,q,r,s}(\boldsymbol{\theta})$	Cross-ratios of the vector $\boldsymbol{\theta}$
$\boldsymbol{\lambda}$	Cross-ratio coordinates
$\boldsymbol{\lambda}^*$	Cross-ratio coordinates for the leaf of uniform distributions
$\mathcal{L}_{\boldsymbol{\lambda}}(\boldsymbol{\Lambda})$	Level set of the cross-ratio function $\boldsymbol{\Lambda}$ for regular value $\boldsymbol{\lambda}$
$\boldsymbol{\Theta}(\boldsymbol{\lambda})$	Point-of-reference in the level set $\mathcal{L}_{\boldsymbol{\lambda}}(\boldsymbol{\Lambda})$
$V_\delta(\boldsymbol{\lambda})$	δ-neighborhood of the cross-ratios $\boldsymbol{\lambda}$
$\Phi(x,t)$, $\Phi^t(x)$	Flow of an ODE
$\mathrm{D}\boldsymbol{F}(\boldsymbol{x}), \mathrm{D}_{\boldsymbol{x}}\boldsymbol{F}$	Derivative of the function $\boldsymbol{F}$ at $\boldsymbol{x}$
$\mathrm{D}_{x_j}\boldsymbol{F}(\boldsymbol{x})$	Partial derivative of $\boldsymbol{F}$ with respect to the variable x_j at $\boldsymbol{x}$
id	Identity map
id_n	n-by-n identity matrix

$\operatorname{Re} z$	Real part of $z \in \mathbb{C}$
$\operatorname{Im} z$	Imaginary part of $z \in \mathbb{C}$
$\bar{z}$	Complex conjugate of $z \in \mathbb{C}$
Δ^{s}, Δ^{u}	Synchronous fixed points
Σ^i, Ξ^i	Two-cluster fixed points
ω	Control parameter for an Active Rotator
κ	Coupling strength
ϵ	Perturbation parameter
μ	Floquet multiplier
f, g	Common fields in Watanabe-Strogatz integrable systems
$\boldsymbol{\phi}_{\boldsymbol{\lambda}}(t)$	Periodic solution with cross-ratios $\boldsymbol{\lambda}$ for a Watanabe-Strogatz integrable system
$T(\boldsymbol{\lambda})$	Period of $\boldsymbol{\phi}_{\boldsymbol{\lambda}}(t)$
$\mathcal{C}_{\boldsymbol{\lambda}}$	Periodic orbit of $\boldsymbol{\phi}_{\boldsymbol{\lambda}}(t)$
$\hat{\boldsymbol{F}}(\boldsymbol{\lambda})$	Time-average of the vector field $\boldsymbol{F}$ over $\mathcal{C}_{\boldsymbol{\lambda}}$

LIST OF ACRONYMS

ODE	Ordinary Differential Equation
AR	Active Rotator
NHIM	Normally Hyperbolic Invariant Manifold
NAIM	Normally Attracting Invariant Manifold
WS	Watanabe-Strogatz
SNIC	Saddle-Node Bifurcation on an Invariant Circle
THB	Transcritical Homoclinic Bifurcation
QIF	Quadratic Integrate-And-Fire

Id fieri potest, ut fallar.

1

INTRODUCTION

Nec deus intersit, nisi dignus vindice nodus.

The world around us is the result of the interactions between its constituents. Its abundance with the most intricate and complex structures is so overwhelming that for the largest part of human history, it was inconceivable that the natural world could be anything less than the creation of supernatural, omnipotent beings. It is one of the great achievements of mankind to realize that even the most complicated collective dynamics need not be orchestrated or constructed by some higher power but can emerge from simple rules describing how one part influences the other, from flocks of birds to the human brain. The natural world is in this respect in stark contrast to the world of human-made objects, which are top to bottom constructions while natural phenomena typically self-organize from bottom to top. The armamentarium for the mathematical analysis of dynamical systems comes from the theory of nonlinear dynamics.

Despite what it might occasionally seem, things do not just happen at random and to either predict what some physical system will look like in the future or to decipher what it looked like in the past, given all available information in the present, is the trade of physics. Granted that most processes in nature occur continuously in time and depending on how different properties or observables of said systems influence their evolution (i. e., how the present or past values of the observables determine their rate of change), this naturally leads to a description in terms of differential equations of some kind. In particular and broadly speaking, if the rate of change for the state of a system at some given time only depends on its current state itself, its evolution may be described by an Ordinary Differential Equation (ODE). The theory of ODEs is part of the theory of dynamical systems whose applications range from physics [Hol90; Sug+94] over engineering [Str+05; Roh+12] and biology [Win01; Izh10] to social science [HK02; Lor07] and economy [Hsi91; And18], to name just a few.

Oscillators and synchronization.

Collective periodic dynamics of ensembles of simple subsystems play a fundamental role in a vast number of complex phenomena [PRK03]. For example, it is commonly believed today that the brain's functionality is an emergent phenomenon, i. e., information processing does not happen in the single cells of the nervous system (neurons) but through the interaction of many neurons [Sin93; Fri15]. Likewise, there is an ongoing debate whether, and if, how pathological phenomena like epilepsy, Parkinson's disease, and Alzheimers are related to, e. g.,

excessive amounts of synchrony in the firing of many neurons [US06; Jir+13; BLL21]. A heart, pumping blood, functions because its cells contract or relax in a precisely coordinated manner [MMJ86]. In the social sciences, there exist attempts to model consensus formation in large social groups by minimal models of simple oscillating units/elements,[1] representing individual people, where consensus is reached if the majority of units oscillate in phase [PLR06; HS11]. These examples have in common that they feature some type of synchronization between the individual elements under appropriate circumstances. If the circumstances are right, a significant proportion of an ensemble of units will show a large-scale coordinated behavior. One may characterize synchronization as emerging large-scale or global dynamics through interactions of individual units on a local scale. Maybe one of the most visually impressive examples of synchronization occurs in swarms of fireflies [Buc38; Buc88]. In some firefly species, the males periodically produce flashes of light in order to attract females. If a swarm of males produces such flashes in an uncoordinated manner, the swarm will appear to nearby females as one flickering mass and may likely be ignored as ambient light. Instead, the males react to their neighbors and tend to "fire" in unison with their competitors. While this is of course not a conscious decision, the result is nevertheless impressive. After a short while, almost all males will fire in unison which has a much greater potential to spark the interest of any females nearby. Summarizing, one may say that the coupling between individual units plays a role that is just as important for generating large-scale behavior as the individual dynamics of the single unit. In particular, even if the single units are at rest on their own, depending on the nature of the coupling, the ensemble may very well show highly complex dynamics, often involving collective periodic behavior [TZ14; KF19].

Neuroscience and excitability.

One particularly prolific field of research within the theory of oscillatory elements and synchronization is that of neuroscience, i. e., the study of how cells of the nervous system function and interact and how this gives rise to phenomena like memory, intelligence, and ultimately, consciousness [DA05; CS99; Tra09]. One of the main concepts from neuroscience, which inspired this work, is the *excitability* of neurons. Simply put, a neuron being excitable means that, while staying typically at rest when isolated, it will produce a (possibly periodic) output in terms of *nerve impulses*, also called *action potentials* or *spikes*, if it is sufficiently and appropriately stimulated by, e. g., incoming spikes from other neurons. Their excitability makes neurons the building blocks of the nervous system, somewhat akin to logic gates, built from transistors, being the building blocks of modern computers. As it turns out, the neurobiological concept of excitability translates directly to single neurons being able to be modeled as dynamical systems which are close to some limit cycle bifurcation. For this reason, the study of the collective dynamics of excitable elements can yield insights, for example, on

1 Throughout this monograph, we use the words "unit" and "element" interchangeably.

how the functionality of nervous systems emerges from the interplay between neurons. In turn, this study revealed and inspired a wealth of mathematical structures and concepts which are very much worth studying in their own right.

Whether and how individual elements that are at rest on their own, can show nontrivial ensemble dynamics via appropriate coupling has been subject to ongoing research for a considerable time. As one of maybe the earliest examples, Smale investigated in 1976 the interaction of two "dead" cells that become "alive" via diffusive coupling between their respective enzyme concentrations [Sma76]. Here, a cell being "dead" is understood to be at rest while being "alive" means its enzyme concentrations vary periodically. As Smale points out, the underlying model goes back even further to Turing's seminal paper [Tur53] on reaction-diffusion systems in biology, originally published in 1953.

Keep it simple, stupid.

The bread and butter of physical modeling is to find the right level of abstraction to describe a given real-world phenomenon. If the model is simplified too much, its dynamics will not mimic the sought behavior or, even worse, its dynamics will be trivial. On the other hand, abstraction is necessary in order to get a firm enough grip of the system's key properties that can be quantified and subsequently described by some equation. From a practical point of view, a simple model is preferable to a complicated one and a model that can be described by simple equations is often preferable to one whose equations are complicated. This is all the more true for ODEs because they are notoriously hard to solve. When it comes to periodic behavior, it is often possible to derive a simple description where the state of each unit is described by a single periodic real variable. This "phase description" has turned out to be very powerful even (or maybe *especially*), but by far not exclusively, in the field of neuroscience, where the actual electro-chemical mechanisms inside each cell may often be neglected in favor of a description in terms of a single abstract phase-like variable [Vel06; Gal09; DB14; Son+14; ACN16; Cha+17]. Often, one considers the case where single units are spiking by themselves, i. e., they show periodic behavior, even if isolated. The seminal Kuramoto model [Kur75; Ace+05] and its many variations [SK86a; SK86b; YS99; Str00; KB02; MP04; HK15] deal with cases like this and yield a variety of different dynamics, depending on the specific setup, from the spontaneous onset of (partial) synchronization through coupling [Kur84; Str00; Ace+05; WYD21] over chaotic behavior [MPT05], phase-locked solutions [Ros+21], explosive synchronization [VZP15], and clustered states [BSY19] to so-called Chimera states [AS04; Olm15; LK21]. Remarkably enough, all of these completely different types of dynamics can be observed in some variation of the Kuramoto model despite its (at least in its original guise) rather simple form. For ensembles of excitable elements, the Active Rotator model by Shinomoto and Kuramoto [SK86b] plays a similar role and captures the essence of interacting (class I) excitable elements. It can be characterized as a classic planar Heisenberg model with all-to-all coupling (originally involving noise) under the assumption of an additional constant driving force. As already noted, this model is distinguished by,

e. g., the Kuramoto model by the fact that its elements are not necessarily oscillating in a self-sustained manner but can stay at rest if uncoupled which, as it turns out, can make its analysis more complicated in some respect. Nevertheless, it is equally able to produce rich dynamics, including synchronized periodic motion, pulse and spiral propagation, pattern formation, or collective bursting, depending on the respective setup [SSK88; Gia+12; TZ14; ZT16; KSN16; DGP17; Fra+21]. What makes the model by Shinomoto and Kuramoto especially interesting is that it can feature what is known today as Watanabe-Strogatz integrability.

Watanabe-Strogatz integrability.

The beginnings of Watanabe-Strogatz integrability (or theory) date back about 30 years when several groups of researchers noted the existence of so-called splay states in systems describing arrays of overdamped superconducting Josephson junctions [Jos62], coupled to a common load [AGM91; TS92; NW92]. To their surprise, these solutions possessed a high degree of neutral stability for a wide range of system parameters. Following several works which tried to explain these remarkable observations via averaging theory [SSW92] or by considering the thermodynamic limit [Gol+92; SM93], Watanabe and Strogatz showed rigorously in their seminal works [WS93; WS94] how these findings can be understood by considering a set of just three coupled differential equations whose dynamics fully encode the dynamics of the whole array, regardless of the number of junctions. They already noted that their results could be generalized to a wider class of dynamical systems, consisting of identical angular[2] variables, coupled to common fields via their respective zeroth and first Fourier modes. While their original work was, as others put it in [EM14], an "algebraic tour-de-force" construction of special constants of motion, later on, a more geometric view became popular, which illuminated the degenerate dynamics of such systems by means of complex projective geometry. Watanabe-Strogatz integrability has since been an active field of research which involves techniques and concepts from Lie theory [MMS09], invariant manifold theory [MS09], averaging theory [Eld+21], and equivariance of ODEs [Mir94], most of which are also employed in this work.

The Ott-Antonsen ansatz.

Watanabe-Strogatz theory is not the only systematic framework for studying synchronization effects in oscillatory systems. Notably, the Ott-Antonsen ansatz [OA08; OA09] equally yields a low-dimensional description of, in its case, infinite ensembles of angular variables. Both theories have distinct realms: While Watanabe-Strogatz theory holds for finite ensembles of identical[3] angular variables, the Ott-Antonsen ansatz applies to heterogeneous ensembles in the thermodynamic limit of infinitely many units. Nevertheless, both frameworks are closely related to each other [PR15]. Not the least for the richness of the involved mathematical structures and techniques, these two frameworks are of continuing high interest.

2 Often, people also speak of phase or phase-like variables even when these quantities are generally not growing linearly in time.

3 In the sense of identical coupling to some common fields in which case one also speaks of "identically driven" units.

Perturbations.

As of now, there exist no general perturbation theories for Watanabe-Strogatz or Ott-Antonsen theory, although there exist, e. g., results for finite ensembles of weakly heterogeneous units [VRP16] or infinite ensembles of generally heterogeneous units [PR11] for the former case. Recent results in this direction also employ a circular cumulant representation for such systems under individual noise [Gol+18; Gol19; Tyu+18; Tyu+19]. In any case, these results focus on situations where individual units become distinguishable, i. e., nonidentical.

Our main objective.

In contrast to the above-mentioned works, our main objective is to investigate how periodic ensemble dynamics for general but *identical* (class I) excitable elements emerge through repulsive coupling. The idea for this comes from a recent work by Zaks and Tomov [ZT16] who observed intricate ensemble dynamics for sufficiently strong repulsion between individual units. This observation lead to the question of how generic these dynamics actually are since the model studied there possesses the Möbius group symmetry that characterizes Watanabe-Strogatz integrable models, a property that natural systems rarely possess. To investigate this question for the case of angular variables, we first need to gain a deeper understanding of the consequences of integrability for the model by Shinomoto and Kuramoto. Then, we can generalize the model to remove the degeneracy that arises from its integrability. As a result, we may see the original model as a base case for which we can develop a perturbation theory to account for more general types of dynamics. To go even further, we can study more complicated models with similar properties, e. g., by considering units that are not just one- but higher-dimensional with a similar type of coupling. We pay particular attention to periodic ensemble dynamics that involve (clustered) splay states, which are periodic solutions that feature a specific type of spatio-temporal symmetry. Splay states (also known as, e. g., (discrete) "rotating wave", "wagon wheel", or "ponies on a merry-go-round" solutions) are in fact a common phenomenon in Watanabe-Strogatz integrable systems [AGM91; AGK91; NW92; SM93; Mir94; Dip+12; Che+17] and similar setups [Zil+07; ZZ09; Per+10; Ber+21] and can lead to, e. g., "attractor crowding", which for large ensembles can lead to hopping between distinct attractors under the influence of even weak external noise [WH89; TW90]. The same is true for clustered periodic states, which can be observed in models from neuroscience to electro-chemistry [Oku93; HMM93; KZH06; LY12; SK14; KHK19; Kem+21; Fie+21]. In a nutshell, this thesis is mainly dedicated to studying the effects of repulsive coupling between class I excitable units and their description in terms of global variables, its motivation being the excavation of the mathematical principles that underlie the complex dynamics of such systems. It is divided into five parts.

Outline.

Part I introduces the theoretical background and mathematical techniques that our work relies on. In Chapter 2, we discuss the neuroscientific concept of (class I) excitability, how it translates to the theory of nonlinear dynamics, and describe the notion of the (generalized) Active Rotator as well as sinusoidal coupling between such elements. We also introduce the first two models that are central to our work. In Chap-

ter 3, we give a brief overview over the most important mathematical concepts that we use to study the dynamics of these models: the theory of normally attracting invariant manifolds, discrete symmetry groups of ODEs and the resulting spatio-temporal symmetries for periodic solutions for such equations, and a theorem from averaging theory for periodic solutions of ODEs. We feel that it is not just educational but necessary to discuss these concepts in some depth, since they are not necessarily part of the standard repertoire of, e. g., neuroscience. (At least they were and to some extend still are clandestine knowledge to the author.) We also discuss how to determine the stability of clustered periodic solutions against perturbations that split one or several clusters of the ensemble. Chapter 4 focuses on Watanabe-Strogatz theory. We show, in particular, that the set of group parameters and conserved quantities from Watanabe-Strogatz theory can be used as alternative coordinates on the space of angular variables in (strict) cyclic order. As a result, *any* system of coupled identical angular variables can be written alternatively in these new coordinates, regardless of whether it is integrable or not. This enables us to study general systems of identical angular variables within the Watanabe-Strogatz framework, which is essential for the following part of this monograph.

Results. Part II contains our results on the dynamics of the above-mentioned angular models: the classic Active Rotator model and the generalized Active Rotator model. In Chapter 5, we discuss the existence and stability of two-cluster states where we focus on periodic solutions. We show that such solutions emerge, in the most generic way, by one of two global bifurcation scenarios and discuss how these scenarios are connected to the criticality of a pitchfork bifurcation of a special synchronous fixed point of the system. We then show that the stability of periodic two-cluster states depends on the ratio of cluster sizes and how an observed change in stability for such states can be understood through Watanabe-Strogatz theory. Chapter 6 deals with the existence and stability of splay states and related periodic states for the classic model. Employing the theory of normally attracting invariant manifolds, we show that for a broad class of Watanabe-Strogatz integrable systems, splay states must not only exist but are also embedded in a continuum of nonhyperbolic periodic orbits whose union forms a normally attracting invariant manifold. In particular, this result applies to the classic Active Rotator model. The hyperbolic structure of the manifold enables us in Chapter 7 to determine the stability of the splay state for the generalized Active Rotator model via techniques from averaging theory and gives a simple criterion to determine which orbits of the continuum persist under a given perturbation. It also allows us to understand a "nonlocal transfer of stability" between periodic two-cluster states and splay states in a minimal model of just four classic Active Rotators and allows for an unfolding of this nongeneric bifurcation scenario to a "local transfer of stability". We note that similar techniques were recently used in a related context to prove the existence of Chimera states in oscillatory systems on star networks [Eld+21].

Morris-Lecar neurons.

Part III focuses on coupled Morris-Lecar neurons, which are, to some degree, a higher-dimensional analog of Active Rotators. In particular, we study how the results from Part II generalize to ensembles of general class I excitable units. We show how for this system splay states and periodic two-cluster emerge in similar bifurcations to the ones discussed in the second part and observe, again for the simplest nontrivial case of four such neurons, a now local transfer of stability between the two types of periodic solutions. This suggests that while Watanabe-Strogatz theory can be employed to investigate bifurcations in systems of repulsively coupled Active Rotators, the observed scenarios are not a consequence of this integrability but generalize to general systems of identical (class I) excitable units. However, higher-dimensional systems like coupled Morris-Lecar neurons can also give rise to potentially stable periodic solutions which do not find their analogs in angular dynamics. Specifically, we observe states where the ensemble splits in two groups which display qualitatively different dynamics, so that in an admittedly very loose sense one may speak of "Chimera-like" states.

"Chimera-like" states.

Chimera states, in a strict sense, always involve an ensemble of identical units that splits into two groups where one group is synchronized while the other group is in a state of decoherence [Kem+16]. For our model, this will not be the case so that one has to be careful with the name "Chimera" to avoid confusion. Our usage of the word is to be understood more in the sense of [ZP17] where Chimera states are defined as states in which an ensemble splits in a fully synchronized macroscopic component and a "cloud" of distinct units.

Part IV constitutes the conclusion of our work while part V consists of an appendix with background information and calculations which would otherwise interrupt the flow of the main chapters.

Style.

A note on style: For this thesis, we employ a style that structures the text body into definitions, lemmas, theorems, proofs, etc. which is more commonly known from the mathematical literature while this monograph is a thesis in physics (even though the border between mathematics and physics is blurry in this field of research, to say the least). Nevertheless, we deliberately chose this style because we feel that it helps not only to organize the writing process but also makes the content better digestible and allows to reference intermediate results more easily. After all, the purpose of this style is not to distinguish mathematics from physics but to make a complicated topic more accessible.

Part I

FOUNDATIONS

Mathematics succeeds in dealing with tangible reality by being conceptual. We cannot cope with the full physical complexity; we must idealize.

— Pólya György [Pól77]

2

COUPLED ACTIVE ROTATORS

ABSTRACT

This chapter gives an overview over the theoretical background of the (generalized) Active Rotator model, to which this thesis is mostly dedicated. We start by introducing the notion of *excitability* from neuroscience in Section 2.1 and discuss how this physiological property of neurons can be understood within the framework of nonlinear dynamics. In particular, this leads to the introduction of the (generalized) *Active Rotator*, which obeys a simple one-dimensional ordinary differential equation. In Section 2.2, we discuss systems of coupled identical Active Rotators and the distinction between *attractive* and *repulsive* coupling. We are then ready to introduce the first two models of this thesis in Section 2.3, one being the deterministic Shinomoto-Kuramoto model with classic identical Active Rotators under repulsive sinusoidal coupling and the other one being a similar model, where we consider ensembles of generalized Active Rotators under the same kind of coupling.

2.1 CLASS I EXCITABILITY AND ACTIVE ROTATORS

WHAT IS EXCITABILITY? On of the key physiological properties of neurons is their *excitability* [JW94; AA98; KS09; Win01; Izh10]. The transmission of information in the nervous system happens via electrical signals which themselves are produced by neurons. The in- and outside of every neuron harbor different concentrations of various kinds of ions, e. g., Ca^{2+}, K^+, and Na^+ where the membrane of the cell acts as a partially permeable physical barrier, separating its inside from the outside. The result of this gradient of ion concentrations is a net electric potential difference V between the cell's interior and exterior, called the *membrane potential* or *membrane voltage*. The cell membrane is partially permeable for the ions because it is equipped with ion channels and pumps, which let ions either diffuse through the membrane with their respective concentration and electric gradients (channels) or actively pump them from the interior to the exterior and vice versa against these gradients (pumps). Both mechanisms are usually selective, i. e., different channels and pumps act on different types of ions. Whether channels are open or not and the activity of the pumps and thus the overall conductance of the membrane for ion currents are them-

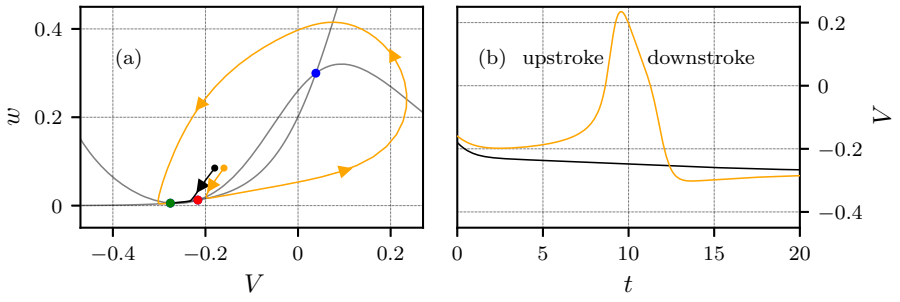

Figure 1: Subthreshold perturbation (black line) and spike (orange line) for a class I excitable neuron. Panel (a) shows the phase plot in the membrane voltage V and a single gating variable w for a so-called Morris-Lecar neuron. The subthreshold perturbation converges exponentially to the resting state $(V^{\mathrm{s}}, w^{\mathrm{s}})$ (green dot) of the neuron while in a spike-generating perturbation, the state first approaches a saddle (red dot) and then traces a large-scale contour in phase space (the unstable manifold of the saddle), thus producing the spike. Gray lines indicate the nullclines of the system and the blue dot marks an unstable focus. For better visual display, we consider here perturbations that change *both*, the membrane voltage and the gating variable. In Panel (b), we show the time series for V for both perturbations. The upstroke of the spike is characterized by a rapid growth of V which is followed by a downstroke in which V converges to V^{s}.

selves (nonlinearly) voltage-dependent. Hence, a single Neuron can be modeled as an electric circuit with nonlinear feedback, making it accessible to methods from the theory of nonlinear dynamics. For such a conductance-based neuron model, the state of the neuron is characterized by the membrane voltage V and the (normalized) conductances $w_{\mathrm{Ca}^{2+}}$, $w_{\mathrm{K}^{+}}$, etc. of the membrane for each type of ion. Since the channels and pumps act as gates for the respective types of ions, the variables w_x with $x \in \{\mathrm{Ca}^{2+}, \mathrm{K}^{+}, \mathrm{Na}^{+}, \dots\}$ are known as *gating variables*. Based on how, and in particular how fast, ion channels and pumps react to changes in V, one classifies three different types of gating variables: *excitation*, *recovery*, and *adaptation variables* [Izh10]. The interplay between the membrane potential and the gating variables can often be modeled by some ODE of the form

$$\begin{aligned} \dot{V} &= f(V, \boldsymbol{w}, I) \\ \dot{\boldsymbol{w}} &= g(V, \boldsymbol{w}) \end{aligned} \tag{2.1}$$

where $\boldsymbol{w} \coloneqq (w_1, \dots, w_n) \in \mathbb{R}^n$ is a tuple of the n gating variables and $I \in \mathbb{R}$ is a transmembrane current, which in nature arises through synaptic connections to other neurons and typically only affects the membrane voltage. In experiments, one can mimic such a current by inserting an electrode into the neuron and applying a (small) external voltage. I acts as a control parameter for equation (2.1).

A single isolated neuron is typically at rest, which translates to the existence of a stable fixed point $(V^{\mathrm{s}}, \boldsymbol{w}^{\mathrm{s}})$ for (2.1). Let $\delta(t)$ denote the Dirac delta function. Applying a pulse-like input signal $I(t) = I_{\mathrm{in}}\delta(t)$ of signal strength I_{in} perturbs the neuron from its state of rest at time $t = 0$. For the subsequent evolution of its state, one generally distinguishes

between two qualitatively different scenarios, depicted in Figure 1. In Panel (a), we show the phase space for a so-called Morris-Lecar neuron, which possesses a single gating variable w and is discussed in more detail in Chapter 8, together with its essential invariant objects. The two gray lines depict the nullclines of the system. Their intersections mark three distinct fixed points: the stable fixed point at $(V^{\mathrm{s}}, w^{\mathrm{s}})$ (green dot), a saddle (red dot), and an unstable focus (blue dot). A black and orange dot mark two distinct initial states, each representing one of the two perturbation scenarios, mentioned above. In Panel (b), we show the time series $V(t)$ for both perturbations. Note that, even though in-vivo and in (2.1), perturbations typically only affect the membrane voltage V, here, we depict two perturbations that also change the gating variable w. This is for the sole reason of a better visual display and does not alter the outcome.

If the perturbation of the state is too small (black dot), it decays exponentially and rapidly settles at $(V^{\mathrm{s}}, w^{\mathrm{s}})$ again (black lines in Panels (a) and (b)). On the other hand, if the perturbation from the signal $I(t)$ is sufficiently strong, the perturbed state will not immediately converge to $(V^{\mathrm{s}}, w^{\mathrm{s}})$ but will produce a so-called *spike* in its membrane potential, depicted in orange in both panels. The spike is characterized by a short period, during which V grows rapidly (upstroke), followed by a period of exponential convergence to the state of rest (downstroke), see Panel (b). During the spike, the state of the neuron traces a large-scale contour in phase space before eventually converging to $(V^{\mathrm{s}}, w^{\mathrm{s}})$. We note that the distinction between subthreshold and spike-generating perturbations in our example lies in whether the perturbed state lies to the left (subthreshold) or right (spike-generating) of the *stable manifold* of the saddle in phase space.

It is precisely the ability to produce spikes that is called *excitability*: If a neuron receives a sufficiently strong input from other neurons (in form of a series of spikes), it can produce one or several spikes itself. This can in turn elicit the same behavior in other neurons or suppress their ability to produce spikes, depending on the specific type of coupling between them. In the former case, one speaks of *excitatory* coupling while the latter case is known as *inhibitory* coupling. Thus, their excitability enables neurons to react to each other which in turn is the cornerstone of information processing in neural networks.[1]

CLASSES OF EXCITABILITY Mainly for historical reasons, one distinguishes between three types of excitability, referred to as *class I, II,* and *III*, respectively. This distinction goes back to Hodgkin [Hod48], who observed that neurons can be classified by how they react to a stimulus. In practice, the classification is based on the fact that applying a sufficiently strong constant current[2] I to a neuron makes it spike

1 Of course, we are not implying that excitability is the *only* imaginable way how neurons could communicate. It is simply the way, that nature has settled on and it is otiose to discuss how information processing would work if they were not excitable.

2 In the literature, this is also known simply as a DC current.

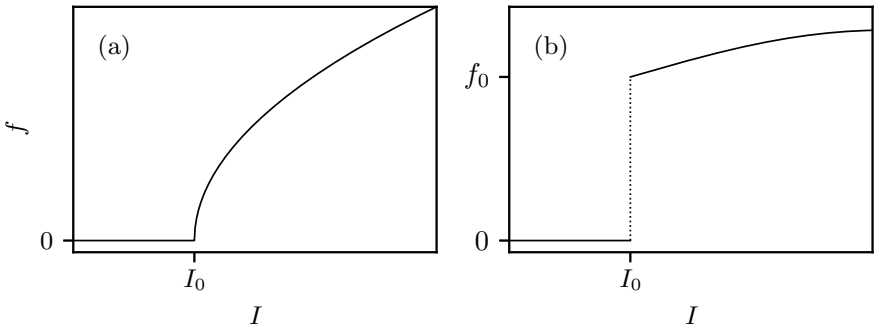

Figure 2: Idealized depiction for the current-frequency relation for a class I excitable neuron in Panel (a) and class II excitable neuron in Panel (b).

periodically with some frequency f. Such periodic series of spikes are commonly referred to as *spike trains.*

Spike trains.

For class I excitable neurons, the transition between quiescence and periodic activity is continuous, i. e., the frequency can be made arbitrarily small by tuning I. Below a critical value I_0, the neuron does not produce or *fire* any spikes, which can be interpreted as a spike train with frequency zero. Above the threshold, the frequency of the spike train continuously increases. This relation between current I and spike frequency f is schematically depicted in Panel (a) of Figure 2.

On the other hand, for class II excitable neurons, the transition between quiescence and periodic oscillation is discontinuous. In other words, starting with small I and slowly increasing the applied current will result in a transition from subthreshold behavior (i. e., no spike trains or $f = 0$) to periodic spiking with finite frequency $f > f_0 > 0$, see Panel (b) in the same figure. In class III excitable neurons, a single spike is generated for sufficiently strong input currents, whereas periodic spike trains may only be achieved for extremely large currents.

It was later suggested that the class of excitability of a neuron is connected to the corresponding dynamical system (2.1) being close to a limit cycle bifurcation in parameter space [RE89]. Focusing on codimension 1 bifurcations, it can be shown that class II excitability is related to inherently two-dimensional bifurcation scenarios such as sub- or supercritical Hopf bifurcations while class I excitability is related to a so-called Saddle-Node Bifurcation on an Invariant Circle (SNIC) [Izh00], also known as Saddle-Node Homoclinic Bifurcation [Kuz13].

The top row of Figure 3 depicts the phase plots for a SNIC scenario for a Morris-Lecar neuron. In Panel (a), saddle (red dot) and node (green dot) are well separated and are connected by the unstable manifold of the saddle (orange line). This robust contour is the invariant circle on which the SNIC occurs in Panel (b) where it forms the homoclinic orbit of a saddle-node (green-red dot). After the bifurcation, the contour becomes a stable periodic orbit in Panel (c). The unstable manifold from Panel (a) is exactly the hidden large-scale contour that the spike in Figure 1 traces.

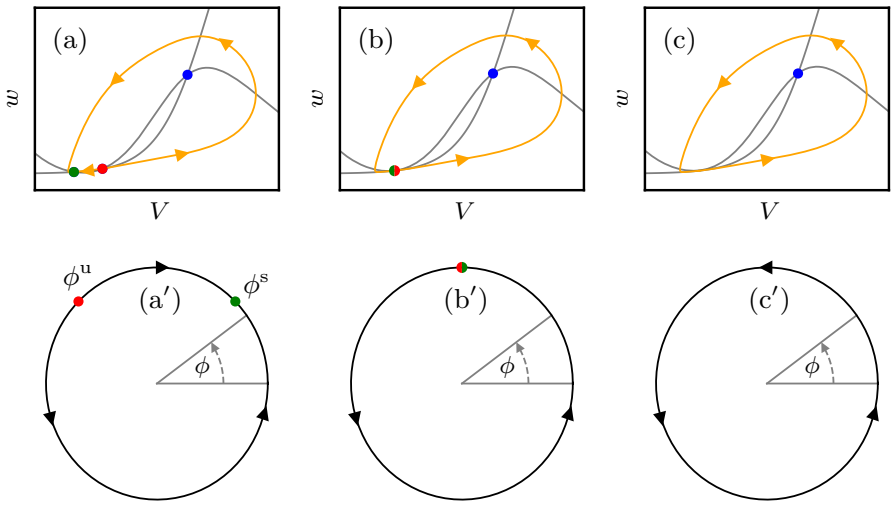

Figure 3: SNIC for a Morris-Lecar neuron (top) and an Active Rotator (bottom). Again, a red dot denotes a saddle, a green dot a stable node, and a blue dot an unstable focus. Arrowheads indicate the direction of the flow along respective contours. Saddle and node are connected by the two branches of the unstable manifold (orange line) of the saddle. This contour forms an invariant circle in the phase space. While saddle and node are well-separated in Panel (a), at the SNIC in Panel (b), they form a saddle-node (green-red dot) for which the unstable manifold of the former saddle becomes a homoclinic orbit. After the bifurcation, in Panel (c), a stable periodic orbit forms from the former homoclinic orbit. The bottom row represents a reduction of the dynamics of the top row along the invariant circle in terms of an angular variable ϕ. In Panel (a′), there exists a stable fixed point ϕ^{s} and an unstable one ϕ^{u}. At the SNIC in Panel (b′), these two merge to a saddle-node (green-red dot). After the bifurcation, no fixed points are left and the system possesses a periodic solution in Panel (c′). For the Active Rotator model, the phase space as a whole is the invariant circle of the SNIC.

Thus, two dynamical regimes exist for such a neuron: In the excitable regime, it produces spikes if appropriately excited while it stays at rest if no input is present. After the bifurcation, in the second regime, the stable state of rest has vanished and the neuron produces a periodic spike train even without any further input.

The fact that an invariant circle exists for a class I excitable unit hints that a dimensional reduction is possible: Since the contour is stable with respect to perturbations in normal direction (this leads to the periodic orbit in Panel (c) of Figure 3 to be equally stable), any initial state close by will converge exponentially to this contour and then follow it to the stable node or keep rotating if no such node exists. In this case, it is reasonable to describe the state of the system by its position on the invariant circle, akin to the one-dimensional descriptions of higher-dimensional oscillators by means of phase reduction techniques [Win01; PRK03]. In fact, extending the concept of the so-called isochron to excitable elements yields a low-dimensional reduced description for such

elements [IAJ98].[3] This motivates the following angular model for class I excitable elements.

THE ADLER EQUATION AND ACTIVE ROTATORS Arguably, the simplest incarnation of class I excitable elements comes in the form of the Adler equation [Adl46], which reads

$$\dot{\phi} = \omega - \sin\phi \tag{2.2}$$

Throughout this thesis, we define $\mathbb{S}^1 := \mathbb{R}/2\pi\mathbb{Z}$ and distinguish it in particular from the unit circle $\partial\mathbb{D} := \{z \in \mathbb{C} \,;\, |z| = 1\}$ in the complex plane.

with $|\omega| < 1$. Here, we assume $\phi \in \mathbb{R}/2\pi\mathbb{Z} =: \mathbb{S}^1$, so that we identify all points $\phi, \varphi \in \mathbb{R}$ for which $\phi - \varphi$ is an integer multiple of 2π and the phase space of (2.2) is indeed a circle.

As for any potentially class I excitable system, we can distinguish two regimes for the dynamics of (2.2), as depicted in the bottom row of Figure 3. For $-1 < \omega < 1$, equation (2.2) possesses exactly one stable fixed point $\phi^{\mathrm{s}} = \arcsin\omega$ and one unstable fixed point $\phi^{\mathrm{u}} = \pi - \arcsin\omega$ so that no periodic solutions exist in this regime, see Panel (a′). A SNIC occurs for the two critical values $\omega = \pm 1$, where the invariant circle is the phase space $\mathbb{S}^1$ itself which forms a homoclinic orbit for the saddle-node $\phi^{\mathrm{sn}} = \pi$ in Panel (b′). For $|\omega| > 1$, no fixed points exist whatsoever and we obtain a periodic solution $\phi(t)$ of period $T = 2\pi/\sqrt{\omega^2 - 1}$, as depicted in Panel (c′). The sign of ω determines the sense of rotation of the oscillation. Negative values lead to clockwise and positive values to counterclockwise rotation.

The system (2.2) is commonly known as an *Active Rotator*, a name that Shinomoto and Kuramoto introduced in 1986 [SK86b]. What makes the Rotator *Active* is a nonzero choice of ω which acts, in Shinomoto's and Kuramoto's own words, as a "constant driving force" to the Rotator. However, in what follows, we exclude the cases $\omega = \pm 1$ and $|\omega| > 1$ and refer only to the case $|\omega| < 1$ as a (classic) Active Rotator since only then, the system (2.2) is excitable.

Active Rotators in disguise.

A close connection exists between the Active Rotator model and two other important neurophysical models, the *theta neuron* (also known as theta model or Ermentrout-Kopell canonical model) and the Quadratic Integrate-And-Fire (QIF) neuron [EK86]. These neuron models, introduced by Ermentrout and Kopell in 1986, also show class I excitability for a suitable parameter choice. The theta model reads

$$\dot{\theta} = (1 - \cos\theta) + a(1 + \cos\theta)$$

with $\theta \in \mathbb{S}^1$ while the QIF neuron model reads

$$\dot{x} = a + x^2$$

with $x \in \hat{\mathbb{R}} := \mathbb{R} \cup \{\infty\}$. Intuitively, the extended real line $\hat{\mathbb{R}}$ can be seen as the real line with a single additional "point at infinity" ∞ so that its "end points" $\pm\infty$ are identified or "glued" together. In this picture, the QIF model can feature periodic motion for $a > 0$ where the state $x(t)$ first diverges in finite time to $+\infty$ and "returns" from

3 In the terminology of [HI12], one may speak of the *canonical* model for such systems.

$-\infty$ in finite time, thus, traversing the whole space $\hat{\mathbb{R}}$. All three models, the theta neuron, the QIF neuron, and the Active Rotator model are in fact equivalent. Theta and QIF neuron are connected via the Weierstraß substitution $\sin\theta = 2x/(1+x^2)$, $\cos\theta = (1-x^2)/(1+x^2)$. Rescaling $t \mapsto (1-a)t$ and setting $\phi = \theta + \pi/2$ then yields the Active Rotator from the theta neuron with $\omega = (1+a)/(1-a)$.

Classic Active Rotators are first order approximations for class I excitable elements.

The right hand side of (2.2) for the classic Active Rotator contains only zeroth and first order Fourier modes. In the context of general (higher-dimensional) class I excitable elements, it thus serves as a first order Fourier series expansion of the vector field, restricted to the involved invariant circle of the system's SNIC, whereas the Fourier expansion of the actual vector field on that contour generically involves infinitely many modes.[4] We therefore generalize the notion of the Active Rotator to account for these higher order modes in the dynamics of a single excitable element. This leads to the following definition:

Definition 2.1 *Consider the ODE $\dot{\phi} = f(\phi, \delta)$ with $\phi \in \mathbb{S}^1$ and $\delta \in \mathbb{R}$ and assume that $f : \mathbb{S}^1 \times \mathbb{R} \to \mathbb{R}$ is smooth and that the following three conditions are fulfilled:*

1. *For $\delta < 0$, f possesses exactly two regular zeros ϕ^{s} and ϕ^{u}, i. e., $f(\phi^{\mathrm{s}}, \delta) = f(\phi^{\mathrm{u}}, \delta) = 0$ with $\mathrm{D}_\phi f\,(\phi^{\mathrm{s}}, \delta) < 0$ and $\mathrm{D}_\phi f\,(\phi^{\mathrm{u}}, \delta) > 0$.*
2. *For $\delta > 0$, f possesses no zeros in ϕ.*
3. *At $\delta = 0$, the system goes through a saddle-node bifurcation.*

$\mathrm{D}_\phi f(\phi^{\mathrm{s}}, \delta)$ denotes the partial derivative of f with respect to its first variable, evaluated at $(\phi^{\mathrm{s}}, \delta)$.

For $\delta < 0$, we call the system an Active Rotator (AR).

Remarks 2.2

1. *The function f can also be interpreted as 2π-periodic in $\phi \in \mathbb{R}$.*
2. *$\mathrm{D}_\phi f\,(\phi^{\mathrm{s}}, \delta)$ and $\mathrm{D}_\phi f\,(\phi^{\mathrm{u}}, \delta)$ always have opposite signs since f is, in particular, continuously differentiable.*
3. *ϕ^{s} denotes the stable fixed point of the system while ϕ^{u} denotes its unstable fixed point.*

Since f is smooth and defined on $\mathbb{S}^1 \times \mathbb{R}$, we can expand it in terms of a Fourier series in ϕ:

$$f(\phi, \delta) = \sum_{n=0}^{\infty} a_n(\delta)\cos n\phi + b_n(\delta)\sin n\phi \tag{2.3}$$

where the real parameters a_n and b_n depend smoothly on δ. In what follows, we always make the following assumption:

4 As a matter of fact and assuming that the invariant contour is in indeed a *normally attracting invariant manifold*, see Chapter 3, this expansion does not only describe the dynamics on the contour but also serves as a *local model* for the dynamics in a neighborhood of the contour [HI12]. We will come back to this and in particular discuss the concept of local models in Chapter 6.

Assumption 2.3 *The first four Fourier coefficients in* (2.3) *are fixed to*

$$a_0 = \omega,\ b_0 = 0,\ a_1 = 0,\ \textit{and}\ b_1 = -1$$

for some $\omega \in \mathbb{R}$.

Note that for any Fourier expansion (2.3), this can always be achieved by an appropriate rescaling of time t and shift of angle ϕ as long as $a_1 \neq 0$ or $b_1 \neq 0$:

If $b_1 = 0$ and therefore $a_1 \neq 0$, we simply rescale $t \mapsto t' = a_1 t$ and shift $\phi \mapsto \phi' = \phi - \frac{\pi}{2}$ so that in these new coordinates and with $c_n = (a_n - ib_n)/2$ and $\bar{c}_n = (a_n + ib_n)/2$, we have

For every complex number z, we denote its complex conjugate as $\bar{z}$.

$$\begin{aligned}\frac{\mathrm{d}\phi'}{\mathrm{d}t'} &= \frac{1}{a_1}\frac{\mathrm{d}\phi}{\mathrm{d}t} \\ &= \frac{a_0}{a_1} + \cos\left(\phi' + \frac{\pi}{2}\right) + \sum_{n=2}^{\infty} \frac{c_n}{a_1} \mathrm{e}^{in\left(\phi' + \frac{\pi}{2}\right)} + \frac{\bar{c}_n}{a_1} \mathrm{e}^{-in\left(\phi' + \frac{\pi}{2}\right)} \\ &= \omega - \sin\phi' + \sum_{n=2}^{\infty} c'_n \mathrm{e}^{in\phi'} + \bar{c}'_n \mathrm{e}^{-in\phi'}\end{aligned}$$

with

$$\omega = \frac{a_0}{a_1} \text{ and } c'_n = \frac{c_n}{a_1} \mathrm{e}^{i\frac{n\pi}{2}}.$$

$$\operatorname{sign} x = \begin{cases} +1 & \text{if } x > 0 \\ -1 & \text{if } x < 0 \\ 0 & \text{if } x = 0 \end{cases}$$

On the other hand, for $b_1 \neq 0$, we can rescale $t \mapsto t' = At$ and shift $\phi \mapsto \phi' = \phi + B$ with $A = \operatorname{sign} b_1 \sqrt{a_1^2 + b_2^2}$ and $B = \pi + \arctan\frac{a_1}{b_1}$ such that, in these new coordinates,

$$\begin{aligned}\frac{\mathrm{d}\phi'}{\mathrm{d}t'} &= \frac{1}{A}\frac{\mathrm{d}\phi}{\mathrm{d}t} \\ &= \frac{a_0}{A} + \frac{a_1}{A}\cos\left(\phi' - B\right) + \frac{b_1}{A}\sin\left(\phi' - B\right) + \\ &\quad + \sum_{n=2}^{\infty} \frac{c_n}{A} \mathrm{e}^{in(\phi' - B)} + \frac{\bar{c}_n}{A} \mathrm{e}^{-in(\phi' - B)} \\ &= \omega - \sin\phi' + \sum_{n=2}^{\infty} c'_n \mathrm{e}^{in\phi'} + \bar{c}'_n \mathrm{e}^{-in\phi'}\end{aligned}$$

with

$$\omega = \frac{a_0}{A} \text{ and } c'_n = \frac{c_n}{A} \mathrm{e}^{-inB}$$

where we used the fact that

$$\frac{a \operatorname{sign} b}{\sqrt{a^2 + b^2}} \cos\phi + \frac{b \operatorname{sign} b}{\sqrt{a^2 + b^2}} \cos\phi = \sin\left(\phi + \arctan\frac{a}{b}\right).$$

We may thus always write

$$\dot{\phi} = \omega - \sin\phi + h(\phi)$$

with

$$h(\phi) = \sum_{n=2}^{\infty} a_n \sin n\phi + b_n \cos n\phi.$$

In the case of $h(\phi) = 0$, we reobtain the classic definition of Shinomoto and Kuramoto. We will later see how the choice of h determines the stability of splay states and periodic two-cluster states for a specific class of ensembles of Active Rotators.

2.2 COUPLED IDENTICAL ACTIVE ROTATORS

While the dynamics of a single Active Rotator is rather simple, complex dynamics can be observed for ensembles of Active Rotators. Since 1986, dynamics for ensembles of Active Rotators were and still are subject of a prolific field of research and have been studied in a wide variety of scenarios, including Active Rotators with noise [Zak+03; Tes+07; DGP17], in heterogeneous ensembles [Son+14; KF19], with nontrivial network structure [Son+13; KSN16], or various types of coupling [TZ14; ZT16; Bač+18] to name a few. In most of these cases, the individual Active Rotators obey the Adler equation. Noteworthy, even a single Active Rotator can exhibit complex dynamics, e. g., if one promotes the parameter ω to an adaptive variable under the influence of Gaussian white noise [Fra+20].

For clarity, it is beneficial to distinguish between a unit j and its state x_j, e. g., ϕ_j for the angular model or $(V_j, \boldsymbol{w}_j)$ for more realistic neuron models.

In this work, the focus lies on systems of N identical units $j \in \{1, \dots, N\}$ where the angular velocity $\dot{\phi}_j$ of unit j is a function of its "internal" or "on-site" dynamics $f(\phi_j)$ and its interaction with all other units of the ensemble. We assume that

$$\dot{\phi}_j = f(\phi_j) + \sum_{k \neq j}^{N} g(\phi_k - \phi_j) \tag{2.4}$$

holds with smooth functions f and g. Here, $g(\phi_k - \phi_j)$ determines the influence of unit k on unit j. When we speak of *identical* units, we mean that the functions f and g do not depend on the index j, e. g., by site-dependent Fourier coefficients. Note that we assume here that the coupling between units is (i) pairwise, (ii) all-to-all, and (iii) depends solely on the mutual angular difference of two units. In the case of phase oscillators, i. e., units that already oscillate on their own, assumption (iii) follows naturally from (i) for the time-average approximation of general pairwise coupling functions $\tilde{g}(\phi_k, \phi_j)$ [SVM07; Kur84; PRK03]. Even though this averaging argument cannot be readily applied to ensembles of Active Rotators since it relies on the fact that each unit by itself already features some periodic motion, we adopt assumption (iii) within this thesis.

Phase space and state space.

The phase space for systems of type (2.4) is the N-dimensional torus

$$\mathbb{T}^N := \underbrace{\mathbb{S}^1 \times \cdots \times \mathbb{S}^1}_{N \text{ times}}.$$

However, it is sometimes convenient to geometrically interpret (2.4) as describing an ensemble of units on the same circle. Whenever we employ this perspective, we will refer to $\mathbb{S}^1$ as the *state space* of (2.4) in contrast to the phase space $\mathbb{T}^N$.

The specific choice for g determines how unit k influences the dynamics of unit j. If one assumes that the influence of j on k is of the same magnitude but opposite direction (in loose resemblance to Newton's third law of motion), then g must be odd, i. e., $g(-\theta) = -g(\theta)$ must hold for all $\theta \in \mathbb{S}^1$. In this case, the Fourier expansion of g can be written entirely in terms of sinusoidal modes $\theta \mapsto \sin m\theta$ with $m \in \mathbb{N}$ so that the coupling in (2.4) vanishes for $\phi_j = \phi_k$. A common choice is

$$g : \theta \mapsto \frac{\kappa}{N} \sin(\theta).$$

This type of coupling in ensembles of ARs was first investigated by Shinomoto and Kuramoto themselves. The coefficient κ determines whether the coupling of ϕ_j to ϕ_k is *attractive* or *repulsive*. The factor $1/N$ serves as a convenient scaling factor.

Attractive and repulsive coupling.

Informally speaking, by attractive and repulsive coupling, we mean the following: If two units j and k are close to each other, regardless of their positions $\phi_j, \phi_k \in \mathbb{S}^1$, i. e., if their mutual distance[5] $d_{jk} := \min(|\phi_j - \phi_k| \bmod 2\pi, 2\pi - |\phi_j - \phi_k| \bmod 2\pi)$ is small, then *attractive* coupling tends to *decrease* this distance while *repulsive* coupling *increases* it. Note, however, that this does not mean that, e. g., for repulsively coupled units, the distance $d_{jk}(t)$ necessarily grows over time. In fact, $d_{jk}(t)$ generally depends on the nonlinear on-site dynamics of each unit. To give a more concise definition of the two types of coupling, we speak of attractive coupling if $g'(0) > 0$ and of repulsive coupling if $g'(0) < 0$. Indeed, within this notion of attractive- and repulsiveness, the effect from coupling between two units, close by, coincides with the informal notion above. We note that in the literature, attractive and repulsive coupling often serve as surrogates for more complex forms of coupling like excitatory and inhibitory coupling between neurons [Tsi+05; GJC11; TR19; LB20]. While this correspondence is not necessarily accurate because, e. g., sufficiently strong repulsive coupling between ARs yields oscillatory behavior of the otherwise quiescent "neurons" [ZT16] while actual inhibitory coupling leads to the suppression of firing for one neuron if another one fires, it may serve as a rough approximation for actual interactions between neurons. But even (GABA-mediated) repulsive coupling has recently been observed between circadian clock neurons in the mammalian suprachiasmatic nucleus [Myu+15]. Equally, systems that feature both attractive and repulsive coupling have been used in modeling sociological [MPT10], ecological [Gir+16], and physical [DS20] phenomena, see also [MCG20].

Sinusoidal coupling.

A word is at hand, regarding some important aspects of sinusoidal coupling. As mentioned above, the interaction between two neurons usually occurs via spike trains, i. e., one neuron produces a single spike or a

5 This choice for d_{jk} means that, if we picture ϕ_j and ϕ_k as being located on the unit circle, the distance between them is defined by the length of the shorter of the two arcs that connect them.

series of spikes, which can excite or inhibit the same behavior in another neuron. Most often, neurons do not directly "sense" their neighbors' electric fields but instead, the transmission of spike trains occurs via chemical synapses [DA05] in which case one speaks of the *presynaptic* neuron for the one that fires spikes and the *postsynaptic* neuron, which receives the spikes through the synaptic connection. Hence, the interaction between neurons is often modeled via so-called pulse-coupling, where spikes from one neuron can act as instantaneous perturbations for the state of the other. This can be modeled by, e. g., a series of Dirac delta functions in time, neglecting the synaptic filtering [MS90; HMM95; Izh99; GE02] or via continuous pulse-like functions [Lai14; Lai15; Lai18]. The yet simpler sinusoidal coupling as in the Shinomoto-Kuramoto model loosely serves as a first-order Fourier approximation for such more complicated couplings by neglecting second- and higher-order terms in the Fourier expansion of g. We note that in the context of synaptic coupling, this approximation is flawed because synaptic coupling between neurons is directed whereas for sinusoidal coupling, both neurons affect each other. However, other types of electrical connections between neurons and various other types of cells exist, e. g., in the form of gap junctions, for which the coupling between two cells *is* symmetric [DA05; DS93]. For this type of coupling, an approximation in terms of sinusoidal coupling may be to some degree appropriate. Moreover, pure sinusoidal coupling was further used to, e. g., model locomotion in isolated spinal cords of lampreys [CHR82] and plays a role in laser systems [JPP08] and radio engineering [Hak08]. It also emerges naturally for arrays of so-called *Josephson junctions* with parallel resistor-capacitor-inductor load under the condition of negligible capacitor load for each junction where a time-average approximation yields the Kuramoto phase model [WS95].

No overtaking allowed.

An important observation that can be readily made for systems of type (2.4) is that any two units j and k cannot overtake each other in the state space since otherwise they must coincide at some time t' where they couple in the same way to every other unit of the ensemble. This implies that $\dot{\phi}_j(t') = \dot{\phi}_k(t')$ and hence $\phi_j(t) = \phi_k(t)$ for all $t \in \mathbb{R}$ in contradiction to the assumption that they were separated for some $t < t'$. We call a set $A \subseteq \{1, \dots, N\}$ of units a *cluster* if and only if $\phi_j(t) = \phi_k(t)$ for all $j, k \in A$. The above consideration then implies that clusters stay clusters for all time, in other words, they are preserved under the flow of (2.4).

Clusters stay clusters.

M-cluster states.

If the ensemble splits in M mutually distinct clusters $A_1, \dots, A_M$, i. e., if $\bigcup_{i=1,\dots,M} A_i = \{1, \dots, N\}$ and $A_i \cap A_j = \emptyset$ for any two $i \neq j \in \{1, \dots, M\}$, we call $(\phi_1, \dots, \phi_N)$ an *M-cluster state*.

We close this section with some remarks on notation.

Convention 2.4

1. *A tuple $(x_1, \dots, x_n)$ of n elements x_j is denoted by a boldface symbol*

$$\boldsymbol{x} \coloneqq (x_1, \dots, x_n).$$

Vector-valued functions are equally denoted by boldfaced symbols. Further, if a function F acts element-wise on $\boldsymbol{x}$, i. e., if $F : x_j \mapsto F(x_j)$ for all $j = 1, \dots, n$, we write

$$F(\boldsymbol{x}) \coloneqq (F(x_1), \dots, F(x_n))$$

for its diagonal action and will explicitly say so.

2. *For any function $\boldsymbol{F} : \boldsymbol{x} \mapsto \boldsymbol{F}(\boldsymbol{x})$, we denote its partial derivative with respect to the variable x_j as $\mathrm{D}_{x_j}\boldsymbol{F}$ and the total derivative of $\boldsymbol{F}$ at $\boldsymbol{x} = (x_1, \dots, x_n)$ as $\mathrm{D}\boldsymbol{F}(\boldsymbol{x})$ or $\mathrm{D}_{\boldsymbol{x}}\boldsymbol{F}$.*

2.3 THE MODELS

In thesis, we study the dynamics of class I excitable elements with repulsive coupling. For the most part, we focus on systems of N (generalized) Active Rotators under repulsive, sinusoidal, all-to-all, and pairwise coupling. The first model of interest is the classic Shinomoto-Kuramoto model

$$\dot{\phi}_j = \omega - \sin\phi_j + \frac{\kappa}{N}\sum_{k=1}^{N}\sin(\phi_k - \phi_j) \tag{2.5}$$

itself. As already mentioned above, single units are Active Rotators exactly if $|\omega| < 1$ and repulsiveness of the coupling translates to the condition $\kappa < 0$. In what follows, we refer to (2.5) as the "original" or "unperturbed" AR-model. This model, which plays the prominent role in Chapter 6, was studied in the same setup in [ZT16] which was the starting point and main motivation for our investigations. We investigate in Chapter 6 the implications from the highly degenerate dynamics of this model which constitutes a rather nongeneric behavior (in the sense that it relies on the existence of some hidden symmetry that causes the degeneracy). Since the underlying symmetry is in general not present for general class I excitable elements, we consider a second model

$$\begin{aligned} \dot{\phi}_j &= \omega - \sin\phi_j + \epsilon h(\phi_j) + \frac{\kappa}{N}\sum_{k=1}^{N}\sin(\phi_k - \phi_j) \\ h(\phi) &= \sum_{n=2}^{\infty} a_n \sin n\phi + b_n \cos n\phi \end{aligned} \tag{2.6}$$

of general Active Rotators with repulsive sinusoidal coupling, where $\epsilon h(\phi_j)$ accounts for the higher Fourier mode contributions to the on-site dynamics in the general case. We refer to (2.6) as the "generalized" or "perturbed" AR-model. The parameter ϵ serves as a control parameter for the higher order terms. The two models coincide for $\epsilon = 0$ while for small nonzero ϵ, we can treat $\epsilon h(\phi_j)$ as a perturbation to the original on-site dynamics.

Is the Active Rotator model an adequate neuron model?

We stress that the Active Rotator model, both in its classic and its generalized form, is only of limited use for the description of any

kind of actual neurophysiological system, nor was it intended to be by Shinomoto and Kuramoto. (Although they do not give a physical motivation in [SK86b], it seems that their work was inspired by the classic Heisenberg model in a planar setup with all-to-all distance-independent coupling.) The reason for this lies mainly in the sinusoidal coupling term with its limitations for the description of coupled neurons, as we discussed above. It is rather a toy model that can give insight into *possible* ensemble dynamics of general coupled excitable elements just as the Kuramoto model can give insights into possible dynamics for ensembles of self-sustained oscillatory units. The popularity for *both* models arguably comes from the fact that they are of especially simple form and are mathematically tractable rather than from being realistic descriptions of real world phenomena.

No small-scale periodic solutions allowed.

Finally, we note that the dynamics of (2.5) and (2.6) is of gradient type because they belong to the class of models of the form

$$\dot{\phi}_j = f(\phi_j) + \frac{1}{N}\sum_{k=1}^{N} g(\phi_k - \phi_j)$$

with odd coupling function

$$g(\theta) = \sum_{m=0}^{\infty} b_m \sin m\theta.$$

For systems of this type, the equations of motion read $\dot{\phi}_j = -\mathrm{D}_{\phi_j} V(\boldsymbol{\phi})$ with potential

$$V(\boldsymbol{\phi}) \coloneqq -\sum_k \int f(\phi_k)\,\mathrm{d}\phi_k - \frac{1}{2N}\sum_{k,l}\sum_{m=0}^{\infty}\frac{b_m}{m}\cos m(\phi_l - \phi_k).$$

Being of gradient type immediately rules out the existence of small-scale periodic solutions [6], i. e., periodic solutions for which the angles ϕ_j do not traverse the full state space $\mathbb{S}^1$ during a period [GH13]. A direct consequence from the absence of small-scale periodic solutions is that any kind of periodic motion cannot emerge in local bifurcations, say, in a Hopf bifurcation. For $\kappa = 0$, i. e., when (2.5) and (2.6) become decoupled, there exist no periodic solutions whatsoever and it is certainly not obvious that periodic solutions emerge once we introduce coupling. If such a solution exists at all for some $\kappa \neq 0$, it must emerge in a *global* bifurcation, e. g., a SNICs or a homo- or heteroclinic bifurcation, involving (possibly multiple) saddles.

In the next chapter, we introduce the mathematical concepts and tools that will be used in Part II to investigate the classic and the generalized AR-model.

6 Compare for example the swinging of a pendulum, which constitutes a "small-scale" *libration*, with one that rotates around its pivot, which constitutes a "large-scale" *rotation* [Str18].

3

MANIFOLDS, SYMMETRIES, AND AVERAGING

ABSTRACT

In this chapter, we give a brief overview over the four most important mathematical concepts and methods, that our work relies on. We start by discussing Floquet theory in Section 3.1 where in particular, we derive a criterion on asymptotic stability of clustered periodic orbits with respect to perturbations that *split* one or several clusters. We use this concept in Chapter 5 to determine the stability of periodic two-cluster states. In Section 3.2, we discuss the concept of Normally Attracting Invariant Manifolds (NAIMs) for vector fields which generalizes the notions of exponentially stable fixed points and limit cycles. This is used in Chapter 6 to show that for the classic Active Rotator model (2.5), there exists a family of periodic orbits whose union is normally attracting and naturally invariant. One of the main insights from the theory of NAIMs is that such manifolds are *structurally stable*, i. e., they persist for sufficiently small perturbations to the vector field, which we use in Chapter 7 to investigate the generalized AR-model. In Section 3.3, we discuss the notion of *equivariance* of ODEs under the action of finite groups. The main insight from this concept is the robustness of spatio-temporal symmetries for periodic orbits under perturbations to the vector field that leave it equivariant under a given symmetry group. We use this in Chapter 6 and Chapter 7 to show that one of the periodic solutions of (2.5) and (2.6) is a splay state. Finally, in Section 3.4, we state a theorem from averaging theory for periodic orbits. This theorem is used in Chapter 7 to understand the asymptotic dynamics of the generalized model (2.6) by investigating the dynamics on the NAIM of the classic model (2.5).

3.1 FIXED POINTS, FLOQUET THEORY, AND POINCARÉ MAPS

Within the theory of dynamical systems, invariant subsets play an important role. This is due to the fact that the dynamics on these subsets are often simpler and may allow for a lower dimensional description than in the full phase space. Further, under certain conditions, such a subset can be used to describe the *asymptotic* dynamics of the system, i. e., for the cases $t \to \pm\infty$. In what follows, we informally discuss the most important concepts for our work. For a rigorous and detailed overview, we refer to the literature, e. g., [KH97; Wig03; GH13; Kuz13].

For $\mathbb{R}^n$, we may interchangeably call $\boldsymbol{f}$ a function or a vector field. For the general case of ODEs on manifolds, one has to be more careful.

Consider a dynamical system, described by the ODE $\dot{\boldsymbol{x}} = \boldsymbol{f}(\boldsymbol{x})$ where $\boldsymbol{f} : \mathbb{R}^n \to \mathbb{R}^n$ is a sufficiently smooth function. Arguably the simplest invariant subsets of such a system are *fixed points* and *periodic orbits*. A fixed point $\boldsymbol{x}^{\mathrm{f}}$ is defined by the condition $\boldsymbol{f}(\boldsymbol{x}^{\mathrm{f}}) = \boldsymbol{0}$ and describes a steady state of the system, i. e., a solution $\boldsymbol{x}(t) = \boldsymbol{x}^{\mathrm{f}}$ for all $t \in \mathbb{R}$. Concerning small deviations away from this steady state in the initial condition, $\boldsymbol{x}(0) = \boldsymbol{x}^{\mathrm{f}} + \delta\boldsymbol{x}$ for some small $\delta\boldsymbol{x}$, the Hartman-Grobman theorem [Gro59; Har60] states that the dynamics of $\boldsymbol{x}(t)$ can, under certain conditions, be sufficiently approximated around $\boldsymbol{x}^{\mathrm{f}}$ by the linearized equation $\delta\dot{\boldsymbol{x}} = \mathrm{D}\boldsymbol{f}(\boldsymbol{x}^{\mathrm{f}}) \cdot \delta\boldsymbol{x}$ where

$$\mathrm{D}\boldsymbol{f}\left(\boldsymbol{x}^{\mathrm{f}}\right) \coloneqq \left(\mathrm{D}_{x_j} f_i\left(\boldsymbol{x}^{\mathrm{f}}\right)\right)_{i,j=1,\dots,n}$$

is the derivative of $\boldsymbol{f}$ at $\boldsymbol{x}^{\mathrm{f}}$ and f_i denotes the ith component of $\boldsymbol{f}$. In particular, if all eigenvalues of $\mathrm{D}\boldsymbol{f}(\boldsymbol{x}^{\mathrm{f}})$ have strictly negative real parts, $\delta\boldsymbol{x}(t) \to \boldsymbol{0}$ and $\boldsymbol{x}^{\mathrm{f}}$ is called *exponentially* stable. If all eigenvalues have nonzero real parts, $\boldsymbol{x}^{\mathrm{f}}$ is called *hyperbolic*. The key observation for hyperbolic fixed points is that they are robust under small changes in $\boldsymbol{f}$, meaning that they persist if one perturbs $\boldsymbol{f} \mapsto \boldsymbol{f} + \boldsymbol{h}$ where $\boldsymbol{h} : \mathbb{R}^n \to \mathbb{R}^n$ denotes a C^1-small function [Kuz13].

Determining the asymptotic stability of a T-periodic solution $\boldsymbol{x}^{\mathrm{p}}(t)$ with orbit $\mathcal{C}$ for the system $\dot{\boldsymbol{x}} = \boldsymbol{f}(\boldsymbol{x})$, with $\boldsymbol{f} : \mathbb{R}^n \to \mathbb{R}^n$ being sufficiently smooth, is the subject of Floquet theory [Chi99; GH13]. Its core idea is very similar to the linearization of $\boldsymbol{f}$ around a fixed point. Again, one considers a small deviation $\delta\boldsymbol{x}$ from the periodic solution so that one replaces $\boldsymbol{x}^{\mathrm{p}}(t) \mapsto \boldsymbol{x}^{\mathrm{p}}(t) + \delta\boldsymbol{x}(t)$ which yields to linear order the nonautonomous equation

$$\delta\dot{\boldsymbol{x}} = \mathrm{D}\boldsymbol{f}\left(\boldsymbol{x}^{\mathrm{p}}(t)\right) \cdot \delta\boldsymbol{x} \tag{3.1}$$

for $\delta\boldsymbol{x}$ with a now T-periodic matrix $\mathrm{D}\boldsymbol{f}\left(\boldsymbol{x}^{\mathrm{p}}(t)\right)$. For periodic nonautonomous linear ODEs like (3.1), there exists a *fundamental set* of solutions $\{\boldsymbol{y}^j(t)\}_{j=1,\dots,n}$, i. e., a set of n linearly independent solutions $\boldsymbol{y}^j(t)$ of (3.1), with initial conditions $\boldsymbol{y}_j(0) = \boldsymbol{e}_j$ where $\boldsymbol{e}_j \in \mathbb{R}^n$ is the jth canonical basis vector of the $\mathbb{R}^n$. The solutions $\boldsymbol{y}^j$ form a comoving frame of reference along the orbit of $\boldsymbol{x}^{\mathrm{p}}(t)$ and thus serve as a time dependent basis for any perturbation away from $\boldsymbol{x}^{\mathrm{p}}(t)$. Arranging the $\boldsymbol{y}^j(t)$ in a matrix

$$Y(t) \coloneqq \left[\boldsymbol{y}^1(t), \dots, \boldsymbol{y}^n(t)\right],$$

$Y(t)$ and, by T-periodicity, $Y(t+T)$ also solve (3.1) so that by uniqueness of solutions for ODEs and linearity of (3.1), $Y(t+T) = \mathcal{M}_{\mathcal{C}} \cdot Y(t)$ holds for some t-independent matrix

$$\mathcal{M}_{\mathcal{C}} \coloneqq Y(t+T) \cdot Y^{-1}(t),$$

called the *monodromy matrix* of the periodic solution. Assuming that $\mathcal{M}_{\mathcal{C}}$ is diagonalizable,[1] any initial perturbation $\delta\boldsymbol{x}(t_0)$ can uniquely be

1 Here, our argument is not as general as possible since we assume $\mathcal{M}_{\mathcal{C}}$ to be diagonalizable. For a general argument, see [Chi99].

expressed as a linear combination $\delta\boldsymbol{x}(t_0) = \sum_j c_j(t_0)\boldsymbol{v}^j$ of the eigenvectors $\boldsymbol{v}^j$ of $\mathcal{M}_\mathcal{C}$ with corresponding eigenvalues μ^j, called *Floquet multipliers*. The reason for this is the following: After time T, we have

$$\begin{aligned}\delta\boldsymbol{x}(t_0+T) &= \mathcal{M}_\mathcal{C}\cdot\delta\boldsymbol{x}(t_0)\\ &= \sum_{j=1}^{n} c_j(t_0)\mathcal{M}_\mathcal{C}\cdot\boldsymbol{v}^j\\ &= \sum_{j=1}^{n} c_j(t_0)\mu^j\boldsymbol{v}^j\\ &= \sum_{j=1}^{n} c(t_0+T)\boldsymbol{v}^j\end{aligned}$$

and thus, each coordinate $c_j(t_0)$ in direction of $\boldsymbol{v}^j(t_0)$ is multiplied by μ^j after one period T which determines whether this coordinate grows or increases over the course of a period. One of the Floquet multipliers, say μ^1, corresponds to deviations that lie tangent to the periodic orbit such that $\delta\boldsymbol{x}(t_0) = c(t_0)\boldsymbol{v}^1$ is parallel to $\dot{\boldsymbol{x}}^\mathrm{p}(t_0)$. Such a deviation, to linear order, stays some finite distance ahead or behind $\boldsymbol{x}^\mathrm{p}(t)$ along $\mathcal{C}$. In particular, one finds $c(t_0+T)\boldsymbol{v}^1 = c(t_0)\boldsymbol{v}^1$ and thus $\mu^1 = 1$ because the so-perturbed state, following the same periodic orbit, is T-periodic, as well. The multiplier μ^1 is called the *trivial Floquet multiplier*. One sees that if $\delta\boldsymbol{x}(t_0)$ can be expressed in terms of the $\boldsymbol{v}^j$ with $j = 2,\ldots,n$, $|\delta\boldsymbol{x}(t_0) + mT)|$ converges to zero exponentially fast for $m\to\infty$ if and only if all $|\mu^j| < 1$ for $j = 2,\ldots,n$. This leads to the following definition:

Definition 3.1 *A periodic orbit $\mathcal{C}$ of the system $\dot{\boldsymbol{x}} = \boldsymbol{f}(\boldsymbol{x})$ is exponentially stable if and only if all of its nontrivial Floquet multipliers μ^j, $j = 2,\ldots,n$ fulfill $|\mu^j| < 1$.*

If $|\mu^j| < 1$, we call $\boldsymbol{v}^j$ an *exponentially stable* direction, if $|\mu^j| > 1$, we call it *exponentially unstable*. If any nontrivial Floquet multiplier μ^j with $2 \le j \le n$ has absolute value $|\mu^j| = 1$, we call $\boldsymbol{v}^j$ a *neutral direction* of $\boldsymbol{x}^\mathrm{p}(t)$ and the orbit $\mathcal{C}$ *nonhyperbolic*. Otherwise, we call $\mathcal{C}$ *hyperbolic*.

In practice, $\mathcal{M}_\mathcal{C}$ can often only be determined numerically for a given system because of the time-dependence of (3.1). This can be done by implementing a so-called *Poincaré map*. For this, one starts by defining an $(n-1)$-dimensional hypersurface Σ, called *Poincaré section*, that lies transversal to $\mathcal{C}$. Geometrically, this means that at, say $t = 0$, $\boldsymbol{x}^\mathrm{p}(0) =: \boldsymbol{y}^0 \in \Sigma$ while $\dot{\boldsymbol{x}}^\mathrm{p}(0)$ does not lie tangent to Σ.[2] There then exists an open neighborhood $U \subset \Sigma$ of $\boldsymbol{y}^0$, such that for any point $\boldsymbol{y} \in U$, used as an initial state for $\dot{\boldsymbol{x}} = \boldsymbol{f}(\boldsymbol{x})$, the trajectory $\boldsymbol{x}(t)$ with $\boldsymbol{x}(0) = \boldsymbol{y}$ will return to U at $t \approx T$. Hence, this procedure defines a so-called *first return map* or *Poincaré map* $\mathcal{P} : U \to U$ with a fixed point at $\boldsymbol{y}^0 = \boldsymbol{x}^\mathrm{p}(0) = \boldsymbol{x}^\mathrm{p}(T)$. In general, finding periodic orbits of $\dot{\boldsymbol{x}} = \boldsymbol{f}(\boldsymbol{x})$

2 We denote points in the $(n-1)$-dimensional space Σ with the letter $\boldsymbol{y}$ to distinguish them from points $\boldsymbol{x}$ in the n-dimensional phase space $\mathbb{R}^n$. In a slight abuse of notation we consider points in Σ also as points in $\mathbb{R}^n$.

corresponds to finding fixed points of $\mathcal{P}$ for a suitable choice of Σ. Stability of the orbit can be determined from the stability of $\mathcal{P}$. In fact, the eigenvalues of the derivative $\mathrm{D}\mathcal{P}\left(\boldsymbol{y}^0\right)$ are exactly the $n-1$ nontrivial Floquet multipliers of the monodromy matrix as they both describe the linearized dynamics, transversal to $\boldsymbol{x}^{\mathrm{p}}(t)$ over one period [Wig03]. However, just as $\mathcal{M}_{\mathcal{C}}$, the map $\mathcal{P}$, as well as its derivative $\mathrm{D}\mathcal{P}(\boldsymbol{y})$, can usually only be computed numerically. How we implemented this for the case of angular variables $\boldsymbol{\phi} \in \mathbb{T}^N$, is content of the next section.

3.1.1 *Numerical Computation of Floquet Multipliers*

A simple choice for the Poincaré section Σ of a system of angular variables $\boldsymbol{\phi} = (\phi_1, \ldots, \phi_N)$ is to define $\Sigma \coloneqq \left\{\boldsymbol{\phi} \in T^N \,;\, \phi_1 = c\right\}$ with a suitable $c \in [-\pi, +\pi)$ and then integrate the system $\dot{\boldsymbol{\phi}} = f(\boldsymbol{\phi})$ with initial condition $\boldsymbol{\phi}(0) \in \Sigma$ until its trajectory crosses Σ a second time. One has to make sure that this crossing happens only after one full rotation of ϕ_1 around $\mathbb{S}^1$. This can be achieved by assuring that $\dot{\phi}_1$ at the second intersection has the same sign as at $t = 0$. For our purposes, $c = -2$ was a suitable choice for the systems (2.5) and (2.6).

Here, we have $i, j \in \{2, \ldots, N\}$ since $\phi_1 = c$ is always fixed.

To approximate the entry $(\mathrm{D}\mathcal{P}(\boldsymbol{\phi}^0))_{ij} = \mathrm{D}_{\phi_j}\mathcal{P}_i\left(\boldsymbol{\phi}^0\right)$ for the derivative of the Poincaré map $\mathcal{P}$ at the point $\boldsymbol{\phi}^0 = \boldsymbol{\phi}(0) \in \Sigma$ for the orbit of $\boldsymbol{\phi}(t)$, we may consider two initial conditions $\boldsymbol{\phi}^{\pm} \in \Sigma$ where $\phi_k^{\pm} = \phi_k^0$ except for the jth entry $\phi_j^{\pm} = \phi_j^0 \pm \delta\phi$ for some small $\delta\phi > 0$. Then

$$\Big(\mathrm{D}\mathcal{P}(\boldsymbol{\phi}^0)\Big)_{ij} = \frac{\mathcal{P}_i(\boldsymbol{\phi}^+) - \mathcal{P}_i(\boldsymbol{\phi}^-)}{2\,\delta\phi} + \mathcal{O}(\delta\phi^3) \tag{3.2}$$

can be approximated up to cubic order in $\delta\phi$. Floquet multipliers can then be determined by any matrix-diagonalization algorithm. We used this implementation to determine the Floquet multipliers for splay states where this method works well.[3] For periodic two-cluster states however, this numerical procedure can fail if the system is close in parameter space to a limit cycle creating bifurcation, e. g., a double-SNIC, discussed in Chapter 5. The reason for this is the following: Assume that unit j belongs to cluster A with coordinate ϕ_A. Integrating the perturbed states $\boldsymbol{\phi}^{\pm}(t)$ until their next intersection with Σ, the angles $\phi_j^{\pm}(t) = \phi_j(t) \pm \delta\phi(t)$ can come so close to rest of A for some time t', that they cannot be distinguished from ϕ_A within floating point accuracy and thus numerical integration results in $\phi_j^{\pm}(t) = \phi_A^{\pm}(t)$ for all $t > t'$ (since the dynamics of the angles now coincide within finite numerical accuracy). Hence, $\mathcal{P}(\boldsymbol{\phi}^{\pm})$ yields a two-cluster state whereas in the exact dynamics, $\phi_j^{\pm}(T)$ would be distinct from $\phi_A(T)$. This distorts the numerator in (3.2) considerably with the overall effect that we find a numerically estimated value of 0 for one of the Floquet multipliers. Of course, this contradicts the fact that $\mathcal{P}$ must be invertible at $\boldsymbol{\phi}^0$.

To solve this purely computational problem, we make use of the fact that for clustered periodic orbits of a system of identical angular

3 A similar implementation was used for the case of coupled Morris-Lecar neurons, discussed in Chapter 8.

variables, we may directly calculate the Floquet multipliers in a semi-analytical fashion that avoids the problem, described above. This is what we discuss in the next section.

3.1.2 *Splitting Floquet Multipliers for Periodic M-Cluster States*

Deriving analytic expressions for Floquet multipliers is in general not possible. The reason for this is that in order to derive such expressions, one has to solve the ODE $\dot{\boldsymbol{x}} = \boldsymbol{f}(\boldsymbol{x})$ of the dynamical system, first. After that, the nonautonomous ODE for the monodromy matrix would have to be solved, which constitutes the next hurdle to overcome. However, if the system is sufficiently well-behaved, one may compute the multipliers in a semi-analytic fashion. This works as follows: (i) Implement a Poincaré map $\mathcal{P}$ for the system with a suitable numerical integration scheme for ODEs. (We used a fourth-order Runge-Kutta scheme.) (ii) Numerically determine the fixed points of $\mathcal{P}$. (We used the Newton-Raphson algorithm.) (iii) Sample the trajectory of the found periodic orbit in form of a time series $(k\,\Delta t, \boldsymbol{\phi}(k\,\Delta t))$ where Δt denotes the time step between two samples and $k = 1, \ldots, T/\Delta t$. These three steps can usually be achieved without any computational problems. Finally, in step (iv), one integrates certain quantities over the time series, which depend on the eigenvalues of the derivative $\mathrm{D}\boldsymbol{f}$ of the vector field $\boldsymbol{f}$ along the orbit and determines the sought Floquet multipliers from them. One can then compute the Floquet multipliers to arbitrary accuracy by adjusting the time step Δt for the numerical sampling of the periodic orbit. In what follows, we derive how to compute Floquet multipliers with respect to what we call *splitting* and *non-splitting* perturbations in the case of clustered periodic states for ensembles of identical angular variables, which are coupled pairwise, symmetrically, all-to-all, and only via their mutual angular differences. Consequently, we refer to the corresponding multipliers as *splitting* and *non-splitting multipliers*. The exact meaning behind the terms splitting and non-splitting is discussed in the remarks, thereafter.

Splitting and non-splitting perturbations.

Assertion 3.2 *For an ensemble of N identical angular variables $\boldsymbol{\phi} = (\phi_1, \ldots, \phi_N) \in \mathbb{T}^N$, obeying the equation $\dot{\boldsymbol{\phi}} = \boldsymbol{F}(\boldsymbol{\phi})$ with*

$$\dot{\phi}_j = f(\phi_j) + \frac{\kappa}{N} \sum_{l=1}^{N} g(\phi_l - \phi_j) =: F_j(\boldsymbol{\phi}) \tag{3.3}$$

and given a tuple of positive integers $(n_0 < n_1 < n_2 < \cdots < n_M)$ where $n_0 = 0$ and $n_M = N$, let $\boldsymbol{\phi}^{\mathrm{p}}(t)$ be a T-periodic M-cluster solution, such that

$$\phi^{\mathrm{p}}_{n_{k-1}+1}(t) = \cdots = \phi^{\mathrm{p}}_{n_k}(t) =: \phi_{A_k}(t)$$

for $k \in \{1, \ldots, M\}$ and with $\phi_{A_k} \neq \phi_{A_{k'}}$ if $k \neq k'$. We say that the units $n_{k-1} + 1, \ldots, n_k$ belong to cluster A_k which is of size $m_k := n_k - n_{k-1}$. Then, the system has

- *M non-splitting Floquet multipliers μ^k with $k \in \{1, \ldots, M\}$ of multiplicity 1, and*
- *for each $m_k > 1$ an A_k-splitting Floquet multiplier μ^{A_k} of multiplicity $m_k - 1$.*

The multipliers are given by

$$\mu^\alpha = \exp\left(\int_0^T \lambda^\alpha(t)\ \mathrm{d}t\right)$$

where $\lambda^\alpha(t)$ is the corresponding eigenvalue[4] *of the derivative $\mathrm{D}\boldsymbol{F}(\boldsymbol{\phi}^\mathrm{p}(t))$ of $\boldsymbol{F}$ evaluated at the point $\boldsymbol{\phi}^\mathrm{p}(t)$.*

Before we proof the assertion, we make the following remarks to explain what we mean when we speak of splitting and non-splitting perturbations:

Remarks 3.3

1. *A non-splitting perturbation $\delta\boldsymbol{\phi}(t)$ of a periodic M-cluster state $\boldsymbol{\phi}^\mathrm{p}(t)$ is a perturbation that leaves all clusters whole but shifts the position of at least one of them. Hence, if the units i and j belong to cluster A_k, we have $\delta\phi_i(t) = \delta\phi_j(t)$, i. e., they are shifted by the same amount in the same direction.*
2. *An A_k-splitting perturbation $\delta\boldsymbol{\phi}(t)$ of a periodic M-cluster state $\boldsymbol{\phi}^\mathrm{p}(t)$ is a perturbation, for which $\delta\boldsymbol{\phi}_j(t) = 0$ if the unit j does not belong to cluster A_k. Additionally, $\sum_{j=1}^N \delta\phi_j(t) = 0$ holds. This means, that an A_k-splitting perturbations splits the cluster A_k into smaller clusters or single units while the positions of all other clusters stay the same. The condition $\sum_{j=1}^N \delta\phi_j(t) = 0$ intuitively means that the perturbation does not change the "center-of-mass" of A_k.*
3. *The splitting Floquet multipliers μ^{A_k} can have the same value but we consider them anyway as distinct multipliers of multiplicity $m_k - 1$, each.*
4. *Any perturbation $\delta\boldsymbol{\phi}$ can be decomposed into splitting and non-splitting components: First, shift every cluster according to the non-splitting components, then split each cluster according to the splitting components. In particular, stability of $\boldsymbol{\phi}^\mathrm{p}(t)$ with respect to splitting and non-splitting perturbations determines its stability against any perturbation.*
5. *For periodic two-cluster states, we have $M = 2$ and the two clusters $A_1 = A$ and $A_2 = B$. Let each cluster consist of $m_A > 1$ and $m_B > 1$ units. We then have two non-splitting Floquet multipliers μ^1 and μ^2 of multiplicity 1, each, and two splitting Floquet multipliers μ^A and μ^B of multiplicity $m_A - 1$ and $m_B - 1$, respectively.*

4 I. e., of the same splitting or non-splitting type.

Next, we proof the assertion.

Proof. Consider equation (3.3) and assume that a T-periodic M-cluster state $\boldsymbol{\phi}^{\mathrm{p}}(t)$ exists. To determine its asymptotic stability one has to first linearize the system (3.3) around $\boldsymbol{\phi}^{\mathrm{p}}(t)$ which yields

$$\delta\dot{\boldsymbol{\phi}} = \mathrm{D}\boldsymbol{F}\left(\boldsymbol{\phi}^{\mathrm{p}}(t)\right) \cdot \delta\boldsymbol{\phi} \tag{3.4}$$

where the derivative $\mathrm{D}\boldsymbol{F}\left(\boldsymbol{\phi}^{\mathrm{p}}(t)\right)$ is evaluated along the periodic orbit and $\delta\boldsymbol{\phi}(t) = \boldsymbol{\phi}(t) - \boldsymbol{\phi}^{\mathrm{p}}(t)$ is the deviation of a generic perturbed solution $\boldsymbol{\phi}(t)$ from $\boldsymbol{\phi}^{\mathrm{p}}(t)$ with $\|\delta\boldsymbol{\phi}(0)\| \ll 1$. Solving this nonautonomous differential equation over a period T determines the monodromy matrix $\mathcal{M}_{\boldsymbol{\phi}^{\mathrm{p}}(t)}$. For any M-cluster state $\boldsymbol{\phi} \in \mathbb{T}^N$, the derivative $\mathrm{D}\boldsymbol{F}(\boldsymbol{\phi})$ at $\boldsymbol{\phi}$ forms a block matrix

By $\|\cdot\|$ we denote the Euclidean norm in $\mathbb{R}^N$.

For the rest of the proof, the indices $i, j, k \in \{1, \dots, M\}$ are used to index clusters, while indices m and n index matrix entries.

$$\mathrm{D}\boldsymbol{F}(\boldsymbol{\phi}) = \begin{pmatrix} B^{11} & \dots & B^{1M} \\ \vdots & \ddots & \vdots \\ B^{M1} & \dots & B^{MM} \end{pmatrix}$$

where the diagonal blocks B^{ii} are m_i-by-m_i matrices of the form

$$B^{ii}_{mn} = \begin{cases} f'(\phi_{A_i}) - \dfrac{m_i - 1}{N}\kappa g'(0) - \displaystyle\sum_{k\neq i}^{M} \frac{m_k}{N}\kappa g'(\phi_{A_k} - \phi_{A_i}) & \text{if } m = n \\ \dfrac{1}{N}\kappa g'(0) & \text{if } m \neq n \end{cases}$$

and the off-diagonal blocks B^{ij} with $i \neq j$ are m_i-by-m_j matrices with entries

$$B^{ij}_{mn} = \frac{1}{N}\kappa g'(\phi_{A_j} - \phi_{A_i}).$$

$\mathrm{D}\boldsymbol{F}(\boldsymbol{\phi})$ is fully diagonalizable: It has M eigenvalues λ^k of multiplicity 1 and for each j with $m_j > 1$ an eigenvalue λ^{A_j} with multiplicity $m_j - 1$ [Oku93]. The eigenvectors $\boldsymbol{v}^k$, corresponding to λ^k are of the form

$$\boldsymbol{v}^k = (\underbrace{v^k_1, \dots, v^k_1}_{m_1 \text{ times}}, \dots, \underbrace{v^k_j, \dots, v^k_j}_{m_j \text{ times}}, \dots, \underbrace{v^k_M, \dots, v^k_M}_{m_M \text{ times}})^T \tag{3.5}$$

where the v^k_m are mutually distinct. One can see this by inserting $\boldsymbol{v}^k$ in the eigenvalue equation $\left(\mathrm{D}\boldsymbol{F}(\boldsymbol{\phi}) - \lambda^k \,\mathrm{id}_N\right) \cdot \boldsymbol{v}^k = \boldsymbol{0}$, where id_N denotes the N-by-N identity matrix and λ^k is not necessarily explicitly known. The result is a reduced system of M homogeneous linear equations in the λ^k. But $\det\left(\mathrm{D}\boldsymbol{F}(\boldsymbol{\phi}) - \lambda^k \,\mathrm{id}_N\right) = 0$ implies that the coefficient matrix of this reduced system is also singular (its corresponding eigenvalues are exactly the λ^k) and thus it possesses nontrivial solutions in the M entries v^k_m.

The eigenvalues λ^{A_k} are of the form[5]

$$\lambda^{A_k} = f'(\phi^{A_k}) - \kappa \sum_{j=1}^{M} \frac{m_j}{N} g'(\phi^{A_j} - \phi^{A_k})$$

5 Only the λ^{A_k} can be written explicitly, for the λ^k, there exists in general no closed form.

and a basis for their respective eigenspaces is given by $\left\{\boldsymbol{v}_l^{A_k}\,;\,2\le l\le m_k\right\}$ (l indexes the m_k-1 basis vectors and n below indexes the N entries of each basis vector) with entries

$$\left(\boldsymbol{v}_l^{A_k}\right)_n=\begin{cases}+1 & \text{if } n=n_{k-1}+1\\ -1 & \text{if } n=n_{k-1}+l\\ 0 & \text{else}\end{cases} \tag{3.6}$$

as one easily checks. In other words, the basis vectors reflect the situation, where the first unit of cluster A_k (with index $j=n_{k-1}+1$) together with another unit of the same cluster (with index $j=n_{k-1}+l$) are displaced in opposite directions from the rest of cluster A_k. Hence, we end up with $M+\sum_k(m_k-1)=\sum_k^M(n_k-n_{k-1})=N$ linearly independent vectors which then form a basis of the N-dimensional tangential space $\mathbb{R}^N$ at $\boldsymbol{\phi}$ so that $\mathrm{D}\boldsymbol{F}(\boldsymbol{\phi})$ is indeed diagonalizable. Therefore, the linearized system (3.4) yields, in the basis of eigenvectors of $\mathrm{D}\boldsymbol{F}\left(\boldsymbol{\phi}^{\mathrm{p}}(t)\right)$, a set of N decoupled linear homogeneous nonautonomous differential equations of the form

$$\delta\dot{x}^k=\lambda^k(t)\,\delta x^k \tag{3.7a}$$

$$\delta\dot{x}^{A_k}=\lambda^{A_k}(t)\,\delta x^{A_k} \tag{3.7b}$$

where $\lambda^\alpha(t)\coloneqq\lambda^\alpha(\boldsymbol{\phi}^{\mathrm{p}}(t))$ denotes for every $\alpha\in\{1,\dots,M,A_1,\dots,A_M\}$ the respective eigenvalue of $\mathrm{D}\boldsymbol{F}\left(\boldsymbol{\phi}^{\mathrm{p}}(t)\right)$. We can readily write down the solutions for (3.7) at $t=T$ as

$$\delta x^\alpha(T)=\delta x^\alpha(0)\,\exp\left(\int_0^T\lambda^\alpha(t)\,\mathrm{d}t\right).$$

The initial condition for (3.7) specifies the perturbation type for which, from the form of the eigenvectors $\boldsymbol{v}^k$ and $\boldsymbol{v}^{A_k}$, we can distinguish two different scenarios: (i) A perturbation that shifts the positions of the clusters $\{A_k\}$ tangentially to the eigenvector $\boldsymbol{v}^k$ at $\boldsymbol{\phi}^{\mathrm{p}}(0)$ is described by (3.7a). These perturbations are *non-splitting* because they leave the clusters whole at $t=0$ as can be read from (3.5). Since all units are identical, the clusters stay intact for all t which justifies the name. (ii) A perturbation that splits cluster A_k while leaving the "centers-of-mass" $\frac{1}{N}\sum_{i\in A_j}\phi_i$ for each A_j unchanged is described by (3.7b). Any such perturbation lies tangential to some linear combination of the $\boldsymbol{v}_l^{A_k}$ at $\boldsymbol{\phi}^{\mathrm{p}}(0)$ which thus holds true for all t. This, together with the form (3.6) of the $\boldsymbol{v}_l^{A_k}$, justifies the name *splitting* perturbation.

There exists a direct connection between the eigenvalues of $\mathrm{D}\boldsymbol{F}\left(\boldsymbol{\phi}^{\mathrm{p}}(t)\right)$ and the Floquet multipliers of $\boldsymbol{\phi}^{\mathrm{p}}(t)$ because the solutions of (3.7) yield a system of fundamental solutions of (3.4). Constructing the matrix

$$\Phi(t)\coloneqq\Big[\boldsymbol{\phi}^1(t),\dots,\boldsymbol{\phi}^M(t),\underbrace{\boldsymbol{\phi}^{A_1}(t),\dots,\boldsymbol{\phi}^{A_1}(t)}_{m_1-1\text{ columns}},\dots,\underbrace{\boldsymbol{\phi}^{A_M}(t),\dots,\boldsymbol{\phi}^{A_M}(t)}_{m_M-1\text{ columns}}\Big]$$

from this system and diagonalizing with help of the orthogonal basis, spanned by the $\boldsymbol{v}^k$ and $\boldsymbol{v}^{A_k}$, the monodromy matrix $\mathcal{M}_{\boldsymbol{\phi}^{\mathrm{p}}(t)}$ is given by

$$\begin{aligned}\mathcal{M}_{\boldsymbol{\phi}^{\mathrm{p}}(t)} &= \Phi(t+T)\cdot\Phi^{-1}(t)\\ &= \operatorname{diag}\Big(\mu^1,\dots,\mu^M,\underbrace{\mu^{A_1},\dots,\mu^{A_1}}_{m_1-1\text{ entries}},\dots,\underbrace{\mu^{A_M},\dots,\mu^{A_M}}_{m_M-1\text{ entries}}\Big)\end{aligned}$$

with the Floquet multipliers

$$\begin{aligned}\mu^k &\coloneqq \frac{\delta x^k(T)}{\delta x^k(0)} = \exp\left(\int_0^T \lambda^k(t)\,\mathrm{d}t\right)\\ \mu^{A_k} &\coloneqq \frac{\delta x^{A_k}(T)}{\delta x^{A_k}(0)} = \exp\left(\int_0^T \lambda^A(t)\,\mathrm{d}t\right).\end{aligned}$$

Multiplicities of the Floquet multipliers are inherited from the respective multiplicities of the λ^α. This completes the proof. □

In Chapter 5, we will be particularly interested in the splitting stability of periodic two-cluster states. For this, we state the following corollary as a stability criterion for these states:

Corollary 3.4 *For a given T-periodic two-cluster state $\boldsymbol{\phi}^{\mathrm{p}}(t)$ of the system* (3.3)*, let $p = m_A/N$ and $(1-p) = m_B/N$ denote the proportions of units in cluster A and B, respectively. Then, the Floquet multipliers for splitting perturbations of both clusters are given by*

$$\begin{aligned}\mu^A &= \exp\left(\int_0^T \lambda^A(t)\,\mathrm{d}t\right)\\ \mu^B &= \exp\left(\int_0^T \lambda^B(t)\,\mathrm{d}t\right)\end{aligned}\tag{3.8}$$

with

$$\begin{aligned}\lambda^A(t) &= f'(\phi_A^{\mathrm{p}}) - \kappa\, p\, g'(0) - \kappa(1-p)\, g'(\phi_B^{\mathrm{p}} - \phi_A^{\mathrm{p}})\\ \lambda^B(t) &= f'(\phi_B^{\mathrm{p}}) - \kappa(1-p)\, g'(0) - \kappa\, p\, g'(\phi_A^{\mathrm{p}} - \phi_B^{\mathrm{p}}),\end{aligned}$$

evaluated along the periodic orbit of $(\underbrace{\phi_A^{\mathrm{p}}(t),\dots,\phi_A^{\mathrm{p}}(t)}_{m_A\ \text{times}},\underbrace{\phi_B^{\mathrm{p}}(t),\dots,\phi_B^{\mathrm{p}}(t)}_{m_B\ \text{times}})^T$.

With this, we end our discussion of stability for periodic orbits. Next we discuss the notion of normally attracting invariant manifolds, which are generalizations of exponentially stable fixed points and periodic orbits.

3.2 NORMALLY ATTRACTING INVARIANT MANIFOLDS

Hyperbolic fixed points and exponentially (un)stable periodic orbits for systems of the type $\dot{\boldsymbol{x}} = \boldsymbol{f}(\boldsymbol{x})$ share one remarkable property: they are persistent under small perturbations of the vector field $\boldsymbol{f}$ [Chi99; Kuz13]. However, the involved calculations and arguments to show

this are relatively simple due to the simple geometry of points and closed curves and cannot easily be generalized to higher-dimensional manifolds. If one is interested in higher-dimensional invariant sets and their stability and persistence, the considerations become much more involved. A natural generalization of hyperbolic fixed points and periodic orbits is that of the Normally Hyperbolic Invariant Manifold (NHIM), introduced by Fenichel in 1971 [FM71; Fen74; Fen77]. In this context, hyperbolic fixed points and periodic orbits are examples for zero- and one-dimensional NHIMs. In particular, Fenichel showed that compact NHIMs are generally persistent under small perturbations of the vector field $\boldsymbol{f}$. The converse is also true, as was shown by Mañé in [Mañ78]: Persistent invariant manifolds must be normally hyperbolic.

This section is structured as follows: First, we discuss the main concepts of the theory of normally hyperbolic invariant manifolds, following mainly [Wig94; HPS77; Eld13]. Hereby, we focus on the special case of Normally Attracting Invariant Manifolds (NAIMs) which are not just hyperbolic but also *exponentially stable* and therefore serve as a generalization of stable fixed points and limit cycles. For brevity, we only give an informal definition for manifolds and their tangent and normal bundles. For a rigorous definition, we refer to [HPS77].

With C^k, we denote the set of k-times continuously differentiable functions.

For our purposes, it is sufficient to consider manifolds as subsets of some $\mathbb{R}^n$. Informally speaking, an m-dimensional C^k-submanifold of the $\mathbb{R}^n$ is then a subset $\mathcal{M} \subset \mathbb{R}^n$ that "looks" locally around any point $\boldsymbol{x} \in \mathcal{M}$ like the $\mathbb{R}^m$ where the map between the neighborhood of $\boldsymbol{x}$ and $\mathbb{R}^m$ is a C^k-diffeomorphism. For each point $\boldsymbol{x} \in \mathcal{M}$, one can define the *tangent space* $T_{\boldsymbol{x}}\mathcal{M}$ as the set of all vectors $\boldsymbol{v} \in T_{\boldsymbol{x}}\mathbb{R}^n \cong \mathbb{R}^n$ with basis point at $\boldsymbol{x}$ that lie tangent to $\mathcal{M}$. Subsequently, one can define for every $\boldsymbol{x} \in \mathcal{M}$ a *normal space* $\mathcal{N}_{\boldsymbol{x}}$ as the span of a set of vectors $\boldsymbol{v}_1, \dots, \boldsymbol{v}_k \in T_{\boldsymbol{x}}\mathbb{R}^n$ which do not lie tangent to $\mathcal{M}$ at $\boldsymbol{x}$, i. e., $\boldsymbol{v}_j \notin T_{\boldsymbol{x}}\mathcal{M}$ for all $j = 1, \dots, k$.[6] Following the notation in [Eld13], the *tangent bundle* $T\mathcal{M}$ and *normal bundle* $\mathcal{N}$ are then defined as

$$T\mathcal{M} \coloneqq \{(\boldsymbol{x}, \boldsymbol{v}) \in \mathcal{M} \times \mathbb{R}^n \,;\, \boldsymbol{v} \in T_{\boldsymbol{x}}\mathcal{M}\}$$
$$\mathcal{N} \coloneqq \{(\boldsymbol{x}, \boldsymbol{v}) \in \mathcal{M} \times \mathbb{R}^n \,;\, \boldsymbol{v} \in \mathcal{N}_{\boldsymbol{x}}\}\,.$$

With this, we are ready to give a definition for normally attracting invariant submanifolds. Recall that the flow Φ of the ODE $\dot{\boldsymbol{x}} = \boldsymbol{f}(\boldsymbol{x})$ maps every pair $(\boldsymbol{x}^0, t)$ to the solution[7] $\Phi(\boldsymbol{x}^0, t) \coloneqq \boldsymbol{x}(t)$ of the ODE with initial condition $\boldsymbol{x}(0) = \boldsymbol{x}^0$.

Definition 3.5 (Normally attracting invariant manifold) *Let $k \geq 1$ and $\dot{\boldsymbol{x}} = \boldsymbol{f}(\boldsymbol{x})$ with $\boldsymbol{x} \in \mathbb{R}^n$ and $\boldsymbol{f} \in C^k$ be a dynamical system with flow $\Phi : \mathbb{R}^n \times \mathbb{R} \to \mathbb{R}^n$. A given C^k-submanifold $\mathcal{M} \subset \mathbb{R}^n$ is then*

6 The choice of name for this space is slightly confusing since usually, the normal space at $\boldsymbol{x}$ is defined as the space of all vectors that lie perpendicular to $\mathcal{M}$ at $\boldsymbol{x}$. However, in the literature on NAIMs, one speaks of normal spaces and bundles, anyway, even when their elements are not normal in the usual sense. The only condition is that $T_{\boldsymbol{x}}\mathcal{M}$ and the normal space (or normal spaces) together span the full $T_{\boldsymbol{x}}\mathbb{R}^n$, i. e., they are complementary to each other [Eld].

7 If that solution is defined for t.

called a k-normally attracting invariant manifold of $\boldsymbol{f}$ if it fulfills the following three criteria:

(i) $\mathcal{M}$ *is invariant under the flow, i. e.,* $\Phi(\mathcal{M}, t) = \mathcal{M}\ \forall t \in \mathbb{R}$.

(ii) There exists a continuous splitting

$$T_{\mathcal{M}}\mathbb{R}^n = T\mathcal{M} \oplus \mathcal{N}$$

of the tangent bundle $T\mathbb{R}^n$, restricted to $\mathcal{M}$, into the tangent bundle $T\mathcal{M}$ of $\mathcal{M}$ and a normal bundle $\mathcal{N}$ with continuous projections $\pi_{\mathcal{M}}$ and $\pi_{\mathcal{N}}$. Further, this splitting is invariant under the linearized flow $\mathrm{D}\Phi^t = \mathrm{D}\Phi^t_{\mathcal{M}} \oplus \mathrm{D}\Phi^t_{\mathcal{N}}$ where $\Phi^t(\boldsymbol{x}) \coloneqq \Phi(\boldsymbol{x}, t)$.

(iii) There exist real numbers a and b with $a < k\,b \leq 0$, and $C > 0$ such that the following exponential growth conditions hold on $T_{\mathcal{M}}\mathbb{R}^n$:

$$\begin{aligned} \forall t \leq 0, (\boldsymbol{x}, \boldsymbol{\nu}) \in T\mathcal{M}: &\qquad \left\| \mathrm{D}\Phi^t_{\mathcal{M}}(\boldsymbol{x}) \cdot \boldsymbol{\nu} \right\| \leq C\,\mathrm{e}^{bt}\,\|\boldsymbol{\nu}\| \\ \forall t \geq 0, (\boldsymbol{x}, \boldsymbol{\nu}) \in \mathcal{N}: &\qquad \left\| \mathrm{D}\Phi^t_{\mathcal{N}}(\boldsymbol{x}) \cdot \boldsymbol{\nu} \right\| \leq C\,\mathrm{e}^{at}\,\|\boldsymbol{\nu}\|\,. \end{aligned}$$

Remarks 3.6

1. *Condition (i) means that for every initial condition $\boldsymbol{x}^0 \in \mathcal{M}$ of $\dot{\boldsymbol{x}} = \boldsymbol{f}(\boldsymbol{x})$, the solution $\boldsymbol{x}(t)$ stays in $\mathcal{M}$ for all t.*

2. *The continuous splitting in condition (ii) means that for every $\boldsymbol{x} \in \mathcal{M}$, one can choose a base of $T_{\boldsymbol{x}}\mathcal{M}$ and of $\mathcal{N}_{\boldsymbol{x}}$, respectively, such that the basis vectors vary continuously with $\boldsymbol{x}$ over $\mathcal{M}$ and together always span the full $\mathbb{R}^n$. This may be thought of as a generalization of the fundamental system for periodic orbits as a comoving frame of reference from the previous section. The respective projections $\pi_{\mathcal{M}}$ and $\pi_{\mathcal{N}}$ yield the tangential and normal components for every vector $\boldsymbol{v} \in T_{\boldsymbol{x}}\mathbb{R}^n$.*

3. *The invariance of the splitting under the linearized flow means that any deviation away from a point $\boldsymbol{x} \in \mathcal{M}$ in tangential or normal[8] direction to $\mathcal{M}$ stays tangent or normal, respectively, up to linear order under the flow Φ. In other words, the evolution of the perturbation can be uniquely decomposed into its tangent and normal component and these components decouple. This is akin to the observation that perturbations that lie tangent to a periodic orbit stay on that periodic orbit to linear order while perturbations normal to the orbit stay normal as one checks with help of the fundamental system, discussed in the previous section.*

4. *The rate conditions (iii) generalize the concept of Floquet multipliers for periodic orbits. Particularly, e^{bT}, corresponds to the tangential multiplier μ^1 while e^{aT} corresponds to the nontrivial multipliers μ^j, $j = 2, \ldots, n$. The main difference is that the tangential multipliers are not necessarily trivial anymore, i. e., perturbations may expand or contract exponentially in tangential direction.*

8 In the general sense, see the footnote on the previous page.

5. *Intuitively speaking, the rate conditions state that any deviation from $\mathcal{M}$ decays exponentially* faster *in normal direction to $\mathcal{M}$ than it expands in tangential direction. In particular, if $\mathcal{M}$ is a periodic orbit, the tangential expansion rate is zero, i. e., $b = 0$.*

As already mentioned above, NAIMs have the remarkable property of being persistent under small perturbations of the vector field $\boldsymbol{f}$. This is the made rigorous with the following theorem, cf. Theorem. 1 of [FM71] or Theorem. 4.1 in [HPS77]:

Theorem 3.7 (Persistence of NAIMs) *Let $\mathcal{M} \subset \mathbb{R}^n$ be a compact k-normally attracting invariant manifold of the system $\dot{\boldsymbol{x}} = \boldsymbol{f}(\boldsymbol{x})$. Then, there exists an $\epsilon > 0$ such that for every vector field $\tilde{\boldsymbol{f}}$ with $\left\|\tilde{\boldsymbol{f}} - \boldsymbol{f}\right\|_{C^1} \leq \epsilon$, there exists a unique invariant C^k-manifold $\tilde{\mathcal{M}}$ for $\tilde{\boldsymbol{f}}$ which is diffeomorphic to $\mathcal{M}$, normally attracting, and $\mathcal{O}\left(\left\|\tilde{\boldsymbol{f}} - \boldsymbol{f}\right\|_{C^1}\right)$-close to $\mathcal{M}$.*

Throughout this work, we use Landau's big-$\mathcal{O}$ notation for order functions, i. e., $f(\epsilon) = \mathcal{O}(g(\epsilon))$ means that there exist constants $K \geq 0$ and $\epsilon_0 \geq 0$ such that $0 \leq |f(\epsilon)| \leq K\,|g(\epsilon)|$ for all $0 \leq \epsilon \leq \epsilon_0$.

In principle, there are different choices to define the C^1-norm $\|\boldsymbol{f}\|_{C^1}$ of a differentiable function $\boldsymbol{f} : \mathbb{R}^n \to \mathbb{R}^n$ which are, in our context of finite-dimensional spaces, all equivalent [Wer06]. Here, we use

$$\|\boldsymbol{f}\|_{C^1} \coloneqq \sup_{\boldsymbol{x}\in\mathbb{R}^n} \|\boldsymbol{f}(\boldsymbol{x})\| + \sup_{\boldsymbol{x}\in\mathbb{R}^n} \sup_{\|\boldsymbol{v}\|=1} \|\mathrm{D}\boldsymbol{f}(\boldsymbol{x}) \cdot \boldsymbol{v}\|$$

where $\|\boldsymbol{v}\| \coloneqq \sqrt{\sum_{i=1}^n v_i^2}$ is the Euclidean norm of the vector $\boldsymbol{v} \in \mathbb{R}^n$. Hence, if $\|\boldsymbol{f}\|_{C^1} \leq \epsilon$, not only is $\boldsymbol{f}$ small, i. e., $\|\boldsymbol{f}(\boldsymbol{x})\| < \epsilon$ for all $\boldsymbol{x}$ but also the derivative $\mathrm{D}\boldsymbol{f}$ is small, meaning that for every $\boldsymbol{x} \in \mathbb{R}^n$ and every unit vector $\boldsymbol{v} \in \mathbb{R}^n$, the norm $\|\mathrm{D}\boldsymbol{f}(\boldsymbol{x}) \cdot \boldsymbol{v}\|$ of the image $\mathrm{D}\boldsymbol{f}(\boldsymbol{x}) \cdot \boldsymbol{v}$ of $\boldsymbol{v}$ under the linear map $\mathrm{D}\boldsymbol{f}(\boldsymbol{x})$ is smaller than ϵ.

A remark is at hand, regarding the scope of Theorem 3.7.

Remark 3.8 *Theorem 3.7 generally holds as long as the manifold $\mathcal{M}$ has no boundary $\partial\mathcal{M}$ or if the vector field on $\partial\mathcal{M}$ is strictly pointing outward in which case one speaks of* "overflowing invariance" *[FM71]. In this thesis, we deal with manifolds that have a boundary and are generally not overflowing invariant. However, this problem can be circumvented by modifying the vector field in a small neighborhood around the boundary so that the new vector field is overflowing on $\partial\mathcal{M}$ and coincides with the original vector field outside that neighborhood. In particular, all results for the NAIM of the modified vector field also hold for our $\mathcal{M}$, sufficiently far away from $\partial\mathcal{M}$ [Eld+21].*

With this, we conclude our discussion of NAIMs. In the next section, we discuss spatio-temporal symmetries, which play an important role in the description of so-called splay states.

3.3 SPATIO-TEMPORAL SYMMETRIES

Lie theory, named after Sophus Lie, is concerned with symmetries of vector fields under the action of continuous transformation groups and the resulting symmetries of solutions of ODEs [Olv00; Can02]. While

the central objects in Lie theory, known as *Lie groups*, are themselves manifolds and therefore generally of infinite order, finite transformation groups can also give rise to certain so-called *spatio-temporal symmetries* for solutions of ODEs [Gol+98; BG01]. Following Golubitsky and Stewart [GS00], we briefly outline the concept of equivariance under discrete symmetry groups. We use this in Chapter 6 and Chapter 7 to show that for sufficiently large ensemble size N and sufficiently repulsive coupling strength κ, both the original system (2.5) and the perturbed system (2.6) of identical ARs give rise to so-called splay states which are periodic solutions with a specific type of spatio-temporal symmetry.

Note that a (finite) group $(\Gamma, \circ)$ consists of a set $\Gamma = \{\gamma_i \,;\, i \in I\}$ with some (finite) index set I (in what follows, we drop the index i for simplicity if no ambiguity is created by this), together with a binary operation $\circ : \Gamma \times \Gamma \to \Gamma$, such that the following three conditions hold:

(i) There exists an *identity element* $e \in \Gamma$ such that $e \circ \gamma = \gamma \circ e = \gamma$ for all $\gamma \in \Gamma$.

(ii) For each $\gamma \in \Gamma$, there exists an *inverse element*, denoted $\gamma^{-1} \in \Gamma$, such that $\gamma \circ \gamma^{-1} = \gamma^{-1} \circ \gamma = e$.

(iii) For every three elements γ_1, γ_2, and γ_3 of Γ, the binary operation is associative, i. e., $\gamma_1 \circ (\gamma_2 \circ \gamma_3) = (\gamma_1 \circ \gamma_2) \circ \gamma_3$.

If no ambiguity is created, we simply write Γ instead of $(\Gamma, \circ)$ for the group. We say that Γ is *acting (from the left)* on the vector space $\mathbb{R}^n$ if there exists a map $\Gamma \times \mathbb{R}^n \ni (\gamma, \boldsymbol{x}) \mapsto \gamma\boldsymbol{x} \in \mathbb{R}^n$ that is linear in $\boldsymbol{x}$, i. e., for every $\gamma \in \Gamma$, all $\boldsymbol{x}, \boldsymbol{y} \in \mathbb{R}^n$, and all $a, b \in \mathbb{R}$, we have $\gamma(a\boldsymbol{x} + b\boldsymbol{y}) = a\gamma\boldsymbol{x} + b\gamma\boldsymbol{y}$. Hence, Γ can be seen as a group of linear transformations $\gamma : \mathbb{R}^n \to \mathbb{R}^n$, where any two transformations γ_1 and γ_2 map any point $\boldsymbol{x} \in \mathbb{R}^n$ to the point $\gamma_1(\gamma_2\boldsymbol{x}) = (\gamma_1 \circ \gamma_2)\boldsymbol{x}$ so that compositions of transformations obey the group properties of Γ. Note that this notion of group action can be generalized to general manifolds.

The main concept of this section is that of *equivariance* of vector fields and autonomous ODEs under finite group actions:

Definition 3.9 *Let Γ be a finite group, acting on $\mathbb{R}^n$ and consider the ODE $\dot{\boldsymbol{x}} = \boldsymbol{f}(\boldsymbol{x})$ with smooth vector field $\boldsymbol{f}$. Then, $\boldsymbol{f}$ is equivariant under Γ if for every $\gamma \in \Gamma$ and every $\boldsymbol{x} \in \mathbb{R}^n$, $\boldsymbol{f}(\gamma\boldsymbol{x}) = \gamma\boldsymbol{f}(\boldsymbol{x})$ holds. In this case, we also call $\dot{\boldsymbol{x}} = \boldsymbol{f}(\boldsymbol{x})$ equivariant under Γ.*

Intuitively speaking, if the vector field $\boldsymbol{f}$ or the corresponding ODE is equivariant under Γ, the transformations γ do not change the resulting dynamics qualitatively. The equations "look the same" under such transformations, because $\mathrm{d}(\gamma\boldsymbol{x})/\mathrm{d}t = \gamma\dot{\boldsymbol{x}} = \gamma\boldsymbol{f}(\boldsymbol{x}) = \boldsymbol{f}(\gamma\boldsymbol{x})$. For example, permuting the N identical units in (2.5) or (2.6) does not change qualitatively the dynamics of the ensemble, it results in a mere relabeling of units. In this case, we refer to Γ as a (finite) *symmetry group* of the equation $\dot{\boldsymbol{x}} = \boldsymbol{f}(\boldsymbol{x})$

Periodic solutions of ODEs give rise to the following two subgroups of Γ, cf. [GS00]:

Definition 3.10 *Let $\dot{\boldsymbol{x}} = \boldsymbol{f}(\boldsymbol{x})$ be equivariant under the finite group Γ and let $\boldsymbol{x}^{\mathrm{p}}(t)$ denote a T-periodic solution of this equation with periodic orbit $\mathcal{C} \coloneqq \{\boldsymbol{x}^{\mathrm{p}}(t)\,;\, t \in \mathbb{R}\} \subset \mathbb{R}^n$. Then, the two subgroups*

$$K \coloneqq \{\gamma \in \Gamma\,;\, \gamma\,\boldsymbol{x}^{\mathrm{p}}(t) = \boldsymbol{x}^{\mathrm{p}}(t)\ \forall t\}$$
$$H \coloneqq \{\gamma \in \Gamma\,;\, \gamma\,\mathcal{C} = \mathcal{C}\}$$

of Γ are called the group of spatial symmetries *and the* group of spatio-temporal symmetries[9] *of $\boldsymbol{x}^{\mathrm{p}}(t)$, respectively. Here, we write $\gamma\,\mathcal{C} \coloneqq \{\gamma\,\boldsymbol{x}^{\mathrm{p}}(t)\,;\, t \in \mathbb{R}\}$.*

The meaning behind the names for K and H is clear: each element of K leaves every point of the periodic orbit invariant while each element of H maps every point of the orbit to some other point on it.

For every $\gamma \in H$, there exists a unique $\tau \in [0, T)$ such that $\gamma\boldsymbol{x}^{\mathrm{p}}(t) = \boldsymbol{x}^{\mathrm{p}}(t-\tau)$ or equivalently $\gamma\boldsymbol{x}^{\mathrm{p}}(t+\tau) = \boldsymbol{x}^{\mathrm{p}}(t)$ for every $t \in \mathbb{R}$. To see this, note that we must have $\gamma\boldsymbol{x}^{\mathrm{p}}(t_0+\tau) = \boldsymbol{x}^{\mathrm{p}}(t_0)$ for some $t_0 \in [0, T)$ by definition of H. But since both $\gamma\boldsymbol{x}^{\mathrm{p}}(t+\tau)$ and $\boldsymbol{x}^{\mathrm{p}}(t)$ solve $\dot{\boldsymbol{x}} = \boldsymbol{f}(\boldsymbol{x})$ and coincide at $t = t_0$, uniqueness of solutions for ODEs guarantees that they coincide for all t . We say that $\boldsymbol{x}^{\mathrm{p}}(t)$ is equipped with a spatial symmetry, given by K, and a spatio-temporal symmetry, given by H.

The main statements for our purposes are given in the following theorem and corollary, due to Buono and Golubitsky [BG01]:

Theorem 3.11 *Let Γ be a finite group, acting on $\mathbb{R}^n$ and $\dot{\boldsymbol{x}} = \boldsymbol{f}(\boldsymbol{x})$ a Γ-equivariant ODE with smooth $\boldsymbol{f}$. Further, let $\boldsymbol{x}(t)$ be a T-periodic solution of the system with spatial symmetry group K and spatio-temporal symmetry group H. Further, let $N(K)$ denote the normalizer of K. Then,*

The normalizer of a subgroup G of the group Γ is the subgroup $N(G) \coloneqq \{\gamma \in \Gamma\,;\, \gamma G = G\gamma\}$ where $\gamma G = G\gamma$ means that for every $g \in G$, we have $\gamma \circ g \circ \gamma^{-1} \in G$ [Car37].

$$\eta\boldsymbol{x}\left(t + \frac{T}{m}\right) = \boldsymbol{x}(t)$$

for some fixed $\eta \in N(K)$ and fixed $m \in \mathbb{N}$ if and only if the following four conditions are fulfilled:

(a) $H/K \cong \mathbb{Z}_m$ is cyclic, $m \geq 2$, and $\eta \in H$ projects onto a generator of H/K,

(b) there exists an $\boldsymbol{x}_0 \in \mathbb{R}^n$ such that $\boldsymbol{x}_0$ is invariant under K, i.e., $K\boldsymbol{x}_0 = \boldsymbol{x}_0$,

$\dim \mathrm{Fix}(K)$ *denotes the dimension of the vector space* $\mathrm{Fix}(K)$.

(c) $\dim \mathrm{Fix}(K) \geq 2$, where $\mathrm{Fix}(K) \coloneqq \{\boldsymbol{x} \in \mathbb{R}^n\,;\, K\boldsymbol{x} = \boldsymbol{x}\}$ is the subspace of fixed points of K. If $\dim \mathrm{Fix}(K) = 2$, then $H = N(K)$ and η acts on $\mathrm{Fix}(K)$ by rotation through $\pm\frac{2\pi}{m}$,

(d) H fixes a connected component of $\mathrm{Fix}(K)\backslash L_K$, where

$$L_K \coloneqq \bigcup_{\gamma \notin K} \mathrm{Fix}(\gamma) \cap \mathrm{Fix}(K).$$

9 Actually, the group of spatio-temporal symmetries in [GS00] is defined slightly differently but, as is shown there, the actual group of spatio-temporal symmetries and H are isomorphic.

The details of this theorem are not really important for us. What is more important is that from it, the following corollary follows, which guarantees that exponentially stable periodic orbits are not only persistent under C^1-small perturbations $\boldsymbol{h}$ of the vector field $\boldsymbol{f}$ but also that their spatial and spatio-temporal symmetries persist if $\boldsymbol{h}$ is equally equivariant under Γ as $\boldsymbol{f}$:

Corollary 3.12 *Let the groups K and H satisfy conditions (a)-(d) of Theorem 3.11. Then, exponentially stable periodic solutions with spatial symmetry group K and spatio-temporal symmetry group H are robust in Γ-equivariant systems of ODEs on $\mathbb{R}^n$.*

3.4 AVERAGING THEORY

Averaging theory is a powerful tool for handling systems in which timescale separations occur between fast oscillating variables and slow varying ones [SVM07; Chi99]. We employ averaging theory in Chapter 7 to determine the dynamics of the perturbed system (2.6) in terms of the degenerate dynamics of the original system (2.5). This approach relies on the following theorem, cf. Theorems 7.9 in [Chi99] and Theorem 6.3.2 and 6.3.3 in [SVM07]:

Theorem 3.13 *Consider any system of the form*

$$\begin{aligned} \dot{\boldsymbol{x}} &= \epsilon \boldsymbol{F}(\boldsymbol{x}, \psi) + \epsilon^2 \boldsymbol{F}_2(\boldsymbol{x}, \psi, \epsilon) \\ \dot{\psi} &= \Omega(\boldsymbol{x}) + \epsilon\, G(\boldsymbol{x}, \psi, \epsilon) \end{aligned} \tag{3.9}$$

where $\boldsymbol{x} \in \mathbb{R}^n$ and $\psi \in \mathbb{S}^1$ and assume that there exists a $c > 0$ such that $\Omega(\boldsymbol{x}) > c$ for all $\boldsymbol{x} \in \mathbb{R}^n$. If the averaged system

$$\dot{\boldsymbol{y}} = \epsilon \hat{\boldsymbol{F}}(\boldsymbol{y})$$

with

$$\hat{\boldsymbol{F}}(\boldsymbol{y}) \coloneqq \frac{1}{2\pi} \int_0^{2\pi} \boldsymbol{F}(\boldsymbol{y}, \psi)\, \mathrm{d}\psi$$

possesses a hyperbolic fixed point $\boldsymbol{y}^{\mathrm{f}} \in \mathbb{R}^n$ and $\epsilon > 0$ is sufficiently small, (3.9) possesses a periodic solution $(\boldsymbol{x}^{\mathrm{p}}(t), \psi(t))$ whose orbit is of the same stability type as $\boldsymbol{y}^{\mathrm{f}}$ and $\left\| \boldsymbol{x}^{\mathrm{p}}(t) - \boldsymbol{y}^{\mathrm{f}} \right\| = \mathcal{O}(\epsilon)$ holds for all t.

Remarks 3.14

1. *The periodic orbit having the same stability type as $\boldsymbol{y}^{\mathrm{f}}$ means that the dimensions of the stable and unstable manifolds of $\boldsymbol{y}^{\mathrm{f}}$ and the periodic orbit of $(\boldsymbol{x}^{\mathrm{p}}(t), \psi(t))$ coincide.*

2. *For $\epsilon < 0$, the stable and unstable manifold of the periodic orbit switch: The dimension of the orbit's stable manifold equals the dimension of the unstable manifold of $\boldsymbol{y}^{\mathrm{f}}$ and the dimension of its unstable manifold is equals that of the stable manifold of $\boldsymbol{y}^{\mathrm{f}}$.*

3. *Since for small* $|\epsilon|$, $\boldsymbol{x}^{\mathrm{p}}(t)$ *stays close to* $\boldsymbol{y}^{\mathrm{p}}$, *we can weaken the condition on* Ω *to* $\Omega(\boldsymbol{y}) > c > 0$ *for all* $\boldsymbol{y} \in V$ *in some (possibly small) open neighborhood* V *of* $\boldsymbol{y}^{\mathrm{f}}$.

Theorem 3.13 states that if the dynamics of $\boldsymbol{x}$ is slow in comparison to that of ψ, we can "average out" the fast oscillations of $\psi(t)$ in the first equation of (3.9) and still recover a good approximation for the dynamics in $\boldsymbol{x}$. In the context of Watanabe-Strogatz theory, we will make use of averaging techniques to investigate the existence and stability of periodic orbits in the perturbed system (2.6) by averaging the perturbation function $\boldsymbol{h}$ over periodic solutions of the original model (2.5). Watanabe-Strogatz theory is the content of the next chapter.

4

WATANABE-STROGATZ INTEGRABILITY

ABSTRACT

In this chapter, we outline the main concepts of Watanabe-Strogatz (WS) theory on which our work relies to a large extend. We start by discussing the group of Möbius transformations and its action on $\mathbb{T}^N$ in Section 4.1. Möbius transformations constitute the fundamental geometric objects of WS-theory and are used to determine the dynamics for ensembles of angular variables in terms of the group parameters of the Möbius group. We further discuss the so-called cross-ratios, which are generally invariant under any Möbius transformation. We then show that the group parameters and cross-ratios can be employed as a suitable alternative coordinate system to the angular variables $(\phi_1, \dots, \phi_N)$ on the subspace of ordered tuples in $\mathbb{T}^N$. In Section 4.2, we recall the fundamental theorem of WS-theory which states that for a fairly general class of angular models, the ensemble dynamics can be fully described by a set of just three coupled ODEs. This (partial) integrability yields a low-dimensional description for these models and, in particular, for the system (2.5). Finally, in Section 4.3, we discuss how the alternative coordinate system from Section 4.1 can be used to describe the dynamics of general ensembles of identical angular variables which allows to generalize the formalism of WS-theory to such systems.

The concepts, discussed here, form the foundation in the derivation of the results of Chapter 6 and 7 but WS-integrability also plays an important role in Chapter 5 for the understanding of stability of periodic two-cluster states. Since WS-theory only yields nontrivial results for ensembles that contain at least four distinct units, in this chapter, we always assume $N \geq 4$. Some passages and in particular the propositions and proofs in Section 4.1 are verbatim quotes from [RZP].

4.1 WATANABE-STROGATZ VARIABLES

MÖBIUS TRANSFORMATIONS Watanabe and Strogatz were the first to show that systems of N identical angular variables $(\phi_1, \dots, \phi_N) =: \boldsymbol{\phi}$, obeying

$$\dot{\phi}_j = f(\boldsymbol{\phi})\mathrm{e}^{i\phi_j} + g(\boldsymbol{\phi}) + \bar{f}(\boldsymbol{\phi})\mathrm{e}^{-i\phi_j} \tag{4.1}$$

with common fields $f : \mathbb{T}^N \to \mathbb{C}$ and $g : \mathbb{T}^N \to \mathbb{R}$, can be described by just three coupled ODEs such that these systems become (partially)

The functions f and g denote general functions of $\boldsymbol{\phi}$ and do not necessarily act element wise.

integrable. However, their derivation was rather complicated and did not make immediately clear what the underlying reason for this fact was. Fifteen years later, Marvel, Mirollo, and Strogatz gave a simple geometric proof of the same theorem which relies on Lie theory, applied to the group of Möbius transformations [MMS09]. This revealed that Möbius transformations are the fundamental geometric objects of WS-theory.

The *general* Möbius group is the set of holomorphic automorphisms[1] of the extended complex plane $\hat{\mathbb{C}} \coloneqq \mathbb{C} \cup \{\infty\}$, cf. [Ahl79]. They are exactly those functions $\mu : \hat{\mathbb{C}} \to \hat{\mathbb{C}}$ of the form

$$\mu(z) \coloneqq \frac{az+b}{cz+d}$$

with complex coefficients a, b, c, d for which $ad - bc \neq 0$ holds[2] and we set $\mu(\infty) \coloneqq a/c$ and $\mu(-d/c) = \infty$. Geometrically, Möbius transformations are those maps under which all circles and lines in the complex plane are mapped onto circles and lines.[3] The group operation on this set is then naturally the composition of functions. However, this group is yet to large for the purposes of WS-theory. In fact, what is known in the literature on WS-integrability as *the* Möbius group is the subgroup of orientation-preserving Möbius transformations that map the open unit disk $\mathbb{D} \coloneqq \{z \in \mathbb{C} \,;\, |z| < 1\}$ onto itself. By analytic continuation, these maps can be extended to the complex unit circle $\partial\mathbb{D} \coloneqq \{z \in \mathbb{C} \,;\, |z| = 1\}$. Hence, throughout this thesis, we work with the following definition, cf. [Ols10]:

Complex open unit disk $\mathbb{D}$ and unit circle $\partial\mathbb{D}$.

Definition 4.1 *The Möbius group $\mathcal{G}$ is the group of transformations $G_{\alpha,\psi} : \partial\mathbb{D} \to \partial\mathbb{D}$ of the form*

$$G_{\alpha,\psi}(z) \coloneqq \frac{\alpha + \mathrm{e}^{i\psi} z}{1 + \bar{\alpha}\mathrm{e}^{i\psi} z} \tag{4.2}$$

with group parameters $\alpha \in \mathbb{D}$ and $\psi \in \mathbb{S}^1$. The group operation is the composition of transformations. For any $\boldsymbol{\theta} \in \mathbb{T}^N$, we set

$$\mathrm{e}^{i\boldsymbol{\theta}} \coloneqq \left(\mathrm{e}^{i\theta_1}, \ldots, \mathrm{e}^{i\theta_N}\right)$$

and write in a slight abuse of notation

$$G_{\alpha,\psi}\left(\mathrm{e}^{i\boldsymbol{\theta}}\right) \coloneqq \left(G_{\alpha,\psi}\left(\mathrm{e}^{\theta_1}\right), \ldots, G_{\alpha,\psi}\left(\mathrm{e}^{i\theta_N}\right)\right).$$

for the diagonal action of $\mathcal{G}$ on $\mathbb{T}^N$.

$\mathcal{G}$ is in fact a three-dimensional Lie group and can equivalently be defined as the group of orientation-preserving holomorphic automorphisms of $\mathbb{D}$ [SS10; Ols10]. We discuss the group properties of $\mathcal{G}$ in

1 I. e., bijective maps of $\hat{\mathbb{C}}$ onto itself which, together with their inverses, are complex differentiable.

2 For $ad - bc = 0$, f is actually a constant map and can therefore in particular not be an automorphism of $\hat{\mathbb{C}}$.

3 Actually, for the extended complex plane, lines can be seen as circles through the point at infinity ∞.

Appendix A. In particular, every $G_{\alpha,\psi}$ maps $\partial\mathbb{D}$ bijectively onto itself since for every $z \in \partial\mathbb{D}$ we find

$$\begin{aligned}|G_{\alpha,\psi}(z)|^2 &= \frac{(\alpha + \mathrm{e}^{i\psi}z)(\bar{\alpha} + \mathrm{e}^{-i\psi}\bar{z})}{(1 + \bar{\alpha}\mathrm{e}^{i\psi}z)(1 + \alpha\mathrm{e}^{-i\psi}\bar{z})} \\ &= \frac{|\alpha|^2 + \bar{\alpha}\mathrm{e}^{i\psi}z + \alpha\mathrm{e}^{-i\psi}\bar{z} + |z|^2}{1 + \bar{\alpha}\mathrm{e}^{i\psi}z + \alpha\mathrm{e}^{-i\psi}\bar{z} + |\alpha|^2} \\ &= 1\end{aligned}$$

so that $G_{\alpha,\psi}$ is well-defined. The diagonal action of $\mathcal{G}$ induces the following equivalence relation on $\mathbb{T}^N$:

Definition 4.2 *Any two points $\boldsymbol{\vartheta}, \boldsymbol{\theta} \in \mathbb{T}^N$ are equivalent if and only if there exists a $G_{\alpha,\psi} \in \mathcal{G}$ such that $\mathrm{e}^{i\boldsymbol{\vartheta}} = G_{\alpha,\psi}\left(\mathrm{e}^{i\boldsymbol{\theta}}\right)$ in which case we write $\boldsymbol{\vartheta} \sim \boldsymbol{\theta}$. For any $\boldsymbol{\theta} \in \mathbb{T}^N$, we write*

$$[\boldsymbol{\theta}] \coloneqq \left\{\boldsymbol{\vartheta} \in \mathbb{T}^N \,;\, \boldsymbol{\vartheta} \sim \boldsymbol{\theta}\right\}$$

for its equivalence class.

The fact that $\sim$ really is an equivalence relation is asserted by the following proposition:

Proposition 4.3 *The relation $\sim$ is an equivalence relation on $\mathbb{T}^N$.*

Proof. This follows immediately from the group properties of $\mathcal{G}$: Consider any three points $\boldsymbol{\vartheta} \sim \boldsymbol{\theta} \sim \boldsymbol{\phi} \in \mathbb{T}^N$. Then,

1. The identity map $\boldsymbol{\theta} \mapsto \boldsymbol{\theta}$ is given by $G_{0,0} \in \mathcal{G}$ and thus guarantees that $\boldsymbol{\theta} \sim \boldsymbol{\theta}$ so that $\sim$ is reflexive.
2. There exists a $G_{\alpha,\psi} \in \mathcal{G}$ such that $\mathrm{e}^{i\boldsymbol{\vartheta}} = G_{\alpha,\psi}\left(\mathrm{e}^{i\boldsymbol{\theta}}\right)$. The inverse $G^{-1}_{\alpha,\psi} \in \mathcal{G}$ then fulfills $\mathrm{e}^{i\boldsymbol{\theta}} = G^{-1}_{\alpha,\psi}\left(\mathrm{e}^{i\boldsymbol{\vartheta}}\right)$ and thus $\boldsymbol{\theta} \sim \boldsymbol{\vartheta}$ so that $\sim$ is symmetric.
3. There exists a $G_{\beta,\chi} \in \mathcal{G}$ with $\mathrm{e}^{i\boldsymbol{\theta}} = G_{\beta,\chi}\left(\mathrm{e}^{i\boldsymbol{\phi}}\right)$ and thus $\mathrm{e}^{i\boldsymbol{\vartheta}} = G_{\alpha,\psi} \circ G_{\beta,\chi}\left(\mathrm{e}^{i\boldsymbol{\phi}}\right)$ where $G_{\alpha,\psi} \circ G_{\beta,\chi} \in \mathcal{G}$ so that $\boldsymbol{\vartheta} \sim \boldsymbol{\phi}$ and $\sim$ is transitive.

□

Since all units couple in the same way to f and g in (4.1), the units ϕ_j can never overtake each other. (Note that this does not necessarily mean that the ϕ_j are identical. They can still contribute differently to the common fields.) In particular, we can restrict ourselves without loss of generality to the case where all angles $\boldsymbol{\phi} = (\phi_1, \ldots, \phi_N)$ are in (strict) cyclic order. This gives rise to the following definition:

Definition 4.4 *For fixed N, the set $\mathbb{T}^N_{\text{ordered}} \subset \mathbb{T}^N$ of angles in cyclic order is defined as* *Angles in cyclic order.*

$$\mathbb{T}^N_{\text{ordered}} \coloneqq \left\{\boldsymbol{\theta} \in \mathbb{T}^N \,;\, \theta_1 < \cdots < \theta_N < \theta_1 + 2\pi\right\}.$$

Of course, on $\mathbb{T}^N_{\text{ordered}}$ we still find that $\mathcal{G}$ induces an equivalence relation $\sim$ with respective equivalence classes $[\boldsymbol{\theta}]$ for every $\boldsymbol{\theta} \in \mathbb{T}^N_{\text{ordered}}$.

CROSS-RATIOS For any four mutually distinct[4] $z_1, z_2, z_3, z_4 \in \mathbb{C}$, the so-called *cross-ratio* (z_1, z_2, z_3, z_4) is defined as

$$(z_1, z_2, z_3, z_4) \coloneqq \frac{(z_1 - z_2)\,(z_3 - z_4)}{(z_1 - z_4)\,(z_3 - z_2)}.$$

It is a well-known fact that Möbius transformations preserve cross-ratios which is ultimately a consequence of the fact that Möbius transformations map circles to circles [Ahl79]. It is equally known that (z_1, z_2, z_3, z_4) is real-valued if all four points z_j lie on $\partial\mathbb{D}$. This leads to the following proposition which will be used to parameterize the partition of $\mathbb{T}^N_{\text{ordered}}$ in equivalence classes:

Proposition 4.5 *For any $G_{\alpha,\psi} \in \mathcal{G}$ and $\boldsymbol{\theta} \in \mathbb{T}^N_{\text{ordered}}$, let $\boldsymbol{\vartheta} \in \mathbb{T}^N_{\text{ordered}}$ be defined by $\mathrm{e}^{i\boldsymbol{\vartheta}} = G_{\alpha,\psi}\left(\mathrm{e}^{i\boldsymbol{\theta}}\right)$. Further, let $\Lambda_{p,q,r,s} : \mathbb{T}^N_{\text{ordered}} \to \mathbb{R}$ be defined as*

$$\begin{aligned}\Lambda_{p,q,r,s}(\boldsymbol{\theta}) &\coloneqq \left(\mathrm{e}^{i\theta_p}, \mathrm{e}^{i\theta_s}, \mathrm{e}^{i\theta_q}, \mathrm{e}^{i\theta_r}\right)\\ &= \frac{\left(\mathrm{e}^{i\theta_p} - \mathrm{e}^{i\theta_s}\right)\left(\mathrm{e}^{i\theta_q} - \mathrm{e}^{i\theta_r}\right)}{\left(\mathrm{e}^{i\theta_p} - \mathrm{e}^{i\theta_r}\right)\left(\mathrm{e}^{i\theta_q} - \mathrm{e}^{i\theta_s}\right)}\\ &= \frac{\sin\frac{\theta_p-\theta_s}{2}\sin\frac{\theta_q-\theta_r}{2}}{\sin\frac{\theta_p-\theta_r}{2}\sin\frac{\theta_q-\theta_s}{2}}.\end{aligned}$$

Then,

$$\Lambda_{p,q,r,s}(\boldsymbol{\vartheta}) = \Lambda_{p,q,r,s}(\boldsymbol{\theta})$$

for any cross-ratio $\Lambda_{p,q,r,s}$.

Proof. For a proof, we refer to [Ahl79]. □

In principle, for any $\boldsymbol{\theta} \in \mathbb{T}^N$, there exist N^4 different cross-ratios. However, it was shown in [MMS09] that for $N > 3$, one can choose $N - 3$ functionally independent cross-ratios such that all other cross-ratios can be written as some algebraic expression of these $N - 3$ ones. With the following definition, we fix a convenient choice of cross-ratios for our purposes which will be used in Chapter 6:

Definition 4.6 *Let the set $V \subset \mathbb{R}^{N-3}$ be defined as*

$$V \coloneqq \left\{\boldsymbol{\lambda} \in (0,1)^{N-3}\,;\, 1 > \lambda_1 > \cdots > \lambda_{N-3} > 0\right\}.$$

The cross-ratio function $\boldsymbol{\Lambda}$. *The cross-ratio function $\boldsymbol{\Lambda} : \mathbb{T}^N_{\text{ordered}} \to V$ is defined as*

$$\begin{aligned}\boldsymbol{\Lambda}(\boldsymbol{\theta}) &\coloneqq (\Lambda_1(\boldsymbol{\theta}), \ldots, \Lambda_{N-3}(\boldsymbol{\theta}))\\ \Lambda_k(\boldsymbol{\theta}) &\coloneqq \Lambda_{1,2,3,k+3}(\boldsymbol{\theta}) = \frac{\sin\frac{\theta_1-\theta_{k+3}}{2}\sin\frac{\theta_2-\theta_3}{2}}{\sin\frac{\theta_2-\theta_{k+3}}{2}\sin\frac{\theta_1-\theta_3}{2}}\end{aligned} \tag{4.3}$$

with $k = 1, \ldots, N-3$.

4 The cross-ratio is in fact well-defined also for $z_1 = z_2 \neq z_3 = z_4$. Further, it can be extended to the case $z_1, z_2, z_3, z_4 \in \hat{\mathbb{C}}$.

Since each Λ_k depends, besides θ_1, θ_2, and θ_3, only on θ_{k+3}, the $N-3$ components of $\boldsymbol{\Lambda}$ are clearly functionally independent of each other. Next, we note some important properties of the spaces $\mathbb{T}^N_{\text{ordered}}$ and V and the cross-ratio function $\boldsymbol{\Lambda}$:

Lemma 4.7 *The following two assertions hold:*

1. *The set $\mathbb{T}^N_{\text{ordered}}$ is invariant under the action of $\mathcal{G}$.*
2. *The cross-ratios* (4.3) *define a function $\boldsymbol{\Lambda} : \mathbb{T}^N_{\text{ordered}} \to V$.*

Proof. The first assertion follows from the fact that all Möbius transformations $G_{\alpha,\psi} \in \mathcal{G}$ are orientation-preserving [Ahl79]. Thus, for every $\boldsymbol{\theta} \in \mathbb{T}^N_{\text{ordered}}$, i. e., for which $\theta_1 < \cdots < \theta_N < \theta_1 + 2\pi$ holds, let $\mathrm{e}^{i\boldsymbol{\vartheta}} = G_{\alpha,\psi}\left(\mathrm{e}^{i\boldsymbol{\theta}}\right)$. Then $\vartheta_1 < \cdots < \vartheta_N < \vartheta_1 + 2\pi$ by preservation of orientation and hence $\boldsymbol{\vartheta} \in \mathbb{T}^N_{\text{ordered}}$.

The second assertion holds true by observing that[5]

$$\mathrm{D}_{\theta_{k+3}}\Lambda_k(\boldsymbol{\theta}) = \frac{1}{2}\frac{\sin\frac{\theta_1-\theta_2}{2}\sin\frac{\theta_2-\theta_3}{2}}{\sin\frac{\theta_1-\theta_3}{2}\sin^2\frac{\theta_2-\theta_{k+3}}{2}} < 0, \quad k = 1, \ldots, N-3$$

so that all Λ_k are strictly monotonically decreasing in θ_{k+3} on $\mathbb{T}^N_{\text{ordered}}$. In particular, we find $\Lambda_k(\boldsymbol{\theta}) > \Lambda_{k+1}(\boldsymbol{\theta})$ on $\mathbb{T}^N_{\text{ordered}}$. Additionally, we find that $\lim_{\theta_{k+3}\downarrow\theta_3}\Lambda_k(\boldsymbol{\theta}) = 1$ and $\lim_{\theta_{k+3}\uparrow\theta_1+2\pi}\Lambda_k(\boldsymbol{\theta}) = 0$ so that $\boldsymbol{\Lambda}$ indeed maps $\mathbb{T}^N_{\text{ordered}}$ to V. □

The fact that Möbius transformations leave cross-ratios invariant hints that the equivalence classes on $\mathbb{T}^N_{\text{ordered}}$ can be interpreted as level sets of $\boldsymbol{\Lambda}$. To make this assertion rigorous is the purpose of the following lemma:

Lemma 4.8 *For any two $\boldsymbol{\vartheta}, \boldsymbol{\theta} \in \mathbb{T}^N_{\text{ordered}}$, we have*

$$\boldsymbol{\vartheta} \sim \boldsymbol{\theta} \Leftrightarrow \boldsymbol{\Lambda}(\boldsymbol{\vartheta}) = \boldsymbol{\Lambda}(\boldsymbol{\theta})$$

and in particular, we have

$$[\boldsymbol{\theta}] = \left\{\boldsymbol{\vartheta} \in \mathbb{T}^N_{\text{ordered}} \,;\, \boldsymbol{\Lambda}(\boldsymbol{\vartheta}) = \boldsymbol{\Lambda}(\boldsymbol{\theta})\right\}$$

on $\mathbb{T}^N_{\text{ordered}}$, i. e., for every $\boldsymbol{\theta} \in \mathbb{T}^N_{\text{ordered}}$, the equivalence class $[\boldsymbol{\theta}] \subset \mathbb{T}^N_{\text{ordered}}$ is exactly the level set of the cross-ratio function $\boldsymbol{\Lambda}$ for the value $\boldsymbol{\Lambda}(\boldsymbol{\theta})$.

Proof. ($\Rightarrow$): Since $\boldsymbol{\vartheta} \sim \boldsymbol{\theta}$, there exists a $G_{\alpha,\psi} \in \mathcal{G}$ with $\mathrm{e}^{i\boldsymbol{\vartheta}} = G_{\alpha,\psi}\left(\mathrm{e}^{i\boldsymbol{\theta}}\right)$. Then $\boldsymbol{\Lambda}(\boldsymbol{\vartheta}) = \boldsymbol{\Lambda}(\boldsymbol{\theta})$ follows from Proposition 4.5.

5 Due to the strict cyclic order, all arguments of the sine functions fall in the open interval $(-\pi, 0)$.

($\Leftarrow$): Let $\boldsymbol{\Lambda}(\boldsymbol{\vartheta}) = \boldsymbol{\Lambda}(\boldsymbol{\theta})$ for some $\boldsymbol{\vartheta}, \boldsymbol{\theta} \in \mathbb{T}^N_{\text{ordered}}$. We construct a suitable $G_{\alpha,\psi} \in \mathcal{G}$. Consider the two general[6] Möbius transformations $\mu_{\boldsymbol{\theta}} : \hat{\mathbb{C}} \to \hat{\mathbb{C}}$ and $\mu_{\boldsymbol{\vartheta}} : \hat{\mathbb{C}} \to \hat{\mathbb{C}}$ with

$$\mu_{\boldsymbol{\theta}}(z) \coloneqq \frac{\left(z - \mathrm{e}^{i\theta_1}\right)\left(\mathrm{e}^{i\theta_2} - \mathrm{e}^{i\theta_3}\right)}{\left(z - \mathrm{e}^{i\theta_2}\right)\left(\mathrm{e}^{i\theta_1} - \mathrm{e}^{i\theta_3}\right)}$$
$$\mu_{\boldsymbol{\vartheta}}(z) \coloneqq \frac{\left(z - \mathrm{e}^{i\vartheta_1}\right)\left(\mathrm{e}^{i\vartheta_2} - \mathrm{e}^{i\vartheta_3}\right)}{\left(z - \mathrm{e}^{i\vartheta_2}\right)\left(\mathrm{e}^{i\vartheta_1} - \mathrm{e}^{i\vartheta_3}\right)}.$$

These maps fulfill

$$\begin{aligned}
\mu_{\boldsymbol{\theta}}\left(\mathrm{e}^{i\theta_1}\right) &= 0 = \mu_{\boldsymbol{\vartheta}}\left(\mathrm{e}^{i\vartheta_1}\right) \\
\mu_{\boldsymbol{\theta}}\left(\mathrm{e}^{i\theta_2}\right) &= \infty = \mu_{\boldsymbol{\vartheta}}\left(\mathrm{e}^{i\vartheta_2}\right) \\
\mu_{\boldsymbol{\theta}}\left(\mathrm{e}^{i\theta_3}\right) &= 1 = \mu_{\boldsymbol{\vartheta}}\left(\mathrm{e}^{i\vartheta_3}\right)
\end{aligned}$$

so that the function $G(z) = \mu_{\boldsymbol{\vartheta}}^{-1} \circ \mu_{\boldsymbol{\theta}}(z)$ maps $\mathrm{e}^{i\theta_k} \mapsto \mathrm{e}^{i\vartheta_k}$ for $k = 1, 2, 3$. In particular, G is a bijective conformal map from $\partial\mathbb{D}$ to $\partial\mathbb{D}$. It is also orientation-preserving since $\mathrm{e}^{i\theta_1}, \mathrm{e}^{i\theta_2}, \mathrm{e}^{i\theta_3} \in \partial\mathbb{D}$ and $\mathrm{e}^{i\vartheta_1}, \mathrm{e}^{i\vartheta_2}, \mathrm{e}^{i\vartheta_3} \in \partial\mathbb{D}$ are in the same cyclic order by assumption. G is therefore an element of $\mathcal{G}$. Additionally, assumption $\Lambda_k(\boldsymbol{\theta}) = \Lambda_k(\boldsymbol{\vartheta})$ implies that

$$\mu_{\boldsymbol{\theta}}\left(\mathrm{e}^{i\theta_{k+3}}\right) = \Lambda_k(\boldsymbol{\theta}) = \Lambda_k(\boldsymbol{\vartheta}) = \mu_{\boldsymbol{\vartheta}}\left(\mathrm{e}^{i\vartheta_{k+3}}\right).$$

and thus $G\left(\mathrm{e}^{i\theta_k}\right) = \mathrm{e}^{i\vartheta_k}$ holds also for all $k = 4, \ldots, N$. We therefore conclude that $G\left(\mathrm{e}^{i\boldsymbol{\theta}}\right) = \mathrm{e}^{i\boldsymbol{\vartheta}}$ which finishes the proof. □

Level sets $\mathcal{L}_{\boldsymbol{\lambda}}(\boldsymbol{\Lambda})$.

Lemma 4.8 implies that we can parameterize the partition of $\mathbb{T}^N_{\text{ordered}}$ in equivalence classes $[\boldsymbol{\theta}] \subset \mathbb{T}^N_{\text{ordered}}$ via the cross-ratios $\boldsymbol{\lambda} \in V$ such that we may identify equivalence classes and level sets:

$$[\boldsymbol{\theta}] \equiv \mathcal{L}_{\boldsymbol{\lambda}}(\boldsymbol{\Lambda}) \coloneqq \left\{\boldsymbol{\vartheta} \in \mathbb{T}^N_{\text{ordered}} \,;\, \boldsymbol{\Lambda}(\boldsymbol{\vartheta}) = \boldsymbol{\lambda}\right\}$$

where $\boldsymbol{\lambda} = \boldsymbol{\Lambda}(\boldsymbol{\theta})$. Now, each $\boldsymbol{\theta} \in \mathbb{T}^N_{\text{ordered}}$ is an element of the level set $\mathcal{L}_{\boldsymbol{\lambda}}(\boldsymbol{\Lambda})$ of the function $\boldsymbol{\Lambda}$ with $\boldsymbol{\lambda} = \boldsymbol{\Lambda}(\boldsymbol{\theta})$. Next, we introduce a suitable coordinate system on each level set $\mathcal{L}_{\boldsymbol{\lambda}}(\boldsymbol{\Lambda})$.

WATANABE-STROGATZ COORDINATES The ultimate goal of this section is to establish a coordinate system on $\mathbb{T}^N_{\text{ordered}}$ in terms of the two Möbius group parameters α and ψ as well as the $N - 3$ cross-ratios $\boldsymbol{\lambda}$. The group parameters themselves do not yet establish a proper coordinate system on $\mathcal{L}_{\boldsymbol{\lambda}}(\boldsymbol{\Lambda})$. Instead, they only yield a description how to get from any point $\boldsymbol{\theta} \in \mathcal{L}_{\boldsymbol{\lambda}}(\boldsymbol{\Lambda})$ to any other point $\boldsymbol{\vartheta} \in \mathcal{L}_{\boldsymbol{\lambda}}(\boldsymbol{\Lambda})$ by *some* Möbius transformation while we want to uniquely determine where exactly $\boldsymbol{\theta}$ lies on $\mathcal{L}_{\boldsymbol{\theta}}(\boldsymbol{\Lambda})$ in terms of α and ψ. The underlying reason

6 I. e., transformations of type $\mu(z) \coloneqq \frac{az+b}{cz+d}$ with $a, b, c, d \in \mathbb{C}$ and $ad - bc \neq 0$.

for this ambiguity lies in the fact that we are still lacking a unique "point-of-reference" for every $\mathcal{L}_{\boldsymbol{\lambda}}(\boldsymbol{\Lambda})$ with respect to which every other point in the same level set can be determined by a given α and ψ. To introduce such a point $\boldsymbol{\Theta}(\boldsymbol{\lambda})$ for each $\mathcal{L}_{\boldsymbol{\lambda}}(\boldsymbol{\Lambda})$, is purpose of the following definition:

Definition 4.9 *The function* $\boldsymbol{\Theta} : V \to \mathbb{T}^N_{\text{ordered}}$*, defined by*[7]

$$\begin{aligned}
\boldsymbol{\Theta}(\boldsymbol{\lambda}) &\coloneqq (\Theta_1(\boldsymbol{\lambda}), \dots, \Theta_N(\boldsymbol{\lambda})) \\
\Theta_k(\boldsymbol{\lambda}) &\coloneqq -\pi + \frac{2\pi}{N}(k-1), && \text{if } k = 1, 2, 3 \\
\Theta_k(\boldsymbol{\lambda}) &\coloneqq -i \operatorname{Log} \frac{\mathrm{e}^{\frac{2\pi i}{N}} \left(\lambda_{k-3} + \lambda_{k-3}\, \mathrm{e}^{\frac{2\pi i}{N}} - 1\right)}{-\lambda_{k-3} + (1 - \lambda_{k-3})\, \mathrm{e}^{\frac{2\pi i}{N}}}, && \text{if } k = 4, \dots, N,
\end{aligned} \tag{4.4}$$

determines the point-of-reference $\boldsymbol{\Theta}(\boldsymbol{\lambda}) \in \mathcal{L}_{\boldsymbol{\lambda}}(\boldsymbol{\Lambda})$ *for given* $\boldsymbol{\lambda} \in V$*.*

We need to check whether the above made choice is suitable for our purposes by showing that it defines for *each* level set $\mathcal{L}_{\boldsymbol{\lambda}}(\boldsymbol{\Lambda})$ a unique point-of-reference. In other words, we have to check that the image of $\boldsymbol{\Theta}$ intersects *each* $\mathcal{L}_{\boldsymbol{\lambda}}(\boldsymbol{\Lambda})$ in exactly one point. If this is the case, we can define for every point $\boldsymbol{\theta} \in \mathbb{T}^N_{\text{ordered}}$ its WS-coordinates $(\alpha, \psi, \boldsymbol{\lambda})$ via the relation

$$\mathrm{e}^{i\boldsymbol{\theta}} = G_{\alpha,\psi}\left(\mathrm{e}^{i\boldsymbol{\Theta}(\boldsymbol{\lambda})}\right)$$

so that $\boldsymbol{\lambda}$ determines in *which* level set $\mathcal{L}_{\boldsymbol{\lambda}}(\boldsymbol{\Lambda})$ the point $\boldsymbol{\theta}$ lies while α and ψ determine *where* $\boldsymbol{\theta}$ is located in $\mathcal{L}_{\boldsymbol{\lambda}}(\boldsymbol{\Lambda})$ with respect to $\boldsymbol{\Theta}(\boldsymbol{\lambda})$. To show that this is actually the case is done by the following lemma:

Lemma 4.10 *The map* $\boldsymbol{\Theta} : V \to \mathbb{T}^N_{\text{ordered}}$*, defined by* (4.4)*, is smooth and a right inverse of the function* $\boldsymbol{\Lambda}$*, i. e.,* $\boldsymbol{\Lambda} \circ \boldsymbol{\Theta}(\boldsymbol{\lambda}) = \boldsymbol{\lambda}$ *and thus,* $\boldsymbol{\Theta}(\boldsymbol{\lambda}) \in \mathcal{L}_{\boldsymbol{\lambda}}(\boldsymbol{\Lambda})$*.*

Proof. $\boldsymbol{\Theta}$ is well-defined and smooth since the numerator in the second line of (4.4) vanishes only for $\lambda_k = 1/\left(1 + \mathrm{e}^{\frac{2\pi i}{N}}\right) \notin \mathbb{R}$ while the denominator vanishes only for $\lambda_k = \mathrm{e}^{\frac{2\pi i}{N}} / \left(-1 + \mathrm{e}^{\frac{2\pi i}{N}}\right) \notin \mathbb{R}$. Equation (4.4) solves $\boldsymbol{\Lambda}(\boldsymbol{\Theta}) = \boldsymbol{\lambda}$ for $\boldsymbol{\Theta}$ and so is the right inverse of $\boldsymbol{\Lambda}$ by construction. Finally, we need to show that $\boldsymbol{\Theta}$ indeed maps V to $\mathbb{T}^N_{\text{ordered}}$. For this, we assert that for every $k \geq 4$, $\Theta_k(\boldsymbol{\lambda})$ is strictly monotonically decreasing in λ_{k-3} and that $\Theta_3(\boldsymbol{\lambda}) > \Theta_4(\boldsymbol{\lambda})$. The assertion then follows from the fact that $1 > \lambda_1 > \cdots > \lambda_{N-3} > 0$ and

$$\begin{aligned}
\lim_{\lambda_1 \uparrow 1} \Theta_4(\boldsymbol{\lambda}) &= -\pi + \frac{2\pi}{N} 2 \\
\lim_{\lambda_{N-3} \downarrow 0} \Theta_N(\boldsymbol{\lambda}) &= \pi
\end{aligned}$$

7 Here and in what follows, we use the principal value $\operatorname{Log} z$ for the logarithm $\log z$ but for convenience, let its imaginary part lie in the interval $[-\pi, +\pi)$ instead of $(-\pi, +\pi]$.

because that way, the $\Theta_k(\boldsymbol{\lambda})$ are in strict order and for $k \geq 4$ lie all in the interval $(\Theta_3(\boldsymbol{\lambda})), +\pi)$. But since $N \geq 4$, we find

$$\mathrm{D}_{\lambda_{k-3}}\Theta_k(\boldsymbol{\lambda}) = \frac{-2\sin\frac{2\pi}{N}}{1 - \underbrace{2\lambda_{k-3}(1-\lambda_{k-3})}_{\in(0,1/2]}\underbrace{\left(1+\cos\frac{2\pi}{N}\right)}_{\in[1,2)}} < 0$$

so that Θ_k is indeed strictly monotonically decreasing in λ_{k-3} for all $k = 4, \ldots, N$ which finishes the proof. □

Before we come to the main result, we make the following remark which becomes important in Chapter 6 and Chapter 7:

Remark 4.11 *In what follows, particular focus lies on the point*

$$\begin{aligned} \boldsymbol{\theta}^* &\coloneqq (\theta_1^*, \ldots, \theta_N^*) \\ \theta_j^* &\coloneqq -\pi + \frac{2\pi}{N}(j-1) \end{aligned} \tag{4.5}$$

of evenly spaced angles on $\mathbb{S}^1$*. For this point, we find*

$$\begin{aligned} \boldsymbol{\lambda}^* &\coloneqq (\lambda_1^*, \ldots, \lambda_{N-3}^*) \\ \lambda_k^* &\coloneqq \Lambda_k(\boldsymbol{\theta}^*) = \frac{\sin\frac{\pi(k+2)}{N}}{2\cos\frac{\pi}{N}\sin\frac{\pi(k+1)}{N}} \end{aligned} \tag{4.6}$$

for its corresponding cross-ratios.

We are now able to state the final result of this section which asserts the existence of a well-defined coordinate system in terms of WS-variables on $\mathbb{T}^N_{\text{ordered}}$:

Proposition 4.12 *The map* $\boldsymbol{m} : \mathbb{D} \times \mathbb{S}^1 \times V \to \mathbb{T}^N_{\text{ordered}}$ *with*

$$\boldsymbol{m}(\alpha, \psi, \boldsymbol{\lambda}) \coloneqq -i \operatorname{Log} G_{\alpha,\psi}\left(\mathrm{e}^{i\boldsymbol{\Theta}(\boldsymbol{\lambda})}\right) = -i \operatorname{Log} \frac{\alpha + \mathrm{e}^{i\psi}\mathrm{e}^{i\boldsymbol{\Theta}(\boldsymbol{\lambda})}}{1 + \bar{\alpha}\,\mathrm{e}^{i\psi}\mathrm{e}^{i\boldsymbol{\Theta}(\boldsymbol{\lambda})}}$$

is a smooth diffeomorphism.

Proof. In order to show that $\boldsymbol{m}$ is a smooth diffeomorphism, we need to show that it is smooth, bijective, and that its derivative $\mathrm{D}\boldsymbol{m}$ has full rank everywhere, see [Rud76].

Smoothness of $\boldsymbol{m}$: Because it is a composition of the smooth maps $(\alpha, \psi, \boldsymbol{\theta}) \mapsto G_{\alpha,\psi}(\mathrm{e}^{i\boldsymbol{\theta}})$, $\boldsymbol{\Theta}$, and the Log-function, $\boldsymbol{m}$ is smooth.

Injectivity of $\boldsymbol{m}$: Suppose that for $(\alpha, \psi, \boldsymbol{\lambda}), (\alpha', \psi', \boldsymbol{\lambda}') \in \mathbb{D} \times \mathbb{S}^1 \times V$ the equality $\boldsymbol{m}(\alpha, \psi, \boldsymbol{\lambda}) = \boldsymbol{m}(\alpha', \psi', \boldsymbol{\lambda}')$ holds. We then find

$$\begin{aligned} -i \operatorname{Log} G_{\alpha,\psi}\left(\mathrm{e}^{i\boldsymbol{\Theta}(\boldsymbol{\lambda})}\right) &= -i \operatorname{Log} G_{\alpha',\psi'}\left(\mathrm{e}^{i\boldsymbol{\Theta}(\boldsymbol{\lambda}')}\right) \\ \Rightarrow \mathrm{e}^{i\boldsymbol{\Theta}(\boldsymbol{\lambda})} &= G^{-1}_{\alpha,\psi} \circ G_{\alpha',\psi'}\left(\mathrm{e}^{i\boldsymbol{\Theta}(\boldsymbol{\lambda}')}\right). \end{aligned}$$

By Lemma 4.8, this implies

$$\begin{aligned} &\boldsymbol{\Theta}(\boldsymbol{\lambda}) \in [\boldsymbol{\Theta}(\boldsymbol{\lambda}')] = \mathcal{L}_{\boldsymbol{\lambda}'}(\boldsymbol{\Lambda}) \\ &\Rightarrow \boldsymbol{\lambda} = \boldsymbol{\Lambda} \circ \boldsymbol{\Theta}(\boldsymbol{\lambda}) = \boldsymbol{\lambda}'. \end{aligned}$$

Further, $\boldsymbol{\Theta}(\boldsymbol{\lambda})$ always possesses at least three distinct coordinates (e.g. Θ_1, Θ_2, and Θ_3). But since any Möbius map is uniquely defined by the images of three distinct points [Ols10], we have

$$\begin{aligned} G_{\alpha,\psi}\left(\mathrm{e}^{i\boldsymbol{\Theta}(\boldsymbol{\lambda})}\right) &= G_{\alpha',\psi'}\left(\mathrm{e}^{i\boldsymbol{\Theta}(\boldsymbol{\lambda})}\right) \\ \Leftrightarrow\ \ G_{\alpha,\psi} &= G_{\alpha',\psi'} \\ \Leftrightarrow (\alpha,\psi) &= (\alpha',\psi') \end{aligned}$$

and thus $(\alpha,\psi,\boldsymbol{\lambda}) = (\alpha',\psi',\boldsymbol{\lambda}')$ so that $\boldsymbol{m}$ is injective.

Surjectivity of $\boldsymbol{m}$: For any $\boldsymbol{\theta} \in \mathbb{T}^N_{\text{ordered}}$, the cross-ratios $\boldsymbol{\lambda} = \boldsymbol{\Lambda}(\boldsymbol{\theta}) \in V$ are well defined. Thus, since $\boldsymbol{\Theta}(\boldsymbol{\lambda})$ and $\boldsymbol{\theta}$ are both elements of $\mathcal{L}_{\boldsymbol{\lambda}}(\boldsymbol{\Lambda}) = [\boldsymbol{\Theta}(\boldsymbol{\lambda})] = [\boldsymbol{\theta}]$, there exists a $G_{\alpha,\psi} \in \mathcal{G}$ with $G_{\alpha,\psi}\left(\mathrm{e}^{i\boldsymbol{\Theta}(\boldsymbol{\lambda})}\right) = \mathrm{e}^{i\boldsymbol{\theta}}$. But this implies the existence of an $(\alpha,\psi,\boldsymbol{\lambda}) \in \mathbb{D}\times\mathbb{S}^1\times V$ which is mapped by $\boldsymbol{m}$ to $\boldsymbol{\theta}$.

At last, we show that the derivative $\mathrm{D}\boldsymbol{m}$ has full rank everywhere. Note that we have to treat $\mathbb{D}$ as a real space in order to apply NAIMs-theory later on. Since $\mathbb{D}$ is then two dimensional, we could for example use $\mathrm{D}_{\mathrm{Re}\,\alpha}$ and $\mathrm{D}_{\mathrm{Im}\,\alpha}$ as partial derivatives on $\mathbb{D}$. Instead, we treat α and $\bar{\alpha}$ as independent variables, and use the Wirtinger derivatives [RS00] which are defined as

$$\begin{aligned} \mathrm{D}_{\alpha} &\coloneqq \mathrm{D}_{\mathrm{Re}\,\alpha} - i\mathrm{D}_{\mathrm{Im}\,\alpha} \\ \mathrm{D}_{\bar{\alpha}} &\coloneqq \mathrm{D}_{\mathrm{Re}\,\alpha} + i\mathrm{D}_{\mathrm{Im}\,\alpha}. \end{aligned}$$

Then, for each $x \in \{\alpha,\bar{\alpha},\psi,\lambda_1,\ldots,\lambda_{N-3}\}$, let

$$\mathrm{D}_x\boldsymbol{m} = (\mathrm{D}_x m_1,\ldots,\mathrm{D}_x m_N)^T$$

denote the respective column of the derivative

$$\mathrm{D}\boldsymbol{m} = \left[\mathrm{D}_{\alpha}\boldsymbol{m},\mathrm{D}_{\bar{\alpha}}\boldsymbol{m},\mathrm{D}_{\psi}\boldsymbol{m},\mathrm{D}_{\lambda_1}\boldsymbol{m},\ldots,\mathrm{D}_{\lambda_{N-3}}\boldsymbol{m}\right].$$

From the identity

$$\boldsymbol{\Lambda}(\boldsymbol{m}(\alpha,\psi,\boldsymbol{\lambda})) = \boldsymbol{\lambda}$$

we note first that $\mathrm{D}_{\boldsymbol{\theta}}\boldsymbol{\Lambda}\cdot\mathrm{D}_{\boldsymbol{\lambda}}\boldsymbol{m} = \mathrm{id}_{N-3}$ or more explicitly

$$\begin{pmatrix} \mathrm{D}_{\theta_1}\Lambda_1 & \ldots & \mathrm{D}_{\theta_N}\Lambda_1 \\ \vdots & \ddots & \vdots \\ \mathrm{D}_{\theta_1}\Lambda_{N-3} & \ldots & \mathrm{D}_{\theta_N}\Lambda_{N-3} \end{pmatrix} \cdot \begin{pmatrix} \mathrm{D}_{\lambda_1}m_1 & \ldots & \mathrm{D}_{\lambda_{N-3}}m_1 \\ \vdots & \ddots & \vdots \\ \mathrm{D}_{\lambda_1}m_N & \ldots & \mathrm{D}_{\lambda_{N-3}}m_N \end{pmatrix} = \mathrm{id}_{N-3} \tag{4.7}$$

where id_{N-3} is the $(N-3)$-dimensional identity matrix. Thus, $\mathrm{D}_{\boldsymbol{\lambda}}\boldsymbol{m}$ has a left inverse $\mathrm{D}_{\boldsymbol{\theta}}\boldsymbol{\Lambda}$ and therefore has in particular full column rank $N-3$.

Secondly, we have from the same identity

$$\mathrm{D}_{\boldsymbol{\theta}}\boldsymbol{\Lambda}\cdot\mathrm{D}_{\alpha}\boldsymbol{m} = \mathrm{D}_{\boldsymbol{\theta}}\boldsymbol{\Lambda}\cdot\mathrm{D}_{\bar{\alpha}}\boldsymbol{m} = \mathrm{D}_{\boldsymbol{\theta}}\boldsymbol{\Lambda}\cdot\mathrm{D}_{\psi}\boldsymbol{m} = 0 \tag{4.8}$$

so the three column vectors $\mathrm{D}_\alpha \boldsymbol{m}$, $\mathrm{D}_{\bar\alpha}\boldsymbol{m}$, and $\mathrm{D}_\psi \boldsymbol{m}$ stand orthogonal to the column vectors $\mathrm{D}_{\theta_j}\boldsymbol{\Lambda}$ and are thus linearly independent of the column vectors $\mathrm{D}_{\lambda_k}\boldsymbol{m}$. For if any (nontrivial) linear combination

$$\boldsymbol{y} = a\,\mathrm{D}_\alpha \boldsymbol{m} + b\,\mathrm{D}_{\bar\alpha}\boldsymbol{m} + c\,\mathrm{D}_\psi \boldsymbol{m}$$

was in the span of the $\mathrm{D}_{\lambda_k}\boldsymbol{m}$, i. e., if we would have

$$\boldsymbol{y} = \sum_{j=1}^{N-3} c_j \mathrm{D}_{\lambda_j}\boldsymbol{m}$$

with $c_k \neq 0$ for some $k \in \{1, \dots, N-3\}$, we would find

$$0 = \mathrm{D}_{\boldsymbol{\theta}}\Lambda_k \cdot \boldsymbol{y} = \sum_{j=1}^{N-3} c_j \mathrm{D}_{\boldsymbol{\theta}}\Lambda_k \cdot \mathrm{D}_{\lambda_j}\boldsymbol{m} = c_k$$

where the first equality follows from (4.8) and the last from (4.7). This contradicts the assumption that $c_k \neq 0$.

Finally, the three vectors $\mathrm{D}_\alpha \boldsymbol{m}$, $\mathrm{D}_{\bar\alpha}\boldsymbol{m}$, and $\mathrm{D}_\psi \boldsymbol{m}$ are linearly independent. To see this, let us consider the $(N-3)$-by-3 matrix $A = [\mathrm{D}_\alpha \boldsymbol{m}, \mathrm{D}_{\bar\alpha}\boldsymbol{m}, \mathrm{D}_\psi \boldsymbol{m}]$ which then has $\operatorname{rank} A \leq 3$. For any matrix, its rank is equal to that of its largest order square submatrix with nonzero determinant [Bos21]. Let the submatrix $\hat{A}$ consist of the first three components of each column of A. It is of the form

$$\hat{A} = \begin{pmatrix} \frac{i}{-\alpha+\mathrm{e}^{i\psi}} & \frac{i\mathrm{e}^{i\psi}}{-1+\bar\alpha\mathrm{e}^{i\psi}} & \frac{\mathrm{e}^{i\psi}\left(|\alpha|^2-1\right)}{\left(-\alpha+\mathrm{e}^{i\psi}\right)\left(-1+\bar\alpha\mathrm{e}^{i\psi}\right)} \\ \frac{i}{-\alpha+\mathrm{e}^{i\psi}\mathrm{e}^{\frac{2\pi i}{N}}} & \frac{i\mathrm{e}^{i\psi}\mathrm{e}^{\frac{2\pi i}{N}}}{-1+\bar\alpha\mathrm{e}^{i\psi}\mathrm{e}^{\frac{2\pi i}{N}}} & \frac{\left(|\alpha|^2-1\right)\mathrm{e}^{i\psi}\mathrm{e}^{\frac{2\pi i}{N}}}{\left(-\alpha+\mathrm{e}^{i\psi}\mathrm{e}^{\frac{2\pi i}{N}}\right)\left(-1+\bar\alpha\mathrm{e}^{i\psi}\mathrm{e}^{\frac{2\pi i}{N}}\right)} \\ \frac{i}{-\alpha+\mathrm{e}^{i\psi}\mathrm{e}^{\frac{4\pi i}{N}}} & \frac{i\mathrm{e}^{i\psi}\mathrm{e}^{\frac{4\pi i}{N}}}{-1+\bar\alpha\mathrm{e}^{i\psi}\mathrm{e}^{\frac{4\pi i}{N}}} & \frac{\left(|\alpha|^2-1\right)\mathrm{e}^{i\psi}\mathrm{e}^{\frac{4\pi i}{N}}}{\left(-\alpha+\mathrm{e}^{i\psi}\mathrm{e}^{\frac{4\pi i}{N}}\right)\left(-1+\bar\alpha\mathrm{e}^{i\psi}\mathrm{e}^{\frac{4\pi i}{N}}\right)} \end{pmatrix},$$

with determinant

$$\det \hat{A} = \frac{X}{Y_1 Y_2}$$

where

$$\begin{aligned} X &= -\left(1-\mathrm{e}^{\frac{2\pi i}{N}}\right)^3\left(1+\mathrm{e}^{\frac{2\pi i}{N}}\right)\left(1-|\alpha|^2\right)\mathrm{e}^{3i\psi}\mathrm{e}^{\frac{2\pi i}{N}} \\ Y_1 &= \left(\alpha-\mathrm{e}^{i\psi}\right)\left(\alpha-\mathrm{e}^{i\psi}\mathrm{e}^{\frac{2\pi i}{N}}\right)\left(\alpha-\mathrm{e}^{i\psi}\mathrm{e}^{\frac{4\pi i}{N}}\right) \\ Y_2 &= \left(1-\bar\alpha\mathrm{e}^{i\psi}\right)\left(1-\bar\alpha\mathrm{e}^{i\psi}\mathrm{e}^{\frac{2\pi i}{N}}\right)\left(1-\bar\alpha\mathrm{e}^{i\psi}\mathrm{e}^{\frac{4\pi i}{N}}\right). \end{aligned}$$

This determinant is nonvanishing: By the triangle inequality, we have

$$\begin{aligned} |Y_1| &\leq (1+|\alpha|)^3 \\ |Y_2| &\leq (1+|\alpha|)^3 \end{aligned}$$

while for $N \geq 3$ and with $\left|1 \pm \mathrm{e}^{i\theta}\right| = \sqrt{2}\sqrt{1 \pm \cos\theta}$ and $1 - \cos\theta \geq \theta^2/8$ for all $\theta \in \left[-\frac{2\pi}{3}, \frac{2\pi}{3}\right]$, we have

$$\begin{aligned} |X| &= \left|1 - \mathrm{e}^{\frac{2\pi i}{N}}\right|^3 \left|1 + \mathrm{e}^{\frac{2\pi i}{N}}\right| \left(1 - |\alpha|^2\right) \\ &= 4\sqrt{\left(1 - \cos\frac{2\pi}{N}\right)^3 \left(1 + \cos\frac{2\pi}{N}\right)} \left(1 - |\alpha|^2\right) \\ &\geq 4\frac{1}{\sqrt{8^3 2}} \left(\frac{2\pi}{N}\right)^3 \left(1 - |\alpha|^2\right) = \left(\frac{\pi}{N}\right)^3 \left(1 - |\alpha|^2\right) \end{aligned}$$

where in the third line we also used $1 + \cos\theta \geq 1/2$ for all $\theta \in \left[-\frac{2\pi}{3}, \frac{2\pi}{3}\right]$. Thus we find

$$\left|\det \hat{A}\right| \geq \left(\frac{\pi}{N}\right)^3 \frac{1 - |\alpha|^2}{(1 + |\alpha|)^6} > 0$$

so that $\hat{A}$ has full rank 3 and so has A. Hence, $\mathrm{D}_\alpha \boldsymbol{m}$, $\mathrm{D}_{\bar{\alpha}} \boldsymbol{m}$, and $\mathrm{D}_\psi \boldsymbol{m}$ are linearly independent. Therefore, all column vectors of $\mathrm{D}\boldsymbol{m}$ are linearly independent.

□

For any system $\dot{\boldsymbol{\phi}} = \boldsymbol{f}(\boldsymbol{\phi})$ of identical angular variables, Proposition 4.12 allows for an alternative and equivalent description in terms of the WS-variables α, ψ, and $\boldsymbol{\lambda}$. If a solution $(\alpha(t), \psi(t), \boldsymbol{\lambda}(t))$ for the system in these variables can be found, one can recover the original dynamics by virtue of $\boldsymbol{m}$. The key feature of WS-integrable systems (4.1) is then that the governing equations in these WS-variables are particularly simple in the sense that the cross-ratios $\boldsymbol{\lambda}(t) = (\lambda_1(t), \ldots, \lambda_{N-3}(t))$ are constants of motion. In the next section, we discuss the fundamental theorem of WS-theory.

4.2 INTEGRABILITY

The fundamental theorem of WS-theory, due to [WS94] states that for any system of the form (4.1), its flow is completely determined by a one-parameter family of Möbius transformations. It can be stated as follows (here we follow the formulation and notation in [MMS09]):

Theorem 4.13 *Consider an ensemble of $N > 3$ mutually distinct angular variables $\boldsymbol{\phi} = (\phi_1, \ldots, \phi_N) \in \mathbb{T}^N$, obeying the equations*

$$\dot{\phi}_j = f(\boldsymbol{\phi})\, \mathrm{e}^{i\phi_j} + g(\boldsymbol{\phi}) + \bar{f}(\boldsymbol{\phi})\, \mathrm{e}^{-i\phi_j} \tag{4.9}$$

for $j = 1, \ldots, N$ where $f : \mathbb{T}^N \to \mathbb{C}$ and $g : \mathbb{T}^N \to \mathbb{R}$ are smooth functions. Then, the time-evolution of $\boldsymbol{\phi}(t)$ is determined through

$$\mathrm{e}^{i\phi_j(t)} = G_{\alpha(t),\psi(t)}\left(\mathrm{e}^{i\theta_j}\right) \tag{4.10}$$

where $\boldsymbol{\theta} = (\theta_1, \ldots, \theta_N) \in \mathbb{T}^N$ is constant and $\alpha(t)$ and $\psi(t)$ are solutions of

$$\begin{aligned} \dot{\alpha} &= i\left(f(\boldsymbol{\phi})\alpha^2 + g(\boldsymbol{\phi})\alpha + \bar{f}(\boldsymbol{\phi})\right) \\ \dot{\psi} &= f(\boldsymbol{\phi})\alpha + g(\boldsymbol{\phi}) + \bar{f}(\boldsymbol{\phi})\bar{\alpha} \end{aligned} \tag{4.11}$$

and the functions f and g now implicitly depend on α and ψ via the flow relation (4.10).

Note that the first line in (4.11) actually represents two equations since its right hand side is not holomorphic. It is to be understood as two equations for, e. g., $\operatorname{Re}\alpha$ and $\operatorname{Im}\alpha$ or α and $\bar{\alpha}$.

Theorem 4.13 has been proven in various ways from purely algebraic proofs [Goe95; PR08] over geometric ones, relying on concepts from Lie theory [MMS09], to those, using arguments from complex analysis [EM14] or complex projective geometry [Ste11]. We refer to these works for a proof of the theorem.

Choosing initial conditions and constraints.

A few remarks are at hand, concerning some intricacies of Theorem 4.13. First, the theorem gives us some freedom of choice regarding the initial conditions for (4.11), depending on the choice of the constant $\boldsymbol{\theta}$. Different choices can be more suitable in different settings. With the N degrees of freedom from $\boldsymbol{\theta} \in \mathbb{T}^N$ and the three degrees of freedom from the group parameters α and ψ, we need to impose three conditions on the tuple $(\alpha, \psi, \boldsymbol{\theta})$ in addition to the N initial conditions from $\boldsymbol{\phi}(0)$ in order to uniquely determine the dynamics of $\boldsymbol{\phi}(t)$ via the group action (4.10). Watanabe and Strogatz themselves discussed two possible options in [WS94]. The first one, preferred by them, is to impose $\sum_{j=1}^{N} \mathrm{e}^{i\theta_j} = 0$ and $\sum_{j=1}^{N} \theta_j = 0 \bmod 2\pi$ on $\boldsymbol{\theta}$ so that the θ_j become, in their own words, "incoherent". Then, $\alpha(0)$ and $\psi(0)$ can be chosen such that $\mathrm{e}^{i\boldsymbol{\phi}(0)} = G_{\alpha(0),\psi(0)}\left(\mathrm{e}^{i\boldsymbol{\theta}}\right)$ which they deemed the natural way to impose the three constraints because in this picture, the flow on $\mathbb{D} \times \mathbb{S}^1$ is the same for all choices of $\boldsymbol{\theta}$ that lie in the same equivalence class while different initial conditions $\boldsymbol{\phi}_1(0), \boldsymbol{\phi}_2(0) \in [\boldsymbol{\theta}]$ with $\boldsymbol{\phi}_1(0) \neq \boldsymbol{\phi}_2(0)$ of (4.9) lead to different initial conditions $(\alpha_1(0), \psi_1(0)) \neq (\alpha_2(0), \psi_2(0))$ of (4.11). This naturally corresponds to the fact that the vector field and therefore flow on each $[\boldsymbol{\theta}]$ does not depend on which representative $\boldsymbol{\vartheta} \in [\boldsymbol{\theta}]$ one chooses.

A second option, which was considered unnatural by Watanabe and Strogatz, is to always impose the initial condition $\alpha(0) = \psi(0) = 0$ such that $\boldsymbol{\theta} = \boldsymbol{\phi}(0)$ and therefore let the vector field in (4.11) on $\mathbb{D} \times \mathbb{S}^1$ explicitly depend on $\boldsymbol{\phi}(0)$ such that in particular two distinct initial conditions $\boldsymbol{\phi}_1(0) \neq \boldsymbol{\phi}_2(0)$ with $[\boldsymbol{\phi}_1(0)] = [\boldsymbol{\phi}_2(0)]$ yield different equations of motion in α and ψ even though their corresponding dynamics in $\boldsymbol{\phi}$ take place in the same equivalence class. This is a direct consequence of the fact that the Möbius parameters α and ψ do not define a coordinate system on a given level set by themselves but are only relative coordinates, as mentioned before.[8] In our work, we follow a third option, that is somewhat similar to the natural choice of constraints

8 In some sense, this is similar to the distinction between affine spaces and vector spaces. For the former, vectors do not readily determine specific points in, say, some $\mathbb{R}^n$ but only differences between points so that "An affine space is nothing more than a vector space whose origin we try to forget about [...]" [Ber09]. In this informal view, an affine space becomes a vector space once we define a specific origin or point-of-reference and only then do vectors uniquely determine points in $\mathbb{R}^n$ just as α and ψ parameterize a given level set $\mathcal{L}_{\boldsymbol{\lambda}}(\boldsymbol{\Lambda})$ only once we distinguish a single point-of-reference $\boldsymbol{\Theta}(\boldsymbol{\lambda})$ for that level set.

by Watanabe and Strogatz. The unique point-of-reference $\boldsymbol{\Theta}(\boldsymbol{\lambda})$ from Lemma 4.10 and Proposition 4.12 yields three constraints on $\boldsymbol{\theta}$ by fixing $(\theta_1, \theta_2, \theta_3) = (\Theta_1(\boldsymbol{\lambda}), \Theta_2(\boldsymbol{\lambda}), \Theta_3(\boldsymbol{\lambda})) = (-\pi, -\pi+2\pi/N, -\pi+4\pi/N)$ so that we may choose the initial conditions for (4.11) by imposing $\boldsymbol{\phi}(0) = G_{\alpha(0),\psi(0)}\left(\mathrm{e}^{i\boldsymbol{\Theta}(\boldsymbol{\lambda})}\right)$ with $\boldsymbol{\lambda} = \boldsymbol{\Lambda}(\boldsymbol{\phi}(0))$.

Computational aspects.

As a second remark, we note that, while the equations (4.11) look simple at first sight, they obfuscate some conceptual problems when it comes to solving them in practice. Since f and g only depend implicitly on α and ψ as well as on the constant $\boldsymbol{\theta}$ via (4.10), it is in general not feasible to write them down explicitly. A closed form can usually only be found for specific choices of $\boldsymbol{\theta}$ and thus distinguished level sets $\mathcal{L}_{\boldsymbol{\lambda}}(\boldsymbol{\Lambda})$. We will encounter this problem in Chapter 6 when we investigate a continuum of periodic orbits. As a consequence, the equations (4.11) are rarely useful for numerical work. While for large N, one only has to solve a system of three coupled ODEs instead of N, one usually still has to store the values for each $\phi_j(t)$ to determine f and g. With this, any performance gain that might come with the dimensional reduction of the problem is immediately compensated by complicated auxiliary computations for f and g at every time step. Even worse, while the system (4.9) is usually eligible for vectorization of numerical integration algorithms, this cannot be expected for (4.11) so that in consequence, solving (4.11) numerically is less efficient than solving (4.9). With this, we end our discussion of Theorem 4.13. Next, we make use of Proposition 4.12 to restate (4.11) in terms of the full set of WS-variables $(\alpha, \psi, \boldsymbol{\lambda})$ and discuss how to extend them to nonintegrable systems.

4.3 GENERAL DYNAMICS IN WATANABE-STROGATZ VARIABLES

By Proposition 4.12, every point $\boldsymbol{\theta} \in \mathbb{T}^N_{\text{ordered}}$ is uniquely determined by the three WS-variables $(\alpha, \psi, \boldsymbol{\lambda}) \in \mathbb{D} \times \mathbb{S}^1 \times V$. In particular, $\boldsymbol{\theta}$ lies in the level set $\mathcal{L}_{\boldsymbol{\lambda}=\boldsymbol{\Lambda}(\boldsymbol{\theta})}(\boldsymbol{\Lambda}) = [\boldsymbol{\Theta}(\boldsymbol{\Lambda}(\boldsymbol{\theta}))]$. Since this holds true for every $\boldsymbol{\theta} \in \mathbb{T}^N_{\text{ordered}}$, the level sets form a partition of $\mathbb{T}^N_{\text{ordered}}$, i. e., we have

$$\mathbb{T}^N_{\text{ordered}} = \bigcup_{\boldsymbol{\lambda} \in V} \mathcal{L}_{\boldsymbol{\lambda}}(\boldsymbol{\Lambda})$$

with mutually disjoint three-dimensional submanifolds $\mathcal{L}_{\boldsymbol{\lambda}}(\boldsymbol{\Lambda})$. Theorem 4.13 then implies that the dynamics of $\boldsymbol{\phi}$ for a WS-integrable system (4.9) can be determined from the corresponding system (4.11) for α and ψ via the Möbius action (4.10) so that $\boldsymbol{\phi}(t) \in [\boldsymbol{\phi}(0)]$ for all t. In other words, the partition of $\mathbb{T}^N_{\text{ordered}}$ through the level sets $\mathcal{L}_{\boldsymbol{\lambda}}(\boldsymbol{\Lambda})$ is invariant under the flow of (4.9) and therefore, the dynamics of (4.9) in WS-variables $(\alpha, \psi, \boldsymbol{\lambda})$ is fully determined by the system

$$\begin{aligned} \dot{\alpha} &= i\left(f(\boldsymbol{\phi})\alpha^2 + g(\boldsymbol{\phi})\alpha + \bar{f}(\boldsymbol{\phi})\right) \\ \dot{\psi} &= f(\boldsymbol{\phi})\alpha + g(\boldsymbol{\phi}) + \bar{f}(\boldsymbol{\phi})\bar{\alpha} \\ \dot{\boldsymbol{\lambda}} &= \mathbf{0}. \end{aligned} \tag{4.12}$$

Consider on the other hand a general system $\dot{\boldsymbol{\phi}} = \boldsymbol{F}(\boldsymbol{\phi})$ of identical angles $(\phi_1, \ldots, \phi_N) =: \boldsymbol{\phi} \in \mathbb{T}^N_{\text{ordered}}$ which is generally *not* WS-integrable. For such a system, the corresponding equations in WS-coordinates read

$$\begin{aligned}
\dot{\alpha} &= \mathrm{D}_{\boldsymbol{\phi}}\alpha \cdot \dot{\boldsymbol{\phi}} = \mathrm{D}_{\boldsymbol{\phi}}\alpha \cdot \boldsymbol{F}(\boldsymbol{\phi}) \\
\dot{\psi} &= \mathrm{D}_{\boldsymbol{\phi}}\psi \cdot \dot{\boldsymbol{\phi}} = \mathrm{D}_{\boldsymbol{\phi}}\psi \cdot \boldsymbol{F}(\boldsymbol{\phi}) \\
\dot{\boldsymbol{\lambda}} &= \mathrm{D}_{\boldsymbol{\phi}}\boldsymbol{\Lambda} \cdot \dot{\boldsymbol{\phi}} = \mathrm{D}_{\boldsymbol{\phi}}\boldsymbol{\Lambda} \cdot \boldsymbol{F}(\boldsymbol{\phi})
\end{aligned}$$

by the chain rule. From this, we see that it is always possible to separate the components of $\boldsymbol{F}$ that are compatible with WS-integrability from the nonintegrable components, i. e., to write

$$\boldsymbol{F}(\boldsymbol{\phi}) = \boldsymbol{F}_{\text{WS}}(\boldsymbol{\phi}) + \boldsymbol{F}_{\text{non-WS}}(\boldsymbol{\phi}),$$

defined by the relations

$$\begin{aligned}
\mathrm{D}_{\boldsymbol{\phi}}\boldsymbol{\Lambda} \cdot \boldsymbol{F}_{\text{WS}}(\boldsymbol{\phi}) &= \mathbf{0} \\
\mathrm{D}_{\boldsymbol{\phi}}\alpha \cdot \boldsymbol{F}_{\text{non-WS}}(\boldsymbol{\phi}) = \mathrm{D}_{\boldsymbol{\phi}}\psi \cdot \boldsymbol{F}_{\text{non-WS}}(\boldsymbol{\phi}) &= 0
\end{aligned}$$

for every $\boldsymbol{\phi}$ so that

$$\begin{aligned}
\dot{\alpha} &= \mathrm{D}_{\boldsymbol{\phi}}\alpha \cdot \boldsymbol{F}_{\text{WS}}(\boldsymbol{\phi}) \\
\dot{\psi} &= \mathrm{D}_{\boldsymbol{\phi}}\psi \cdot \boldsymbol{F}_{\text{WS}}(\boldsymbol{\phi}) \\
\dot{\boldsymbol{\lambda}} &= \mathrm{D}_{\boldsymbol{\phi}}\boldsymbol{\Lambda} \cdot \boldsymbol{F}_{\text{non-WS}}(\boldsymbol{\phi})
\end{aligned}$$

from which we can conclude with (4.8) that

$$\begin{aligned}
\boldsymbol{F}_{\text{WS}}(\boldsymbol{\phi}) &\in \operatorname{span}\left(\mathrm{D}_{\alpha}\boldsymbol{m}\,, \mathrm{D}_{\bar{\alpha}}\boldsymbol{m}\,, \mathrm{D}_{\psi}\boldsymbol{m}\right) \\
\boldsymbol{F}_{\text{non-WS}}(\boldsymbol{\phi}) &\in \operatorname{span}\left(\mathrm{D}_{\lambda_1}\boldsymbol{m}\,, \ldots, \mathrm{D}_{\lambda_{N-3}}\boldsymbol{m}\right).
\end{aligned}$$

In other words, $\boldsymbol{F}_{\text{WS}}(\boldsymbol{\phi})$ denotes the components of $\boldsymbol{F}(\boldsymbol{\phi})$, that lie tangent to $\mathcal{L}_{\boldsymbol{\lambda}}(\boldsymbol{\Lambda})$ at the point $\boldsymbol{\phi} = \boldsymbol{m}(\alpha, \psi, \boldsymbol{\lambda})$ while $\boldsymbol{F}_{\text{non-WS}}(\boldsymbol{\phi})$ denotes the components of $\boldsymbol{F}(\boldsymbol{\phi})$ normal to it. We make use of this fact when we investigate the generalized Active Rotator model (2.6) in Chapter 7.

With this, we end our discussion of Watanabe-Strogatz integrability. In the next part of this thesis, we discuss the results of our work on the systems (2.5) and (2.6). We start with the results on states that consist of two clusters.

Part II

ENSEMBLES OF ACTIVE ROTATORS

If you cannot solve the proposed problem, try to solve first a simpler related problem.

— Pólya György [Pól77]

5

TWO-CLUSTER STATES

ABSTRACT

In this chapter, we investigate the emergence and stability of periodic two-cluster states for the case of the generalized Active Rotator model

$$\begin{aligned}\dot{\phi}_j &= \omega - \sin\phi_j + \epsilon h(\phi_j) + \frac{\kappa}{N}\sum_{k=1}^{N}\sin(\phi_k - \phi_j)\\ h(\phi) &= \sum_{n=2}^{\infty} a_n \sin n\phi + b_n \cos n\phi,\end{aligned} \tag{2.6}$$

as introduced in Chapter 2. For this, we assume that the ensemble splits in two clusters $A = \{1, \ldots, m_A\}$ and $B = \{m_A + 1, \ldots, N\}$ of $m_A > 1$ and $m_B = N - m_A > 1$ units each so that

$$\begin{aligned}\phi_A &= \phi_1 = \cdots = \phi_{m_A}\\ \phi_B &= \phi_{m_A+1} = \cdots = \phi_N\end{aligned}$$

where we also include the case of full synchrony $\phi_A = \phi_B$. If the two clusters are of equal size, i. e., if $m_A = m_B = N/2$, we call the two-cluster state *symmetric*. Otherwise, we refer to it as *asymmetric*.

After making some general remarks in Section 5.1, we start by introducing a reduced description of the system in terms of cluster coordinates ϕ_A and ϕ_B in Section 5.2, which allows for determining the emergence and stability of periodic two-cluster states against non-splitting perturbations, independently of the ensemble size N, and is a well-known tool for the study of clustered solutions [LY12]. In Section 5.3, we discuss local bifurcations of fixed points in this reduced description which play an important role in the creation of periodic two-cluster states. In Section 5.4, we discuss the two most generic codimension 1 bifurcations, yielding periodic two-cluster states: the double-heteroclinic bifurcation and the double-SNIC. Afterwards, in Section 5.5, we discuss the stability of the emerging periodic states in dependence on the perturbation term $\epsilon h(\phi_j)$ and how the observed behavior can be explained within the framework of WS-theory.

The results on limit cycle bifurcation scenarios and stability of periodic two-cluster states constitute the main results of this chapter and were published in [RZ21a].

5.1 GENERAL REMARKS

To make the discussion more definite, we consider two paradigmatic choices for the perturbation function h in (2.6). By definition, h contains only terms of second or higher order Fourier modes $\sin n\phi$ and $\cos n\phi$, $n \geq 2$. We therefore consider one example that is particularly simple in its form to make some explicit calculations more tangible, and a second one that serves as a representative for generic perturbations, involving infinitely many modes. For this, we choose

$$h(\phi) = \sin 2\phi \tag{5.1a}$$

$$h(\phi) = \frac{1}{\sin\phi - 2} + \frac{1}{\sqrt{3}} + \left(\frac{4}{\sqrt{3}} - 2\right)\sin\phi. \tag{5.1b}$$

Note that in (5.1b), the two terms $1/\sqrt{3}$ and $(4/\sqrt{3}-2)\sin\phi$ solely serve the purpose to cancel out the zeroth and first order Fourier modes of $1/(\sin\phi - 2)$ so that this choice only contains higher order modes.

Although all quantitative results in this chapter apply only to the two choices for h above, we argue that they are universal for systems of type (2.6) at least for sufficiently small $|\epsilon|$. The reason for this is twofold. Firstly, the found bifurcation scenarios are in some sense minimal: They involve only saddles and fixed points that are either already present in the uncoupled case $\kappa = 0$ or emerge in the most generic fixed point bifurcations that can occur for systems of type (2.6), see Section 5.3. Secondly, the main result of Section 5.5 is that a change of stability for symmetric periodic two-cluster states occurs at $\epsilon = 0$ while asymmetric periodic two-cluster states do not show such behavior. As we will show, this is an immediate consequence of the system becoming WS-integrable at $\epsilon = 0$ where in fact *any* symmetric periodic two-cluster state is neutrally stable while asymmetric periodic two-cluster states are always exponentially unstable at $\epsilon = 0$, regardless of the specific form of h.

As a first step in our investigation, we replace the ensemble and cluster sizes in (2.6) by the parameter p, describing the relative size of one of the clusters. This allows to make general statements about existence and stability of two-cluster states, independently of N.

5.2 A REDUCED DESCRIPTION

As already established in Chapter 2, for systems of identical ARs, it holds that (i) units cannot overtake each other in the state space $\mathbb{S}^1$ and thus, (ii) clustered states stay clustered for all time. Introducing the parameter $p = m_A/N$, this means that the two-cluster subspaces

$$\mathbb{T}_p \coloneqq \left\{\boldsymbol{\phi} \in \mathbb{T}^N \,;\, \phi_1 = \cdots = \phi_{pN} = \phi_A,\ \phi_{pN+1} = \cdots = \phi_N = \phi_B\right\},$$

which are homeomorphic to the two-dimensional torus $\mathbb{T}^2$, are invariant under the flow of (2.6). For finite N, the parameter p takes values in $\{2/N, \ldots, (N-2)/N\}$ but for our purposes we simply assume $p \in (0, 1)$. In particular, symmetric two-cluster states are elements of the space

$\mathbb{T}_{1/2}$. Note that different choices for m_A and m_B and subsequently of p yield different subspaces $\mathbb{T}_p \subset \mathbb{T}^N$ which intersect only in the diagonal space $\Delta \coloneqq \left\{ \boldsymbol{\phi} \in \mathbb{T}^N \,;\, \phi_1 = \cdots = \phi_N \right\}$ (the space of complete synchrony). Hence, the dynamics on these spaces can be described by the two-dimensional reduced system

$$\begin{aligned} \dot{\phi}_A &= \omega - \sin\phi_A + \epsilon h(\phi_A) + (1-p)\,\kappa \sin(\phi_B - \phi_A) \\ \dot{\phi}_B &= \omega - \sin\phi_B + \epsilon h(\phi_B) + p\,\kappa \sin(\phi_A - \phi_B) \end{aligned} \tag{5.2}$$

since only those units interact with each other that do not belong to the same cluster. Equation (5.2) thus describes a system of two generally nonidentical units, close to a SNIC, a setup that was investigated rigorously by Baesens and MacKay in [BM13] for the case of the units being sufficiently close to their respective SNICs.

The reduced system (5.2) features an important property in the symmetric case $p = 1/2$: It is equivariant under permutations of cluster A and B. According to the argument, made in Chapter 3, this equivariance results in a spatio-temporal symmetry one for its periodic solutions: after one half-period $T/2 > 0$, the instantaneous cluster positions are permuted, i. e., $\phi_A(t + T/2) = \phi_B(t)$ and vice versa for all $t \in \mathbb{R}$. Therefore, with respect to $\mathbb{T}_{1/2}$, any periodic state is a splay state. This observation becomes important in Section 5.5, when we investigate the asymptotic stability of such states.

Let ϕ^{s} and ϕ^{u} denote the stable and the unstable fixed point of the single AR $\dot{\phi} = \omega - \sin\phi + \epsilon\, h(\phi)$. For $\kappa = 0$, the system (5.2) possesses exactly four steady states: the stable synchronous fixed point $\Delta^{\mathrm{s}} = (\phi^{\mathrm{s}}, \phi^{\mathrm{s}})$, the unstable synchronous fixed point $\Delta^{\mathrm{u}} = (\phi^{\mathrm{u}}, \phi^{\mathrm{u}})$, as well as the two saddles $\Sigma^1 = (\phi^{\mathrm{u}}, \phi^{\mathrm{s}})$ and $\Sigma^2 = (\phi^{\mathrm{s}}, \phi^{\mathrm{u}})$. In a slight abuse of notation, we identify these fixed points with the corresponding ones of (2.6), i. e., with the synchronous fixed points

We refer to all states that lie on the diagonal Δ as synchronous *and to all states that do not lie in Δ as* asynchronous *states.*

$$\begin{aligned} \Delta^{\mathrm{s}} &= (\underbrace{\phi^{\mathrm{s}}, \ldots, \phi^{\mathrm{s}}}_{N \text{ entries}}) \\ \Delta^{\mathrm{u}} &= (\underbrace{\phi^{\mathrm{u}}, \ldots, \phi^{\mathrm{u}}}_{N \text{ entries}}) \end{aligned}$$

in the diagonal space Δ and the two saddles

$$\begin{aligned} \Sigma^1 &= (\underbrace{\phi^{\mathrm{u}}, \ldots, \phi^{\mathrm{u}}}_{m_A \text{ entries}}, \underbrace{\phi^{\mathrm{s}}, \ldots, \phi^{\mathrm{s}}}_{m_B \text{ entries}}) \\ \Sigma^2 &= (\underbrace{\phi^{\mathrm{s}}, \ldots, \phi^{\mathrm{s}}}_{m_A \text{ entries}}, \underbrace{\phi^{\mathrm{u}}, \ldots, \phi^{\mathrm{u}}}_{m_B \text{ entries}}) \end{aligned}$$

of the full system. Since ϕ^{s} and ϕ^{u} are hyperbolic, so are the reduced fixed points and thus they persist for sufficiently small $|\kappa| > 0$.

Coming next to the existence of periodic solutions, one may ask for which choices of $(\omega, \epsilon, \kappa, p)$ such solutions exist at all. The former two parameters determine only the on-site dynamics of each cluster so we may fix them and determine for which choices of (κ, p) the system (5.2)

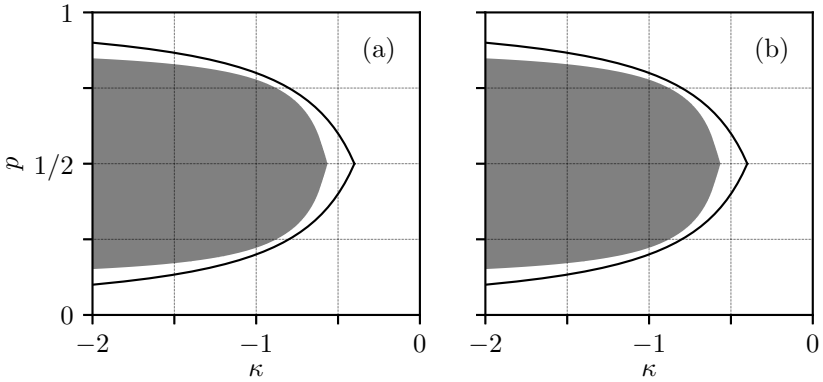

Figure 4: Existence of periodic orbits for the system (5.2) in dependence on coupling strength κ and relative proportion p of cluster A with fixed parameters $\omega = 0.8$ and $\epsilon = 0.1$. Panels (a) and (b) show numerical results for the choices (5.1a) and (5.1b) for h, respectively. In the white shaded area, no periodic two-cluster states exist while in the gray area, a periodic orbit with $m_A = pN$ and $m_B = (1-p)N$ exists for any given N. Black lines indicate the approximate bounds (5.3) and (5.4) for the existence of periodic states.

possesses periodic states. Figure 4 depicts the regime of existence of periodic states (gray shaded area) of the system (5.2) for perturbation types (5.1a) and (5.1b), respectively. In the white shaded area, no periodic orbits exist. The meaning of the black lines will be explained further below. On-site parameters are fixed at $\omega = 0.8$ and $\epsilon = 0.1$. From this, one can make two preliminary observations. First, in order to yield any periodic two-cluster states, coupling needs to be sufficiently repulsive. In this numerical experiment, we only find such orbits for κ smaller than approximately $-2/3$. Secondly, in order to exist, periodic orbits must be sufficiently balanced in cluster size for given κ. In general, we observe that the larger $|\kappa|$ is, i. e., the more repulsive the interaction gets, the larger the disparity of cluster sizes can be to still yield a periodic orbit. This observation is in accordance to our expectation: If repulsion between clusters is weak and size disparity is large, the smaller cluster has little impact on the dynamics of the larger one. Hence, the latter converges approximately to the coordinate ϕ^{s} of the single unit's stable state of rest, as if isolated. Since clusters cannot overtake each other, the small cluster cannot show any large scale periodic motion. However, small scale motions are equally forbidden as the system is of gradient type as we showed in Chapter 2. Hence, the system must come to rest. This argument leads to a rough estimate on the bounds of existence for periodic two-cluster states in κ and p for $|\epsilon| \ll 1$.

For this, let the on-site dynamics be given by $f(\phi) = \omega - \sin\phi + \epsilon h(\phi)$ and $p < 1/2$ which implies that cluster B is the larger one. Assuming, without loss of generality, $\omega > 0$, we may view the influence of the smaller cluster A as a small time-dependent perturbation $p\kappa g(t)$ to the dynamics of B so that we write $\dot{\phi}_B = f(\phi_B) + p\kappa g(t)$. Repulsion

between clusters is the strongest if $\phi_A - \phi_B = \pm\pi/2$ and the influence of A on B is bounded by $\pm p\kappa$ which yields

$$\left|\dot{\phi}_B\right| = |\omega - \sin\phi_B + \epsilon h(\phi_B) + p\kappa g(t)| \leq |\omega - \sin\phi_B + \epsilon h(\phi_B) - p\kappa|$$

since $p\kappa < 0$. The flow of ϕ_B then possesses a fixed point ϕ_B^* if the right hand side of this equation can become zero for some ϕ_B. For $|\epsilon| \ll 1$, this implies $\omega - p\kappa \lesssim 1$ so that we conclude for the existence of periodic two-cluster states with cluster sizes pN and $(1-p)N$ that

$$p > p_{\min} \approx -\frac{1-\omega}{\kappa} \tag{5.3}$$

and $p_{\min}$ is a lower bound for p. By symmetry, the upper bound can be approximated as

$$p_{\max} \approx 1 + \frac{1-\omega}{\kappa}. \tag{5.4}$$

We plot these bounds as black lines in Figure 4. Comparing with the actual domain of existence, we find that they indeed bound the regime of existence for periodic two-cluster states. However, as true boundaries for this regime, they are not very accurate. In order to gain a more thorough understanding of this regime, we have to investigate the actual bifurcations that lead to periodic two-cluster states. These bifurcations are expected (i) to be global and involve the fixed points Δ^{s}, Δ^{u}, Σ^1, and Σ^2 and (ii) to take place in the subspaces $\mathbb{T}_p$. Thus, we first need to investigate the possible bifurcation scenarios for the fixed points in $\mathbb{T}_p$. Doing so, we focus mainly on the case $p = 1/2$. Afterwards, we discuss how the scenarios change qualitatively if one considers $p \neq 1/2$.

5.3 FIXED POINT BIFURCATIONS IN $\mathbb{T}_p$

For fixed p and sufficiently small $|\kappa|$, the two-cluster subspace $\mathbb{T}_p$ contains exactly four fixed points Δ^{s}, Δ^{u}, Σ^1, and Σ^2. Of these, only the two saddles are expected to play a role in any global bifurcation, leading to periodic two-cluster states: The synchronous fixed point Δ^{u} is completely unstable for $\kappa < 0$ and does not go through any bifurcation while Δ^{s} only takes part in a Transcritical Homoclinic Bifurcation (THB) at κ_0 which yields different periodic states, discussed in Chapter 6. However, the four fixed points do not exist independently of each other, but can go through local bifurcations as well, which is what we discuss next. For simplicity, we focus for now on the case $p = 1/2$, i. e., the case of symmetric two-cluster states.[1] This is in accordance with our empirical observations. For values of p far off $1/2$, integration for randomly chosen initial conditions rarely lead to stable periodic two-cluster states in our numerical studies. The reason for this will become clear when we discuss stability in Section 5.5.

1 Note that in doing so, we assume N to be even. In our numerical experiments, the results for uneven N looked rather similar with symmetric two-cluster states being replaced by states, consisting of two equally sized clusters and a singleton.

5.3.1 *Destabilization of* Δ^{s}

It was shown in [ZT16], that Δ^{s} is, for sufficiently small $|\kappa|$, the only attractor of systems like (2.6) but looses stability in a THB [AKS90; AS92] at some $\kappa_0 < 0$, i. e., when the coupling becomes sufficiently repulsive. For the choice (5.1a) of h, the critical value for κ and the on-site parameters ω and ϵ are interrelated by the expression[2]

$$\begin{aligned} 0 = &-1 + 12\epsilon^2 - 48\epsilon^4 + 64\epsilon^6 + \kappa_0^2 + 4\epsilon^2\kappa_0^2 - \\ &- 32\epsilon^4\kappa_0^2 - 4\epsilon\kappa_0^3 + 4\epsilon^2\kappa_0^4 + \omega^2 - 80\epsilon^2\omega^2 - \\ &- 128\epsilon^4\omega^2 + 32\epsilon^2\kappa_0^2\omega^2 + 64\epsilon^2\omega^4. \end{aligned} \tag{5.5}$$

This expression can be solved for κ_0 in terms of a power series in ϵ which reads up to quadratic order

$$\kappa_0 = -\sqrt{1-\omega^2} + 2(1-\omega^2)\epsilon + 2\omega^2\frac{4\omega^2-5}{\sqrt{1-\omega^2}}\epsilon^2 + \mathcal{O}(\epsilon^3). \tag{5.6}$$

As described in [ZT16], the destabilization of Δ^{s} through the THB is a highly degenerate event. Firstly, the derivative $\mathrm{D}\boldsymbol{F}(\Delta^{\mathrm{s}})$ of the right hand side of (2.6) possesses an eigenvalue of multiplicity $N-1$, which becomes zero at κ_0. Secondly, at the THB, $\Delta^{\mathrm{s}} \in \mathbb{T}^N$ coalesces with $\sim 2^{N-1}$ saddles, which are asynchronous for $\kappa \neq \kappa_0$. These saddles are all two-cluster steady states that lie in different subspaces $\mathbb{T}_p \subset \mathbb{T}^N$ so that for every $\mathbb{T}_p$ with $p \neq 1/2$, either one of the two $\Sigma^i \in \mathbb{T}_p$ which already exist for $\kappa = 0$ coincides with Δ^{s} or one of two new asynchronous fixed points Ξ^i which may emerge in additional saddle-node bifurcations, discussed further below.

When we write Σ^i (and later Ξ^i, see below), it is always assumed that $i \in \{1, 2\}$.

The homoclinic bifurcation of Δ^{s} at κ_0 is transcritical only with respect to the two-cluster subspaces $\mathbb{T}_p$ with $p \neq 1/2$. There, the saddles $\Sigma^i, \Xi^i \in \mathbb{T}_p$ exist for all κ in an open neighborhood of κ_0, are unstable in $\mathbb{T}_p$ for $\kappa > \kappa_0$, and stable in $\mathbb{T}_p$ for $\kappa < \kappa_0$, cf. [ZT16].[3] However, the symmetric $\Sigma^i, \Xi^i \in \mathbb{T}_{1/2}$ play an exceptional role due to the equivariance of (2.6) under permutations of clusters A and B for $p = 1/2$. In $\mathbb{T}_{1/2}$, the transcritical bifurcation is replaced by a pitchfork bifurcation, as demonstrated in the next section. Thus, for the case $p = 1/2$, the participating fixed points Σ^i or Ξ^i only exist for either $\kappa > \kappa_0$ in case of a subcritical pitchfork or for $\kappa < \kappa_0$ for a supercritical pitchfork, see Figure 5. Here, a solid line indicates a stable (in $\mathbb{T}_{1/2}$) fixed point while a dashed line indicates an unstable one. The green line represents the synchronous fixed point Δ^{s} while black lines represent two-cluster saddles. Whether the pitchfork is sub- or supercritical can have implications on what global bifurcations, leading to periodic orbits, are possible.

2 The expressions (5.5) and (5.6) as well as similar ones for the case of perturbation type (5.1b) are derived in Appendix B.

3 Note that this does not imply that they are stable in the full phase space $\mathbb{T}^N$ for $\kappa < \kappa_0$. They are in fact unstable in $\mathbb{T}^N$ since they are generally unstable against splitting perturbations, in accordance with [ZT16].

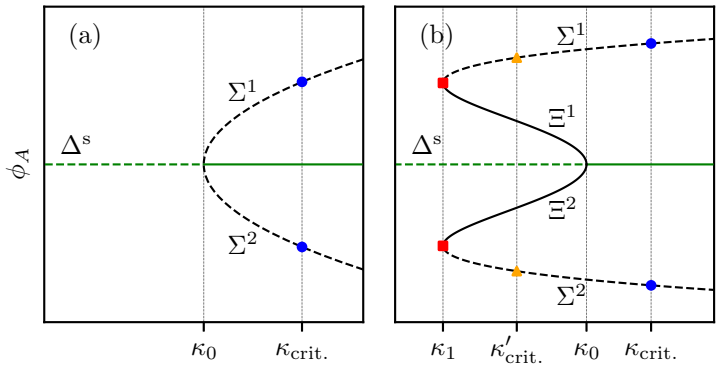

Figure 5: Schematic depiction of the simplest possible bifurcation scenarios, involving Δ^s and the saddles $\Sigma^i, \Xi^i \in \mathbb{T}_{1/2}$, $i \in \{1, 2\}$. Solid lines represent stable fixed points (in $\mathbb{T}_{1/2}$) while dashed lines indicate unstable ones. Panel (a): A subcritical pitchfork occurs at κ_0. Global bifurcations that yield periodic two-cluster states, involve the saddles Σ^i and thus must occur for some $\kappa_{crit.} > \kappa_0$ (blue dots). Panel (b): A supercritical pitchfork occurs at κ_0 and yields new stable steady states Ξ^i which generically vanish in simultaneous saddle-node bifurcations with the Σ^i for some $\kappa_1 < \kappa_0$. Periodic two-cluster states can emerge in two possible ways. Either, they are created in a double-heteroclinic bifurcation for some $\kappa_1 < \kappa'_{crit.} < \kappa_0$ (yellow triangles) or $\kappa_{crit.} \geq \kappa_0$ (blue dots), or in a double-SNIC at κ_1 (red squares). In case of a double-heteroclinic bifurcation, multistability in $\mathbb{T}_{1/2}$ can occur: If the periodic orbit emerges at $\kappa_{crit.} > \kappa_0$ and is stable, it is a second attractor besides Δ^s. Basins of attraction are separated by the unstable manifolds of the Σ^i.

In principle, there are no limitations as to what kinds of limit cycle bifurcations can occur in $\mathbb{T}_{1/2}$ with respect to κ. Depending on the form of the perturbation term $h(\phi)$, one might encounter saddle-node limit cycle bifurcations, giving rise to pairs of stable and unstable periodic orbits or heteroclinic bifurcations that involve additional saddles which themselves may emerge in independent local fixed point bifurcations. However, if we are parsimonious with assumptions on the existence of additional invariant sets being involved in the creation of periodic two-cluster states, only two possible scenarios, depicted in Figure 5, are expected.

If the pitchfork is subcritical, the two saddles Σ^i merge with Δ^s at κ_0, rendering it unstable, see Panel (a). In this case, since for $\kappa < \kappa_0$, the only fixed points left are Δ^s and Δ^u, which are both unstable in $\mathbb{T}_{1/2}$ and seem to not be involved in any further bifurcations, any occurring periodic orbits are expected to emerge for some $\kappa_0 < \kappa_{crit.} < 0$ and must involve both saddles Σ^i (blue dots), due to symmetry. On the other hand, if the pitchfork is supercritical, it yields two new asynchronous fixed points Ξ^i, stable in $\mathbb{T}_{1/2}$, which take over the role of Δ^s as attractors in that space as depicted in Panel (b). Generically, the new steady states Ξ^i and the saddles Σ^i can vanish for some $\kappa_1 < \kappa_0$ in two simultaneous saddle-node bifurcations (again due to permutation symmetry). In this case, two distinct scenarios, leading to periodic orbits, are possible. Either, these states are formed in a global bifurcation that involve only the Σ^i, e. g., in form of two simultaneous heteroclinic

bifurcations (henceforth called a *double-heteroclinic bifurcation*). This can, for example, happen for some $\kappa_0 \leq \kappa_{\text{crit.}} < 0$ (blue dots in Figure 5) or for some $\kappa_1 < \kappa'_{\text{crit.}} < \kappa_0$ (yellow triangles), i. e., before or after the pitchfork occurs. A second type of scenario would consist of two simultaneous SNICs (henceforth called a *double*-SNIC) at κ_1 (red squares). Again, for $\kappa < \kappa_1$ no creation of periodic orbits can take place without assuming additional more complex bifurcation scenarios.

This means in particular that a subcritical pitchfork should always imply a double-heteroclinic bifurcation while observing a double SNIC implies that Δ^{s} went through a supercritical pitchfork, before. We demonstrate in what follows that the proposed scenarios indeed occur. Before we come to this, we discuss first a criterion for the criticality of the pitchfork bifurcation of Δ^{s}.

5.3.2 *Criterion of Criticality for the Pitchfork Bifurcation of* Δ^{s}

In this section, we show that a pitchfork bifurcation of Δ^{s} occurs in $\mathbb{T}_{1/2}$ and determine whether it is sub- or supercritical. For this, we consider a more general class of systems

$$\begin{aligned} \dot{\phi}_A &= F(\phi_A) + \frac{\kappa}{2} G(\phi_B - \phi_A) \\ \dot{\phi}_B &= F(\phi_B) + \frac{\kappa}{2} G(\phi_A - \phi_B) \end{aligned} \tag{5.7}$$

where F and G are assumed to be sufficiently smooth and $G(0) = 0$. If Δ^{s} is a stable fixed point for $\kappa = 0$, we have $F(\phi^{\text{s}}) = 0$ and $F'(\phi^{\text{s}}) < 0$. Criticality is then determined via the following proposition:

Proposition 5.1 *Let $\Delta^{\text{s}} = (\phi^{\text{s}}, \phi^{\text{s}})$ denote the synchronous fixed point of the system (5.7) of two coupled Active Rotators where ϕ^{s} denotes the stable fixed point of the single AR $\dot{\phi} = F(\phi)$. If the coupling function G is odd and does not vanish identically and the first three derivatives of F at ϕ^{s} and G at 0 exist, the system undergoes a pitchfork bifurcation at $\kappa_0 = F'(\phi^{\text{s}})/G'(0)$. Moreover, this pitchfork is supercritical if the quantity*

$$c \coloneqq \frac{3F''(\phi^{\text{s}})^2 G'(0)}{F'(\phi^{\text{s}})\left(F'''(\phi^{\text{s}})G'(0) - 4F'(\phi^{\text{s}})G'''(0)\right)} \tag{5.8}$$

fulfills $0 < c < 1$. For $c < 0$ or $c > 1$, the pitchfork is subcritical.

To prove this proposition, we first make the following simple geometric observation:

Assertion 5.2 *Any two parabolas $y_1(x) = a_1 + b_1 x^2/2$ and $y_2(x) = a_2 + b_2 x^2/2$ with either (a) $b_1 > b_2 > 0$, (b) $0 > b_1 > b_2$, or (c) $b_1 > 0 > b_2$ intersect if and only if $a_1 < a_2$, as depicted in Panels (a), (b), and (c) in Figure 6. On the other hand, if (d) $b_1 < 0 < b_2$, they intersect if and only if $a_1 > a_2$, cf. Panel (d).*

Remark 5.3 *The first three cases amount to the condition $b_1 > b_2$. To distinguish them anyway is necessary for the "graphic" proof in Figure 6.*

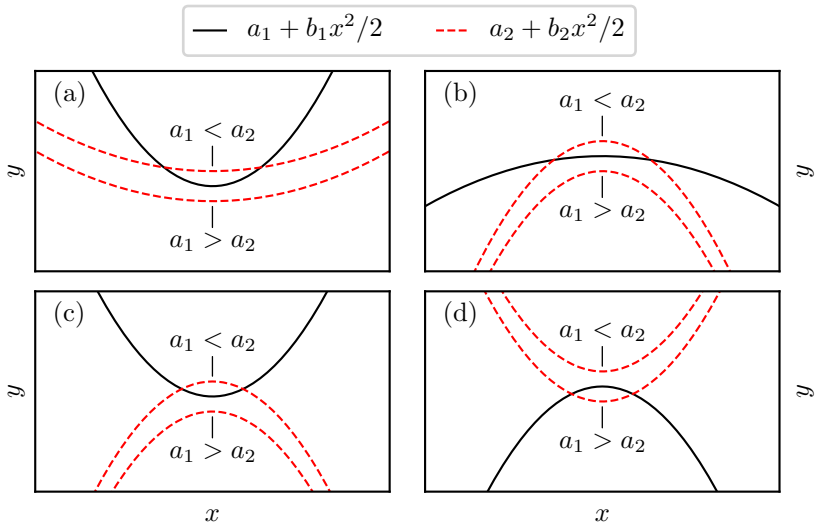

Figure 6: Two parabolas $y_1(x) = a_1 + b_1x^2/2$ and $y_2(x) = a_2 + b_2x^2/2$ with either $b_1 > b_2 > 0$, $0 > b_1 > b_2$, or $b_1 > 0 > b_2$ intersect if and only if $a_1 < a_2$, see Panels (a), (b), and (c). On the other hand, if $b_1 < 0 < b_2$ holds, the parabolas only intersect if $a_1 > a_2$, see Panel (d).

Note also that case (d) is equivalent to (c) as can be seen by switching indices.

We now prove Proposition 5.1.

Proof. Without loss of generality, assume $G'(0) > 0$ which in particular implies repulsive coupling for $\kappa < 0$. Since the system (5.7) is invariant under permutations of the clusters, so are the ϕ_A- and ϕ_B-nullclines. It is convenient to make a change of coordinates to $x = (\phi_A - \phi_B)/2$ and $y = (\phi_A + \phi_B)/2$ which essentially constitutes a clockwise rotation of the system by $\pi/4$. Note that in these coordinates, Δ^s reads $\Delta^s = (0, \phi^s)$. Further, permutation invariance of the original system translates to a mirror symmetry along the y-axis. We find

$$\dot{x} = f(x, y)$$
$$\dot{y} = g(x, y)$$

with

$$f(x, y) = \frac{1}{2}[F(x + y) - F(y - x)] - \frac{\kappa}{2}G(2x)$$
$$g(x, y) = \frac{1}{2}[F(x + y) + F(y - x)]$$

for which $f(-x, y) = -f(x, y)$ and $g(-x, y) = g(x, y)$ hold. The x-nullcline $y_x(x)$ and y-nullcline $y_y(x)$ are then defined by $0 = f(x, y_x(x))$ and $0 = g(x, y_y(x))$, respectively. The x-nullcline has a trivial branch $x = 0$, which corresponds to the fact that the diagonal $\phi_A = \phi_B$ is invariant under the flow of (5.7). We can therefore factor out this branch

by considering y_x as the solution of $0 = f(x, y_x(x))/x$. Mirror symmetry around the y-axis implies that the nullclines are even functions

$$y_x(x) = a_x + \frac{1}{2} b_x x^2 + \mathcal{O}(x^4) \tag{5.10a}$$

$$y_y(x) = a_y + \frac{1}{2} b_y x^2 + \mathcal{O}(x^4). \tag{5.10b}$$

Fixed points constitute intersections of nullclines. To determine whether the assumed pitchfork of Δ^{s} at κ_0 is sub- or supercritical we make use of Assertion 5.2 by determining and comparing the quadratic coefficients b_x and b_y in the series expansions (5.10) and evaluating which case of the assertion applies to the them.

We start with computing the y-nullcline. Inserting (5.10b) into $0 = g(x, y)$ yields

$$0 = F(a_y) + \frac{1}{2} \left[b_y F'(a_y) + F''(a_y) \right] x^2 + \mathcal{O}(x^4)$$

and by collecting powers of x, we find

$$\begin{aligned} 0 &= F(a_y) \\ 0 &= b_y F'(a_y) + F''(a_y). \end{aligned}$$

The first equation is just the fixed point equation for a single Active Rotator and thus has solutions ϕ^{s} and ϕ^{u} where only the first one is of interest for us. The second equation can then be solved for b_y, which yields

$$b_y = -\frac{F''(\phi_s)}{F'(\phi_s)}.$$

Since ϕ^{s} is stable and does not depend on κ, the denominator is negative and we have

$$\begin{aligned} \operatorname{sign} b_y &= \operatorname{sign} F''(\phi^{\mathrm{s}}) \\ \frac{\mathrm{d}a_y}{\mathrm{d}\kappa} &= 0. \end{aligned}$$

Next, we determine the quadratic expansion for the nontrivial branch of the x-nullcline, defined by $0 = f(x, y_x(x))/x$, for which the Taylor expansion in x reads

$$\begin{aligned} 0 = &- \frac{\kappa}{2x} G(0) + \left[F'(a_x) - \kappa G'(0) \right] - \kappa G''(0)\, x + \\ &+ \frac{1}{6} \left[3 b_x F''(a_x) + F'''(a_x) - 4\kappa G'''(0) \right] x^2 + \mathcal{O}(x^4). \end{aligned}$$

Collecting powers of x and noting that the terms of odd power of x vanish identically since G is odd, we are left with

$$\begin{aligned} 0 &= F'(a_x) - \kappa G'(0) \\ 0 &= 3 b_x F''(a_x) + F'''(a_x) - 4\kappa G'''(0). \end{aligned}$$

From the first equation we read the critical coupling $\kappa_0 = F'(\phi^{\mathrm{s}})/G'(0) < 0$ since at the bifurcation, we have $a_x = \phi^{\mathrm{s}}$. However, in general we have to consider a_x as a function of κ. Solving the equations for b_x yields

$$b_x = \frac{4F'(a_x)G'''(0) - F'''(a_x)G'(0)}{3F''(a_x)G'(0)}.$$

To summarize, we find that

$$\operatorname{sign} b_x = \operatorname{sign} b_y \cdot \operatorname{sign}\left(4F'(\phi^{\mathrm{s}})G'''(0) - F'''(\phi^{\mathrm{s}})G'(0)\right)$$
$$\operatorname{sign} \frac{\mathrm{d}a_x}{\mathrm{d}\kappa}(\phi^{\mathrm{s}}) = \operatorname{sign} \frac{\mathrm{d}\kappa}{\mathrm{d}a_x}(\phi^{\mathrm{s}}) = \frac{F''(\phi^{\mathrm{s}})}{G'(0)} = \operatorname{sign} b_y.$$

Note also that the quantity c in (5.8) is given by

$$c := \frac{b_y}{b_x|_{a_x=\phi^{\mathrm{s}}}} = \frac{3F''(\phi^{\mathrm{s}})^2 G'(0)}{F'(\phi^{\mathrm{s}})\left(F'''(\phi^{\mathrm{s}})G'(0) - 4F'(\phi^{\mathrm{s}})G'''(0)\right)}.$$

We are now able to finally prove the proposition. Note first that Δ^{s} is always unstable for $\kappa < \kappa_0$ and goes through some bifurcation at κ_0. To determine whether it is a sub- or supercritical pitchfork, it suffices to determine whether $y_x(x)$ and $y_y(x)$ intersect at $\kappa = \kappa_0 + \delta\kappa$ or $\kappa = \kappa_0 - \delta\kappa$ in the vicinity of $x = 0$ for sufficiently small $\delta\kappa > 0$ because these intersections yield the two other fixed points that coalesce with Δ^{s} in $\mathbb{T}_{1/2}$ in the pitchfork at κ_0. Note that we have $a_y = \phi^{\mathrm{s}} = a_x(\kappa_0)$ with $\mathrm{d}a_x/\mathrm{d}\kappa(\kappa_0) \neq 0$ so that if the nullclines intersect for $\kappa_0 + \delta\kappa$, they cannot intersect for $\kappa_0 - \delta\kappa$ because of Assertion 5.2 and hence the bifurcation is a subcritical pitchfork. On the other hand, if they intersect for $\kappa_0 - \delta\kappa$, they cannot intersect for $\kappa_0 + \delta\kappa$ for the same reason and thus, the bifurcation is a supercritical pitchfork. We now have to distinguish six cases to determine criticality, where we approximate the nullclines up to quadratic order and compare with the cases (a)-(d) from Assertion 5.2. For the first four cases, we have $4F'(\phi^{\mathrm{s}})G'''(0) - F'''(\phi^{\mathrm{s}})G'(0) > 0$:

1. $b_y > b_x > 0$ implies $\mathrm{d}a_x/\mathrm{d}\kappa > 0$ and $c > 1$. Hence, comparing with case (a) of Assertion 5.2 with $y_1(x) = y_y(x)$ and $y_2(x) = y_x(x)$, the nullclines intersect only for $\kappa_0 + \delta\kappa$ where $a_y = a_x(\kappa_0) < a_x(\kappa_0 + \delta\kappa)$ and the pitchfork is subcritical.

2. $b_x > b_y > 0$ implies $\mathrm{d}a_x/\mathrm{d}\kappa > 0$ and $0 < c < 1$. Hence, comparing with case (a) of Assertion 5.2 with $y_1(x) = y_x(x)$ and $y_2(x) = y_y(x)$, the nullclines intersect only for $\kappa_0 - \delta\kappa$ where $a_x(\kappa_0 - \delta\kappa) < a_x(\kappa_0) = a_y$ and the pitchfork is supercritical.

3. $0 > b_y > b_x$ implies $\mathrm{d}a_x/\mathrm{d}\kappa < 0$ and $0 < c < 1$. Hence, comparing with case (b) of Assertion 5.2 with $y_1(x) = y_x(x)$ and $y_2(x) = y_y(x)$, the nullclines intersect only for $\kappa_0 - \delta\kappa$ where $a_x(\kappa_0 - \delta\kappa) > a_x(\kappa_0) = a_y$ and the pitchfork is supercritical.

4. $0 > b_x > b_y$ implies $\mathrm{d}a_x/\mathrm{d}\kappa < 0$ and $c > 1$. Hence, comparing with case (b) of Assertion 5.2 with $y_1(x) = y_x(x)$ and $y_2(x) = y_y(x)$, the nullclines intersect only for $\kappa_0 + \delta\kappa$ where $a_y = a_x(\kappa_0) < a_x(\kappa_0 + \delta\kappa)$ and the pitchfork is subcritical.

Assuming $4F'(\phi^{\mathrm{s}})G'''(0) - F'''(\phi^{\mathrm{s}})G'(0) < 0$ yields the remaining two cases:

5. $b_y > 0 > b_x$ implies $\mathrm{d}a_x/\,\mathrm{d}\kappa > 0$ and $c < 0$. Hence, comparing with case (c) of Assertion 5.2 with $y_1(x) = y_y(x)$ and $y_2(x) = y_x(x)$, the nullclines intersect only for $\kappa_0+\delta\kappa$ where $a_y = a_x(\kappa_0) < a_x(\kappa_0 + \delta\kappa)$ and the pitchfork is subcritical.

6. $b_x > 0 > b_y$ implies $\mathrm{d}a_x/\,\mathrm{d}\kappa < 0$ and $c < 0$. Hence, comparing with case (d) of Assertion 5.2 with $y_1(x) = y_y(x)$ and $y_2(x) = y_x(x)$, the nullclines intersect only for $\kappa_0+\delta\kappa$ where $a_x(\kappa_0+\delta\kappa) < a_x(\kappa_0) = a_y$ and the pitchfork is subcritical.

This completes the proof. □

In case of systems of type (5.2) with $p = 1/2$, the quantity c in Proposition 5.1 reads

$$c = \frac{3(\sin\phi^{\mathrm{s}} + \epsilon h''(\phi^{\mathrm{s}}))^2}{(\cos\phi^{\mathrm{s}} - \epsilon h'(\phi^{\mathrm{s}})(3\cos\phi^{\mathrm{s}} - 4\epsilon h'(\phi^{\mathrm{s}}) - \epsilon h'''(\phi^{\mathrm{s}}))}$$

which yields

$$c_1 = \frac{(\sin\phi^{\mathrm{s}} - 4\epsilon\sin 2\phi^{\mathrm{s}})^2}{\cos\phi^{\mathrm{s}}(\cos\phi^{\mathrm{s}} - 2\epsilon\cos 2\phi^{\mathrm{s}})} \tag{5.11}$$

for $h(\phi) = \sin 2\phi$. The corresponding expression for our second perturbation $h(\phi) = 1/(\sin\phi - 2) + 1/\sqrt{3} + (4/\sqrt{3} - 2)\sin\phi$ is given by

$$c_2 = -\frac{3X^2}{(\epsilon Y_1 - 1)(\epsilon Y_2 + 3)}$$

with

$$\begin{aligned}
X &= \frac{\epsilon}{3}\left(\frac{3}{(\sin\phi^{\mathrm{s}} - 2)^2} - 4\sqrt{3} + 6\right)\tan\phi^{\mathrm{s}} + \frac{2\epsilon\cos\phi^{\mathrm{s}}}{(\sin\phi^{\mathrm{s}} - 2)^3} + \tan\phi^{\mathrm{s}} \\
Y_1 &= -\frac{1}{(\sin\phi^{\mathrm{s}} - 2)^2} + \frac{4}{\sqrt{3}} - 2 \\
Y_2 &= \frac{3}{(\sin\phi^{\mathrm{s}} - 2)^2} - \frac{12}{(\sin\phi^{\mathrm{s}} - 2)^3} - \frac{18}{(\sin\phi^{\mathrm{s}}) - 2)^4} - 4\sqrt{3} + 6.
\end{aligned}$$

A change of criticality occurs if c becomes either one or zero. These degenerate cases constitute codimension 2 bifurcations in the parameter space, spanned by ω, ϵ, and κ. For the case (5.1a), this one-dimensional set fulfills

$$\begin{aligned}
0 = &+ 4\Big[1 - 2\omega^2\Big]^2 + \Big[1796\omega^6 - 1924\omega^4 + 545\omega^2 - 48\Big]\epsilon^2 + \\
&+ 4\Big[16384\omega^8 - 22272\omega^6 + 9390\omega^4 - 1393\omega^2 + 48\Big]\epsilon^4 - \\
&- 4\Big[256\omega^4 - 273\omega^2 + 64\Big]\epsilon^6
\end{aligned} \tag{5.12}$$

for $c_1 = 1$, as shown in Appendix C. The second case $c_1 = 0$ is of no importance because it did not occur in our work. We refrain from

deriving a similar expression for perturbation type (5.1b) due to its complicated form. Note that the switch in criticality constitutes also the curve in the parameter space along which the two-dimensional surface of saddle-node bifurcations branches off the equally two-dimensional surface of pitchfork bifurcations because the saddle-node bifurcation exclusively accompanies the supercritical pitchfork.

A word is at hand, considering the case $p \neq 1/2$. Here, the permutation symmetry between the clusters is removed so that pitchforks cannot occur. Instead, the pitchforks are replaced by either (i) a transcritical bifurcation of one of the saddles Σ^i with Δ^{s}, in which these two switch stabilities, followed by a saddle-node bifurcation with the second Σ^{i+1} (here, we set $2+1 \equiv 1$) for the subcritical case. The bifurcation diagram looks then similar to Panel (a) in Figure 5 where the parabola is now shifted either up or down. (ii) For the supercritical case, we find a saddle-node bifurcation in which the Ξ^i are born, followed by a transcritical bifurcation of one of them (the saddle of the pair) with Δ^{s}, where it switches stability with Δ^{s}. Then, the two saddle-node bifurcations of the Σ^i and Ξ^i occur, even though not necessarily for the same κ. Graphically, this amounts to a vertical shift of the quartic curve in Panel (b) of Figure 5 accompanied by a distortion of the two asynchronous branches.

With these considerations, we end our discussion of the fixed point bifurcations in $\mathbb{T}_p$ and come to the bifurcation scenarios that yield periodic two-cluster states.

5.4 LIMIT CYCLE BIFURCATIONS IN $\mathbb{T}_p$

As mentioned in the beginning of this chapter, periodic two-cluster states must be created in global bifurcations which, in their simplest form, only involve the four fixed points Δ^{s}, Δ^{u}, Σ^1, and Σ^2, and possibly the asynchronous fixed points Ξ^1 and Ξ^2, if the pitchfork at κ_0 for $p = 1/2$ is supercritical if we assume that there are no further fixed points present. These bifurcations are expected to take place in the respective two-cluster subspaces $\mathbb{T}_p$ because they must also be observed in the reduced description (5.2). In our investigations, we observed two types of bifurcations, leading to periodic states. Either via a double-heteroclinic bifurcation or, reminiscent to the single SNIC-element, a double-SNIC. We discuss both bifurcations in what follows. For definiteness, we consider only the perturbation type (5.1a) of the form $h(\phi) = \sin 2\phi$. The same scenarios can however be found for the generic perturbation (5.1b) which further supports the argument that these scenarios are generic for systems of type (2.6).

In order to discuss the scenarios, we plot the phase diagrams together with the necessary invariant structures, as exemplified in Figure 7. Periodic boundary conditions for ϕ_A and ϕ_B are always indicated by black arrowheads along the boundaries of the square plot so that opposite sides of it are identified with each other. For now, the vector field of (5.2) is depicted as small black arrows in the square. In later diagrams,

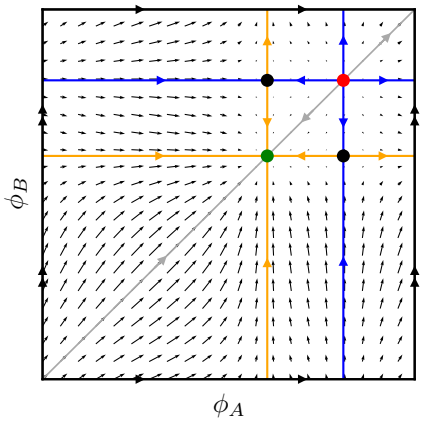

Figure 7: Example phase plot of the system (5.2) with $h(\phi) = \sin 2\phi$ and for $p = 1/2$. System parameters are set to $\omega = 0.8$, $\epsilon = -0.2$, and $\kappa = 0$. Black arrowheads at the boundary indicate the periodic boundary conditions in ϕ_A and ϕ_B. The gray diagonal line indicates the invariant diagonal space Δ with the fixed points Δ^{s} (green dot) and Δ^{u} (red dot). The saddles Σ^1 and Σ^2 (black dots) are connected via their stable manifolds (blue lines) with Δ^{u} and their unstable manifolds (orange lines) with Δ^{s}. Arrowheads indicate the flow along each invariant contour.

we do not show the field any longer to not clutter the plots. At $\kappa = 0$, the system is the product of two independent clusters A and B. Thus, the stable manifolds of the saddles (black discs) are of the form $\{\phi^{\mathrm{u}}\}\times\mathbb{S}^1$ for $\Sigma^1 = (\phi^{\mathrm{u}}, \phi^{\mathrm{s}})$ and $\mathbb{S}^1 \times \{\phi^{\mathrm{u}}\}$ for $\Sigma^2 = (\phi^{\mathrm{s}}, \phi^{\mathrm{u}})$ and connect the saddles with Δ^{u} (red dot). These manifolds are depicted as blue lines in what follows. On the other hand, the unstable manifold of Σ^1 is of the form $\mathbb{S}^1 \times \{\phi^{\mathrm{s}}\}$ while the unstable manifold of Σ^2 is given by $\{\phi^{\mathrm{s}}\} \times \mathbb{S}^1$. These manifolds connect the saddles with Δ^{s} (green dot) and are depicted as orange lines. The flow along the manifolds is indicated by arrowheads. Additionally, the invariant diagonal space Δ is depicted with the direction of its flow as a gray line, connecting Δ^{s} and Δ^{u}.

All of these manifolds are, as products of NHIMs, themselves NHIMs [FM71; HPS77] and are thus persistent for sufficiently small $|\kappa| > 0$ and are the building blocks for the sought bifurcation scenarios. Our discussion is mainly qualitative because it is in general not possible to determine analytic expressions for the critical coupling $\kappa_{\mathrm{crit.}}$ at which, e. g., a double-heteroclinic bifurcation occurs. Standard numerical techniques to determine such bifurcations are the orthogonal collocation method and the shooting method [Kuz13]. We employ a variation of the latter one. Its main idea is simple and easy to implement for planar systems. For a heteroclinic bifurcation at $\kappa_{\mathrm{crit.}}$, the unstable manifold of, say, Σ^1 coincides with the stable manifold of Σ^2. Thus, if κ deviates by a small amount $\delta\kappa > 0$ from $\kappa_{\mathrm{crit.}}$, the unstable manifold misses Σ^2 and instead, after a fast approach, departs from it, trailing the unstable manifold of Σ^2. For $\kappa_{\mathrm{crit.}} + \delta\kappa$ and $\kappa_{\mathrm{crit.}} - \delta\kappa$, this departure happens in opposite directions, depending on which side of the stable manifold

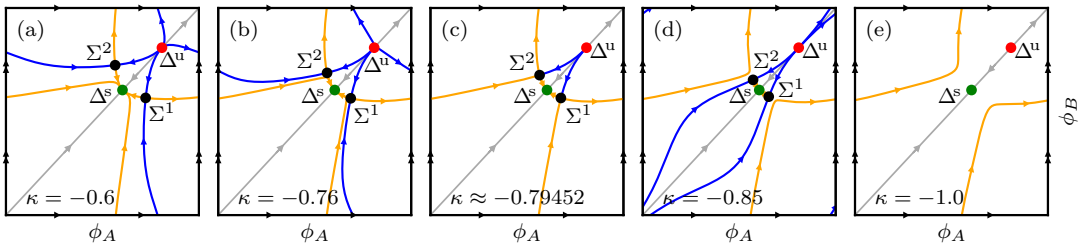

Figure 8: Example of a double-heteroclinic bifurcation, leading to a symmetric ($p = 1/2$) periodic two cluster state. On-site parameters are set to $\omega = 0.8$ and $\epsilon = -0.2$. From the left to the right, the coupling becomes more repulsive. Starting with a moderately repulsive coupling in Panel (a) and well separated stable and unstable manifolds of the Σ^i, these manifolds approach each other in Panel (b). Panel (c) shows the double-heteroclinic bifurcation: both saddles are connected by a heteroclinic cycle (orange line). In Panel (d), a stable periodic orbit (orange closed line) has formed while the synchronous fixed point Δ^{s} is also still stable. In Panel (e), the saddles have merged with Δ^{s} in a subcritical pitchfork, rendering it unstable, transversal to the diagonal Δ. At this point, the symmetric periodic orbit remains the only attractor in $\mathbb{T}_{1/2}$.

of Σ^2 the "shot" from Σ^1 arrives at. Hence, by narrowing down the interval in which the flip in the direction of departure occurs, one can determine $\kappa_{\mathrm{crit.}}$.

We start our discussion of bifurcation scenarios with the double-heteroclinic bifurcation.

5.4.1 *The Double-Heteroclinic Bifurcation*

5.4.1.1 *Symmetric Two-Cluster States*

We start with discussing the symmetric case $p = 1/2$. Fixing on-site parameters $\omega = 0.8$ and $\epsilon = -0.2$, in Figure 8, we show, from the left to the right, a typical double-heteroclinic bifurcation scenario for increasing repulsiveness in the case of a subcritical pitchfork bifurcation. On the torus $\mathbb{T}_{1/2}$, for moderate coupling in Panel (a), we start with the unstable manifolds (orange lines) which connect the saddles Σ^i with the still stable diagonal fixed point Δ^{s}. On the other hand, the stable manifolds (blue lines) of the Σ^i connect them with the unstable node Δ^{u}. As repulsion increases in Panel (b), the long branches of the unstable manifold of Σ^i and the stable manifold of Σ^{i+1} (where we set $2+1 \equiv 1$) approach each other until they merge for the critical coupling $\kappa_{\mathrm{crit.}}$ in Panel (c). At this point, a heteroclinic cycle (cf. [Fie20]) forms, connecting Σ^1 and Σ^2 with each other. Its subsequent breakup in Panel (d) results in the periodic two-cluster state (orange line). Stability of this orbit within $\mathbb{T}_{1/2}$ is determined through the competition between expansion and contraction near the saddles Σ^i, i. e., by the sum $\lambda^-(\Sigma^i)+\lambda^+(\Sigma^i)$ of eigenvalues of the Jacobian of (5.2) at Σ^i at the bifurcation [Fie20]. In general, this sum reads

$$\lambda^-(\phi_A, \phi_B) + \lambda^+(\phi_A, \phi_B) = f'(\phi_A) + f'(\phi_B) - \kappa \cos(\phi_A - \phi_B).$$

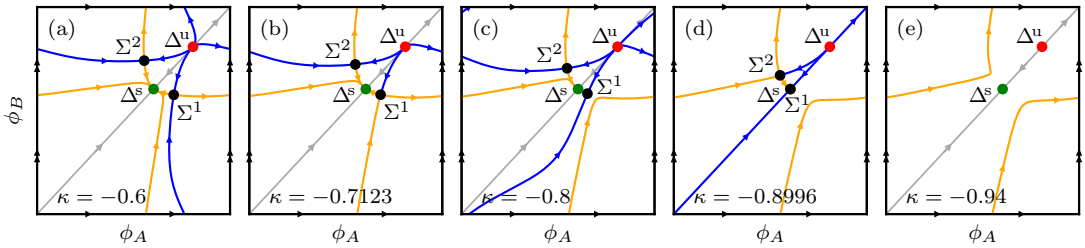

Figure 9: Unfolding of the double-heteroclinic bifurcation for $p = 2/5$. On-site parameters are fixed at $\omega = 0.8$ and $\epsilon = -0.2$. Starting with moderate coupling strength in Panel (a), coupling becomes more repulsive from the left to the right. Panel (b) shows a heteroclinic orbit from Σ^2 to Σ^1 (vertical orange line). Increasing $|\kappa|$ further results in the unstable manifold of Σ^2 forming a closed contour with its two branches ending at Δ^s in Panel (c). Panel (d) shows the moment when a homoclinic orbit for Σ^2 forms which results in the creation of an asymmetric periodic two-cluster state after which the Σ^i vanish in a saddle-node bifurcation, see Panel (e).

If this quantity is positive, i. e., if $|\lambda^-(\Sigma^i)| < \lambda^+(\Sigma^i)$, expansion dominates contraction and the limit cycle is unstable. If it is negative, contraction dominates and the limit cycle is stable. According to numerical results, $\lambda^-(\Sigma^i) + \lambda^+(\Sigma^i)$ is indeed always negative at κ_0, so that contraction prevails and the periodic orbit is always stable in $\mathbb{T}_{1/2}$.

A rigorous treatment of two interacting units sufficiently close to a SNIC can be found in [BM13]. The double-heteroclinic bifurcation, discussed here, corresponds to the T-point in Figure 16 of [BM13]. Note that in Panel (d), the system is bi-stable since both the periodic orbit and Δ^s are stable. Their basins of attraction are separated by the stable manifolds of the saddles Σ^i. This holds until the saddles finally merge with Δ^s in the subcritical pitchfork bifurcation. After this point, the periodic orbit has become the only attractor of the system, as depicted in Panel (e).

Note that one can also observe double-heteroclinic bifurcations in case of supercritical pitchforks of Δ^s with $\kappa_1 < \kappa_{\text{crit.}} < \kappa_0$ which look essentially like the scenario, described above. The only difference is that the involved unstable manifolds end in the Ξ^i rather than Δ^s. We come back to this when we discuss double-SNICs in Section 5.4.2.1.

Obviously, the double-heteroclinic bifurcation is not generic in the sense that its two simultaneous heteroclinic bifurcations of the saddles occur simultaneously due to the permutation symmetry of (5.2) for $p = 1/2$. In the next section, we discuss how the picture changes when this degeneracy is removed by setting $p \neq 1/2$.

5.4.1.2 *Asymmetric Two-Cluster States*

As discussed in Section 5.2, periodic two-cluster states with large disparity in cluster sized only exist for sufficiently strong repulsive coupling. For p close to $1/2$, the bifurcation scenario looks more or less the same as for the symmetric case.

In Figure 9, we show a typical bifurcation for $p = 2/5$ which represents, e. g., a two-cluster state with four and six units per respective cluster. On-site parameters are fixed at $\omega = 0.8$ and $\epsilon = -0.2$. Again, we start with moderate coupling in Panel (a) and increase repulsiveness from the left to the right. Now, the permutation symmetry of the system is removed and we find that the saddles go first through a heteroclinic bifurcation in Panel (b). In this bifurcation, the heteroclinic connection from Σ^2 to Σ^1 detaches from Σ^1 and instead connects Σ^2 in both directions of its unstable manifold with Δ^{s}, as depicted in Panel (c). In Panel (d), this connection forms a homoclinic orbit which subsequently detaches from Σ^2, giving rise to the periodic orbit, shown in Panel (e). Note that in Panel (d), the saddle Σ^1 is also very close to Δ^{s}, i. e., the system is close the THB at κ_0. However, this is purely incidental and is due to the choice of on-site parameters. In general, the homoclinic bifurcation of Σ^2 and the THB occur independently of each other. Between the two depicted phase plots in Panels (d) and (e), the saddles Σ^1 and Σ^2 vanish eventually in a saddle-node bifurcation. This bifurcation, together with the transcritical bifurcation of Σ^1 and Δ^{s}, which is not shown here, are the residuals of the subcritical pitchfork for $p = 1/2$, due to the removal of the permutation symmetry. In particular, Σ^1 becomes stable at κ_0, before merging with Σ^2.

With this, we conclude that for $p \neq 1/2$ the degeneracy of the double-heteroclinic bifurcation is lifted which is replaced by a heteroclinic bifurcation, followed by a homoclinic one. Stability of the resulting periodic orbit is, as in the previous section, a matter of whether the sum $\lambda^+ + \lambda^-$ of eigenvalues of the Jacobian of the vector field at Σ^2 is positive or negative by a well-known theorem by Andronov and Leontovich [And+73; Fie20]. Since numerical results suggest that it is always negative, the periodic two-cluster state is asymptotically stable in $\mathbb{T}_p$.

Comparing Figure 9 with Figure 8, we note that while the heteroclinic connection in Panel (b) of the former forms before the double-heteroclinic bifurcation in the symmetric case, the homoclinic bifurcation occurs only for significantly larger $|\kappa|$. This corresponds to our observation in Section 5.2 where we discussed how for periodic two-cluster states with larger disparity between cluster sizes to exist, the coupling must be more repulsive than for the symmetric case.

In the next section, we discuss the double-SNIC which can be observed only if the pitchfork of Δ^{s} at κ_0 is supercritical.

5.4.2 *The Double-SNIC*

The double-heteroclinic bifurcation for $p = 1/2$ or its unfolding for $p \neq 1/2$ are generic in the sense that they must occur if both clusters are sufficiently close to their respective SNIC [BM13]. In this section, we discuss a bifurcation which can be observed if this is not the case: the double-SNIC. We start again with the symmetric case $p = 1/2$.

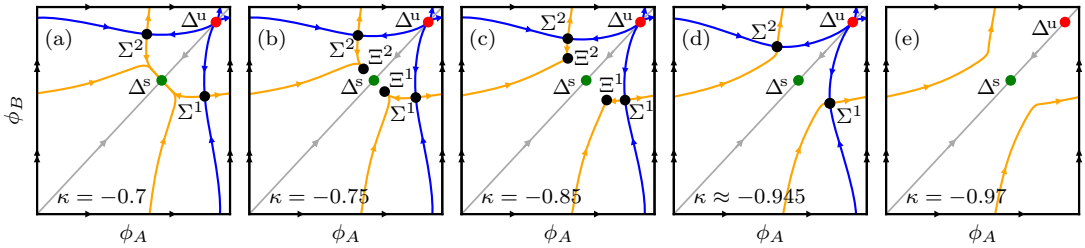

Figure 10: Example for a double-SNIC for a supercritical pitchfork of Δ^{s}. On-site parameters are fixed at $\omega = 0.6$ and $\epsilon = 0.2$. Again, coupling strength increases from the left to the right, starting with moderate coupling in Panel (a). Panel (b) shows the phase plot after the supercritical pitchfork at κ_0. The two new stable asynchronous fixed points Ξ^i take over the role of Δ^{s} as attractors of the system. After the cusped closed contour, formed by the unstable manifolds of the Σ^i, becomes smoothed out in Panel (c). Eventually, the Σ^i and Ξ^i vanish in two simultaneous SNICs in Panel (d). The result is a stable symmetric periodic two-cluster state in Panel (e).

5.4.2.1 *Symmetric Two-Cluster States*

Figure 10 shows a typical double-SNIC if the pitchfork of Δ^{s} at κ_0 is supercritical. On-site parameters are set to $\omega = 0.6$ and $\epsilon = 0.2$. Starting with moderate coupling in Panel (a), we find in Panel (b) that the two asynchronous fixed points Ξ^1 and Ξ^2, stable in $\mathbb{T}_{1/2}$, have formed in the pitchfork and take over the role of Δ^{s} as end points of the unstable manifolds of the Σ^i. At first, the two incoming branches at each Ξ^i end in cusps which subsequently get smoothed out in Panel (c). Panel (d) depicts the simultaneous SNICs where both Ξ^i merge with the Σ^i. From this, the periodic two-cluster state in Panel (e) is finally formed. Its stability is inherited from the two heteroclinic connections of the saddle-nodes in Panel (d), just as for a single SNIC. Since the occurring saddle-nodes are stable in normal direction to the contour, the periodic orbit is also stable in $\mathbb{T}_{1/2}$.

We stress again, that criticality of the pitchfork at κ_0 is not a sufficient condition to conclude that periodic orbits are created in a double-SNIC. In fact, the locus of the heteroclinic bifurcation in Panel (b) of Figure 5, can wander, depending on ω and ϵ, along the saddle branches of the bifurcation diagram. When it ends at the turning point at κ_1 such that periodic orbits are born in double-SNICs, this constitutes an *orbit flip* [Kuz13]. In this codimension 2 event, the direction from where the unstable manifold of saddle Σ^i approaches the stable fixed point Ξ^{i+1} changes from one side to the other along the leading eigenvector of $\mathrm{D}\boldsymbol{F}(\Xi^{i+1})$. For example, the orbit flip from double-heteroclinic to double-SNIC for $\omega = 0.6$ occurs at $\epsilon_{\mathrm{flip}} \approx -0.0245$ when the pitchfork is still supercritical. It becomes subcritical only for $\epsilon < \epsilon_1 \approx -0.1342$, according to the degenerate criticality condition $c_1 = 1$ from Section 5.3.2. Hence, in the regime $\epsilon_1 < \epsilon < \epsilon_{\mathrm{flip}}$ the bifurcation scenario looks as follows: Increasing repulsiveness, we observe first a supercritical pitchfork in which the Ξ^i emerge. Increasing $-\kappa$ further yields a double-heteroclinic bifurcation through which the periodic orbit is created.

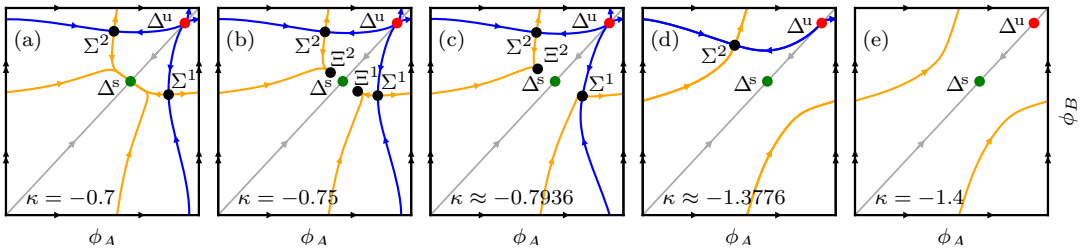

Figure 11: Removing degeneracy of the double-SNIC from the previous section by setting $p = 2/5$. On-site parameters are fixed at $\omega = 0.6$ and $\epsilon = 0.2$ with $|\kappa|$ increasing from the left to the right. Starting with moderate coupling in Panel (a), a stable asynchronous fixed point Ξ^2 and a saddle Ξ^1 form. The latter one goes through a transcritical bifurcation with Δ^{s} thereby switching stability. The result is shown in Panel (b): the unstable manifolds of the Σ^i now end at the respective Ξ^i. In Panel (c), Ξ^1 and Σ^1 vanish in a first SNIC, yielding the two branches of the unstable manifold of Σ^2 to form a closed contour. Panel (d) depicts the second SNIC between Ξ^2 and Σ^2. The result is a stable asymmetric periodic two-cluster orbit, shown in Panel (e).

Increasing $-\kappa$ even more results in two simultaneous saddle-node bifurcations (This scenario corresponds to the case, depicted by yellow triangles in Panel (b) of Figure 5). At $\epsilon = \epsilon_{\mathrm{flip}}$, the last two bifurcations coincide and for $\epsilon > \epsilon_{\mathrm{flip}}$, the periodic orbit emerges in a double-SNIC.

As we will see next, the picture looks again rather similar for the case $p \neq 1/2$ of asymmetric clusters.

5.4.2.2 *Asymmetric Two-Cluster States*

In Figure 11, we show numerical results for the asymmetric case $p = 2/5$, again fixing on-site parameters to $\omega = 0.6$ and $\epsilon = 0.2$. As for the double-heteroclinic bifurcation, the difference to the symmetric double-SNIC is two-fold. Firstly, the supercritical pitchfork is replaced by a saddle-node bifurcation, yielding a saddle Ξ^1 and a stable node Ξ^2. The saddle Ξ^1 and Δ^{s} then go through a transcritical bifurcation at κ_0, where Ξ^1 an Δ^{s} switch stability. The result is depicted in Panel (b): two stable fixed points Ξ^i, to the left and right of Δ^{s}, respectively, have taken over its role as endpoints of the unstable manifolds of the Σ^i. The second difference lies in the fact that the two SNICs now happen consecutively. First, Ξ^1 vanishes together with Σ^1 in Panel (c), which results in the unstable manifold of Σ^2 to connect it with Ξ^2. Then, in a second SNIC, see Panel (d), Ξ^2 and Σ^2 vanish, rendering the invariant circle (orange line) a periodic two-cluster state in Panel (e). As for the symmetric case, the periodic orbit is stable in $\mathbb{T}_p$. Note that again, the contours, formed by the unstable manifolds start cusped and get eventually smoothed out before their respective SNICs.

Note further that, as for the double-heteroclinic bifurcation, we observe that the first SNIC in Panel (c) occurs before the double-SNIC in the symmetric case while the second one in Panel (d) occurs only for significantly more repulsiveness. This again reflects the observation that

for periodic two-cluster states with unequal sizes to form, the coupling must be more repulsive, see Section 5.2.

This concludes our discussion of the found bifurcation scenarios, leading to periodic two-cluster states. We argue that they constitute the most generic bifurcations in which such states can emerge in the sense that they do not require any additional invariant structures and more complicated bifurcations. While the double-heteroclinic scenario is truly generic for two clusters, sufficiently close to their respective SNICs, the double-SNIC has, to our knowledge, not been discussed in the context of repulsively coupled class I excitable elements. Next, we discuss the asymptotic stability of the observed periodic orbits in the full phase space $\mathbb{T}^N$.

5.5 LIMIT CYCLE STABILITY

As we established in Corollary 3.4, two types of asymptotic stability of periodic two-cluster states can be distinguished: it can be splitting or non-splitting. While the reduced system (5.2) offers full information regarding the existence of periodic two-cluster solutions of (2.6) and their asymptotic stability against perturbations that leave both clusters whole we cannot deduce from it whether these orbits are stable against splitting perturbations.

Both, double-heteroclinic bifurcations and double-SNICs create periodic orbits with infinite period T for $\kappa \to \kappa_{\text{crit.}}$. A small deviation from $\kappa_{\text{crit.}}$ still yields an orbit of large period, where the system spends the dominating part of the period in a slow passage through the immediate vicinity of the saddle point (in case of a double-heteroclinic bifurcation) or the "ghosts" of the saddle-nodes (in case of a double-SNIC). Hence, right after the bifurcation, splitting stability is inherited from the saddle or saddle-node: if the saddle (or saddle-node) is stable with respect to splitting perturbations, so is the periodic orbit. The reason for this lies in the fact that the splitting and non-splitting eigenvalues of the vector field Jacobian $\mathrm{D}\boldsymbol{F}$ and hence the respective Floquet multipliers (3.8) depend continuously on the cluster coordinates ϕ_A and ϕ_B of the periodic orbit and thus, if the saddle or saddle-node is stable against splitting perturbations, so is any state close by. Further into the domain of existence for the periodic state, this inheritance is not necessarily the case any more since the orbit spends less time near the saddle or the ghost of the saddle-node.

Since the numerical evidence, presented in the previous section on bifurcations, indicates that the periodic orbits are stable against non-splitting perturbations, we only need to determine the two Floquet multipliers

$$\begin{aligned} \mu^A &= \exp\left(\int_0^T \lambda^A(t)\ \mathrm{d}t\right) \\ \mu^B &= \exp\left(\int_0^T \lambda^B(t)\ \mathrm{d}t\right), \end{aligned} \tag{3.8}$$

defined in Corollary 3.4, which characterize the stability against splitting perturbations of clusters A and B, respectively. For the symmetric case, μ^A and μ^B coincide due to the periodic orbit being a splay state in the reduced description, as we discussed before.

We start with the following proposition, concerning μ^A and μ^B for general WS-integrable models. It matches a similar finding for a system of Kuramoto-Sakaguchi oscillators under common multiplicative noise [Gon+19].

Proposition 5.4 *Let $\boldsymbol{\phi}(t)$ be a T-periodic two-cluster solution of a WS-integrable system $\dot{\boldsymbol{\phi}} = \boldsymbol{F}(\boldsymbol{\phi})$ with distinct clusters A and B where $m_A, m_B \geq 2$. Then the two splitting Floquet multipliers μ^A and μ^B fulfill*

$$\mu^A \mu^B = 1. \tag{5.13}$$

Proof. Without loss of generality, we assume again that the angular variables $\phi_j(t)$ are in cyclic order and that, since the clusters A and B consist of at least two units each, we have $1, 2 \in A$ and $N-1, N \in B$, that is, the first two units of the ensemble belong to cluster A and the last two units belong to cluster B. Since the clusters are distinct, we have $\phi_A(t) \neq \phi_B(t)\ \forall t$ and thus, the cross-ratio

$$\begin{aligned}\Lambda_{1,N-1,N,2}(\boldsymbol{\phi}) &= \frac{\left(\mathrm{e}^{i\phi_1} - \mathrm{e}^{i\phi_2}\right)\left(\mathrm{e}^{i\phi_{N-1}} - \mathrm{e}^{i\phi_N}\right)}{\left(\mathrm{e}^{i\phi_1} - \mathrm{e}^{i\phi_N}\right)\left(\mathrm{e}^{i\phi_{N-1}} - \mathrm{e}^{i\phi_2}\right)} \\ &= \frac{\sin\frac{\phi_1-\phi_2}{2}\,\sin\frac{\phi_{N-1}-\phi_N}{2}}{\sin\frac{\phi_1-\phi_N}{2}\,\sin\frac{\phi_{N-1}-\phi_2}{2}}\end{aligned} \tag{5.14}$$

is well-defined in an open neighborhood of the periodic state in $\mathbb{T}^N$ and is zero for the two-cluster state. Additionally, it is a constant of motion for the WS-integrable system.

For any initial state $\boldsymbol{\phi}(t_0)$ on the periodic orbit, with instantaneous cluster coordinates $\phi_A = \phi_1(t_0) = \phi_2(t_0)$ and $\phi_B = \phi_{N-1}(t_0) = \phi_N(t_0)$, let $\delta\boldsymbol{\phi}$ denote a small splitting perturbation of the form

$$\delta\boldsymbol{\phi} = (\delta, -\delta, 0, \ldots, 0, \delta, -\delta)^T$$

with $0 < \delta \ll 1$. For the perturbed state $\boldsymbol{\phi}(t_0) + \delta\boldsymbol{\phi}$, the Taylor expansion of (5.14) yields

$$\begin{aligned}\lambda_{1,N-1,N,2} &= \Lambda_{1,N-1,N,2}(\boldsymbol{\phi}(t_0) + \delta\boldsymbol{\phi}) \\ &= \frac{2\sin^2\delta}{\cos(\phi_A - \phi_B) - \cos 2\delta} \\ &= -\frac{2\delta^2}{\cos(\phi_A - \phi_B) - 1} + \mathcal{O}(\delta^4).\end{aligned}$$

The perturbation $\delta\boldsymbol{\phi}$ is a linear combination $\delta\boldsymbol{\phi} = \delta\boldsymbol{\phi}_A + \delta\boldsymbol{\phi}_B$ of the two eigenvectors

$$\begin{aligned}\delta\boldsymbol{\phi}_A &= (\delta, -\delta, 0, \ldots, 0)^T \\ \delta\boldsymbol{\phi}_B &= (0, \ldots, 0, \delta, -\delta)^T\end{aligned}$$

of the monodromy matrix $\mathcal{M}_{\boldsymbol{\phi}(t)}$ with respective eigenvalues μ^A and μ^B, see Remarks 3.6. The flow thus transforms $\boldsymbol{\phi}(t_0) + \delta\boldsymbol{\phi}$ after one period T to $\boldsymbol{\phi}(t_0 + T) + \delta\boldsymbol{\phi}' = \boldsymbol{\phi}(t_0) + \delta\boldsymbol{\phi}'$ with

$$\delta\boldsymbol{\phi}' = (\mu^A\delta, -\mu^A\delta, 0, \ldots, 0, \mu^B\delta, -\mu^B\delta)^T + \mathcal{O}(\delta^2).$$

For this new state, we find

$$\begin{aligned}\lambda'_{1,N-1,N,2} &= \Lambda_{1,N-1,N,2}(\boldsymbol{\phi}(t_0) + \delta\boldsymbol{\phi}') \\ &= \frac{2\sin(\mu^A\delta)\sin(\mu^B\delta)}{\cos(\phi_A - \phi_B) - \cos(\mu^A\delta + \mu^B\delta)} + \mathcal{O}(\delta^4) \\ &= \frac{2\mu^A\mu^B\delta^2}{\cos(\phi_A - \phi_B) - 1} + \mathcal{O}(\delta^4).\end{aligned}$$

Being constants of motion, $\lambda_{1,N-1,N,2}$ and $\lambda'_{1,N-1,N,2}$ must coincide and comparing powers of δ yields

$$\mu^A\mu^B = 1$$

which proofs the assertion. □

Proposition 5.4 has two important consequences that we state in the following two corollaries:

Corollary 5.5 *For any symmetric periodic two-cluster state ($p = 1/2$) of a WS-integrable systems, we have $\mu^A = \mu^B = 1$. In particular, this state possesses $N - 2$ neutrally stable directions.*

Proof. This follows from the fact that such a state is a splay in $\mathbb{T}_{1/2}$ and hence, $\mu^A = \mu^B$ and that $\mu^A, \mu^B > 0$ because negative Floquet multipliers would imply a change in the order of the perturbed angles which is prohibited since units cannot overtake each other. Since both multipliers have multiplicity $N/2 - 1$, the orbit has $N - 2$ neutrally stable directions. □

Corollary 5.6 *For any asymmetric periodic two-cluster state ($p \neq 1/2$) of a WS-integrable system, we have either $\mu^A > 1 > \mu^B > 0$ or $\mu^B > 1 > \mu^A > 0$. In particular, such a state is always exponentially unstable and isolated in $\mathbb{T}^N$.*

Proof. This follows from the fact that asymmetric periodic two-cluster states are generally not splay states so that $\mu^A \neq \mu^B$ and that both Floquet multipliers must be positive. Thus being a limit cycle, the periodic orbit of $\boldsymbol{\phi}(t)$ is isolated in $\mathbb{T}^N$ meaning there exists an open neighborhood of it within which every initial state spirals either towards or away from it exponentially fast. □

Without loss of generality, let cluster A be the larger one for the original AR-model (2.5). From our numerical studies, we then find $\mu^A > 1 > \mu^B$ so that A is unstable with respect to splitting perturbations while B is stable with respect to them. Intuitively speaking, cluster B is not strong enough to repel any stray units of A to make them return

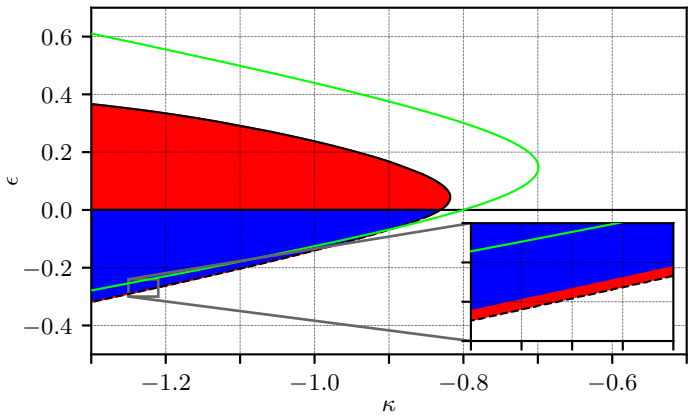

Figure 12: Stability diagram for symmetric periodic two-cluster states of the generalized AR-model (2.6) with perturbation type (5.1a) and fixed $\omega = 0.6$. A white shading indicates that no periodic two-cluster state exists. In the red shaded region, it exists and is unstable while in the blue shaded region, it is stable. The green line depicts the THB of Δ^s at κ_0, according to (5.5). A solid black line indicates a double-SNIC while a dashed black line indicates a double-heteroclinic bifurcation. The inset shows a narrow region of instability, close to the boundary of the region of existence for such periodic states.

to it. On the other hand, cluster A repels stray units of B and pushes them back to it so that cluster B is stable.

After these general considerations for WS-integrable systems, we discuss stability of the generalized AR-model (2.6) with our paradigmatic choices (5.1a) and (5.1b) for the perturbation function h. As before, we start with the symmetric case $p = 1/2$.

5.5.1 *Symmetric Two-Cluster States*

The generalized AR-model

$$\dot{\phi}_j = \omega - \sin\phi_j + \epsilon h(\phi_j) + \frac{\kappa}{N}\sum_{k=1}^{N}\sin(\phi_k - \phi_j) \tag{2.6}$$

becomes WS-integrable at $\epsilon = 0$ for any choice for h. Thus, if a symmetric periodic two-cluster state exists for given values of ω and κ if $\epsilon = 0$, this orbit must be neutrally stable by virtue of Corollary 5.5. Because neutrally stable periodic orbits are generally not robust, this implies that a change in stability must occur at $\epsilon = 0$ for generic choices of h so that the two-cluster state is either stable only for $\epsilon > 0$ and unstable for $\epsilon < 0$ or the other way around as long as $|\epsilon|$ is small. This is supported by numerical results, where we compute the splitting Floquet multipliers according to Corollary 3.4 by integrating the eigenvalues of the Jacobian $D\boldsymbol{F}$ along the periodic orbit. Next, we discuss our numerical findings in more detail.

We begin with Figure 12, which shows numerical results for the stability for the perturbation type (5.1a) and fixed $\omega = 0.6$. In this stability diagram, in the white shaded area, there exist no periodic two-cluster

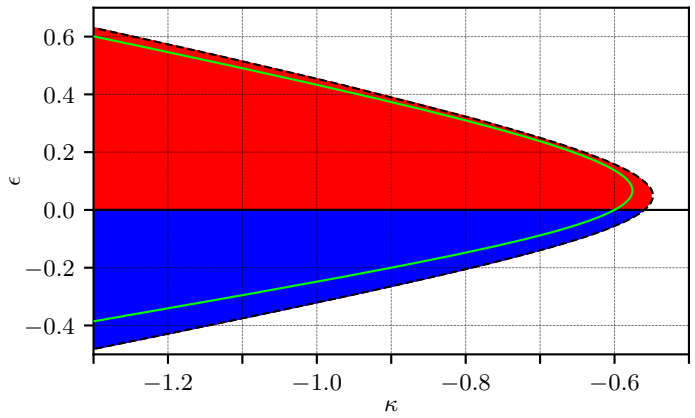

Figure 13: Stability diagram for symmetric periodic two-cluster states for (2.6) with perturbation type (5.1a) and fixed $\omega = 0.8$. In this case, the periodic orbit is always created in a double-heteroclinic bifurcation (dashed black line) and thus exists already before Δ^s becomes unstable in the THB (green line).

states whatsoever. In the red shaded area, an unstable periodic two-cluster state exists. In the blue shaded area, the periodic state exists and is stable. The green line indicates the THB of Δ^s at κ_0, according to (5.5). At the boundary of the regime of existence for periodic solutions, a solid black line indicates a double-SNIC while a dashed black line indicates a double-heteroclinic bifurcation. The latter bifurcation curves were computed numerically by the shooting method and by checking for the occurrence of simultaneous saddle-node bifurcations.

We make two important observations. Firstly, indeed a change of stability occurs at $\epsilon = 0$ which confirms our expectation. Secondly, as shown in the inset, we find that for $\epsilon < 0$ there exists a narrow region of instability close to the double-heteroclinic or double-SNIC. This corresponds to the fact that the splitting stability of the periodic orbit shortly after the bifurcation is inherited from the saddles Σ^i which are unstable against such splittings, as discussed before. Numerical results indicate that the width of this region of instability vanishes for $\epsilon \to 0$, also in accordance with Corollary 5.5.

Note that the intersection of the THB-line and the double-heteroclinic line close to $\epsilon \approx -0.09$ and $\kappa \approx -0.91$ is merely a projection artifact. As already mentioned in Section 5.4.1.1, the THB and double-heteroclinic bifurcation generally occur independently of each other and for distinct choices of the system parameters. Note also that the diagram includes regions of bi-stability: For $\epsilon < 0$ and $\kappa_0 < \kappa < \kappa_{\text{crit.}}$, both Δ^s and the periodic state can be stable.

Figure 13 shows the stability diagram for the case $\omega = 0.8$. Here, the periodic orbit is always created in double-heteroclinic bifurcations and thus exists before the synchronous fixed point Δ^s becomes unstable in the THB. For this case as well, numerical evidence suggests a narrow region of instability for $\epsilon < 0$ and close to $\kappa_{\text{crit.}}$. However, it is too narrow to be resolved graphically.

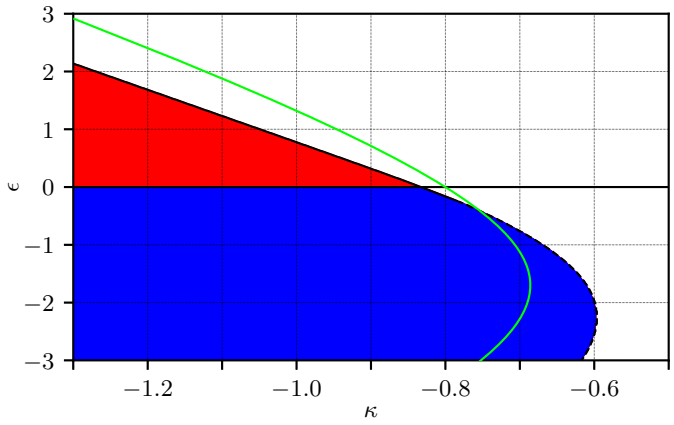

Figure 14: Stability diagram for symmetric periodic two-cluster states for (2.6) with perturbation type (5.1b) and fixed $\omega = 0.6$. As for the perturbation type (5.1a), the periodic orbit is created either in a double-heteroclinic bifurcation (dashed black line) or a double-SNIC (solid black line). The green line, indicating the THB at κ_0 is computed via (B.3).

A noteworthy observation can be made for $\epsilon = 0$. Anticipating the results from Chapter 6, we note that numerical evidence suggests that for $\kappa < \kappa_0$, the symmetric periodic two-cluster state is embedded in a continuum of neutrally stable periodic orbits which arises naturally for WS-integrable systems [WS94]. This corresponds to the fact that in this case, we have $\mu^A = \mu^B = 1$. However, for $\omega = 0.8$, we observe that the periodic two-cluster state exists and is neutrally stable even for some $\kappa > \kappa_0$ where we observe no such continuum of orbits, whatsoever. Note also that while all the periodic orbits of the continuum have $N - 3$ neutral directions, the two-cluster state has $N - 2$, as mentioned before. Thus, the central manifold of the symmetric two-cluster state does generally not coincide with the continuum. While in the regime of existence for $\kappa > \kappa_0$ the periodic two-cluster state is neutrally stable up to linear order, the full nonlinear evolution lets splitting perturbations converge towards Δ^s.

Finally, in Figure 14, we present numerical results concerning the stability of two-cluster states for the generic perturbation (5.1b). As for the case of (5.1a), we find that (i) periodic solutions are created either in double-heteroclinic bifurcations or double-SNICs and (ii) a change of stability occurs at $\epsilon = 0$. This further supports the assertion that this switch is in fact a generic phenomenon for such systems. The green line, indicating the THB at κ_0 is given by (B.3).

With these results, we end our discussion of stability for the symmetric case and come to the asymmetric case of unequal clusters.

5.5.2 *Asymmetric Two-Cluster States*

Since Corollary 5.6 states that all asymmetric periodic two-cluster states are exponentially unstable at $\epsilon = 0$, it follows that there exists an open neighborhood of the line of $\epsilon = 0$ in which no stable asym-

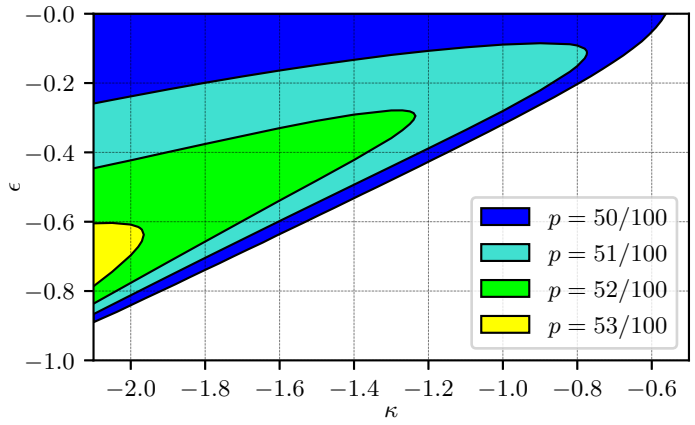

Figure 15: Stability regimes for asymmetric periodic two-cluster for the system (2.6) with perturbation type (5.1a) and $\omega = 0.8$. We consider an ensemble of $N = 100$ units. White shading indicates that no periodic two-cluster states exist. Regimes of multistability are observed. Starting with periodic states with $p = 50/100$ as the only *stable* periodic orbits in the blue area, successively passing to the turquoise, green, and yellow regions, asymmetric orbits with $p = 51/100$, $p = 52/100$, and $p = 53/100$ become stable, as well. Hence, e. g., in the yellow area, we find four different stable periodic two-cluster states.

metric periodic two-cluster states exist for given N. From the results for symmetric states, depicted in Figure 12, 13, and 14, we expect that in the respective regimes of instability for these states the asymmetric orbits are also unstable. On the other hand, the regimes of stability for asymmetric states should be enclosed in the stable region for symmetric states since they are expected to exist only for stronger repulsiveness for given ϵ than in the symmetric case.

This is confirmed by numerical results which show a cascade of regions of multistability, nested with respect to p, see Figure 15. Here, we choose again for definiteness the perturbation type (5.1a), fix $\omega = 0.8$, and consider an ensemble of $N = 100$ units. We only show the results for negative ϵ because for $\epsilon > 0$, as expected, all periodic two-cluster states are found to be unstable. The blue shaded area corresponds to the blue area in Figure 13. In this regime, only symmetric periodic two-cluster states are stable. In the turquoise region, we find that additionally, the periodic two-cluster states with $p = 51/100$ have become stable. In the green area, a third periodic two-cluster state with $p = 52/100$ becomes stable and in the yellow area, we find yet a fourth such state with $p = 53/100$ to become stable. We expect this nested structure to be generic for systems of type (2.6) because if a strongly asymmetric periodic two-cluster state is stable, it is to be expected that a state with less disparity between cluster sizes is also stable. Note that the regions, shown in Figure 15, are not the same as the regions of *existence* for asymmetric periodic two-cluster states but only indicate the regions of *stability*. These states generally exist outside of these stable regions, too. However, in our numerical experiments, the regions of existence

always lie inside the region of existence for symmetric periodic states, in accordance to our observations in Section 5.4.

Note that choosing larger N makes the nesting finer. The larger N is, the more narrow the differently colored areas in Figure 15 become. In particular, with growing N, the region of exclusive stability for symmetric periodic two-cluster states (blue region) continuously shrinks in size, even though it always begins beneath the line at $\epsilon = 0$ for any N.

With this, we end our discussion of stability for periodic two-cluster states and summarize our findings.

5.6 CONCLUSION

We have presented our findings regarding creation, existence, and stability for periodic two-cluster states, both symmetric and asymmetric, which have been published in [RZ21a].

Starting with a reduced description of two-cluster states, we observed two basic global bifurcation scenarios, leading to periodic two-cluster states: the double-heteroclinic bifurcation, where periodic orbits are born from a structurally unstable heteroclinic cycle, and the double-SNIC, where periodic states emerge through two saddle-node bifurcations on an invariant circle, rendering it a limit cycle in $\mathbb{T}_p$. While the former is generic for systems of two class I excitable units, sufficiently close to their respective SNICs, cf. [BM13], the latter has, to our best knowledge, not been discussed before in this context. We discussed both of these scenarios for the degenerate case of equally large clusters and how the picture changes when the clusters differ in size. We also discussed how double-heteroclinic bifurcation and double-SNIC are connected to the criticality of the pitchfork bifurcation of the synchronous fixed point Δ^s at κ_0. Further, we argued why these two scenarios are expected to be generic for systems of type (2.6) which was confirmed in our numerical studies for the generic perturbation type (5.1b). In particular, we found that the emerging periodic states are stable with respect to perturbations that leave the clusters whole.

Regarding splitting perturbations, we showed that symmetric periodic two-cluster states for general WS-integrable systems must always be neutrally stable while asymmetric states are always exponentially unstable with respect to splitting of one of the clusters and stable with respect to splitting perturbations of the other cluster. While it has been shown before that periodic two-cluster states cannot be asymptotically stable for WS-integrable systems, see [EM14], the identity (5.13), which generalizes a similar finding in [Gon+19], can to our knowledge not be found in the existing literature on Watanabe-Strogatz integrability. Equally remarkable is that, although two-cluster states themselves are not accessible via WS-theory since it requires at least three distinct angular variables to apply, their stability can be understood within this framework. Numerical evidence further suggests that neutrally stable symmetric periodic orbits are embedded in a continuum of periodic orbits, if this continuum exists. We will come back to this observation in

Chapter 7. On the other hand, asymmetric periodic two-cluster states cannot be part of this continuum due to their exponential instability. In particular, for odd N, all periodic two-cluster states are isolated and exponentially unstable at $\epsilon = 0$ and, by continuity within an open neighborhood of the $\epsilon = 0$ line while for even N, a switch in stability occurs at $\epsilon = 0$ for symmetric states. We also demonstrated that both, the regions of existence and the regions of stability for periodic two-cluster states, are nested for increasing $|p - 1/2|$. The larger the disparity in size between the two clusters gets, the more repulsive the coupling between them must be in order to yield periodic orbits. If additionally, the orbit is expected to be stable, both, the repulsive strength of the coupling and the deviation from the WS-case must be sufficiently large. This yields a nesting of stable regions for states of large cluster size disparity inside the ones with smaller disparity.

With this, we end this chapter on periodic two-cluster states. In the next chapter, we discuss the existence of splay states and of a continuum of periodic orbits for the original AR-model (2.5) which is equipped with a NAIM-structure in $\mathbb{T}^N$. Afterwards, we investigate the close connection with respect to stability between periodic two-cluster and splay states in Chapter 7.

6

INTEGRABLE DYNAMICS AND THE NORMALLY ATTRACTING CONTINUUM OF PERIODIC ORBITS

ABSTRACT

This chapter is dedicated to the dynamics of the classic AR-model

$$\dot{\phi}_j = \omega - \sin\phi_j + \frac{\kappa}{N}\sum_{k=1}^{N}\sin(\phi_k - \phi_j). \tag{2.5}$$

After some general remarks in Section 6.1, concerning previous findings on the stability of the synchronous state Δ^{s}, we start by expressing the equations of motion for the system in WS-variables in Section 6.2. Afterwards, we show in Section 6.3 that for a broad class of WS-integrable systems and under certain general conditions, a continuum of periodic orbits exists and that the union of these orbits possesses the additional structure of a Normally Attracting Invariant Manifold (NAIM). We also show that one of these orbits features splay state dynamics. In Section 6.4, we apply these results to the model (2.5) and compute the critical coupling strength κ_0 for which the continuum emerges.

Since the units are assumed to be identical, we always consider them in accordance with Chapter 4 and without loss of generality to be in strict cyclic order on $\mathbb{S}^1$. The content of this chapter is based on the results in [RZP]. We note that again some passages and in particular the assertions with their proofs are often verbatim quotes of this work. However, we elaborate some details and calculations in the arguments.

6.1 GENERAL REMARKS

Before we begin with the presentation of our own results, we recapitulate the main findings on the AR-model (2.5) from [ZT16] that are important for us. This serves also as a motivation for this chapter.

Recall from the previous chapter that the system (2.5) possesses a fixed point $\Delta^{\mathrm{s}} = (\phi^{\mathrm{s}}, \dots, \phi^{\mathrm{s}})$, which at $\kappa = 0$ is exponentially stable. For $\kappa > 0$, or *attractive* coupling between the individual units, this fixed point stays stable since not only the on-site component $\omega - \sin\phi_j$ in (2.5) tends to stabilize the unit j at ϕ^{s} but also the coupling binds any two units stronger together. Due to these trivial asymptotic dynamics, the authors of [ZT16] were interested in how the outcome changes if the coupling is repulsive, i. e., when $\kappa < 0$. They found that for general

systems of identical one-dimensional repulsively[1] coupled units, there exists a critical coupling strength κ_0 at which Δ^{s} becomes unstable in a Transcritical Homoclinic Bifurcation (THB)[2], cf. [AKS90]. In this bifurcation, Δ^{s} coalesces with $\sim 2^{N-1}$ two-cluster saddles while a multitude of homoclinic orbits forms. The dynamics along any of these orbit looks as follows: At the beginning and end, all units are located at ϕ^{s} while along the homoclinic orbit, a single unit or a cluster of units separates from the rest of the ensemble, moves in one direction away from it, thereby tracing the state space $\mathbb{S}^1$, and then returns and joins the rest of the ensemble from the other side while the remaining units stay relatively close to ϕ^{s} in state space. Depending on which homoclinic orbit one follows, different units go astray from the bulk before returning from the other side. In this highly degenerate bifurcation, $N-1$ eigenvalues of the vector field's Jacobian at Δ^{s} vanish and a calculation yields

$$\kappa_0 = -\sqrt{1-\omega^2}$$

for the critical coupling strength (recall that $|\omega| < 1$ for Active Rotators).

The question naturally arises what kind of dynamics take place when Δ^{s} ceases to be an attractor and the authors of [ZT16] noted from their numerical studies that a continuum of periodic orbits is formed. We show some exemplary (normalized) time series for some of these orbits in Figure 16 for an ensemble of $N = 10$ units. They differ in their respective conserved cross-ratios $\boldsymbol{\lambda}$ and the timing between any two consecutive units to spike, i. e., when they make a turn around $\mathbb{S}^1$, as seen by the rapid down- and subsequent up-strokes in the plots, which indicate spikes for the respective units. In particular, for a suitable choice $\boldsymbol{\lambda}^*$ of the conserved cross-ratios, a splay state can be observed, as depicted in Panel (a) of Figure 16. Splay states can be characterized as periodic states $\boldsymbol{\phi}(t)$ for which the dynamics of every individual unit $\phi_j(t)$ can be written as

$$\phi_j(t) = \varphi\left(t + j\frac{T}{N}\right) \tag{6.1}$$

for some T-periodic continuous function $\varphi : \mathbb{R} \to \mathbb{S}^1$ so that the time series of all units are copies of each other, shifted by some multiple of $1/T$ in time. Additionally, all of the observed orbits possess two stable directions and $N-3$ neutrally stable ones. This was understood to be the result of the system being WS-integrable which naturally leads to degenerate dynamics, as discussed in Chapter 4. Two questions arose from this: The first one was how generic the observed dynamics actually

1 Actually, their studies were more general, being interested in the case of *mixed* coupling where some units couple attractively and some repulsively.

2 In [ZT16], the authors refer to it as a transcritical *heteroclinic* bifurcation because they consider $\phi_j \in \mathbb{R}$ in which case two points $\theta \in \mathbb{R}$ and $\vartheta = \theta + 2\pi$ are not identified with each other but constitute distinct states in state space $\mathbb{R}$. In particular, the phase space of the system becomes $\mathbb{R}^N$ instead of $\mathbb{T}^N$. Subsequently, all present vector fields are then assumed to be 2π-periodic in each θ_j.

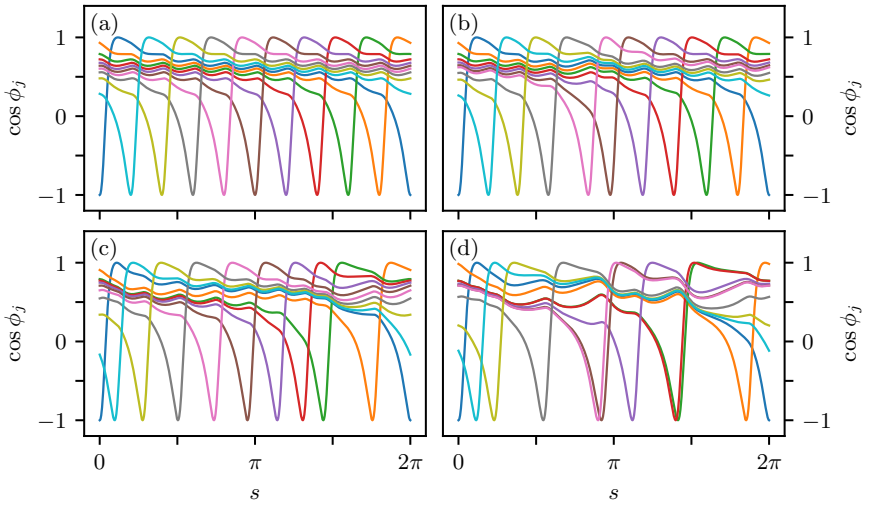

Figure 16: (Normalized) time series of $\cos\phi_j$ for four periodic orbits with different fixed cross-ratios for a system of $N = 10$ Active Rotators obeying (2.5). Different colors indicate different units. System parameters are fixed at $\omega = 0.8$ and $\kappa = -0.7$ and instead over time t, we plot for each orbit over its phase $s = 2\pi\, t/T(\boldsymbol{\lambda})$ where $T(\boldsymbol{\lambda})$ is the solution's period. Panel (a) depicts a splay state while Panels (b)-(d) represent orbits in randomly chosen level sets $\mathcal{L}_{\boldsymbol{\lambda}^*}(\boldsymbol{\Lambda})$ which are generally no splay states.

are, a question that is investigated in Chapter 7 and Chapter 8. The second question, which we intend to answer in this chapter, is about the geometric properties of the continuum itself: whether it is equipped with some additional structures, e. g., if it forms a NAIM in which case results from the theory of NAIMs can be used for further analysis. Here, we show that this is indeed the case and that this observation in fact holds true for a large class of WS-integrable models. We also prove that the continuum for the AR-model (2.5) emerges exactly at κ_0 in accordance with the numerical results from [ZT16].

6.2 THE CLASSIC MODEL IN WATANABE-STROGATZ VARIABLES

We start our investigation of the dynamics of (2.5) by writing it down in WS-variables α, ψ, and $\boldsymbol{\lambda}$ from Proposition 4.12. For this, we note first that (2.5) can be rewritten as

$$\begin{aligned}\dot{\phi}_j &= \omega + \frac{i}{2}\left(\mathrm{e}^{i\phi_j} - \mathrm{e}^{-i\phi_j}\right) - \frac{\kappa}{N}\sum_{k=1}^{N}\frac{i}{2}\left(\mathrm{e}^{i\phi_k}\mathrm{e}^{-i\phi_j} - \mathrm{e}^{-i\phi_k}\mathrm{e}^{i\phi_j}\right)\\ &= \omega + \frac{i}{2}\Big(1 + \kappa\bar{Z}(\boldsymbol{\phi})\Big)\mathrm{e}^{i\phi_j} - \frac{i}{2}\Big(1 + \kappa Z(\boldsymbol{\phi})\Big)\mathrm{e}^{-i\phi_j}\end{aligned} \tag{6.2}$$

where $\boldsymbol{\phi} = (\phi_1, \ldots, \phi_N)$ and Z is the well-known Kuramoto order parameter [Kur75]:

Definition 6.1 *The Kuramoto order parameter* $Z : \mathbb{T}^N \to \overline{\mathbb{D}}$ *is defined as*

$$Z(\boldsymbol{\phi}) \coloneqq \frac{1}{N}\sum_{j=1}^{N} \mathrm{e}^{i\phi_j}$$

where $\overline{\mathbb{D}} \coloneqq \{z \in \mathbb{C}\,;\, |z| \leq 1\}$ *denotes the closed unit disk.*

The order parameter can be interpreted as a measure of synchrony between the angles ϕ_j because if all angles lie close to each other on the circle $\mathbb{S}^1$, we have $|Z| \approx 1$ while for a uniform distribution of angles we find $|Z| = 0$. The first case is one of high synchrony while the latter is one of low synchrony.

Comparing the second line of (6.2) with (4.9) from Theorem 4.13, we find for the common fields

$$\begin{aligned} f &= \frac{i}{2}\left(1 + \kappa\bar{Z}\right) \\ g &= \omega \end{aligned}$$

and in particular, (2.5) is WS-integrable as was already noted in [ZT16]. Furthermore, it belongs to a whole class of WS-integrable systems, for which both f and g can be written as functions of Z and otherwise do not depend explicitly on $\boldsymbol{\phi}$. This leads to the idea to study general systems of this kind which is what we do in what follows.

6.3 A CLASS OF WATANABE-STROGATZ INTEGRABLE SYSTEMS

In Chapter 4, we discussed how for WS-integrable systems like the original AR-model (2.5) a coordinate change to the WS-variables $(\alpha, \psi, \boldsymbol{\lambda})$ reveals that such systems possess $N-3$ constants of motion, the cross-ratios $\boldsymbol{\lambda}$, and that consequently, their dynamics on their respective level set $\mathcal{L}_{\boldsymbol{\lambda}}(\boldsymbol{\Lambda})$ is fully determined by two coupled ODEs for α and ψ. In WS-variables $(\alpha, \psi, \boldsymbol{\lambda})$, the equations of motion then read

$$\begin{aligned} \dot{\alpha} &= i\left(f(\boldsymbol{\phi})\alpha^2 + g(\boldsymbol{\phi})\alpha + \bar{f}(\boldsymbol{\phi})\right) \\ \dot{\psi} &= f(\boldsymbol{\phi})\alpha + g(\boldsymbol{\phi}) + \bar{f}(\boldsymbol{\phi})\bar{\alpha} \\ \dot{\boldsymbol{\lambda}} &= \mathbf{0} \end{aligned} \tag{4.12}$$

where $\boldsymbol{\phi} = \boldsymbol{m}(\alpha, \psi, \boldsymbol{\lambda})$ is determined via the diffeomorphism $\boldsymbol{m}$ from Proposition 4.12. In general, the equations (4.12) are of a more complicated form than the original equations

$$\dot{\phi}_j = f(\boldsymbol{\phi})\mathrm{e}^{i\phi_j} + g(\boldsymbol{\phi}) + \bar{f}(\boldsymbol{\phi})\mathrm{e}^{-i\phi_j} \tag{4.1}$$

so that no closed explicit form for (4.12) exists. However, if the circumstances are right, such an expression can be found which then allows for a more thorough analysis. Hence, for the rest of this section, we consider general WS-integrable systems of the form

$$\dot{\phi}_j = f(Z)\mathrm{e}^{i\phi_j} + g(Z) + \bar{f}(Z)\mathrm{e}^{-i\phi_j} \tag{6.3}$$

or, in WS-variables,

$$\dot{\alpha} = i\left(f(Z)\alpha^2 + g(Z)\alpha + \bar{f}(Z)\right) \tag{6.4a}$$

$$\dot{\psi} = f(Z)\alpha + g(Z) + \bar{f}(Z)\bar{\alpha} \tag{6.4b}$$

$$\dot{\boldsymbol{\lambda}} = \mathbf{0} \tag{6.4c}$$

for which f and g depend on $\boldsymbol{\phi}$ solely via the Kuramoto order parameter Z.[3] To arrive at a closed form of (6.4) in terms of the WS-variables, we therefore have to first express Z entirely in terms of α, ψ, and $\boldsymbol{\lambda}$. Using the Möbius transformation (4.2), we start by defining the auxiliary function $Z_{\boldsymbol{\theta}} : \mathbb{D} \times \mathbb{S}^1 \times \mathbb{T}^N \to \overline{\mathbb{D}}$ with

$$\begin{aligned}
Z_{\boldsymbol{\theta}}(\alpha, \psi, \boldsymbol{\theta}) &\coloneqq \frac{1}{N}\sum_{j=1}^{N} G_{\alpha,\psi}\left(\mathrm{e}^{i\theta_j}\right) \\
&= \frac{1}{N}\sum_{j=1}^{N} \frac{\alpha + \mathrm{e}^{i\psi}\mathrm{e}^{i\theta_j}}{1 + \bar{\alpha}\,\mathrm{e}^{i\psi}\mathrm{e}^{i\theta_j}} \\
&= \frac{1}{N}\sum_{j=1}^{N} (\alpha + \mathrm{e}^{i\psi}\mathrm{e}^{i\theta_j}) \sum_{k=0}^{\infty} (-\bar{\alpha}\,\mathrm{e}^{i\psi}\mathrm{e}^{i\theta_j})^k \\
&= \sum_{k=0}^{\infty} \alpha(-\bar{\alpha}\,\mathrm{e}^{i\psi})^k \frac{1}{N}\sum_{j=1}^{N} \mathrm{e}^{ik\theta_j} + \\
&\quad + \sum_{k=0}^{\infty} \mathrm{e}^{i\psi}(-\bar{\alpha}\,\mathrm{e}^{i\psi})^k \frac{1}{N}\sum_{j=1}^{N} \mathrm{e}^{i(k+1)\theta_j}
\end{aligned}$$

where in the third line we used the fact that $|\alpha| < 1$ and the geometric series formula $\sum_{k=0}^{\infty} z^k = 1/(1-z)$ for $|z| < 1$. Introducing the symbol

$$\left\langle \mathrm{e}^{ik\boldsymbol{\theta}} \right\rangle \coloneqq \frac{1}{N}\sum_{j=1}^{N} \mathrm{e}^{ik\theta_j},$$

we arrive, after reindexing the second sum, at the general expression

$$\begin{aligned}
Z_{\boldsymbol{\theta}}(\alpha, \psi, \boldsymbol{\theta}) &= \alpha \sum_{k=0}^{\infty} (-\bar{\alpha}\,\mathrm{e}^{i\psi})^k \left\langle \mathrm{e}^{ik\boldsymbol{\theta}} \right\rangle + \mathrm{e}^{i\psi} \sum_{k=0}^{\infty} (-\bar{\alpha}\,\mathrm{e}^{i\psi})^k \left\langle \mathrm{e}^{i(k+1)\boldsymbol{\theta}} \right\rangle . \\
&= \alpha + (1 - |\alpha|^2)\,\mathrm{e}^{i\psi} \sum_{k=1}^{\infty} (-\bar{\alpha}\,\mathrm{e}^{i\psi})^{k-1} \left\langle \mathrm{e}^{ik\boldsymbol{\theta}} \right\rangle .
\end{aligned}$$

This equation holds for general $\boldsymbol{\theta} \in \mathbb{T}^N$. Setting $\boldsymbol{\theta} = \boldsymbol{\Theta}(\boldsymbol{\lambda})$ with the point-of-reference function $\boldsymbol{\Theta}$ from (4.4), we define $Z : \mathbb{D} \times \mathbb{S}^1 \times V \to \mathbb{D}$ by $Z(\alpha, \psi, \boldsymbol{\lambda}) \coloneqq Z_{\boldsymbol{\theta}}(\alpha, \psi, \boldsymbol{\Theta}(\boldsymbol{\lambda}))$ (note that $|Z| < 1$ since the $\Theta_j(\boldsymbol{\lambda})$ are always mutually distinct) and thus

$$Z(\alpha, \psi, \boldsymbol{\lambda}) \coloneqq \alpha + (1 - |\alpha|^2)\,\mathrm{e}^{i\psi} \sum_{k=1}^{\infty} (-\bar{\alpha}\,\mathrm{e}^{i\psi})^{k-1} \left\langle \mathrm{e}^{ik\boldsymbol{\Theta}(\boldsymbol{\lambda})} \right\rangle \tag{6.5}$$

3 Since Z is to be understood as a two-dimensional real valued function, we should better write, e. g., $f(\operatorname{Re} Z, \operatorname{Im} Z)$ or $f(Z, \bar{Z})$ where for any $z \in \mathbb{C}$, $\operatorname{Re} z$ and $\operatorname{Im} z$ denote its real and imaginary part. Instead, we simply write, e. g., $f(Z)$ with the understanding that f and g generally depend on both Z and $\bar{Z}$. In particular, they need not be complex differentiable but only real differentiable.

which is the general expression for Z on $\mathbb{T}^N_{\text{ordered}}$ in terms of the WS-variables.

For generic choices of $\boldsymbol{\lambda}$, the expression (6.5) cannot be simplified further and in particular, there is no closed form for the infinite sum in it. However, there exists a specific level set $\mathcal{L}_{\boldsymbol{\lambda}^*}(\boldsymbol{\Lambda})$ on which this can be achieved.

6.3.1 *The Level Set of Uniform Distributions*

In Chapter 2, we defined the point

$$\begin{aligned} \boldsymbol{\theta}^* &\coloneqq (\theta_1^*, \dots, \theta_N^*) \\ \theta_j^* &\coloneqq -\pi + \frac{2\pi}{N}(j-1) \end{aligned} \tag{4.5}$$

of evenly spaced angles θ_j in $\mathbb{S}^1$ which is clearly an element of $\mathbb{T}^N_{\text{ordered}}$. As noted in Remark 4.11, its corresponding cross-ratios $\boldsymbol{\lambda}^* = \boldsymbol{\Lambda}(\boldsymbol{\theta}^*)$ read

$$\begin{aligned} \boldsymbol{\lambda}^* &= (\lambda_1^*, \dots, \lambda_{N-3}^*) \\ \lambda_k^* &= \frac{\sin\frac{\pi(k+2)}{N}}{2\cos\frac{\pi}{N}\sin\frac{\pi(k+1)}{N}}. \end{aligned} \tag{4.6}$$

We call a configuration like $\boldsymbol{\theta}^*$ of evenly spaced angles a uniform distribution of angles. Any uniformly distributed state $\boldsymbol{\vartheta}$ can be constructed from $\boldsymbol{\theta}^*$ by shifting the whole ensemble by some fixed amount $c \in [0, 2\pi)$, in other words, by applying a Möbius transformation

$$\mathrm{e}^{i\boldsymbol{\theta}^*} \mapsto \mathrm{e}^{i\boldsymbol{\vartheta}} = G_{0,c}\left(\mathrm{e}^{i\boldsymbol{\theta}^*}\right)$$

so that $\boldsymbol{\vartheta}$ also lies in $\mathcal{L}_{\boldsymbol{\lambda}^*}(\boldsymbol{\Lambda})$. We therefor refer to $\mathcal{L}_{\boldsymbol{\lambda}^*}(\boldsymbol{\Lambda})$ as the level set of uniform distributions. For this level set, there exists a closed expression for the symbols $\left\langle \mathrm{e}^{ik\boldsymbol{\Theta}(\boldsymbol{\lambda}^*)} \right\rangle$:

Lemma 6.2 *On the set $\mathcal{L}_{\boldsymbol{\lambda}^*}(\boldsymbol{\Lambda})$, the symbols $\left\langle \mathrm{e}^{i\boldsymbol{\Theta}(\boldsymbol{\lambda}^*)} \right\rangle$ are of the form*

$$\left\langle \mathrm{e}^{ik\boldsymbol{\Theta}(\boldsymbol{\lambda}^*)} \right\rangle = \begin{cases} (-1)^k & \text{if } k \in N\mathbb{Z} \\ 0 & \text{else.} \end{cases}$$

Proof. Let $k \in N\mathbb{Z}$, i. e., $k = Nl$ for some integer l and note that $\boldsymbol{\theta}^* = \boldsymbol{\Theta}(\boldsymbol{\lambda}^*)$. Then $\mathrm{e}^{ik\theta_j^*} = \mathrm{e}^{-i\pi k + \frac{2\pi i}{N}Nl(j-1)} = \mathrm{e}^{-i\pi k} = (-1)^k$ for all j and hence, $\left\langle \mathrm{e}^{ik\boldsymbol{\theta}^*} \right\rangle = \frac{1}{N}\sum_{j=1}^N (-1)^k = (-1)^k$. On the other hand, let $k \notin N\mathbb{Z}$. We use the well known identity $\sum_{j=0}^{N-1} z^j = \frac{z^N - 1}{z-1}$ for any $z \neq 1$ which yields

$$\begin{aligned} \left\langle \mathrm{e}^{ik\boldsymbol{\theta}^*} \right\rangle &= \frac{1}{N}\sum_{j=1}^{N} \mathrm{e}^{-i\pi k + \frac{2\pi i}{N}(j-1)k} \\ &= \frac{1}{N}\mathrm{e}^{-i\pi k}\sum_{j=0}^{N-1}\left(\mathrm{e}^{\frac{2\pi i}{N}k}\right)^j \end{aligned}$$

$$
\begin{aligned}
&= \frac{1}{N}\mathrm{e}^{-i\pi k}\frac{\mathrm{e}^{\frac{2\pi i}{N}kN}-1}{\mathrm{e}^{\frac{2\pi i}{N}k}-1}\\
&= \frac{1}{N}\mathrm{e}^{-i\pi k}\frac{\mathrm{e}^{2\pi ik}-1}{\mathrm{e}^{\frac{2\pi i}{N}k}-1}\\
&= 0
\end{aligned}
$$

since $\mathrm{e}^{\frac{2\pi i}{N}k} \neq 1$ for $k \notin N\mathbb{Z}$. □

From this lemma, we conclude that

$$
\begin{aligned}
Z(\alpha,\psi,\boldsymbol{\lambda}^*) &= \alpha - \left(1-|\alpha|^2\right)\,\mathrm{e}^{i\psi}\sum_{k=1}^{\infty}(\bar{\alpha}\,\mathrm{e}^{i\psi})^{kN-1}\\
&= -\sum_{k=1}^{\infty}\bar{\alpha}^{kN-1}\mathrm{e}^{ikN\psi} + \alpha\sum_{k=0}^{\infty}\bar{\alpha}^{kN}\mathrm{e}^{ikN\psi}
\end{aligned}
\tag{6.6}
$$

so that $Z(\alpha,\psi,\boldsymbol{\lambda}^*) = \alpha + \mathcal{O}\left(|\alpha|^N\right)$ and thus can be approximated by α on $\mathcal{L}_{\boldsymbol{\lambda}^*}(\boldsymbol{\Lambda})$ for large ensemble sizes N. This observation has far-reaching consequences. It was first noted in [PR08] where it was used to investigate ensembles of heterogeneous ensembles of angular variables in the thermodynamic limit $N \to \infty$ by means of WS-theory. For systems of the form (6.4), it implies that (6.4a) effectively decouples from ψ and $\boldsymbol{\lambda}$ for $N \gg 1$ and can be studied independently. This ansatz was further elaborated and applied in order to study, e. g., weakly inhomogeneous ensembles of angular variables as well as explosive synchronization and Chimera states in star graphs [VZP15; VRP16; Eld+21].

We also use this observation to determine periodic orbits of systems of the type (6.4) by studying its closed or *truncated* form where Z is replaced by α. Since the dynamics then decouples from ψ and $\boldsymbol{\lambda}$, the problem is reduced to finding (stable) fixed points of (6.4a) for which $\dot{\psi} \neq 0$. We can then use Theorem 3.7 for NAIMs to conclude that similar orbits must exist in the original system (6.4) and that their union in fact forms a NAIM. However, to make this work, we must first elaborate the implications of substituting Z by α to "close" (6.4a). In particular, we must first show that the error that is made by replacing Z by α can be made sufficiently small in C^1-norm by choosing N sufficiently large. The main result of this section is thus an estimate of the error $\eta = Z - \alpha$ and its partial derivatives for large N.

Each level set $\mathcal{L}_{\boldsymbol{\lambda}}(\boldsymbol{\Lambda}) \subset \mathbb{T}^N_{\text{ordered}}$ is diffeomorphic to the space $\mathbb{D}\times\mathbb{S}^1$ so that we identify

$$\mathcal{L}_{\boldsymbol{\lambda}}(\boldsymbol{\Lambda}) \cong \mathbb{D}\times\mathbb{S}^1\times\{\boldsymbol{\lambda}\}$$

where for any two diffeomorphic spaces X and Y, we write $X \cong Y$.[4] For any smooth function $\boldsymbol{F} : \mathbb{T}^N_{\text{ordered}} \to \mathbb{R}^n$, the derivative of its restriction $\boldsymbol{F}|_{\mathcal{L}_{\boldsymbol{\lambda}}(\boldsymbol{\Lambda})}$ to the level set $\mathcal{L}_{\boldsymbol{\lambda}}(\boldsymbol{\Lambda})$ is then given by

$$\tilde{\mathrm{D}}\boldsymbol{F} \coloneqq \mathrm{D}\boldsymbol{F}|_{\mathcal{L}_{\boldsymbol{\lambda}}(\boldsymbol{\Lambda})} \equiv (\mathrm{D}_\alpha\boldsymbol{F}, \mathrm{D}_{\bar{\alpha}}\boldsymbol{F}, \mathrm{D}_\psi\boldsymbol{F})\,.$$

4 In the same way, we identified $\mathbb{T}^N_{\text{ordered}} \cong \mathbb{D}\times\mathbb{S}^1\times V$ in Chapter 4.

In the derivation of $Z(\alpha, \psi, \boldsymbol{\lambda})$, we made use of the geometric series so that (6.5) diverges for $|\alpha| \to 1$. To account for this, from now on we restrict the domain for α such that $Z(\alpha, \psi, \boldsymbol{\lambda})$ stays bounded. Let

$$\mathbb{D}_r \coloneqq \{z \in \mathbb{C} \,;\, |z| < r\}$$

denote the open complex disk of radius r with closure $\overline{\mathbb{D}}_r$. The following lemma gives an estimate for the error $\eta = Z - \alpha$ in C^1-norm on $\mathcal{L}_{\boldsymbol{\lambda}^*}(\boldsymbol{\Lambda})$:

Lemma 6.3 *Consider $\overline{\mathbb{D}}_r$ for any $0 < r < 1$ and let*

$$\begin{aligned} \eta : \mathbb{D} \times \mathbb{S}^1 \times V &\to \mathbb{C} \\ (\alpha, \psi, \boldsymbol{\lambda}) &\mapsto Z(\alpha, \psi, \boldsymbol{\lambda}) - \alpha. \end{aligned}$$

Then,

$$\sup_{(\alpha,\psi)\in\overline{\mathbb{D}}_r\times\mathbb{S}^1} |\eta(\alpha, \psi, \boldsymbol{\lambda}^*)| = \mathcal{O}(r^{N-1}) \tag{6.7}$$

$$\sup_{(\alpha,\psi)\in\overline{\mathbb{D}}_r\times\mathbb{S}^1} \left\|\tilde{\mathrm{D}}\eta(\alpha, \psi, \boldsymbol{\lambda}^*)\right\| = \mathcal{O}(Nr^{N-2}). \tag{6.8}$$

Proof. We start with Equation (6.7). From (6.5) and Lemma 6.2, we infer

$$\begin{aligned} \eta(\alpha, \psi, \boldsymbol{\lambda}^*) &= -\left(1 - |\alpha|^2\right) \mathrm{e}^{i\psi} \sum_{k=1}^{\infty} (\bar{\alpha}\, \mathrm{e}^{i\psi})^{kN-1} \\ &= -\sum_{k=1}^{\infty} \bar{\alpha}^{kN-1} \mathrm{e}^{ikN\psi} + \alpha \sum_{k=1}^{\infty} \bar{\alpha}^{kN} \mathrm{e}^{ikN\psi}, \end{aligned}$$

yielding

$$\begin{aligned} \sup_{(\alpha,\psi)\in\overline{\mathbb{D}}_r\times\mathbb{S}^1} |\eta(\alpha, \psi, \boldsymbol{\lambda}^*)| &= \sup_{(\alpha,\psi)\in\overline{\mathbb{D}}_r\times\mathbb{S}^1} \left| \left(1 - |\alpha|^2\right) \mathrm{e}^{i\psi} \sum_{k=1}^{\infty} (\bar{\alpha}\, \mathrm{e}^{i\psi})^{kN-1} \right| \\ &\leq \sup_{(\alpha,\psi)\in\overline{\mathbb{D}}_r\times\mathbb{S}^1} \left(1 - |\alpha|^2\right) \sum_{k=1}^{\infty} \left|\bar{\alpha}\, \mathrm{e}^{i\psi}\right|^{kN-1} \\ &\leq \sum_{k=1}^{\infty} r^{kN-1} = \mathcal{O}(r^{N-1}). \end{aligned}$$

so that (6.7) holds.

To prove (6.8), we first compute the entries of $\tilde{\mathrm{D}}\eta(\alpha, \psi, \boldsymbol{\lambda}^*)$ to leading order in N. From this, we can expand $\left\|\tilde{\mathrm{D}}\eta(\alpha, \psi, \boldsymbol{\lambda}^*)\right\|$ to leading order. For each $x \in \{\alpha, \bar{\alpha}, \psi\}$, we can then write in a slight abuse of notation $\mathrm{D}_x\eta = \mathrm{Re}\,\mathrm{D}_x\eta + i\,\mathrm{Im}\,\mathrm{D}_x\eta$ for the respective column $(\mathrm{Re}\,\mathrm{D}_x\eta, \mathrm{Im}\,\mathrm{D}_x\eta)^T$ of $\mathrm{D}\eta$. In particular, $|\mathrm{Re}\,\mathrm{D}_x\eta|\,, |\mathrm{Im}\,\mathrm{D}_x\eta| \leq |\mathrm{D}_x\eta| \equiv \|\mathrm{D}_x\eta\|$ holds.

For the first column of $\mathrm{D}\eta(\alpha, \psi, \boldsymbol{\lambda}^*)$, we find

$$\begin{aligned} \mathrm{D}_\alpha\eta(\alpha, \psi, \boldsymbol{\lambda}^*) &= \sum_{k=1}^{\infty} (\bar{\alpha}\, \mathrm{e}^{i\psi})^{kN} \\ |\mathrm{D}_\alpha\eta(\alpha, \psi, \boldsymbol{\lambda}^*)| &\leq \sum_{k=1}^{\infty} |\alpha|^{kN} \leq \sum_{k=1}^{\infty} r^{kN} \end{aligned}$$

for all $(\alpha,\psi)\in\overline{\mathbb{D}}_r\times\mathbb{S}^1$ and thus

$$\sup_{(\alpha,\psi)\in\overline{\mathbb{D}}_r\times\mathbb{S}^1}|\mathrm{Re}\,\mathrm{D}_\alpha\eta(\alpha,\psi,\boldsymbol{\lambda}^*)|=\mathcal{O}(r^N)$$
$$\sup_{(\alpha,\psi)\in\overline{\mathbb{D}}_r\times\mathbb{S}^1}|\mathrm{Im}\,\mathrm{D}_\alpha\eta(\alpha,\psi,\boldsymbol{\lambda}^*)|=\mathcal{O}(r^N).$$

Similarly, we find for the second column

$$\begin{aligned}\mathrm{D}_{\bar\alpha}\eta(\alpha,\psi,\boldsymbol{\lambda}^*)=&-\sum_{k=1}^{\infty}(kN-1)\,\bar\alpha^{kN-2}\,\mathrm{e}^{ikN\psi}\\&+\alpha\sum_{k=1}^{\infty}kN\,\bar\alpha^{kN-1}\,\mathrm{e}^{ikN\psi}\\|\mathrm{D}_{\bar\alpha}\eta(\alpha,\psi,\boldsymbol{\lambda}^*)|\le&\sum_{k=1}^{\infty}\Big[(kN-1)\,|\alpha|^{kN-2}+kN\,|\alpha|^{kN}\Big]\\\le&\sum_{k=1}^{\infty}\Big[(kN-1)\,r^{kN-2}+kN\,r^{kN}\Big]\end{aligned}$$

for all $(\alpha,\psi)\in\overline{\mathbb{D}}_r\times\mathbb{S}^1$ and hence

$$\sup_{(\alpha,\psi)\in\overline{\mathbb{D}}_r\times\mathbb{S}^1}|\mathrm{Re}\,\mathrm{D}_{\bar\alpha}\eta(\alpha,\psi,\boldsymbol{\lambda}^*)|=\mathcal{O}(Nr^{N-2})$$
$$\sup_{(\alpha,\psi)\in\overline{\mathbb{D}}_r\times\mathbb{S}^1}|\mathrm{Im}\,\mathrm{D}_{\bar\alpha}\eta(\alpha,\psi,\boldsymbol{\lambda}^*)|=\mathcal{O}(Nr^{N-2}).$$

Finally, we have

$$\begin{aligned}\mathrm{D}_\psi\eta(\alpha,\psi,\boldsymbol{\lambda}^*)=&\sum_{k=1}^{\infty}ikN\big[-\bar\alpha^{kN-1}+\alpha\bar\alpha^{kN}\big]\mathrm{e}^{ikN\psi}\\|\mathrm{D}_\psi\eta(\alpha,\psi,\boldsymbol{\lambda}^*)|\le&\sum_{k=1}^{\infty}kN\big[\,|\alpha|^{kN-1}+|\alpha|^{kN+1}\,\big]\\\le&\sum_{k=1}^{\infty}kN\big[r^{kN-1}+r^{kN+1}\big]\end{aligned}$$

for all $(\alpha,\psi)\in\overline{\mathbb{D}}_r\times\mathbb{S}^1$ so that

$$\sup_{(\alpha,\psi)\in\overline{\mathbb{D}}_r\times\mathbb{S}^1}|\mathrm{Re}\,\mathrm{D}_\psi\eta(\alpha,\psi,\boldsymbol{\lambda}^*)|=\mathcal{O}(Nr^{N-1})$$
$$\sup_{(\alpha,\psi)\in\overline{\mathbb{D}}_r\times\mathbb{S}^1}|\mathrm{Im}\,\mathrm{D}_\psi\eta(\alpha,\psi,\boldsymbol{\lambda}^*)|=\mathcal{O}(Nr^{N-1}).$$

Writing

$$\|A\|_1=\max_{1\le j\le n}\sum_{i=1}^{m}|A_{ij}|$$

for the induced 1-norm for any m-by-n matrix A and using the inequality $\|A\|\le\sqrt{n}\,\|A\|_1$ for its Euclidean norm, we arrive at

$$\Big\|\tilde{\mathrm{D}}\eta(\alpha,\psi,\boldsymbol{\lambda}^*)\Big\|\le\sqrt{3}\max_{x\in\{\alpha,\bar\alpha,\psi\}}\Big(\Big|\mathrm{Re}\,\tilde{\mathrm{D}}_x\eta(\alpha,\psi,\boldsymbol{\lambda}^*)\Big|+\Big|\mathrm{Im}\,\tilde{\mathrm{D}}_x\eta(\alpha,\psi,\boldsymbol{\lambda}^*)\Big|\Big)$$

and hence

$$\left\|\tilde{\mathrm{D}}\eta(\alpha,\psi,\boldsymbol{\lambda}^*)\right\| = \mathcal{O}(Nr^{N-2}),$$

uniformly for all $(\alpha,\psi) \in \overline{\mathbb{D}}_r \times \mathbb{S}^1$ which proves Equation (6.8). □

By substituting α for Z in (6.4), we neglect certain terms on the right hand side of that equation, i. e., we *truncate* the equations and Lemma 6.3 allows to estimate the error, introduced by this approximation on each level set $\mathcal{L}_{\boldsymbol{\lambda}}(\boldsymbol{\Lambda})$. However, it does not yet give an estimate on the truncated terms in (6.4) which is necessary in order to apply the Persistence Theorem 3.7 later on. This estimate is content of the following lemma:

Lemma 6.4 *Let $0 < r < 1$ and let the vector field $\boldsymbol{\tau} : \mathbb{D} \times \mathbb{S}^1 \times V \to \mathbb{R}^3$ be defined by*

$$\boldsymbol{\tau}(\alpha,\psi,\boldsymbol{\lambda}) = (G(Z(\alpha,\psi,\boldsymbol{\lambda})) - G(\alpha)) \cdot \boldsymbol{Y}(\alpha,\psi) \tag{6.9}$$

where $G : \mathbb{D} \to \mathbb{C}$ and $\boldsymbol{Y} : \mathbb{D} \times \mathbb{S}^1 \to \mathbb{R}^3$ are smooth. Then, given $\epsilon > 0$, there exist an $N_0 \in \mathbb{N}$ such that for all $N \geq N_0$, there exists a δ-neighborhood $V_\delta(\boldsymbol{\lambda}^*)$ of $\boldsymbol{\lambda}^*$ such that

$$\sup_{(\alpha,\psi)\in\overline{\mathbb{D}}_r\times\mathbb{S}^1} \|\boldsymbol{\tau}(\alpha,\psi,\boldsymbol{\lambda})\| + \left\|\tilde{\mathrm{D}}\boldsymbol{\tau}(\alpha,\psi,\boldsymbol{\lambda})\right\| < \epsilon$$

for all $\boldsymbol{\lambda} \in V_\delta(\boldsymbol{\lambda}^*)$.

Proof. **Step 1:** Let $F : \mathbb{D} \to \mathbb{C}$ be defined as $F(Z) \coloneqq G(Z) - G(\alpha)$. We start by bounding the function F and its partial derivatives $\mathrm{D}_x F$ with $x \in \{\alpha, \bar{\alpha}, \psi\}$. Since $\overline{\mathbb{D}}_r$ is convex and $F(\alpha) = 0$, we find by the mean value theorem and with $\eta = Z - \alpha$ that

$$\begin{aligned} F(Z) &= \int_0^1 \eta \cdot \mathrm{D}_z F|_{z=\alpha+t\eta} + \bar{\eta} \cdot \mathrm{D}_{\bar{z}} F|_{z=\alpha+t\eta}\,\mathrm{d}t \\ |F(Z)| &\leq |\eta| \cdot \int_0^1 |\mathrm{D}_z F|_{z=\alpha+t\eta} + |\mathrm{D}_{\bar{z}} F|_{z=\alpha+t\eta}\,\mathrm{d}t. \end{aligned} \tag{6.10}$$

Since F is smooth and $\overline{\mathbb{D}}_r$ is compact, there exist constants $M_1, M_2 > 0$ such that $|\mathrm{D}_z F| < M_1$ and $|\mathrm{D}_{\bar{z}} F| < M_2$ for all $z \in \overline{\mathbb{D}}_r$ and in particular, the integral above is of order $\mathcal{O}(1)$ and subsequently

$$|F(Z(\alpha,\psi,\boldsymbol{\lambda}^*))| = \mathcal{O}(|\eta(\alpha,\psi,\boldsymbol{\lambda}^*)|) = \mathcal{O}(r^{N-1})$$

for all $(\alpha,\psi) \in \overline{\mathbb{D}}_r \times \mathbb{S}^1$ by Lemma 6.3. On the other hand, applying the product and chain rule to (6.10), we find

$$\begin{aligned} \mathrm{D}_x F(Z) = &\int_0^1 \mathrm{D}_z\mathrm{D}_z F|_{z=\alpha+t\eta}\,\mathrm{D}_x(\alpha+t\eta)\,\mathrm{d}t \cdot \eta \\ &+ \int_0^1 \mathrm{D}_{\bar{z}}\mathrm{D}_z F|_{z=\alpha+t\eta}\,\mathrm{D}_x(\bar{\alpha}+t\bar{\eta})\,\mathrm{d}t \cdot \eta \\ &+ \int_0^1 \mathrm{D}_z\mathrm{D}_{\bar{z}} F|_{z=\alpha+t\eta}\,\mathrm{D}_x(\alpha+t\eta)\,\mathrm{d}t \cdot \bar{\eta} \\ &+ \int_0^1 \mathrm{D}_{\bar{z}}\mathrm{D}_{\bar{z}} F|_{z=\alpha+t\eta}\,\mathrm{D}_x(\bar{\alpha}+t\bar{\eta})\,\mathrm{d}t \cdot \bar{\eta} \\ &+ \int_0^1 \mathrm{D}_z F|_{\alpha+t\eta}\,\mathrm{d}t \cdot \mathrm{D}_x\eta + \int_0^1 \mathrm{D}_{\bar{z}} F|_{z=\alpha+t\eta}\,\mathrm{d}t \cdot \mathrm{D}_x\bar{\eta} \end{aligned}$$

so that by the same argument as above, and again with Lemma 6.3, we find with $|\mathrm{D}_x(\alpha + t\eta(\alpha,\psi,\boldsymbol{\lambda}^*))| = \mathcal{O}(1) + \mathcal{O}(Nr^{N-2}) = \mathcal{O}(1)$

$$\begin{aligned}
|\mathrm{D}_x F(Z(\alpha,\psi,\boldsymbol{\lambda}^*))| \leq\ & |\eta| \cdot \int_0^1 \Big[|\mathrm{D}_z\mathrm{D}_z F|_{\,z=\alpha+t\eta} \cdot |\mathrm{D}_x(\alpha+t\eta)| + \\
& + |\mathrm{D}_{\bar z}\mathrm{D}_z F|_{\,z=\alpha+t\eta} \cdot |\mathrm{D}_x(\bar\alpha+t\bar\eta)| + \\
& + |\mathrm{D}_z\mathrm{D}_{\bar z} F|_{\,z=\alpha+t\eta} \cdot |\mathrm{D}_x(\alpha+t\eta)| + \\
& + |\mathrm{D}_{\bar z}\mathrm{D}_{\bar z} F|_{\,z=\alpha+t\eta} \cdot |\mathrm{D}_x(\bar\alpha+t\bar\eta)| \Big] \,\mathrm{d}t + \\
& + |\mathrm{D}_x\eta| \cdot \int_0^1 |\mathrm{D}_z F|_{\,z=\alpha+t\eta} + |\mathrm{D}_{\bar z} F|_{\,z=\alpha+t\eta} \,\mathrm{d}t \\
=\ & \mathcal{O}(|\eta(\alpha,\psi,\boldsymbol{\lambda}^*)|)\cdot\mathcal{O}(1) + \mathcal{O}(|\mathrm{D}_x\eta(\alpha,\psi,\boldsymbol{\lambda}^*)|)\cdot\mathcal{O}(1) \\
=\ & \mathcal{O}(r^{N-1}) + \mathcal{O}(Nr^{N-2}) \\
=\ & \mathcal{O}(Nr^{N-2}).
\end{aligned}$$

Step 2: Since $\boldsymbol{Y}(\alpha,\psi)$ does not depend on N, we have $\|\boldsymbol{Y}(\alpha,\psi)\| = \mathcal{O}(1)$ and $\|\mathrm{D}_x\boldsymbol{Y}(\alpha,\psi)\|_1 = \mathcal{O}(1)$ for all $(\alpha,\psi) \in \overline{\mathbb{D}}_r \times \mathbb{S}^1$ so that

$$\|\boldsymbol{\tau}(\alpha,\psi,\boldsymbol{\lambda}^*)\| = |F(Z(\alpha,\psi,\boldsymbol{\lambda}^*))| \cdot \|\boldsymbol{Y}(\alpha,\psi)\| = \mathcal{O}(r^{N-1})$$

and

$$\begin{aligned}
\left\|\tilde{\mathrm{D}}\boldsymbol{\tau}(\alpha,\psi,\boldsymbol{\lambda}^*)\right\|_1 =\ & \max_x \|\mathrm{D}_x F(Z(\alpha,\psi,\boldsymbol{\lambda}^*)) \cdot \boldsymbol{Y}(\alpha,\psi) + \\
& + F(Z(\alpha,\psi,\boldsymbol{\lambda}^*)) \cdot \mathrm{D}_x\boldsymbol{Y}(\alpha,\psi)\|_1 \\
\leq\ & \max_x |\mathrm{D}_x F(Z(\alpha,\psi,\boldsymbol{\lambda}^*))| \cdot \|\boldsymbol{Y}(\alpha,\psi)\|_1 + \\
& + \max_x |F(Z(\alpha,\psi,\boldsymbol{\lambda}^*))| \cdot \|\mathrm{D}_x\boldsymbol{Y}(\alpha,\psi)\|_1 \\
=\ & \mathcal{O}(Nr^{N-2})\cdot\mathcal{O}(1) + \mathcal{O}(r^{N-1})\cdot\mathcal{O}(1) \\
=\ & \mathcal{O}(Nr^{N-2})
\end{aligned}$$

hold by the previous step. Hence, we find that for all $(\alpha,\psi) \in \overline{\mathbb{D}}_r \times \mathbb{S}^1$

$$\left\|\tilde{\mathrm{D}}\boldsymbol{\tau}(\alpha,\psi,\boldsymbol{\lambda}^*)\right\| \leq \sqrt{3}\left\|\tilde{\mathrm{D}}\boldsymbol{\tau}(\alpha,\psi,\boldsymbol{\lambda}^*)\right\|_1 = \mathcal{O}(Nr^{N-2}).$$

Step 3: From step 2, we infer that there exists an N_0 such that $|\boldsymbol{\tau}(\alpha,\psi,\boldsymbol{\lambda})| < \epsilon/2$ and $\left\|\tilde{\mathrm{D}}\boldsymbol{\tau}(\alpha,\psi,\boldsymbol{\lambda})\right\| < \epsilon/2$, uniformly on $\overline{\mathbb{D}}_r \times \mathbb{S}^1 \times \{\boldsymbol{\lambda}^*\}$ for all $N \geq N_0$. By smoothness of $\boldsymbol{\tau}$, it follows that for all $(\alpha,\psi,\boldsymbol{\lambda}^*) \in \overline{\mathbb{D}}_r \times \mathbb{S}^1 \times \{\boldsymbol{\lambda}^*\}$, there exist open neighborhoods $W(\alpha,\psi) \subseteq \mathbb{D} \times \mathbb{S}^1$ of (α,ψ) and $V_{\delta'}(\boldsymbol{\lambda}^*) \subseteq V$ of $\boldsymbol{\lambda}^*$ with $\delta' = \delta'(\alpha,\psi) > 0$ such that this inequality also holds on $W(\alpha,\psi) \times V_{\delta'}(\boldsymbol{\lambda}^*)$. Covering $\overline{\mathbb{D}}_r \times \mathbb{S}^1 \times \{\boldsymbol{\lambda}^*\}$ with these open sets, there exists a finite subcover since $\overline{\mathbb{D}}_r \times \mathbb{S}^1 \times \{\boldsymbol{\lambda}^*\}$ is compact. We set $\delta \coloneqq \min \delta'$ over this subcover and thus find

$$|\boldsymbol{\tau}(\alpha,\psi,\boldsymbol{\lambda})| + \left\|\tilde{\mathrm{D}}\boldsymbol{\tau}(\alpha,\psi,\boldsymbol{\lambda})\right\| < \epsilon$$

for each $(\alpha,\psi,\boldsymbol{\lambda}) \in \overline{\mathbb{D}}_r \times \mathbb{S}^1 \times V_\delta$ which proves the assertion. □

Lemma 6.4 essentially states that truncating the right hand side of (6.4) introduces an error on each level set, that can be made arbitrarily small by choosing N large enough. With this, we are ready to prove the first main result of this chapter: The existence of a continuous family of periodic orbits for systems of the type (6.4), whose union forms a NAIM in $\mathbb{T}^N_{\text{ordered}}$.

6.3.2 *The Continuum of Periodic Orbits*

It was already argued in [WS94] that any periodic orbit $\mathcal{C}_{\boldsymbol{\lambda}}$ for a WS-integrable system that is hyperbolic in its level set $\mathcal{L}_{\boldsymbol{\lambda}}(\boldsymbol{\Lambda}) \supset \mathcal{C}_{\boldsymbol{\lambda}}$ gives rise to a whole (continuous) family $\{\mathcal{C}_{\boldsymbol{\lambda}'}\,;\, \boldsymbol{\lambda}' \in U(\boldsymbol{\lambda})\}$ of such orbits since varying $\boldsymbol{\lambda}$ within some (small) neighborhood $U(\boldsymbol{\lambda})$ of $\boldsymbol{\lambda}$ equally varies the respective vector field from level set to level set. As long as the vector field depends smoothly on $\boldsymbol{\lambda}$, this change in the vector field will be small so that by persistence of hyperbolic orbits, we find such orbits for all $\boldsymbol{\lambda}' \in U(\boldsymbol{\lambda})$. In this sense, the following theorem is not surprising. However, besides the fact that the argument for such a families of orbits was not made rigorously, we now show that, if the system is of type (6.4), it is equipped with even more structure: if the orbits are exponentially stable in their respective level sets, their union forms a NAIM.

The strategy for the proof goes as follows: As in [PR08] and [Eld+21], we "close" the system (6.4) by substituting α for Z such that (6.4a) decouples from ψ. If the now closed equation (6.4a) allows for a unique exponentially stable fixed point α_0 for which $\dot{\psi}(\alpha_0) \neq 0$ holds, there then exists a periodic solution of the full truncated system. Further, for every $\epsilon > 0$ and N sufficiently large, there exists a neighborhood of $\boldsymbol{\lambda}^*$ such that for every $\boldsymbol{\lambda}$ in that neighborhood, the truncated terms constitute a $\mathcal{O}(\epsilon)$-small perturbation for the closed system in C^1-norm on $\mathcal{L}_{\boldsymbol{\lambda}}(\boldsymbol{\Lambda})$. The union of periodic orbits over that open neighborhood of $\boldsymbol{\lambda}^*$ then forms the desired NAIM for the truncated system. Choosing N large enough, the truncated terms can be treated as small perturbations which guarantees that the orbits themselves and subsequently the NAIM also exist for the full system by means of the Persistence Theorem 3.7.

Theorem 6.5 *Consider the system*

$$\dot{\alpha} = i\left(f(Z)\alpha^2 + g(Z)\alpha + \bar{f}(Z)\right) \tag{6.4a}$$

$$\dot{\psi} = f(Z)\alpha + g(Z) + \bar{f}(Z)\bar{\alpha} \tag{6.4b}$$

$$\dot{\boldsymbol{\lambda}} = \mathbf{0} \tag{6.4c}$$

where $f : \mathbb{D} \to \mathbb{C}$ and $g : \mathbb{D} \to \mathbb{R}$ are smooth functions of the Kuramoto order parameter Z. Further, let the closed equation

$$\dot{\alpha} = i\left(f(\alpha)\alpha^2 + g(\alpha)\alpha + \bar{f}(\alpha)\right) \tag{6.12}$$

possess a unique stable fixed point $\alpha_0 \in \mathbb{D}$ for which

$$f(\alpha_0) \neq 0$$

holds. Then, there exists an $N_0 \in \mathbb{N}$ *such that for all* $N \geq N_0$ *there exists a* δ*-neighborhood* $\overline{V}_\delta(\boldsymbol{\lambda}^*)$ *of* $\boldsymbol{\lambda}^*$ *such that for every* $\boldsymbol{\lambda} \in \overline{V}_\delta(\boldsymbol{\lambda}^*)$ *there exists a unique periodic orbit* $\mathcal{C}_{\boldsymbol{\lambda}} \subset \mathcal{L}_{\boldsymbol{\lambda}}(\boldsymbol{\Lambda})$ *which is exponentially stable in* $\mathcal{L}_{\boldsymbol{\lambda}}(\boldsymbol{\Lambda})$*. Additionally, the union*

$$\mathcal{M}_\delta \coloneqq \bigcup_{\boldsymbol{\lambda} \in \overline{V}_\delta} \mathcal{C}_{\boldsymbol{\lambda}} \subset \mathbb{T}^N_{\text{ordered}}$$

forms a compact NAIM *of dimension* $N-2$ *with invariant boundary.*

Proof. **Step 1:** Substituting Z by α in (6.4) yields the closed system

$$\dot{\alpha} = i\left(f(\alpha)\alpha^2 + g(\alpha)\alpha + \bar{f}(\alpha)\right) \tag{6.13a}$$

$$\dot{\psi} = f(\alpha)\alpha + g(\alpha) + \bar{f}(\alpha)\bar{\alpha} \tag{6.13b}$$

$$\dot{\boldsymbol{\lambda}} = \mathbf{0}. \tag{6.13c}$$

By assumption, α_0 is a stable fixed point of (6.13a). If $\Omega \coloneqq f(\alpha_0)\alpha_0 + g(\alpha_0) + \bar{f}(\alpha_0)\bar{\alpha}_0 \neq 0$, this gives rise to the periodic solution $(\alpha_0, \Omega t, \boldsymbol{\lambda})$ for (6.13) with an exponentially stable periodic orbit $\mathcal{C}^{\text{trunc}}_{\boldsymbol{\lambda}}$. From the definition of Ω, we then infer

$$\alpha_0 \Omega = f(\alpha_0)\alpha_0^2 + g(\alpha_0)\alpha_0 + \bar{f}(\alpha_0)\left|\alpha_0\right|^2.$$

Adding and subtracting $\bar{f}(\alpha_0)$, this results in

$$\alpha_0 \Omega = \underbrace{f(\alpha_0)\alpha_0^2 + g(\alpha_0)\alpha_0 + \bar{f}(\alpha_0)}_{=0 \text{ by (6.13a)}} + \bar{f}(\alpha_0)\left(\left|\alpha_0\right|^2 - 1\right)$$

so that $\Omega = 0$ implies $f(\alpha_0) = 0$ and conversely, $f(\alpha_0) \neq 0$ implies $\Omega \neq 0$.

Step 2: We prove that for any $\delta > 0$, the union

$$\mathcal{M}^{\text{trunc}}_\delta \coloneqq \bigcup_{\boldsymbol{\lambda} \in \overline{V}_\delta} \mathcal{C}^{\text{trunc}}_{\boldsymbol{\lambda}} = \{\alpha_0\} \times \mathbb{S}^1 \times \overline{V}_\delta$$

forms a smooth compact NAIM with invariant boundary for (6.13) in $\mathbb{D} \times \mathbb{S}^1 \times V$ by checking conditions (i)-(iii) of Definition 3.5. Indeed, as a product of the three smooth compact manifolds $\{\alpha_0\}$, $\mathbb{S}^1$, and $\overline{V}_\delta$, it is itself an $(N-2)$-dimensional smooth compact submanifold of $\mathbb{D} \times \mathbb{S}^1 \times V$. Further, it is invariant by construction (as is its boundary which consists of all $\mathcal{C}^{\text{trunc}}_{\boldsymbol{\lambda}}$ with $\boldsymbol{\lambda} \in \partial\overline{V}_\delta$) so that condition (i) is fulfilled.

To show that condition (ii) holds, we need to determine the continuous splitting $T_{\mathcal{M}^{\text{trunc}}_\delta}\mathbb{T}^N_{\text{ordered}} = T\mathcal{M}^{\text{trunc}}_\delta \oplus \mathcal{N}$ and the decomposition $\mathrm{D}\Phi^t(\boldsymbol{p}) = \mathrm{D}\Phi^t_{\mathcal{M}^{\text{trunc}}_\delta}(\boldsymbol{p}) \oplus \mathrm{D}\Phi^t_{\mathcal{N}}(\boldsymbol{p})$ which keeps this splitting invariant. For this, consider any point $\boldsymbol{p} = (\alpha_0, \psi, \boldsymbol{\lambda}) \in \mathcal{M}^{\text{trunc}}_\delta$. We can write any vector $\boldsymbol{v} \in T_{\boldsymbol{p}}\mathbb{T}^N_{\text{ordered}}$ as $\boldsymbol{v} = (v_\alpha, v_\psi, v_{\boldsymbol{\lambda}})^T$ where $v_\alpha \in \mathbb{R}^2$, $v_\psi \in \mathbb{R}^1$, and $v_{\boldsymbol{\lambda}} \in \mathbb{R}^{N-3}$ denote the respective tangential components with respect to the variables α, ψ, and $\boldsymbol{\lambda}$. Then, $T_{\boldsymbol{p}}\mathcal{M}^{\text{trunc}}_\delta$ is spanned by those $\boldsymbol{v}$ with $v_\alpha = 0$ (since $\{\alpha_0\}$ is just a point) while the vectors $(v_\alpha, 0, 0)$

are perpendicular to $T_{\boldsymbol{p}}\mathcal{M}_\delta^{\text{trunc}}$. Further, we can write $\mathrm{D}\Phi^t(\boldsymbol{p})$ in block matrix form as

$$\mathrm{D}\Phi^t(\boldsymbol{p}) = \begin{pmatrix} \exp\left(t\, J|_{\alpha_0}\right) & 0 \\ A & B \end{pmatrix} \tag{6.14}$$

where $J|_{\alpha_0}$ is the Jacobian for the right hand side of (6.12) evaluated at α_0, A is a $(N-2)$-by-2 matrix, and B is of the form

$$B = \begin{pmatrix} 1 & \mathbf{0}^T \\ \mathbf{0} & \mathrm{id}_{N-3} \end{pmatrix} = \mathrm{id}_{N-2}\,. \tag{6.15}$$

To see this, let $\boldsymbol{v} \in T_{\boldsymbol{p}}\mathbb{T}^N_{\text{ordered}}$ denote any tangent vector at $\boldsymbol{p} \in \mathcal{M}_\delta^{\text{trunc}}$. We find α decoupled from ψ and $\boldsymbol{\lambda}$, so that the linearized flow in α at the fixed point α_0 is given by the linear map $v_\alpha \mapsto \exp(t\, J|_{\alpha_0})\cdot v_\alpha$ which yields the two upper blocks of in (6.14).[5] The flow in ψ is given by

$$\psi \mapsto \psi + \int_0^t \left[f(\alpha(t'))\alpha(t') + g(\alpha(t')) + \bar{f}(\alpha(t'))\bar{\alpha}(t')\right] \mathrm{d}t'$$

where $\alpha(t')$ solves (6.4a) and the flow of ψ is in particular independent of $\boldsymbol{\lambda}$. The flow in $\boldsymbol{\lambda}$ is constant, and so its linearization is the $(N-3)\times(N-3)$ identity. From this it follows that the only nonzero entries of the matrix A are in its top row (since the flow of ψ and thus its linearization generally depend on α but not on $\boldsymbol{\lambda}$) while B is of the form (6.15). We conclude from (6.14) that $\mathrm{D}\Phi^t(\boldsymbol{p})$ possesses two simple eigenvalues $\mathrm{e}^{\lambda^\pm} < 1$ where $\lambda^\pm < 0$ denote the eigenvalues of the Jacobian $J|_{\alpha_0}$. Further, we have an eigenvalue 1 of multiplicity $N-2$. The corresponding $N-2$ eigenvectors to the latter eigenvalue span $T\mathcal{M}_\delta^{\text{trunc}}$ since for every $\boldsymbol{v}_{||} = (0, v_\psi, v_{\boldsymbol{\lambda}}) \in T_{\boldsymbol{p}}\mathcal{M}_\delta^{\text{trunc}}$, we have

$$\begin{pmatrix} 0 \\ v_\psi \\ v_{\boldsymbol{\lambda}} \end{pmatrix} \mapsto \mathrm{D}\Phi^t(\alpha,\psi,\boldsymbol{\lambda})\cdot \begin{pmatrix} 0 \\ v_\psi \\ v_{\boldsymbol{\lambda}} \end{pmatrix} = \mathrm{D}\Phi^t_{\mathcal{M}_\delta^t}(\alpha,\psi,\boldsymbol{\lambda})\cdot \begin{pmatrix} 0 \\ v_\psi \\ v_{\boldsymbol{\lambda}} \end{pmatrix} = \begin{pmatrix} 0 \\ v_\psi \\ v_{\boldsymbol{\lambda}} \end{pmatrix} = \boldsymbol{v}_{||}.$$

The span of the two eigenvectors $\boldsymbol{v}^\pm$ that correspond to e^{λ^+} and e^{λ^-}, respectively, then uniquely defines the normal space $\mathcal{N}_{\boldsymbol{p}}$ at $\boldsymbol{p}$. The only nonzero components of $\boldsymbol{v}^\pm$ are v_α and v_ψ due to the fact that the matrix A contains nonzero entries in its first row. Since they are eigenvectors of $\mathrm{D}\Phi^t(\boldsymbol{p})$ with eigenvalues $\mathrm{e}^{\lambda^\pm}$, the dynamics in these directions decouple from the linearized tangential flow $\mathrm{D}\Phi^t_{\mathcal{M}_\delta^t}(\boldsymbol{p})$ and we thus conclude that $\mathrm{D}\Phi^t(\boldsymbol{p})$ indeed can be written as $\mathrm{D}\Phi^t(\boldsymbol{p}) = \mathrm{D}\Phi^t_{\mathcal{M}_\delta^{\text{trunc}}}(\boldsymbol{p}) \oplus \mathrm{D}\Phi^t_{\mathcal{N}}(\boldsymbol{p})$ which keeps the splitting of $T_{\mathcal{M}_\delta^{\text{trunc}}}\mathbb{R}^n = T\mathcal{M}_\delta^{\text{trunc}} \oplus \mathcal{N}$ invariant. The splitting is continuous since all eigenvalues depend continuous on the entries of $\mathrm{D}\Phi^t(\boldsymbol{p})$ and thus of $\boldsymbol{p}$. For the projection $\pi_{\mathcal{M}^{\text{trunc}}} : T_{\mathcal{M}_\delta^{\text{trunc}}}\mathbb{T}^N_{\text{ordered}} \to T\mathcal{M}_\delta^{\text{trunc}}$, we have

$$\pi_{\mathcal{M}_\delta^{\text{trunc}}}(\alpha_0, \psi, \boldsymbol{\lambda}, v_\alpha, v_\psi, v_{\boldsymbol{\lambda}}) = (\alpha_0, \psi, \boldsymbol{\lambda}, 0, v_\psi, v_{\boldsymbol{\lambda}})$$

5 This is a standard result which also plays a crucial role in the proof of the Hartman-Grobman theorem, see [Chi99].

while the projection $\pi_{\mathcal{N}} : T_{\mathcal{M}_\delta^{\text{trunc}}}\mathbb{T}^N_{\text{ordered}} \to \mathcal{N}$ is given by the canonical scalar product

$$\pi_{\mathcal{N}}(\alpha_0, \psi, \boldsymbol{\lambda}, \boldsymbol{v}) = (\alpha_0, \psi, \boldsymbol{\lambda}, (\boldsymbol{v} \cdot \boldsymbol{v}^+)\boldsymbol{v}^+ + (\boldsymbol{v} \cdot \boldsymbol{v}^-)\boldsymbol{v}^-).$$

From this, we see that both projections are readily continuous due to the continuity of the basis vectors $\boldsymbol{v}^\pm(\boldsymbol{p})$.

At last, we show that condition (iii) is fulfilled. We already noted that the eigenvalue 1 corresponds to the tangential flow $\mathrm{D}\Phi^t_{\mathcal{M}_\delta^{\text{trunc}}}$ while $0 < \mathrm{e}^{\lambda^\pm} < 1$ correspond to the contracting normal flow $\mathrm{D}\Phi^t_{\mathcal{N}}$. Hence, for the contraction rates, we find $a = \max(\lambda^+, \lambda^-) < 0$ as well as $b = 0$ and $C = 1$. In particular, we have $a < bm = 0$ for $m > 0$ and thus $\mathcal{M}_\delta^{\text{trunc}}$ is a NAIM.

Step 3: We proceed by showing that (6.4) equally possesses a continuous family of periodic orbits. By closing (6.4) to get equation (6.13), we truncated the vector field

$$\boldsymbol{\tau} = F(Z)\begin{pmatrix} i\alpha^2 \\ \alpha \\ \mathbf{0} \end{pmatrix} + G(Z)\begin{pmatrix} i\alpha \\ 1 \\ \mathbf{0} \end{pmatrix} + \bar{F}(Z)\begin{pmatrix} i \\ \bar{\alpha} \\ \mathbf{0} \end{pmatrix}$$

with

$$F(Z) \coloneqq f(Z) - f(\alpha)$$
$$G(Z) \coloneqq g(Z) - g(\alpha)$$

from (6.4). Identifying $\mathcal{L}_{\boldsymbol{\lambda}}(\boldsymbol{\Lambda}) \cong \mathbb{D} \times \mathbb{S}^1 \times \{\boldsymbol{\lambda}\}$ with the space $\mathbb{D} \times \mathbb{S}^1$, we subsequently truncate

$$\boldsymbol{\tau}|_{\mathcal{L}_{\boldsymbol{\lambda}}(\boldsymbol{\Lambda})} = F(Z)\begin{pmatrix} i\alpha^2 \\ \alpha \end{pmatrix} + G(Z)\begin{pmatrix} i\alpha \\ 1 \end{pmatrix} + \bar{F}(Z)\begin{pmatrix} i \\ \bar{\alpha} \end{pmatrix} \tag{6.16}$$

in every level set $\mathcal{L}_{\boldsymbol{\lambda}}(\boldsymbol{\Lambda})$ for any given $\boldsymbol{\lambda} \in V$ where each of the three terms on the right hand side is of the form (6.9). Choose $1 > r > |\alpha_0|$. Since in $\mathbb{D} \times \mathbb{S}^1$, we can identify all $\mathcal{C}_{\boldsymbol{\lambda}}^{\text{trunc}}$ with the stable limit cycle $\{\alpha_0\} \times \mathbb{S}^1 \subset \mathbb{D}_r \times \mathbb{S}^1$, there exists an $\epsilon > 0$ such that for every perturbation of the vector field that has C^1-norm smaller than ϵ in $\mathbb{D}_r \times \mathbb{S}^1$, the orbits $\mathcal{C}_{\boldsymbol{\lambda}}^{\text{trunc}}$ persists by the Persistence Theorem 3.7. But by Lemma 6.4, there exists an $N_0 \in \mathbb{N}$ such that for all $N \geq N_0$, there exists a δ-neighborhood $\overline{V}_\delta(\boldsymbol{\lambda}^*)$ of $\boldsymbol{\lambda}^*$ such that

$$|\boldsymbol{\tau}(\alpha, \psi, \boldsymbol{\lambda})| + \left\|\tilde{\mathrm{D}}\boldsymbol{\tau}(\alpha, \psi, \boldsymbol{\lambda})\right\| < \epsilon$$

uniformly on $\mathbb{D}_r \times \mathbb{S}^1 \times \overline{V}_\delta$ and thus, the $\mathcal{C}_{\boldsymbol{\lambda}}^{\text{trunc}}$ persist, i. e., the full system (6.4) possesses a periodic orbit $\mathcal{C}_{\boldsymbol{\lambda}} \subset \mathbb{D}_r \times \mathbb{S}^1 \times \{\boldsymbol{\lambda}\} \subset \mathcal{L}_{\boldsymbol{\lambda}}(\boldsymbol{\Lambda})$ for every $\boldsymbol{\lambda} \in \overline{V}_\delta$.

We can further choose δ such that the boundary of the union $\mathcal{M}_\delta$ over these orbits is composed of orbits $\mathcal{C}_{\boldsymbol{\lambda}}$ with $\boldsymbol{\lambda} \in \partial\overline{V}_\delta$ and is thus invariant. Next, we show that $\mathcal{M}_\delta$ is a smooth compact manifold.

Step 4: Note that for $\boldsymbol{\lambda} \in \overline{V}_\delta$, there exists a smooth immersion $\iota_{\boldsymbol{\lambda}} : \mathcal{C}_{\boldsymbol{\lambda}}^{\text{trunc}} \to \mathbb{D}_r \times \mathbb{S}^1 \times \{\boldsymbol{\lambda}\}$ whose image $\iota_{\boldsymbol{\lambda}}(\mathcal{C}_{\boldsymbol{\lambda}}^{\text{trunc}}) = \mathcal{C}_{\boldsymbol{\lambda}}$ lies ϵ-close to $\mathcal{C}_{\boldsymbol{\lambda}}^{\text{trunc}}$ and that $\iota_{\boldsymbol{\lambda}}$ itself depends smoothly on $\boldsymbol{\lambda}$ because the truncated terms (6.16) are smooth in $\boldsymbol{\lambda}$. Hence, the map

$$\begin{aligned} \iota &: \mathcal{M}_\delta^{\text{trunc}} \to \mathbb{D} \times \mathbb{S}^1 \times V \\ \iota &: (\alpha_0, \psi, \boldsymbol{\lambda}) \mapsto (\iota_{\boldsymbol{\lambda}}(\alpha_0, \psi), \boldsymbol{\lambda}), \end{aligned}$$

is (i) smooth, (ii) one-to-one on its image $\mathcal{M}_\delta$, and (iii) its derivative has full rank $N-2$, in other words, ι is equally a smooth immersion and $\mathcal{M}_\delta$, as its image, is a compact smooth manifold [Lee12] which is invariant and $\mathcal{O}(\epsilon)$-close to $\mathcal{M}_\delta^{\text{trunc}}$.

Step 5: Finally, we show that $\mathcal{M}_\delta$ is also normally hyperbolic: For any fixed $\boldsymbol{\lambda} \in V$, let $\Phi_{\boldsymbol{\lambda}}^t$ denote the flow on the level set $\mathcal{L}_{\boldsymbol{\lambda}}(\boldsymbol{\Lambda})$. Then, the flow on $\mathbb{T}^N_{\text{ordered}}$ is of the form

$$(\alpha, \psi, \boldsymbol{\lambda}) \mapsto (\Phi_{\boldsymbol{\lambda}}^t(\alpha, \psi), \boldsymbol{\lambda})$$

and is smooth in $\boldsymbol{\lambda}$ since the vector field on $\mathbb{T}^N_{\text{ordered}}$ and thus $\Phi_{\boldsymbol{\lambda}}^t$ is smooth in $\boldsymbol{\lambda}$. The linearized flow at $\boldsymbol{p} = (\alpha, \psi, \boldsymbol{\lambda}) \in \mathcal{C}_{\boldsymbol{\lambda}} \subset \mathcal{M}_\delta \subset \mathbb{T}^N_{\text{ordered}}$ reads

$$\mathrm{D}\Phi^t(\boldsymbol{p}) = \begin{pmatrix} \tilde{\mathrm{D}}\Phi_{\boldsymbol{\lambda}}^t(\boldsymbol{p}) & \mathrm{D}_{\boldsymbol{\lambda}}\Phi_{\boldsymbol{\lambda}}^t(\boldsymbol{p}) \\ 0 & \mathrm{id}_{N-3} \end{pmatrix}.$$

Let $\mu^\pm < 0$ denote the two nonzero contraction rates of $\mathcal{C}_{\boldsymbol{\lambda}} \subset \mathcal{L}_{\boldsymbol{\lambda}}(\boldsymbol{\Lambda})$ and $\boldsymbol{v}^\pm = (v_\alpha^\pm, v_\psi^\pm, \mathbf{0})$ the corresponding eigenvectors of $\mathrm{D}\Phi^t(\boldsymbol{p})$ and let $\mu^0 = 0$ denote the vanishing contraction rate in tangential direction to $\mathcal{C}_{\boldsymbol{\lambda}}$. The remaining $N-3$ eigenvectors of $\mathrm{D}\Phi^t(\boldsymbol{p})$ are also tangent vectors of $\mathcal{M}_\delta$ at $\boldsymbol{p}$ and have nonvanishing components in $\boldsymbol{\lambda}$-direction since $\mathcal{M}_\delta$ lies transversal to each $\mathcal{L}_{\boldsymbol{\lambda}}(\boldsymbol{\Lambda})$ that it intersects for sufficiently small $\epsilon > 0$. Since $\boldsymbol{\lambda}$ is constant under the flow, the contraction rates in the remaining $N-3$ tangent direction are also zero. Because Φ^t is smooth in $\boldsymbol{\lambda}$, the $\boldsymbol{v}^\pm$ depend smoothly on $\boldsymbol{p}$ so that condition (ii) of Definition 3.5 is readily fulfilled. For the numbers a, b, and C from condition (iii), we find $b = 0$, $a = \max_{\boldsymbol{p} \in \mathcal{M}_\delta}(\mu^\pm(\boldsymbol{p})) < 0 = bm$ for every $m > 0$ and $C = 1$ so that $\mathcal{M}_\delta$ is a smooth m-normally attracting invariant manifold of (6.4). □

We note that the invariant sets $\mathcal{L}_{\boldsymbol{\lambda}}(\boldsymbol{\Lambda})$ yield a *foliation* [MM03] of $\mathcal{M}_\delta^{\text{trunc}}$ in terms of the periodic orbits $\mathcal{C}_{\boldsymbol{\lambda}}^{\text{trunc}}$. Since the perturbation $\boldsymbol{\tau}$ keeps all $\mathcal{L}_{\boldsymbol{\lambda}}(\boldsymbol{\Lambda})$ invariant (because $\tau_{\boldsymbol{\lambda}} = \mathbf{0}$), the NAIM $\mathcal{M}_\delta$ for the original system (6.4) is equally foliated in terms of its periodic orbits $\mathcal{C}_{\boldsymbol{\lambda}}$. Figure 17 gives a schematic depiction of $\mathcal{M}_\delta$ and how its intersection with any level set $\mathcal{L}_{\boldsymbol{\lambda}}(\boldsymbol{\Lambda})$, $\boldsymbol{\lambda} \in V_\delta$, yields the periodic orbit $\mathcal{C}_{\boldsymbol{\lambda}}$ which is exponentially stable in $\mathcal{L}_{\boldsymbol{\lambda}}(\boldsymbol{\Lambda})$ as indicated by gray arrows. Additional periodic orbits $\mathcal{C}_{\boldsymbol{\lambda}'} \subset \mathcal{L}_{\boldsymbol{\lambda}'}(\boldsymbol{\Lambda})$ and $\mathcal{C}_{\boldsymbol{\lambda}''} \subset \mathcal{L}_{\boldsymbol{\lambda}''}(\boldsymbol{\Lambda})$ are depicted, as well. They lie "parallel" to $\mathcal{C}_{\boldsymbol{\lambda}}$ in the sense that they exist in disjoint level sets which partition $\mathbb{T}^N_{\text{ordered}}$.

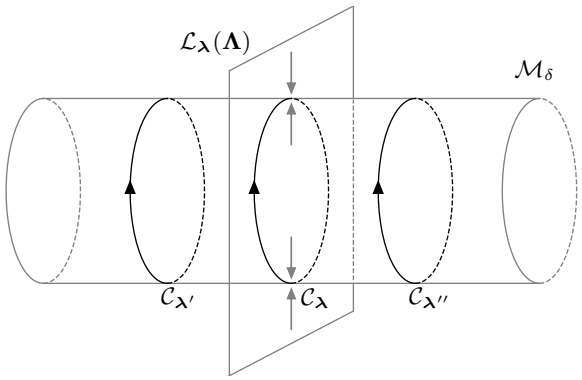

Figure 17: Schematic depiction of the manifold $\mathcal{M}_\delta$ and its periodic orbits. Its intersection with the level set $\mathcal{L}_{\boldsymbol{\lambda}}(\boldsymbol{\Lambda})$ yields the periodic orbit $\mathcal{C}_{\boldsymbol{\lambda}}$. Gray arrows indicate that each $\mathcal{C}_{\boldsymbol{\lambda}}$ is stable in $\mathcal{L}_{\boldsymbol{\lambda}}(\boldsymbol{\Lambda})$. Different periodic orbits $\mathcal{C}_{\boldsymbol{\lambda}'} \subset \mathcal{L}_{\boldsymbol{\lambda}'}(\boldsymbol{\Lambda})$ and $\mathcal{C}_{\boldsymbol{\lambda}''} \subset \mathcal{L}_{\boldsymbol{\lambda}''}(\boldsymbol{\Lambda})$ lie "parallel" to $\mathcal{C}_{\boldsymbol{\lambda}}$.

6.3.3 *Existence of the Splay State*

The manifold $\mathcal{M}_\delta$ intersects in particular the level set $\mathcal{L}_{\boldsymbol{\lambda}^*}(\boldsymbol{\Lambda})$, i. e., there exists a periodic orbit in the level set of uniform distributions. From (6.6), we can deduce that Z and therefore the equations (6.4) are of particularly regular form which hints that the periodic state in $\mathcal{L}_{\boldsymbol{\lambda}^*}(\boldsymbol{\Lambda})$ also features some regular dynamics. This conjecture is confirmed by the following proposition:

Proposition 6.6 *For the manifold $\mathcal{M}_\delta$ from Theorem 6.5, the periodic solution $(\alpha(t), \psi(t), \boldsymbol{\lambda}^*)$ of* (6.4) *with periodic orbit $\mathcal{C}_{\boldsymbol{\lambda}^*} \subset \mathcal{L}_{\boldsymbol{\lambda}^*}(\boldsymbol{\Lambda})$ yields a splay state $\boldsymbol{\phi}_{\boldsymbol{\lambda}^*}(t)$ for systems of the type* (6.3).

Proof. Recall that $\theta_j^* = -\pi + 2\pi(j-1)/N$. For the closed system (6.13), we found the periodic solution $(\alpha_0, \Omega t, \boldsymbol{\lambda}^*)$ with period $T = 2\pi/\Omega$. Its phase dynamics $\boldsymbol{\phi}^{\text{trunc}}_{\boldsymbol{\lambda}^*}(t)$ can be recovered via the diagonal Möbius action (4.10) which yields[6]

$$
\begin{aligned}
\mathrm{e}^{i\phi_j^{\text{trunc}}(t)} &\equiv \frac{\alpha_0 + \mathrm{e}^{i\Omega t + i\theta_j^*}}{1 + \bar{\alpha}_0\, \mathrm{e}^{i\Omega t + i\theta_j^*}} \\
&= \frac{\alpha_0 + \mathrm{e}^{i\Omega t + i\left(-\pi + (j-1)\frac{2\pi}{N}\right)}}{1 + \bar{\alpha}_0\, \mathrm{e}^{i\Omega t + i\left(-\pi + (j-1)\frac{2\pi}{N}\right)}} \\
&= \frac{\alpha_0 + \mathrm{e}^{i\Omega\left(t + j\frac{T}{N}\right) + i\left(-\pi + (N-1)\frac{2\pi}{N}\right)}}{1 + \bar{\alpha}_0\, \mathrm{e}^{i\Omega\left(t + j\frac{T}{N}\right) + i\left(-\pi + (N-1)\frac{2\pi}{N}\right)}} \\
&= \frac{\alpha_0 + \mathrm{e}^{i\Omega\left(t + j\frac{T}{N}\right) + i\theta_N^*}}{1 + \bar{\alpha}_0\, \mathrm{e}^{i\Omega\left(t + j\frac{T}{N}\right) + i\theta_N^*}} \\
&\equiv \mathrm{e}^{i\phi_N^{\text{trunc}}\left(t + j\frac{T}{N}\right)}
\end{aligned}
$$

so that $\phi_j^{\text{trunc}}(t) = \phi_N^{\text{trunc}}\,(t + jT/N)$ holds and $\boldsymbol{\phi}^{\text{trunc}}_{\boldsymbol{\lambda}^*}(t)$ is in fact a splay state, cf. (6.1). We now assert that also the periodic solution

6 When we write down components of $\boldsymbol{\phi}_{\boldsymbol{\lambda}^*}(t)$, we drop the index $\boldsymbol{\lambda}^*$ for better readability.

$(\alpha(t), \psi(t), \boldsymbol{\lambda}^*)$ for the true system (6.4) from Theorem 6.5 yields a splay state $\boldsymbol{\phi}_{\boldsymbol{\lambda}^*}(t)$. For this to be true, the following condition must hold:

$$\mathrm{e}^{i\phi_j(t)} \equiv \frac{\alpha(t) + \mathrm{e}^{i\psi(t)+i\theta_j^*}}{1+\bar{\alpha}(t)\mathrm{e}^{i\psi(t)+i\theta_j^*}} \stackrel{!}{=} \frac{\alpha\Big(t+j\frac{T}{N}\Big) + \mathrm{e}^{i\psi\left(t+j\frac{T}{N}\right)+i\theta_N^*}}{1+\bar{\alpha}\Big(t+j\frac{T}{N}\Big)\mathrm{e}^{i\psi\left(t+j\frac{T}{N}\right)+i\theta_N^*}} \equiv \mathrm{e}^{i\phi_N\left(t+j\frac{T}{N}\right)}$$

which is certainly true if the solution $(\alpha(t), \psi(t), \boldsymbol{\lambda}^*)$ possesses the spatio-temporal symmetry

$$\begin{aligned} \alpha\left(t+j\frac{T}{N}\right) &= \alpha(t) \\ \psi\left(t+j\frac{T}{N}\right) &= \psi(t) + \theta_j^* - \theta_N^* \equiv \psi(t) + j\frac{2\pi}{N} \end{aligned} \tag{6.17}$$

for all $j = 1, \ldots, N$. To see that this is truly the case, we note first that (6.4a) and (6.4b) are equivariant under any transformation that keeps Z and α invariant. Recall that from (6.6), the Kuramoto order parameter on $\mathcal{L}_{\boldsymbol{\lambda}^*}(\boldsymbol{\Lambda})$ is given by

$$Z(\alpha, \psi, \boldsymbol{\lambda}^*) = \alpha - (1 - |\alpha|^2) \sum_{k=1}^{\infty} \bar{\alpha}^{kN-1} \mathrm{e}^{ikN\psi}$$

so that on $\mathcal{L}_{\boldsymbol{\lambda}^*}(\boldsymbol{\Lambda})$, the maps $(\alpha, \psi) \mapsto Z(\alpha, \psi, \boldsymbol{\lambda}^*)$ and $(\alpha, \psi) \mapsto \alpha$ are invariant under the action of the finite group

$$\Gamma \coloneqq \Big\{\gamma_j : \mathbb{D} \times \mathbb{S}^1 \times \{\boldsymbol{\lambda}^*\} \to \mathbb{D} \times \mathbb{S}^1 \times \{\boldsymbol{\lambda}^*\} \; ; \; j = 1, \ldots, N\Big\}$$

of transformations

$$\gamma_j : (\alpha, \psi, \boldsymbol{\lambda}^*) \mapsto \left(\alpha, \psi + j\frac{2\pi}{N}, \boldsymbol{\lambda}^*\right).$$

Hence, for the spatial symmetry group K in Theorem 3.11 for the periodic solution $(\alpha_0, \Omega t, \boldsymbol{\lambda}^*)$, we find $K = \{\gamma_N\}$ (i. e., K contains only the identity element γ_N) while for the spatio-temporal symmetry group, we find $H = N(K) = \Gamma$. Further, we have $\eta = \gamma_{N-1}$ and $m = N$ in Theorem 3.11 since with $\Omega = 2\pi/T$, we find

$$\begin{aligned} \gamma_{N-1}\left(\alpha_0, \Omega\left(t+\frac{T}{N}\right), \boldsymbol{\lambda}^*\right) &= \left(\alpha_0, \Omega t + \frac{\Omega T}{N} + (N-1)\frac{2\pi}{N}, \boldsymbol{\lambda}^*\right) \\ &= \left(\alpha_0, \Omega t + \frac{\Omega T - 2\pi}{N}, \boldsymbol{\lambda}^*\right) \\ &= (\alpha_0, \Omega t, \boldsymbol{\lambda}^*). \end{aligned}$$

Hence, conditions (a)-(d) of that theorem are fulfilled. Since $\mathcal{C}^{\mathrm{trunc}}_{\boldsymbol{\lambda}^*} \subset \mathcal{L}_{\boldsymbol{\lambda}^*}(\boldsymbol{\Lambda})$ is exponentially stable in $\mathcal{L}_{\boldsymbol{\lambda}^*}(\boldsymbol{\Lambda})$ and $(\alpha_0, \Omega t, \boldsymbol{\lambda}^*)$ naturally obeys (6.17), this spatio-temporal symmetry is robust by virtue of Corollary 3.12 and thus, (6.17) also holds for the periodic solution $(\alpha(t), \psi(t), \boldsymbol{\lambda}^*)$ of the true system (6.4). Hence, $\boldsymbol{\phi}_{\boldsymbol{\lambda}^*}(t)$ is a splay state. □

Proposition 6.6 constitutes the second main result of this chapter. To summarize, we showed that systems of the form (6.4) possess, under certain conditions, a NAIM of periodic orbits where one of these orbits features splay state dynamics. Since the original AR-model (2.5) belongs to this class, we can apply Theorem 6.5 and Proposition 6.6 to it and investigate for which parameter choices it possesses such a NAIM. This is content of the remainder of this chapter.

6.4 APPLICATION: ENSEMBLES OF ACTIVE ROTATORS

Recall that the system (2.5) can be written as

$$\dot{\phi}_j = \frac{i}{2}\Big(1+\kappa\bar{Z}\Big)\mathrm{e}^{i\phi_j} + \omega - \frac{i}{2}\Big(1+\kappa Z\Big)\mathrm{e}^{-i\phi_j}$$

such that the functions f and g in (6.3) and (6.4) are of the form

$$f(Z) \coloneqq \frac{i}{2}\left(1+\kappa\bar{Z}\right) \qquad \text{and} \qquad g(Z) \coloneqq \omega.$$

In particular, (6.4) takes the form

$$\begin{aligned}
\dot{\alpha} &= -\frac{1}{2}\Big(1+\kappa\bar{Z}\Big)\alpha^2 + i\omega\alpha + \frac{1}{2}\Big(1+\kappa Z\Big) \\
\dot{\psi} &= \frac{i}{2}\Big(1+\kappa\bar{Z}\Big)\alpha + \omega - \frac{i}{2}\Big(1+\kappa Z\Big)\bar{\alpha} \\
\dot{\boldsymbol{\lambda}} &= \mathbf{0}.
\end{aligned} \tag{6.18}$$

Substituting α for Z then yields the corresponding truncated or closed system

$$\dot{\alpha} = -\frac{1}{2}(1+\kappa\bar{\alpha})\alpha^2 + i\omega\alpha + \frac{1}{2}(1+\kappa\alpha) \tag{6.19a}$$

$$\dot{\psi} = \omega - \operatorname{Im}\alpha \tag{6.19b}$$

$$\dot{\boldsymbol{\lambda}} = \mathbf{0}. \tag{6.19c}$$

We need to determine for which choices of the system parameters ω and κ, the system fulfills the conditions in Theorem 6.5. Note that we always assume $|\omega| < 1$ in order for the individual units to be Active Rotators.

We commence by determining the fixed point α_0 for (6.19a). Writing the equation in polar form by setting $\alpha = \rho\mathrm{e}^{i\beta}$ implies $\dot{\alpha} = \dot{\rho}\mathrm{e}^{i\beta} + i\dot{\beta}\rho\mathrm{e}^{i\beta}$ so that we can write

$$\dot{\rho}\mathrm{e}^{i\beta} + i\dot{\beta}\rho\mathrm{e}^{i\beta} = -\frac{1}{2}\left(1+\kappa\rho\mathrm{e}^{-i\beta}\right)\rho^2\mathrm{e}^{2i\beta} + i\omega\rho\mathrm{e}^{i\beta} + \frac{1}{2}\left(1+\kappa\rho\mathrm{e}^{i\beta}\right)$$

and thus

$$\begin{aligned}
\dot{\rho} + i\dot{\beta}\rho =& -\frac{1}{2}\left(1+\kappa\rho\mathrm{e}^{-i\beta}\right)\rho^2\mathrm{e}^{i\beta} + i\omega\rho + \frac{1}{2}\left(1+\kappa\rho\mathrm{e}^{i\beta}\right)\mathrm{e}^{-i\beta} \\
=& -\frac{1}{2}\rho^2\mathrm{e}^{i\beta} - \frac{\kappa}{2}\rho^3 + i\omega\rho + \frac{1}{2}\mathrm{e}^{-i\beta} + \frac{\kappa}{2}\rho \\
=& \left(-\frac{1}{2}\rho^2\cos\beta - \frac{\kappa}{2}\rho^3 + \frac{1}{2}\cos\beta + \frac{\kappa}{2}\rho\right) + \\
&+ i\left(-\frac{1}{2}\rho^2\sin\beta + \omega\rho - \frac{1}{2}\sin\beta\right).
\end{aligned}$$

The fixed point condition $\dot{\alpha}(\alpha_0) = 0$ then implies that both, the real and the imaginary part of this expression, vanish such that we find

$$-\frac{1}{2}(\rho^2 - 1)\cos\beta - \frac{1}{2}(\rho^2 - 1)\kappa\rho = 0$$
$$-\frac{1}{2}(\rho^2 + 1)\sin\beta + \omega\rho = 0$$

and thus, since $\rho = |\alpha| \neq 1$,

$$\begin{aligned}\cos\beta &= -\kappa\rho \\ \sin\beta &= \frac{2\omega\rho}{(1+\rho^2)}.\end{aligned} \tag{6.20}$$

Eliminating the trigonometric terms by squaring and adding both expression, we get

$$1 = \kappa^2\rho^2 + \frac{4\omega^2\rho^2}{(1+\rho^2)^2}.$$

Substituting $x = \rho^2$ yields the cubic equation

$$0 = \kappa^2 x^3 + (2\kappa^2 - 1)x^2 + (\kappa^2 + 4\omega^2 - 2)x - 1 \tag{6.21}$$

in x. We make the following claim:

Lemma 6.7 *The cubic equation* (6.21) *has exactly one real root* $x \in (0,1)$ *for* $\omega^2 \leq 1$ *if* $\kappa^2 > 1 - \omega^2$ *and no real root in* $(0,1)$ *if* $\kappa^2 \leq 1 - \omega^2$.

Proof. We solve (6.21) for κ^2 and find

$$\kappa^2 = \frac{1}{x} - \frac{4\omega^2}{(1+x)^2}.$$

Next, we show that for any $\omega^2 \leq 1$, the map $(0,1) \ni x \mapsto \frac{1}{x} - \frac{4\omega^2}{(1+x)^2} \in (1-\omega^2, \infty)$ is a bijection from which the claim follows because bijectivity implies conversely that for any $\omega^2 \leq 1$ and every $\kappa^2 > 1 - \omega^2$ there exists a unique $x \in (0,1)$ that solves (6.21) and that there exists no such x for any $\kappa^2 \leq 1 - \omega^2$.
Injectivity: The map is differentiable in $(0,1)$ so that

$$\frac{\mathrm{d}\kappa^2}{\mathrm{d}x} = -\frac{1}{x^2} + \frac{8\omega^2}{(1+x)^3} < 0$$
$$\Leftrightarrow \frac{(1+x)^3}{8x^2} > \omega^2.$$

But $\omega^2 \leq 1 < \frac{(1+x)^3}{8x^2}$ holds because $\frac{(1+x)^3}{8x^2}$ is strictly monotonically decreasing in $(0,1)$ since $\frac{\mathrm{d}}{\mathrm{d}x}\left(\frac{(1+x)^3}{8x^2}\right) = \frac{(x-2)(1+x)^2}{8x^3} < 0 \; \forall x \in (0,1)$ and thus its infimum is $\lim_{x\to 1}\frac{(1+x)^3}{8x^2} = 1$. Hence, κ^2, as a function of x, is strictly monotonically decreasing and therefore injective.

Surjectivity: Because $\kappa^2(x)$ is continuous and strictly monotonically decreasing, its image is the interval (a, b) with

$$a = \lim_{x\to 1} \frac{1}{x} - \frac{4\omega^2}{(1+x)^2} = 1 - \omega^2$$
$$b = \lim_{x\to 0} \frac{1}{x} - \frac{4\omega^2}{(1+x)^2} = \infty$$

so that the map is indeed surjective and thus bijective. □

Lemma 6.7 guarantees that there exists a unique fixed point α_0 of (6.4a) for $|\omega| < 1$ if and only if $\kappa^2 > 1 - \omega^2$. Using (6.20), we can write

$$\alpha_0 = \rho(\cos\beta + i\sin\beta) = -\kappa\rho^2 + 2i\frac{\omega\rho^2}{1+\rho^2}$$

and find that, as long as $\omega \neq 0$,

$$\begin{aligned} f(\alpha_0) &= \frac{i}{2}\left(1 + \kappa\bar{\alpha}_0\right) \\ &= \frac{i}{2}\left(1 - \kappa^2\rho^2 - 2i\frac{\omega\kappa\rho^2}{1+\rho^2}\right) \\ &= \frac{\omega\kappa\rho^2}{1+\rho^2} + \frac{i}{2}\left(1 - \kappa^2\rho^2\right) \\ &\neq 0 \end{aligned}$$

because $\kappa^2 > 1 - \omega^2 > 0$ and $\rho > 0$ hold and additionally

$$\dot{\psi} = \omega - \operatorname{Im}\alpha_0 = \omega\left(1 - \frac{2\rho^2}{1+\rho^2}\right) = \omega\frac{1-\rho^2}{1+\rho^2} =: \Omega \neq 0.$$

Note that the sign of Ω and therefore of ω determines the sense of rotation of the periodic solution $(\alpha_0, \Omega t, \boldsymbol{\lambda})$. This sense of rotation switches when ω changes its sign so that at $\omega = 0$, the closed contours $\mathcal{C}_{\boldsymbol{\lambda}}^{\text{trunc}} = \{(\alpha_0, \psi, \boldsymbol{\lambda})\ ;\ \psi \in \mathbb{S}^1\}$ and thus the manifold $\mathcal{M}_\delta^{\text{trunc}}$ consist of fixed points which possess $N-2$ neutrally stable directions. The same must then hold true for all $\mathcal{C}_{\boldsymbol{\lambda}}$ and $\mathcal{M}_\delta$.

Next, we determine the stability of α_0. Again, we treat α and $\bar{\alpha}$ as independent variables in $\mathbb{D}$ so that we find for the vector field in $\mathbb{D}$

$$\dot{\alpha} = -\frac{1}{2}(1+\kappa\bar{\alpha})\alpha^2 + i\omega\alpha + \frac{1}{2}(1+\kappa\alpha)$$
$$\dot{\bar{\alpha}} = -\frac{1}{2}(1+\kappa\alpha)\bar{\alpha}^2 - i\omega\bar{\alpha} + \frac{1}{2}(1+\kappa\bar{\alpha}).$$

Determining the Jacobian $J \coloneqq \frac{\partial(\dot{\alpha},\dot{\bar{\alpha}})}{\partial(\alpha,\bar{\alpha})}$ for the right hand side of this equation[7] yields

$$J = \begin{pmatrix} -(1+\kappa\bar{\alpha})\alpha + i\omega + \frac{\kappa}{2} & -\frac{\kappa}{2}\alpha^2 \\ -\frac{\kappa}{2}\bar{\alpha}^2 & -(1+\kappa\alpha)\bar{\alpha} - i\omega + \frac{\kappa}{2} \end{pmatrix}.$$

7 Here, we use again the Wirtinger derivatives, see [RS00].

Its eigenvalues are

$$\lambda_\pm = \frac{\kappa(1-2|\alpha|^2)}{2} - \operatorname{Re}\alpha \pm \sqrt{\frac{\kappa^2}{4}|\alpha|^4 - (\omega - \operatorname{Im}\alpha)^2} \tag{6.22}$$

and thus, at the fixed point $\alpha_0 = \rho e^{i\beta}$ we have, again substituting $x = \rho^2$ and using equations (6.20), $\operatorname{Re}\alpha_0 = -\kappa x$ and $\operatorname{Im}\alpha_0 = \frac{2\omega x}{1+x}$ so that (6.22) becomes

$$\lambda_\pm = \frac{\kappa}{2} \pm \sqrt{\frac{\kappa^2}{4}x^2 - \omega^2\left(\frac{1-x}{1+x}\right)^2}.$$

It is now easy to see that $\operatorname{sign}\operatorname{Re}\lambda_\pm = \operatorname{sign}\kappa$. We have two cases: that of $\lambda_\pm \in \mathbb{R}$ and that of $\lambda_\pm \notin \mathbb{R}$. The first case is given by

$$\frac{\kappa^2}{4}x^2 - \omega^2\left(\frac{1-x}{1+x}\right)^2 > 0.$$

But in this case,

$$\frac{\kappa^2}{4} > \frac{\kappa^2}{4}x^2 - \omega^2\left(\frac{1-x}{1+x}\right)^2$$

because $x \in (0,1)$ and we subtract a nonnegative term. Therefore, we conclude that indeed $\operatorname{sign}\operatorname{Re}\lambda_\pm = \operatorname{sign}\kappa$. The second case, on the other hand, is given by

$$\frac{\kappa^2}{4}x^2 - \omega^2\left(\frac{1-x}{1+x}\right)^2 < 0.$$

so that $\operatorname{Re}\lambda_\pm = \frac{\kappa}{2}$ and therefore the statement holds trivially.

The results above on the existence and stability of α_0 assert that the system (6.18) and thus (2.5) indeed fulfill the conditions from Theorem 6.5 and Proposition 6.6 if $0 < |\omega| < 1$ and $\kappa < -\sqrt{1-\omega^2}$. This establishes the final main result of this chapter:

Theorem 6.8 *Let $\boldsymbol{\phi}(t) = (\phi_1(t), \dots, \phi_N(t)) \in \mathbb{T}^N_{\text{ordered}}$ obey*

$$\dot{\phi}_j = \omega - \sin\phi_j + \frac{\kappa}{N}\sum_{k=1}^{N}\sin(\phi_k - \phi_j) \tag{2.5}$$

with parameters $0 < |\omega| < 1$ and $\kappa < -\sqrt{1-\omega^2}$. There then exists an $N_0 \in \mathbb{N}$ such that for all $N \geq N_0$, there exists a closed δ-neighborhood $\overline{V}_\delta = \overline{V}_\delta(\boldsymbol{\lambda}^*) \subset V$ of $\boldsymbol{\lambda}^*$, where for every $\boldsymbol{\lambda} \in \overline{V}_\delta$, there exists a unique periodic orbit $\mathcal{C}_{\boldsymbol{\lambda}} \subset \mathcal{L}_{\boldsymbol{\lambda}}(\boldsymbol{\Lambda})$ which is exponentially stable in $\mathcal{L}_{\boldsymbol{\lambda}}(\boldsymbol{\Lambda})$. Additionally, the union

$$\mathcal{M}_\delta \coloneqq \bigcup_{\boldsymbol{\lambda}\in\overline{V}_\delta} \mathcal{C}_{\boldsymbol{\lambda}} \subset \mathbb{T}^N_{\text{ordered}}$$

forms a compact normally attracting invariant manifold of dimension $N-2$. Further, the periodic solution $\boldsymbol{\phi}_{\boldsymbol{\lambda}^*}(t) \coloneqq \boldsymbol{m}(\alpha(t), \psi(t), \boldsymbol{\lambda}^*)$ with $(\alpha(t), \psi(t), \boldsymbol{\lambda}^*)$ solving (6.18) and orbit $\mathcal{C}_{\boldsymbol{\lambda}^*} \subset \mathcal{M}_\delta$ is a splay state.

Proof. This is a direct application of Theorem 6.5 and Proposition 6.6. □

6.4.1 *Addendum: The Case* $|\omega| > 1$

We end this chapter with a remark on the case $|\omega| > 1$ for which the individual units are oscillatory on their own, even when decoupled. It is reasonable to assume that for $\kappa \neq 0$, this oscillatory motion of the ensemble continues. Since full synchronization of the ensembles is permitted by WS-integrability, so that a fully synchronized state $\phi_1(t) = \cdots = \phi_N(t)$ can be an attractor of the system, see [EM14], it is not at all obvious that we still find a continuum of orbits in this case.

However, we can again look for roots $x \in (0, 1)$ of the cubic equation (6.21), which determined the absolute value of the fixed point α_0 of the closed equation (6.4a). We make the following assertion:

Lemma 6.9 *For any $\omega \in \mathbb{R}$ with $|\omega| > 1$, equation (6.21) possesses exactly one solution $x \in (0, 1)$.*

Proof. For $|\omega| > 1$, the polynomial

$$p(x) = \kappa^2 x^3 + (2\kappa^2 - 1)x^2 + (\kappa^2 + 4\omega^2 - 2)x - 1$$

on the right hand side of (6.21) is strictly monotonically increasing in $(0, 1)$ because its derivative reads

$$\begin{aligned} \mathrm{D}_x p(x) &= 3\kappa^2 x^2 + 2(2\kappa^2 - 1)x + \kappa^2 + 4\omega^2 - 2 \\ &= 3\kappa^2 x^2 + \kappa^2(2x + 1) + 4\omega^2 - 2x - 2 \\ &> 0 \end{aligned}$$

since $4\omega^2 > 4 > 2x + 2$. Further, we have $p(0) = -1$ and $p(1) = 4\kappa^2 + 4\omega^2 - 4 > 0$ so that p has exactly one root in $(0, 1)$, for every κ. □

From this lemma, we can conclude that there exists a unique fixed point α_0, for any κ if $|\omega| > 1$. The same analysis as for the case $|\omega| < 1$ then reveals that $f(\alpha_0) \neq 0$ and that α_0 is stable for repulsive coupling ($\kappa < 0$) and unstable for attractive coupling ($\kappa > 0$). Hence, Theorem 6.5 and Proposition 6.6 apply to the case of oscillatory units and in particular, we find that the whole manifold $\mathcal{M}_\delta$ changes its stability at $\kappa = 0$.

With this, we end our investigation of the degenerate dynamics of the classic AR-model (2.5).

6.5 CONCLUSION

In this chapter, we presented our results concerning the existence and stability of a continuum of periodic orbits for the classic WS-integrable Active Rotator model (2.5). In order to do so, we considered the class of WS-integrable models for which each unit only couples to the rest of the ensemble via the mean field Z, also called Kuramoto order parameter.

We started by expressing Z in terms of the WS-variables α, ψ, and $\boldsymbol{\lambda}$ and showed that if Z is evaluated on the level set $\mathcal{L}_{\boldsymbol{\lambda}^*}(\boldsymbol{\Lambda})$ of uniform

distributions, it can be approximated by α where the resulting error becomes negligible for large N. As a consequence, the error from approximating Z by α becomes equally negligible for all level sets with cross-ratios within a neighborhood of $\boldsymbol{\lambda}^*$. We proceeded by showing that truncating the system through substituting α for Z and thus closing the WS-equation for $\dot{\alpha}$ introduces an error which can be made arbitrarily small in C^1-norm for large N. In particular, this allowed us to study the much simpler dynamics of the truncated system for which we showed that it must, under certain conditions, possess a NAIM which intersects $\mathcal{L}_{\boldsymbol{\lambda}^*}(\boldsymbol{\Lambda})$. Since the error from the truncation can be made arbitrarily small, this implies that the NAIM also exists for the original system for sufficiently large N. Afterwards, we showed that the periodic orbit in $\mathcal{L}_{\boldsymbol{\lambda}^*}(\boldsymbol{\Lambda})$ must be a splay state by means of the equivariance of the system in that subspace. Finally, we returned to the model (2.5) to which our general results can be readily applied. In particular, we computed the critical coupling strength κ_0 at which the continuum of orbits emerges and found that it indeed coincides with the value at which the synchronous fixed point Δ^{s} of the system becomes unstable, thus corroborating the homoclinic nature of the transcritical bifurcation of Δ^{s}.

Theorem 6.5 states that the continuum of orbits exists for sufficiently large N in a neighborhood of $\boldsymbol{\lambda}^*$. At least for the AR-model (2.5), numerical evidence suggests that it already exists for $N = 4$ and extends through the entirety of the space V of cross-ratios.

A word is at hand about several noteworthy points on the continuum of orbits. Throughout this chapter, we assumed all units to be distinct so that there are no clusters present. But if the continuum exists for an ensemble of N units, this implies for an ensemble of kN units, that there similarly exists a continuum of periodic solutions, consisting of N clusters with $k > 1$ units, each, because such an ensemble gives rise to an N-dimensional reduced description in terms of its cluster coordinates, which is of a similar form. In particular, $\mathcal{M}_\delta$ is in general not the only continuum in $\mathbb{T}^N$ but instead, one encounters numerous such continua (not to mention the copies in other part of $\mathbb{T}^N$ that arise from any permutation of units). If the ensemble does not split into clusters of equal but *different* sizes, in the reduced description of cluster coordinates, this makes the clusters nonidentical and thus, WS-theory can in general not be applied to them, even though it is still applicable to the full ensemble. We observed such asymmetric clustered states in our numerical experiments, as well. We note also that, regarding symmetric M-cluster ($M > 2$) states, our results on the stability of $\mathcal{M}_\delta$ only apply to the non-splitting stability of these states. Stability against splitting perturbations must be investigated independently because it is not accessible to the reduced description via cluster coordinates.

From now on, we speak of $\mathcal{M}_\delta$ in a slight abuse of terminology both as a NAIM as well as a continuum of periodic orbits.

In the proof of the existence of $\mathcal{M}_\delta$, we made several assumptions for simplicity which make Theorem 6.5 not as general as possible. Specifically, we assumed that there exists a unique fixed point in (6.13a) and that this fixed point is exponentially stable. But the idea of the proof works similarly for the case of multiple generally hyperbolic fixed

points. The resulting manifolds will than have the same stability type as the respective fixed points. In particular, in Lemma 6.7, where we determined the modulus $\rho = |\alpha_0|$ of the fixed point of (6.13a), we found that there equally exists a unique solution $\tilde{x}$ of the cubic equation (6.21) for $\kappa > +\sqrt{1-\omega^2}$. A stability analysis, similar to the one for α_0, reveals that the resulting fixed point $\tilde{\alpha}_0$ is exponentially *unstable*. As a consequence, for sufficiently *attractive* coupling, there exists a normally *repelling* NHIM $\tilde{\mathcal{M}}_\delta$ of periodic orbits. This repelling manifold emerges in a THB of the unstable synchronous fixed point Δ^{u} instead of Δ^{s}. However, due to its repulsive and therefore asymptotically unstable nature, this manifold is generally of little interest in practice.

As already noted, a change of the sense of rotation for the orbits in $\mathcal{M}_\delta$ occurs when ω changes its sign. At $\omega = 0$, the manifold instead consists of fixed points with $N-2$ neutrally stable directions, each. In this case, different initial states, even in the same level set $\mathcal{L}_{\boldsymbol{\lambda}}(\boldsymbol{\Lambda})$, will generally converge to different steady *asynchronous* states. However, a true Active Rotator will always have $\omega \neq 0$ because it was exactly this nonvanishing "constant driving force" that lead Shinomoto and Kuramoto to coin the name Active Rotator.

Finally, we showed that for $|\omega| > 1$, i. e., when the single units become full blown oscillators on their own, the cubic equation (6.21) possesses a unique real solution for any choice of κ so that in this case, we always encounter a continuum of periodic orbits. Remarkably, this continuum is asymptotically stable for $\kappa > 0$ and unstable for $\kappa < 0$ so that a change of stability for the whole NHIM occurs at $\kappa = 0$. How this stability-changing bifurcation of the manifold looks in detail lies beyond the scope of this thesis but might be worth future research.

The implications from the results of this chapter are profound: Firstly, our results imply that the existence of the continuum of periodic orbits together with its NAIM-structure is a robust phenomenon in WS-integrable systems and is not restricted to systems of the type (6.3) for which the common fields f and g depend solely on Z. Since NAIMs are robust under *any* sufficiently small perturbation, the family $\mathcal{M}_\delta$ still forms a NAIM, even if f and g depend explicitly on $\boldsymbol{\phi}$ as long as this explicit dependence is sufficiently small which might make our results applicable to, e. g., WS-integrable systems that are driven by an external force [Bai+09]. Of course, what constitutes a "sufficiently" small explicit dependence is a highly nontrivial question which to answer lies again beyond the scope of this thesis. The second, and arguably more important, implication is that, while the individual periodic orbits of the continuum, being nonhyperbolic, can cease to exist if one introduces perturbations that violate the conditions for WS-integrability, their *union* $\mathcal{M}_\delta$ forms a robust manifold which persists even when the perturbed system is not integrable. Since $\mathcal{M}_\delta$ is normally attracting, the resulting dynamics will essentially take place on this manifold: For generic initial condition, the corresponding solution moves exponentially fast towards the NAIM and then slowly evolves along it, effectively reducing the dimension of the dynamics by two. The state can then in principle move everywhere on $\mathcal{M}_\delta$ since there exists no more restric-

tions to specific level sets. In particular, the manifold $\mathcal{M}_\delta$ is not just a curiosity of the classic AR-model due to its integrability but is a *general* feature of systems of generalized Active Rotators and, as a matter of fact, also of ensembles of identical Active Rotators with nonsinusoidal coupling.[8] In the next chapter, we make use of this fact when we develop a perturbation theory for (2.5) by means of averaging theory which in particular allows to investigate the asymptotic dynamics of the generalized AR-model (2.6) by looking at the dynamics on $\mathcal{M}_\delta$ for (2.5).

8 Just as any other perturbation, changes in the coupling function leave $\mathcal{M}_\delta$ robust as long as they are small.

7

GENERAL DYNAMICS AND THE AVERAGING PRINCIPLE

ABSTRACT

In this chapter, we leave the classic Active Rotator model (2.5) behind and come back to the generalized model (2.6). While we studied periodic two-cluster states for this model in Chapter 5, we now want to investigate the asymptotic dynamics for such AR-ensembles on the NAIM $\mathcal{M}_\delta$, introduced in the previous chapter. In particular, we are interested in what happens to the infinitely many periodic orbits that composed $\mathcal{M}_\delta$ in the case of the integrable model, when we introduce perturbations which remove this integrability by breaking the Möbius group symmetry of (2.5). For this, we start again by considering the broader class of WS-integrable models of type (6.3) and develop, after some general remarks in Section 7.1, in Section 7.2 a criterion to determine robust periodic orbits in $\mathcal{M}_\delta$ by means of averaging theory for a given perturbation function h. For this, we restrict ourselves to perturbations in the on-site dynamics which in particular includes the generalized AR-model (2.6). In Section 7.3, we draw some general conclusions that immediately follow from this criterion, the most important being that splay states are generally robust solutions for such systems. Afterwards, we conduct a "case study" on a minimal system of four generalized ARs and investigate the stability of the splay state as well as the interplay between this state and the periodic two-cluster states. For this we discuss what we call "broken-symmetry states", which play a vital role in the de-/stabilization of splays states and two-cluster states. Finally, we discuss how the picture generalizes for larger ensemble sizes and illustrate how any given periodic orbit of the continuum can be controlled (i. e., made hyperbolic) by constructing an appropriate perturbation function.

The content of this chapter is based on the results in [RZP] and [RZ21b].

We note again, that we use the symbol $\mathcal{M}_\delta$ to refer both to the NAIM from Theorem 6.5 as well as the continuum of periodic orbits that composed it.

7.1 GENERAL REMARKS

The *continuum* $\mathcal{M}_\delta = \left\{\mathcal{C}_{\boldsymbol{\lambda}} \,;\, \boldsymbol{\lambda} \in \overline{V}_\delta\right\}$ of Theorem 6.5 exists due to the hidden symmetry of the underlying equations of motion (6.3) and the resulting degenerate dynamics are in this sense not generic. What

is generic, however, is the *manifold* $\mathcal{M}_\delta = \bigcup_{\boldsymbol{\lambda}\in\overline{V}_\delta} \mathcal{C}_{\boldsymbol{\lambda}}$. The question thus arises what happens to $\mathcal{M}_\delta$ as (i) a family of periodic orbits and (ii) as an invariant manifold if the vector field is perturbed in such a way that the system ceases to be integrable. The answer to point (ii) is trivial: The NAIM $\mathcal{M}_\delta$ persists because of its normal hyperbolicity. However, the answer to point (i) of the question is not so obvious. Our objective is therefore to determine which, if any, of the infinitely many nonhyperbolic periodic orbits that made up $\mathcal{M}_\delta$ "survive" if we make the system nonintegrable, i. e., which orbits become hyperbolic and thus robust and which do not. It is reasonable to assume that *if* any periodic orbits survive at all, the answer to the question which orbits become robust depends on *how* we perturb the system. Different types of perturbations are sensible: We could consider the case of nonidentical units, as was previously studied in, e. g., [PR08; VRP16]. However, if we want to make use of our considerations from Chapter 4 and Chapter 6 and in particular of the existence of the diffeomorphism $\boldsymbol{m}$ between angular variables and WS-variables, we need to restrict ourselves to the case of perturbations which leave all units identical since only in this case, the ordered torus $\mathbb{T}^N_{\text{ordered}}$ stays invariant under the flow of the perturbed vector field. To determine robust periodic orbits and their stability, we now develop a framework by means of averaging theory [SVM07].

The averaging principle has its origins in works by Laplace and Lagrange in the study of the multi-body problem in Newtonian celestial mechanics [SVM07]. The intuitive idea behind it is that for systems which feature a separation of time scales such that they possess a short-periodic or fast component[1] and some slowly varying or long-time components, one can approximate the dynamics by assuming that the long-time components are (nearly) constant during a full period of the short-periodic variable. The influence of the fast variable on the slow variables can then be approximated by its average over a single full period. The effective dynamics of the slowly varying components under this approximation should then qualitatively resemble their evolution in the true system. For example, the effects of an inner planet's gravitation on the movement of an outer planet (which is thus moving slower in comparison to the former) can be approximated by "smearing out" the inner planet over its orbit and then calculate the effect of the now stationary distribution of mass on the outer planet. In the context of WS-integrability, this is what we expect for the dynamics along the manifold $\mathcal{M}_\delta$ for systems that are "close" to being WS-integrable: There, the fast component is the phase dynamics in direction of the periodic orbits $\mathcal{C}_{\boldsymbol{\lambda}}$ and the slow components are the cross-ratios, which for small perturbations of the on-site dynamics are no longer constants of motion but are slowly varying in time.

As in the last chapter, we start by considering general WS-integrable systems of the form (6.3) where the global fields f and g are functions

1 Here, we only focus on the case of a single fast component. If one deals with multiple short-periodic components, phenomena like resonance have to be taken into consideration.

of the Kuramoto order parameter Z and then study the effects of small perturbations to the right hand side of (6.3). In particular, we always assume the existence of the NAIM $\mathcal{M}_\delta$ from Theorem 6.5 and restrict our attention to the dynamics on this manifold, assuming that it is the only NAIM of the system, since in this case, the asymptotic dynamics of the perturbed system take place entirely on the NAIM. In this case, for arbitrarily chosen initial conditions, the evolution of any state under the flow of the system is composed of a short period of exponential convergence towards $\mathcal{M}_\delta$ after which the state evolves along that manifold so that we can restrict our attention to the dynamics on it.

Maximally extended NAIM.

Theorem 6.5 only guarantees the existence of periodic orbits $\mathcal{C}_{\boldsymbol{\lambda}}$ for values of $\boldsymbol{\lambda}$ in the vicinity of $\boldsymbol{\lambda}^*$. It does not say how far the NAIM $\mathcal{M}_\delta$ actually extends in phase space. However, at least for the case of Active Rotators, numerical results indicate that this extension is "large" in the sense that the manifold is composed of periodic orbits with cross-ratios ranging over the entirety of V, cf. [ZT16]. In other words, regardless of which values we choose for $\boldsymbol{\lambda}$, if the coupling is sufficiently repulsive, there exists a $\mathcal{C}_{\boldsymbol{\lambda}}$ which is part of the continuum for this model. Throughout this chapter, we drop the index δ from $\mathcal{M}_\delta$ and consider its maximal extension

$$\mathcal{M} = \bigcup_{\boldsymbol{\lambda}\in W} \mathcal{C}_{\boldsymbol{\lambda}}$$

where the set $W \subset V$ is the largest open set of cross-ratios, for which for every $\boldsymbol{\lambda} \in W$, there exists a periodic orbit $\mathcal{C}_{\boldsymbol{\lambda}}$, exponentially stable in $\mathcal{L}_{\boldsymbol{\lambda}}(\boldsymbol{\Lambda})$ and where $\mathcal{M}$, as the union over all these orbits is a NAIM.

The generalized Active Rotator model

$$\begin{aligned} \dot{\phi}_j &= \omega - \sin\phi_j + \epsilon h(\phi_j) + \frac{\kappa}{N}\sum_{k=1}^{N}\sin(\phi_k - \phi_j) \\ h(\phi) &= \sum_{n=2}^{\infty} a_n \sin n\phi + b_n \cos n\phi \end{aligned} \tag{2.6}$$

belongs to the class of systems of the form

$$\dot{\phi}_j = f(Z)\mathrm{e}^{i\phi_j} + g(Z) + \bar{f}(Z)\mathrm{e}^{-i\phi_j} + \epsilon h(\phi_j) \tag{7.1a}$$

$$h(\phi) = \sum_{n=2}^{\infty} a_n \sin n\phi + b_n \cos n\phi \tag{7.1b}$$

with constant Fourier coefficients a_n and b_n. In what follows, we always assume h to be smooth. For $\epsilon = 0$, we get back to our general WS-integrable model

$$\dot{\phi}_j = f(Z)\mathrm{e}^{i\phi_j} + g(Z) + \bar{f}(Z)\mathrm{e}^{-i\phi_j} \tag{6.3}$$

from the previous chapter. In particular, since the coefficients a_n and b_n are constant, h represents a perturbation in the on-site dynamics of the ϕ_j while, e. g., choosing $a_n = a_n(Z)$, $b_n = b_n(Z)$ would result in a perturbation in the coupling term of (7.1a).

7.2 THE AVERAGING PRINCIPLE FOR WATANABE-STROGATZ THEORY

We start our considerations by stating an adapted version of Theorem 3.13 for our purposes in the context of WS-integrability.

For the diffeomorphism $\boldsymbol{m}$ from Proposition 4.12, let $\boldsymbol{n} = \boldsymbol{m}^{-1} : \mathbb{T}^N_{\text{ordered}} \to \mathbb{D} \times \mathbb{S}^1 \times V$ denote its inverse. We further write n_α, n_ψ, and $n_{\boldsymbol{\lambda}} \equiv \boldsymbol{\Lambda}$ for its respective components such that for $\boldsymbol{\theta} = \boldsymbol{m}(\alpha, \psi, \boldsymbol{\lambda})$, we have

$$\begin{aligned} n_\alpha(\boldsymbol{\theta}) &\coloneqq \alpha \\ n_\psi(\boldsymbol{\theta}) &\coloneqq \psi \\ n_{\boldsymbol{\lambda}}(\boldsymbol{\theta}) &\coloneqq \boldsymbol{\lambda} = \boldsymbol{\Lambda}(\boldsymbol{\theta}). \end{aligned}$$

Since we assume that the perturbation function h in (7.1) is the same for all units j, we write

$$\boldsymbol{h}(\boldsymbol{\theta}) \coloneqq (h(\theta_1), \dots, h(\theta_N))$$

for its diagonal action on $\mathbb{T}^N_{\text{ordered}}$. Recall from Chapter 4 that, by means of the chain rule, we can then deduce that for every variable $x \in \{\alpha, \psi, \boldsymbol{\lambda}\}$,

$$\dot{x} = \mathrm{D}_{\boldsymbol{\theta}} n_x \cdot \dot{\boldsymbol{\theta}} \equiv \mathrm{D} n_x(\boldsymbol{\theta}) \cdot \dot{\boldsymbol{\theta}}$$

holds. In general, for any $\boldsymbol{\theta} \in \mathbb{T}^N_{\text{ordered}}$ with $\boldsymbol{n}(\boldsymbol{\theta}) = (\alpha, \psi, \boldsymbol{\lambda})$, we write

$$(\mathrm{D}\boldsymbol{\Lambda} \cdot \boldsymbol{h})(\boldsymbol{\theta}) \coloneqq \sum_{j=1}^{N} h(\theta_j) \cdot \mathrm{D}_{\theta_j} \boldsymbol{\Lambda}(\boldsymbol{\theta})$$

for the components of $\boldsymbol{h}(\boldsymbol{\theta})$ that lie perpendicular to the level set $\mathcal{L}_{\boldsymbol{\lambda}}(\boldsymbol{\Lambda})$ at $\boldsymbol{\theta}$.[2] The expressions $(\mathrm{D}n_\alpha \cdot \boldsymbol{h})(\boldsymbol{\theta})$ and $(\mathrm{D}n_\psi \cdot \boldsymbol{h})(\boldsymbol{\theta})$ are similarly defined.

While the perturbation term $\epsilon h(\phi_j)$ in (7.1) consists of higher order Fourier modes, it generally still has some components that lie tangent to $\mathcal{L}_{\boldsymbol{\lambda}}(\boldsymbol{\Lambda})$ and thus contribute to the dynamics of α and ψ. Equation (7.1a) reads therefore in WS-variables

$$\begin{aligned} \dot{\alpha} &= i\left(f(Z)\alpha^2 + g(Z)\alpha + \bar{f}(Z)\right) + \epsilon\,(\mathrm{D}\,n_\alpha \cdot \boldsymbol{h}) \circ \boldsymbol{m}(\alpha, \psi, \boldsymbol{\lambda}) \\ \dot{\psi} &= \left(f(Z)\alpha + g(Z) + \bar{f}(Z)\bar{\alpha}\right) + \epsilon\,(\mathrm{D}\,n_\psi \cdot \boldsymbol{h}) \circ \boldsymbol{m}(\alpha, \psi, \boldsymbol{\lambda}) \\ \dot{\boldsymbol{\lambda}} &= \epsilon\,(\mathrm{D}\boldsymbol{\Lambda} \cdot \boldsymbol{h}) \circ \boldsymbol{m}(\alpha, \psi, \boldsymbol{\lambda}) \end{aligned} \tag{7.2}$$

from which we find that the perturbation term $\epsilon h(\phi_j)$ in (7.1) results in a perturbation term of order $\mathcal{O}(\epsilon)$ to the WS-equations (7.2). Its contribution to the dynamics of α and ψ is thus negligible in comparison

2 Recall that, since $\mathcal{L}_{\boldsymbol{\lambda}}(\boldsymbol{\Lambda})$ is the set of all $\boldsymbol{\theta} \in \mathbb{T}^N_{\text{ordered}}$ with $\boldsymbol{\Lambda}(\boldsymbol{\theta}) = \boldsymbol{\lambda}$, all column vectors $\mathrm{D}_{\theta_j}\boldsymbol{\Lambda}(\boldsymbol{\theta})$ of the gradient $\mathrm{D}\boldsymbol{\Lambda}(\boldsymbol{\theta})$ stand orthogonal to $T_{\boldsymbol{\theta}}\mathcal{L}_{\boldsymbol{\lambda}}(\boldsymbol{\Lambda})$ and span the orthogonal complement $(T_{\boldsymbol{\theta}}\mathcal{L}_{\boldsymbol{\lambda}}(\boldsymbol{\Lambda}))^\perp$ to $T_{\boldsymbol{\theta}}\mathcal{L}_{\boldsymbol{\lambda}}(\boldsymbol{\Lambda})$. Hence, $(\mathrm{D}\boldsymbol{\Lambda} \cdot \boldsymbol{h})(\boldsymbol{\theta})$ denotes the component of $\boldsymbol{h}(\boldsymbol{\theta})$ that is perpendicular to $\mathcal{L}_{\boldsymbol{\lambda}}(\boldsymbol{\Lambda})$ at the point $\boldsymbol{\theta}$.

to the WS-integrable terms in the equations for $\dot{\alpha}$ and $\dot{\psi}$, which are of order $\mathcal{O}(1)$, and can be absorbed into the WS-integrable equations. However, for $\dot{\boldsymbol{\lambda}}$, it results in a slow drift of order $\mathcal{O}(\epsilon)$. Only this drift term in the third equation renders the system nonintegrable by making the level sets $\mathcal{L}_{\boldsymbol{\lambda}}(\boldsymbol{\Lambda})$ noninvariant.

We are now ready to state the averaging principle for WS-theory by giving the desired adapted version of Theorem 3.13:

Proposition 7.1 *Consider the system* (7.1) *with smooth* h*. For* $\epsilon = 0$*, let*

$$\mathcal{M} = \bigcup_{\boldsymbol{\lambda} \in W} \mathcal{C}_{\boldsymbol{\lambda}}$$

denote the largest extension of the NAIM from Theorem 6.5 in $\mathbb{T}^N_{\text{ordered}}$ *such that* W *is the largest open set for which for every* $\boldsymbol{\lambda} \in W \subset V$*, there exists a periodic orbit* $\mathcal{C}_{\boldsymbol{\lambda}} \subset \mathcal{M}$ *which is exponentially stable in* $\mathcal{L}_{\boldsymbol{\lambda}}(\boldsymbol{\Lambda})$ *and* $\mathcal{M}$ *is a NAIM. For every* $\boldsymbol{\lambda} \in W$*, fix a* $\boldsymbol{\theta} = \boldsymbol{\theta}(\boldsymbol{\lambda}) \in \mathcal{C}_{\boldsymbol{\lambda}}$ *and let* $\boldsymbol{\phi}_{\boldsymbol{\lambda}}(t)$ *denote the* $T(\boldsymbol{\lambda})$*-periodic solution of* (6.3) *with initial condition* $\boldsymbol{\phi}_{\boldsymbol{\lambda}}(0) = \boldsymbol{\theta}$*. Then, the following statements hold true:*

1. *The function*

$$\hat{\boldsymbol{F}}_h(\boldsymbol{\lambda}) \coloneqq \frac{1}{T(\boldsymbol{\lambda})} \int_0^{T(\boldsymbol{\lambda})} (\mathrm{D}\boldsymbol{\Lambda} \cdot \boldsymbol{h}) \circ \boldsymbol{\phi}_{\boldsymbol{\lambda}}(t)\, \mathrm{d}t, \tag{7.3}$$

   is continuously differentiable and well-defined and thus in particular independent of the choice of $\boldsymbol{\theta}(\boldsymbol{\lambda}) \in \mathcal{C}_{\boldsymbol{\lambda}}$*.*

2. *There exists an* $\epsilon_0 > 0$ *such that for all* $|\epsilon| < \epsilon_0$*, there exists a NAIM* $\mathcal{M}_\epsilon$ *which is diffeomorphic and* $\mathcal{O}(\epsilon)$*-close to* $\mathcal{M}$*.*

3. *If there exists a* $c > 0$ *such that* $2\pi/T(\boldsymbol{\lambda}) > c > 0$ *for all* $\boldsymbol{\lambda} \in W$*, then, for every hyperbolic fixed point* $\boldsymbol{\lambda}_0 \in W$ *of the averaged system*

$$\dot{\boldsymbol{\lambda}} = \epsilon \hat{\boldsymbol{F}}_h(\boldsymbol{\lambda}), \tag{7.4}$$

   there exists a periodic orbit $\mathcal{C}_{\epsilon,\boldsymbol{\lambda}_0} \subset \mathcal{M}_\epsilon$ *which lies* $\mathcal{O}(\epsilon)$*-close to* $\mathcal{C}_{\boldsymbol{\lambda}_0} \subset \mathcal{M}$ *so that, in particular,* $\|\boldsymbol{\Lambda}(\boldsymbol{\vartheta}) - \boldsymbol{\lambda}_0\| = \mathcal{O}(\epsilon)$ *for every* $\boldsymbol{\vartheta} \in \mathcal{C}_{\epsilon,\boldsymbol{\lambda}_0}$*.*

4. *If* $\boldsymbol{\lambda}_0$ *possess* n_s *stable and* n_u *unstable directions, then, for* $\epsilon > 0$*, the periodic orbit* $\mathcal{C}_{\epsilon,\boldsymbol{\lambda}_0}$ *has* n_s+2 *stable and* n_u *unstable directions. For* $\epsilon < 0$*, it has* $n_u + 2$ *stable and* n_s *unstable directions.*

From now on, we follow the general convention in the theory of normally hyperbolic manifolds to write $\mathcal{M}_\epsilon$ *for the perturbed manifold and* $\mathcal{M}$ *for the original manifold. Although this is a slight abuse of notation with respect to Chapter 6 where* $\mathcal{M}_\delta$ *had a different meaning, there is no chance for confusion since we are exclusively dealing with the extended manifold* $\mathcal{M}$*.*

Proof. 1. Let $\boldsymbol{\phi}_{\boldsymbol{\lambda}}$ be the periodic solution of (6.3) with period $T(\boldsymbol{\lambda}) > 0$ and the initial condition $\boldsymbol{\phi}_{\boldsymbol{\lambda}}(0) = \boldsymbol{\theta} \in \mathcal{C}_{\boldsymbol{\lambda}}$. Then, the average of $\mathrm{D}\boldsymbol{\Lambda} \cdot \boldsymbol{h}$ over $\mathcal{C}_{\boldsymbol{\lambda}}$ on the right hand side of (7.3) exists. For any $\boldsymbol{\theta}' \in \mathcal{C}_{\boldsymbol{\lambda}}$, let $\boldsymbol{\phi}'_{\boldsymbol{\lambda}}(t)$ denote the solution of (6.3) with $\boldsymbol{\phi}'_{\boldsymbol{\lambda}}(0) = \boldsymbol{\theta}'$. Then, there exists a $\tau = \tau(\boldsymbol{\theta}')$ such that $\boldsymbol{\phi}'_{\boldsymbol{\lambda}}(t) = \boldsymbol{\phi}_{\boldsymbol{\lambda}}(t + \tau)$. But since we average over a full period, the integral in (7.3) is invariant under shifts in t and thus is independent of the choice of $\boldsymbol{\theta}$. Further, $\hat{\boldsymbol{F}}_h$ is continuously

differentiable because both $\boldsymbol{\Lambda}$ and $\boldsymbol{h}$ are smooth and $\boldsymbol{\phi}_{\boldsymbol{\lambda}}$ and $T(\boldsymbol{\lambda})$ depend smoothly on the system parameter $\boldsymbol{\lambda}$ [Rud76].

2. Because h is smooth, so is $\boldsymbol{h} : \mathbb{T}^N \to \mathbb{R}^N$. Because $\mathbb{T}^N$ is compact, there exists a constant $K > 0$ such that $\|\boldsymbol{h}\|_{C^1} = K$ and thus

$$\|\epsilon \boldsymbol{h}\|_{C^1} = \mathcal{O}(\epsilon).$$

Thus, by the Persistence Theorem 3.7, there exists an $\epsilon_0 > 0$ such that for all $|\epsilon| < \epsilon_0$, there exists a NAIM $\mathcal{M}_\epsilon$ which is diffeomorphic to $\mathcal{M}$ and lies $\mathcal{O}(\epsilon)$-close to it.

3. By assumption, $\mathcal{M} \cong \mathbb{S}^1 \times W$, i. e., every point $\boldsymbol{\theta} \in \mathcal{M}$ is uniquely determined by (i) its cross-ratios $\boldsymbol{\lambda} = \boldsymbol{\Lambda}(\boldsymbol{\theta})$, determining in which orbit $\mathcal{C}_{\boldsymbol{\lambda}} \subset \mathcal{M}$ it lies, and (ii) its position on $\mathcal{C}_{\boldsymbol{\lambda}}$ which is determined by its phase $s = S(\boldsymbol{\theta}) \in \mathbb{S}^1$. The function S becomes uniquely defined, once we define a Poincaré section $\Sigma \subset \mathcal{M}$ which lies transversal to each orbit $\mathcal{C}_{\boldsymbol{\lambda}} \subset \mathcal{M}$, such that for every $\boldsymbol{\theta} \in \Sigma$, we set $S(\boldsymbol{\theta}) = 0$. If we choose $\Sigma \subset \mathcal{M}$ to be a smooth submanifold of $\mathcal{M}$, the function S is also smooth. This results in a chart

$$\chi : \boldsymbol{\theta} \mapsto (s, \boldsymbol{\lambda}) = (S(\boldsymbol{\theta}), \boldsymbol{\Lambda}(\boldsymbol{\theta}))$$

with coordinates $(s, \boldsymbol{\lambda})$ for $\mathcal{M}$ in which the equations of motion on the NAIM simply read

$$\begin{aligned} \dot{s} &= \frac{2\pi}{T(\boldsymbol{\lambda})} \\ \dot{\boldsymbol{\lambda}} &= \mathbf{0}. \end{aligned}$$

By assumption, $T(\boldsymbol{\lambda})$ is bounded from above for all $\boldsymbol{\lambda} \in W$ and so there exists a $0 < c < 2\pi/T(\boldsymbol{\lambda})$.

We introduce compatible coordinates on $\mathcal{M}_\epsilon$ and determine the equations of motion on it in terms of these coordinates. To do so, we start by noting that, since $\mathcal{M}$ is not only a NAIM but also the union of periodic orbits $\mathcal{C}_{\boldsymbol{\lambda}}$, each stable in its respective level set $\mathcal{L}_{\boldsymbol{\lambda}}(\boldsymbol{\Lambda})$, there exists an open neighborhood $U(\mathcal{M})$ of $\mathcal{M}$ such that χ can be extended to[3]

$$\begin{aligned} &\chi : U \to \mathbb{S}^1 \times V \\ &\chi : \boldsymbol{\vartheta} \mapsto (S(\boldsymbol{\vartheta}), \boldsymbol{\Lambda}(\boldsymbol{\vartheta})) \end{aligned}$$

which is as smooth as the vector field in (7.1a), see [Fen77]. For $|\epsilon|$ sufficiently small, $\mathcal{M}_\epsilon$ lies within $U(\mathcal{M})$ and in particular, every point $\boldsymbol{\vartheta} \in \mathcal{M}_\epsilon$ is uniquely determined by its coordinates

$$(s, \boldsymbol{\lambda}) = (S(\boldsymbol{\vartheta}), \boldsymbol{\Lambda}(\boldsymbol{\vartheta}))$$

because every $\boldsymbol{\vartheta} \in \mathcal{M}_\epsilon$ lies in exactly one isochron in the level set $\mathcal{L}_{\boldsymbol{\lambda}}(\boldsymbol{\Lambda})$ with $\boldsymbol{\lambda} = \boldsymbol{\Lambda}(\boldsymbol{\vartheta})$. Since $\mathcal{M}$ and $\mathcal{M}_\epsilon$ are diffeomorphic and lie $\mathcal{O}(\epsilon)$-close, there further exists a near-identity map

$$\begin{aligned} &\boldsymbol{\rho} : \mathcal{M} \to \mathcal{M}_\epsilon \\ &\boldsymbol{\rho} : \boldsymbol{\theta} \mapsto \boldsymbol{\vartheta} = \boldsymbol{\theta} + \epsilon \boldsymbol{P}(\boldsymbol{\theta}, \epsilon) \end{aligned}$$

3 In the diction of [HI12], χ is the asymptotic phase on U.

which can be extend to a diffeomorphism

$$\boldsymbol{\varrho} : U(\mathcal{M}) \to U(\mathcal{M}_\epsilon)$$

between $U(\mathcal{M})$ and an open neighborhood $U(\mathcal{M}_\epsilon)$ of $\mathcal{M}_\epsilon$. In particular, we have $\boldsymbol{\varrho}|_{\mathcal{M}} = \boldsymbol{\rho}$ and further, $\boldsymbol{\varrho}$ is a near-identity map around $\mathcal{M}$, as well, so that we find

$$\boldsymbol{\varrho}(\boldsymbol{\theta}) = \boldsymbol{\theta} + \epsilon \boldsymbol{P}(\boldsymbol{\theta}, \epsilon) \tag{7.5}$$

for $\boldsymbol{\theta} \in \mathcal{M}$. Writing (7.1a) as

$$\begin{aligned} \dot{\boldsymbol{\vartheta}} &= \boldsymbol{F}_{\mathrm{WS}}(\boldsymbol{\vartheta}) + \epsilon \boldsymbol{h}(\boldsymbol{\vartheta}) \\ \boldsymbol{F}_{\mathrm{WS}}(\boldsymbol{\vartheta}) &\coloneqq \begin{pmatrix} f(Z)\mathrm{e}^{i\vartheta_1} + g(Z) + \bar{f}(Z)\mathrm{e}^{-i\vartheta_1} \\ \vdots \\ f(Z)\mathrm{e}^{i\vartheta_N} + g(Z) + \bar{f}(Z)\mathrm{e}^{-i\vartheta_N} \end{pmatrix}, \end{aligned} \tag{7.6}$$

we can Taylor-expand $\boldsymbol{F}_{\mathrm{WS}}(\boldsymbol{\vartheta}) + \epsilon \boldsymbol{h}(\boldsymbol{\vartheta})$ around $\boldsymbol{\theta} = \boldsymbol{\varrho}^{-1}(\boldsymbol{\vartheta})$ which yields

$$\begin{aligned} \boldsymbol{F}_{\mathrm{WS}}(\boldsymbol{\vartheta}) &= \boldsymbol{F}_{\mathrm{WS}}(\boldsymbol{\theta} + \epsilon \boldsymbol{P}(\boldsymbol{\theta}, \epsilon)) \\ &= \boldsymbol{F}_{\mathrm{WS}}(\boldsymbol{\theta}) + \epsilon \mathrm{D}\boldsymbol{F}_{\mathrm{WS}}(\boldsymbol{\theta}) \cdot \boldsymbol{P}(\boldsymbol{\theta}, \epsilon) + \mathcal{O}(\epsilon^2) \\ \boldsymbol{h}(\boldsymbol{\vartheta}) &= \boldsymbol{h}(\boldsymbol{\theta} + \epsilon \boldsymbol{P}(\boldsymbol{\theta}, \epsilon)) \\ &= \boldsymbol{h}(\boldsymbol{\theta}) + \epsilon \mathrm{D}\boldsymbol{h}(\boldsymbol{\theta}) \cdot \boldsymbol{P}(\boldsymbol{\theta}, \epsilon) + \mathcal{O}(\epsilon^2). \end{aligned} \tag{7.7}$$

For the phase $s = S(\boldsymbol{\vartheta})$, we then find with (7.5), (7.6), and (7.7) by the chain rule

$$\begin{aligned} \dot{s} &= \mathrm{D}S(\boldsymbol{\vartheta}) \cdot \dot{\boldsymbol{\vartheta}} \\ &= \mathrm{D}S(\boldsymbol{\vartheta}) \cdot [\boldsymbol{F}_{\mathrm{WS}}(\boldsymbol{\vartheta}) + \epsilon \boldsymbol{h}(\boldsymbol{\vartheta})] \\ &= \mathrm{D}S(\boldsymbol{\theta} + \epsilon \boldsymbol{P}(\boldsymbol{\theta}, \epsilon)) \cdot [\boldsymbol{F}_{\mathrm{WS}}(\boldsymbol{\theta}) + \mathcal{O}(\epsilon)] \\ &= [\mathrm{D}S(\boldsymbol{\theta}) + \mathcal{O}(\epsilon)] \cdot [\boldsymbol{F}_{\mathrm{WS}}(\boldsymbol{\theta}) + \mathcal{O}(\epsilon)] \\ &= \mathrm{D}S(\boldsymbol{\theta}) \cdot \boldsymbol{F}_{\mathrm{WS}}(\boldsymbol{\theta}) + \mathcal{O}(\epsilon) \\ &= \frac{2\pi}{T \circ \boldsymbol{\Lambda}(\boldsymbol{\theta})} + \mathcal{O}(\epsilon) \end{aligned} \tag{7.8}$$

because for the unperturbed system (6.3), we have by definition of the phase

$$\frac{\mathrm{d}}{\mathrm{d}t} S(\boldsymbol{\theta}) = \mathrm{D}S(\boldsymbol{\theta}) \cdot \dot{\boldsymbol{\theta}} = \mathrm{D}S(\boldsymbol{\theta}) \cdot \boldsymbol{F}_{\mathrm{WS}}(\boldsymbol{\theta}) = \frac{2\pi}{T \circ \boldsymbol{\Lambda}(\boldsymbol{\theta})}.$$

Further, for the cross-ratios $\boldsymbol{\lambda} = \boldsymbol{\Lambda}(\boldsymbol{\vartheta})$, we have by the same argument and because the WS-integrable term $\boldsymbol{F}_{\mathrm{WS}}$ of (7.6) keeps cross-ratios invariant

$$\begin{aligned} \dot{\boldsymbol{\lambda}} &= \mathrm{D}\boldsymbol{\Lambda}(\boldsymbol{\vartheta}) \cdot \dot{\boldsymbol{\vartheta}} \\ &= \mathrm{D}\boldsymbol{\Lambda}(\boldsymbol{\vartheta}) \cdot [\boldsymbol{F}_{\mathrm{WS}}(\boldsymbol{\vartheta}) + \epsilon \boldsymbol{h}(\boldsymbol{\vartheta})] \\ &= \underbrace{\mathrm{D}\boldsymbol{\Lambda}(\boldsymbol{\vartheta}) \cdot \boldsymbol{F}_{\mathrm{WS}}(\boldsymbol{\vartheta})}_{=\mathbf{0}} + \epsilon \mathrm{D}\boldsymbol{\Lambda}(\boldsymbol{\vartheta}) \cdot \boldsymbol{h}(\boldsymbol{\vartheta}) \\ &= \epsilon \mathrm{D}\boldsymbol{\Lambda}(\boldsymbol{\theta} + \epsilon \boldsymbol{P}(\boldsymbol{\theta}, \epsilon)) \cdot \boldsymbol{h}(\boldsymbol{\theta} + \epsilon \boldsymbol{P}(\boldsymbol{\theta}, \epsilon)) \\ &= \epsilon [\mathrm{D}\boldsymbol{\Lambda}(\boldsymbol{\theta}) + \mathcal{O}(\epsilon)] \cdot [\boldsymbol{h}(\boldsymbol{\theta}) + \mathcal{O}(\epsilon)] \\ &= \epsilon \mathrm{D}\boldsymbol{\Lambda}(\boldsymbol{\theta}) \cdot \boldsymbol{h}(\boldsymbol{\theta}) + \mathcal{O}(\epsilon^2). \end{aligned} \tag{7.9}$$

Next, we have to close equations (7.8) and (7.9) by writing them entirely in terms of s and $\boldsymbol{\lambda}$. For this, we need to express $\boldsymbol{\theta}$ in terms of s and $\boldsymbol{\lambda}$. We note first that because of (7.5), we have

$$\begin{aligned}\boldsymbol{\Lambda}(\boldsymbol{\theta}) &= \boldsymbol{\Lambda}(\boldsymbol{\vartheta}) + \mathcal{O}(\epsilon) = \boldsymbol{\lambda} + \mathcal{O}(\epsilon)\\ S(\boldsymbol{\theta}) &= S(\boldsymbol{\vartheta}) + \mathcal{O}(\epsilon) = s + \mathcal{O}(\epsilon).\end{aligned}$$

Let

$$\begin{aligned}\boldsymbol{\theta}_0 &: W \to \Sigma\\ \boldsymbol{\theta}_0 &: \boldsymbol{\lambda} \mapsto \chi^{-1}(0, \boldsymbol{\lambda})\end{aligned}$$

denote the point in $\mathcal{C}_{\boldsymbol{\lambda}} \subset \mathcal{M}$ of phase zero, i. e., $S(\boldsymbol{\theta}_0(\boldsymbol{\lambda})) = 0$. In particular, $\boldsymbol{\theta}_0$ is smooth since χ is smooth. Denoting the flow of the unperturbed equations (6.3), restricted to $\mathcal{M}$, by $\Phi_{\mathrm{WS}}|_{\mathcal{M}} : \mathcal{M} \times \mathbb{R} \to \mathcal{M}$, we can write $\boldsymbol{\theta}$ entirely in terms of s and $\boldsymbol{\lambda}$ as

$$\begin{aligned}\boldsymbol{\theta} &= \Phi_{\mathrm{WS}}|_{\mathcal{M}} \left(\boldsymbol{\theta}_0 \circ \boldsymbol{\Lambda}(\boldsymbol{\theta}), S(\boldsymbol{\theta}) \frac{T \circ \boldsymbol{\Lambda}(\boldsymbol{\theta})}{2\pi}\right)\\ &= \Phi_{\mathrm{WS}}|_{\mathcal{M}} \left(\boldsymbol{\theta}_0(\boldsymbol{\lambda} + \mathcal{O}(\epsilon)), (s + \mathcal{O}(\epsilon)) \frac{T(\boldsymbol{\lambda} + \mathcal{O}(\epsilon))}{2\pi}\right)\\ &= \Phi_{\mathrm{WS}}|_{\mathcal{M}} \left(\boldsymbol{\theta}_0(\boldsymbol{\lambda}) + \mathcal{O}(\epsilon), s \frac{T(\boldsymbol{\lambda})}{2\pi} + \mathcal{O}(\epsilon)\right)\\ &= \Phi_{\mathrm{WS}}|_{\mathcal{M}} \left(\boldsymbol{\theta}_0(\boldsymbol{\lambda}), s \frac{T(\boldsymbol{\lambda})}{2\pi}\right) + \mathcal{O}(\epsilon)\\ &= \boldsymbol{\phi}_{\boldsymbol{\lambda}} \left(s \frac{T(\boldsymbol{\lambda})}{2\pi}\right) + \mathcal{O}(\epsilon)\end{aligned}$$

where $\boldsymbol{\phi}_{\boldsymbol{\lambda}}(t) \equiv \Phi_{\mathrm{WS}}|_{\mathcal{M}}(\boldsymbol{\theta}_0(\boldsymbol{\lambda}), t)$ is the solution of (6.3) with initial condition $\boldsymbol{\phi}_{\boldsymbol{\lambda}}(0) = \boldsymbol{\theta}_0(\boldsymbol{\lambda}) \in \mathcal{C}_{\boldsymbol{\lambda}}$. Subsequently, we arrive at the closed equations

$$\begin{aligned}\dot{s} &= \frac{2\pi}{T(\boldsymbol{\lambda}) + \mathcal{O}(\epsilon)} + \mathcal{O}(\epsilon)\\ &= \frac{2\pi}{T(\boldsymbol{\lambda})} + \mathcal{O}(\epsilon)\\ \dot{\boldsymbol{\lambda}} &= \epsilon \mathrm{D}\boldsymbol{\Lambda} \left(\boldsymbol{\phi}_{\boldsymbol{\lambda}} \left(s \frac{T(\boldsymbol{\lambda})}{2\pi}\right) + \mathcal{O}(\epsilon)\right) \cdot \boldsymbol{h} \left(\boldsymbol{\phi}_{\boldsymbol{\lambda}} \left(s \frac{T(\boldsymbol{\lambda})}{2\pi}\right) + \mathcal{O}(\epsilon)\right) + \mathcal{O}(\epsilon^2)\\ &= \epsilon \left[\mathrm{D}\boldsymbol{\Lambda} \circ \boldsymbol{\phi}_{\boldsymbol{\lambda}} \left(s \frac{T(\boldsymbol{\lambda})}{2\pi}\right) + \mathcal{O}(\epsilon)\right] \cdot \left[\boldsymbol{h} \circ \boldsymbol{\phi}_{\boldsymbol{\lambda}} \left(s \frac{T(\boldsymbol{\lambda})}{2\pi}\right) + \mathcal{O}(\epsilon)\right] + \mathcal{O}(\epsilon^2)\\ &= \epsilon \left(\mathrm{D}\boldsymbol{\Lambda} \cdot \boldsymbol{h}\right) \circ \boldsymbol{\phi}_{\boldsymbol{\lambda}} \left(s \frac{T(\boldsymbol{\lambda})}{2\pi}\right) + \mathcal{O}(\epsilon^2)\end{aligned} \tag{7.10}$$

and in particular, we can readily apply Theorem 3.13 to (7.10). This yields the averaged system

$$\dot{\boldsymbol{\lambda}} = \epsilon \hat{\boldsymbol{F}}_h(\boldsymbol{\lambda}) \tag{7.11}$$

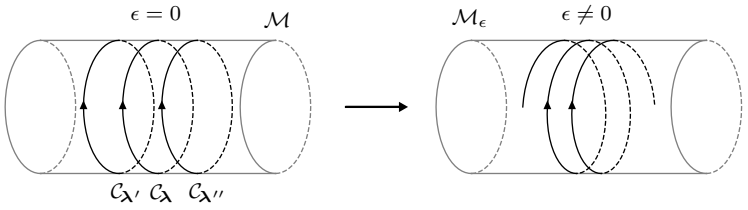

Figure 18: Schematic depiction of the dynamics on the manifolds $\mathcal{M}$ and $\mathcal{M}_\epsilon$. For the WS-integrable system ($\epsilon = 0$) on the left, the manifold is composed of infinitely many periodic orbits along which the flow of the vector field runs in parallel. Switching on the perturbation ($\epsilon \neq 0$) on the right yields a slow drift term in the $\boldsymbol{\lambda}$-components, generally resulting in a spiraling motion along $\mathcal{M}$. Hence, only certain periodic orbits persist in the perturbed case, if any.

with

$$\begin{aligned}\hat{\boldsymbol{F}}_h(\boldsymbol{\lambda}) &\coloneqq \frac{1}{2\pi}\int_0^{2\pi} (\mathrm{D}\boldsymbol{\Lambda}\cdot\boldsymbol{h})\circ\boldsymbol{\phi}_{\boldsymbol{\lambda}}\left(s\frac{T(\boldsymbol{\lambda})}{2\pi}\right)\mathrm{d}s \\ &= \frac{1}{T(\boldsymbol{\lambda})}\int_0^{T(\boldsymbol{\lambda})} (\mathrm{D}\boldsymbol{\Lambda}\cdot\boldsymbol{h})\circ\boldsymbol{\phi}_{\boldsymbol{\lambda}}(t)\,\mathrm{d}t,\end{aligned}$$

i. e., (7.3) where we average over the fast variable s (or t, respectively).

4. Let $\boldsymbol{\lambda}_0$ denote a hyperbolic fixed point of (7.11) with n_s stable and n_u unstable directions. For $0 < \epsilon < \epsilon_0$, we then find for the corresponding periodic orbit $\mathcal{C}_{\epsilon,\boldsymbol{\lambda}_0}$ that it lies $\mathcal{O}(\epsilon)$-close to $\mathcal{C}_{\boldsymbol{\lambda}_0}$ and thus in particular, $\|\boldsymbol{\Lambda}(\boldsymbol{\vartheta}) - \boldsymbol{\lambda}_0\| = \mathcal{O}(\epsilon)$ for every $\boldsymbol{\vartheta} \in \mathcal{C}_{\epsilon,\boldsymbol{\lambda}_0}$. Further, since (7.10) describes the dynamics, restricted to $\mathcal{M}_\epsilon$, the orbit $\mathcal{C}_{\epsilon,\boldsymbol{\lambda}_0}$ has n_s stable directions and n_u unstable directions in $\mathcal{M}_\epsilon$. Because $\mathcal{M}_\epsilon$ is normally attracting and $(N-2)$-dimensional, $\mathcal{C}_{\epsilon,\boldsymbol{\lambda}_0}$ has $n_s + 2$ stable and n_u unstable directions in $\mathbb{T}^N_{\text{ordered}}$. On the other hand, for $-\epsilon_0 < \epsilon < 0$, the fixed point $\boldsymbol{\lambda}_0$ has n_u stable and n_s unstable directions and thus by the same argumen, $\mathcal{C}_{\epsilon,\boldsymbol{\lambda}_0}$ has $n_u + 2$ stable and n_s unstable directions in $\mathbb{T}^N_{\text{ordered}}$. This finishes the proof. □

Proposition 7.1 serves as a tool to determine periodic orbits from the family $\mathcal{M}$ which become robust under a given choice for h. In practice, this works as follows: Fixing $\boldsymbol{\lambda}$, one starts by determining the periodic solution $\boldsymbol{\phi}_{\boldsymbol{\lambda}}(t)$ of the unperturbed system (6.3). Then, one proceeds by numerically evaluating and integrating the expression $\mathrm{D}\boldsymbol{\Lambda}\cdot\boldsymbol{h}$ along the orbit of $\boldsymbol{\phi}_{\boldsymbol{\lambda}}$. If the integral vanishes for $\boldsymbol{\lambda}$ and its derivative with respect to $\boldsymbol{\lambda}$ has no eigenvalues with zero real part, the corresponding orbit $\mathcal{C}_{\boldsymbol{\lambda}}$ will generally be slightly distorted to the orbit $\mathcal{C}_{\epsilon,\boldsymbol{\lambda}}$ due to the perturbation ϵh in (7.1). On the other hand, orbits for which the integral does not vanish do not survive the introduction of the perturbation. Intuitively speaking, the reason for this is that while all $\mathcal{C}_{\boldsymbol{\lambda}} \subset \mathcal{M}$ lie somewhat parallel to their neighboring orbits for the WS-integrable model (6.3), the introduction of ϵh in (7.1a) introduces a slow "drift" in $\boldsymbol{\lambda}$-direction along $\mathcal{M}_\epsilon$ such that a solution $\boldsymbol{\phi}(t) \in \mathcal{M}_\epsilon$ with $\boldsymbol{\lambda} = \boldsymbol{\Lambda}(\boldsymbol{\phi}(0))$, instead of following the orbit $\mathcal{C}_{\boldsymbol{\lambda}}$, is now "pushed" away from this orbit like a cruise ship may drift from its optimal course by

sea currents, coming from different directions. However, if $\hat{\boldsymbol{F}}_h(\boldsymbol{\lambda}) = \mathbf{0}$, the pushes cancel each other out *on average* over the length of $\mathcal{C}_{\boldsymbol{\lambda}}$ such that $\boldsymbol{\phi}(t)$ stays periodic just like the ship reaches its home port again if the sea currents make it drift equally often in opposite directions over its full cruise. Since $\mathcal{C}_{\epsilon,\boldsymbol{\lambda}}$ becomes slightly distorted, the $\boldsymbol{\lambda}$-components of $\boldsymbol{\phi}(t)$ oscillate slowly but stay close to $\boldsymbol{\lambda}$. By the same reasoning, any initial state that does not lie on one of the surviving orbits receives a net drift term in some direction over a full rotation so that its trajectory is not a periodic orbit but slowly spirals along $\mathcal{M}_\epsilon$ in that direction, see Figure 18 for a schematic depiction. In this case, our proverbial ship looses its course and will not find home if the sea currents push it predominantly in one cardinal direction.

One might ask why we are not averaging over the periodic states $\boldsymbol{\phi}_{\boldsymbol{\lambda}}^{\text{trunc}}(t) = \boldsymbol{m}(\alpha_0, \Omega t, \boldsymbol{\lambda})$ from the truncated system (6.13) to compute $\hat{\boldsymbol{F}}_h(\boldsymbol{\lambda})$ since these solutions are much simpler (we even have explicit expressions for them) and, at least for values of $\boldsymbol{\lambda}$ that are close to $\boldsymbol{\lambda}^*$, approximate the full dynamics of (6.3) well. However, as we show in Appendix D, the averaged vector field $\hat{\boldsymbol{F}}_h$ in $\boldsymbol{\lambda}$-direction vanishes identically for all $\boldsymbol{\lambda}$ if we integrate in (7.3) over the orbits $\mathcal{C}_{\boldsymbol{\lambda}}^{\text{trunc}}$. Under these circumstances, we cannot draw any conclusions about robust orbits from the averaging principle and Proposition 7.1 becomes sterile.

In the next section, we discuss the main implications of Proposition 7.1. In particular, we investigate what can be said about the robustness and stability of the splay state for the perturbed system (7.1).

7.3 IMPLICATIONS

Even though the explicit form of the averaged vector field $\hat{\boldsymbol{F}}_h$, defined in (7.3), can in general not be determined because to do so would require (i) to solve the unperturbed equations (6.3) for the periodic solution $\boldsymbol{\phi}_{\boldsymbol{\lambda}}(t)$ and then (ii) integrate the expression $(\mathrm{D}\boldsymbol{\Lambda} \cdot \boldsymbol{h})(\boldsymbol{\theta})$ over a period of this solution, we can still draw some general conclusions for $\hat{\boldsymbol{F}}_h$ by using how the cross-ratios $\Lambda_{p,q,r,s}$ transform under permutations of the units $\theta_p, \theta_q, \theta_r, \theta_s$ [Ric11]. Special focus is thereby put on splay states due to their spatio-temporal symmetry.

7.3.1 *Switch in Stability*

We start with a rather simple observation which is a direct consequence of point 4 of Proposition 7.1. In the averaged system (7.4), the sign of ϵ controls the stability of any hyperbolic fixed point $\boldsymbol{\lambda}_0$ in the sense that changing the sign of ϵ makes stable directions of $\boldsymbol{\lambda}_0$ unstable and vice versa. Thus, the same happens to the stable and unstable directions of the corresponding periodic orbit $\mathcal{C}_{\epsilon,\boldsymbol{\lambda}_0}$ in the true system (7.1) *in* $\mathcal{M}_\epsilon$. The two normally attracting directions, inherited from $\mathcal{M}_\epsilon$ do not change their stability. This means that if a surviving periodic orbit $\mathcal{C}_{\epsilon_0,\boldsymbol{\lambda}_0}$ of (7.1a) is stable for $\epsilon_0 \neq 0$ sufficiently small, the orbit $\mathcal{C}_{-\epsilon_0,\boldsymbol{\lambda}_0}$ is unstable (if it exists). Varying ϵ within the interval $[-\epsilon_0, +\epsilon_0]$, the

orbit $\mathcal{C}_{\epsilon,\boldsymbol{\lambda}_0}$ switches its stability at $\epsilon = 0$, i. e., when the system becomes WS-integrable.

7.3.2 *Persistence and Stability of Splay States*

As established in Proposition 6.6, the periodic orbit $\mathcal{C}_{\boldsymbol{\lambda}^*} \subset \mathcal{M}$ of the continuum gives rise to a splay state which is of the form

$$\phi^j_{\boldsymbol{\lambda}^*}(t) = \varphi\left(t + j\frac{T(\boldsymbol{\lambda}^*)}{N}\right)$$

for some $T(\boldsymbol{\lambda}^*)$-periodic function φ and therefore possesses a spatio-temporal symmetry. The finite group Γ, which is responsible for this in the sense of Theorem 3.11 for equivariant systems, is the group of cyclic permutations of order N:

$$\Gamma = \{\sigma^n \,;\, n = 1, \dots, N\}$$

with

$$\sigma = \begin{pmatrix} 1 & 2 & \dots & N \\ N & 1 & \dots & N-1 \end{pmatrix} \tag{7.12}$$

in standard two-line notation [Car37]. The action of Γ on $\mathbb{T}^N_{\text{ordered}}$ is recursively defined by

$$\begin{aligned} \sigma\boldsymbol{\theta} &\coloneqq (\theta^{\sigma(1)}, \dots, \theta^{\sigma(N)}) = (\theta^N, \theta^1, \dots, \theta^{N-1}) \in \mathbb{T}^N_{\text{ordered}} \\ \sigma^n\boldsymbol{\theta} &\coloneqq \sigma(\sigma^{n-1}\boldsymbol{\theta}), \quad n > 1 \end{aligned} \tag{7.13}$$

For better readability, in the rest of this chapter, we also write θ^j instead of θ_j for the jth component of $\boldsymbol{\theta}$.

for any $\boldsymbol{\theta} \in \mathbb{T}^N_{\text{ordered}}$. In particular, $\sigma^n\boldsymbol{\theta}$ is again an element of $\mathbb{T}^N_{\text{ordered}}$ because a cyclic permutation of the θ^j does not change their cyclic order and obviously, the system (6.3) is equivariant under the action of Γ since all units are identical. In the same spirit as (7.13), we can then for every periodic solution

$$\boldsymbol{\phi}_{\boldsymbol{\lambda}}(t) = \left(\phi^1_{\boldsymbol{\lambda}}(t), \dots, \phi^N_{\boldsymbol{\lambda}}(t)\right)$$

of (6.3) write

$$\begin{aligned} \sigma\boldsymbol{\phi}_{\boldsymbol{\lambda}}(t) &\coloneqq \left(\phi^{\sigma(1)}_{\boldsymbol{\lambda}}(t), \phi^{\sigma(2)}_{\boldsymbol{\lambda}}(t), \dots, \phi^{\sigma(N)}_{\boldsymbol{\lambda}}(t)\right) \\ &= \left(\phi^N_{\boldsymbol{\lambda}}(t), \phi^1_{\boldsymbol{\lambda}}(t), \dots, \phi^{N-1}_{\boldsymbol{\lambda}}(t)\right). \end{aligned}$$

In particular, for the splay state solution $\boldsymbol{\phi}_{\boldsymbol{\lambda}^*}(t)$, we have

$$\begin{aligned} \sigma\boldsymbol{\phi}_{\boldsymbol{\lambda}^*}(t) &\coloneqq \left(\phi^{\sigma(1)}_{\boldsymbol{\lambda}^*}(t), \phi^{\sigma(2)}_{\boldsymbol{\lambda}^*}(t), \dots, \phi^{\sigma(N)}_{\boldsymbol{\lambda}^*}(t)\right) \\ &= \left(\phi^N_{\boldsymbol{\lambda}^*}(t), \phi^1_{\boldsymbol{\lambda}^*}(t), \dots, \phi^{N-1}_{\boldsymbol{\lambda}^*}(t)\right) \\ &= \left(\phi^1_{\boldsymbol{\lambda}^*}\left(t - \frac{T(\boldsymbol{\lambda}^*)}{N}\right), \dots, \phi^N_{\boldsymbol{\lambda}^*}\left(t - \frac{T(\boldsymbol{\lambda}^*)}{N}\right)\right) \\ &= \boldsymbol{\phi}_{\boldsymbol{\lambda}^*}\left(t - \frac{T(\boldsymbol{\lambda}^*)}{N}\right) \end{aligned} \tag{7.14}$$

so that we have $\eta = \sigma$ and $m = N$ in Theorem 3.11. Because of this spatio-temporal symmetry, splay states play a prominent role in $\mathcal{M}$ so that, although they are not hyperbolic, one might ask nevertheless whether they are robust under perturbations which leave the units identical. A necessary condition for this is that $\hat{\boldsymbol{F}}_h(\boldsymbol{\lambda}^*) = \mathbf{0}$ for any possible choice of h. To confirm this conjecture is content of the following two propositions where we handle the case $N = 4$ separately from the case of general N because for four units, we can deduce even more information about $\hat{\boldsymbol{F}}_h$:

Proposition 7.2 *For $N = 4$ and any smooth h, the function $\hat{\boldsymbol{F}}_h$ fulfills*

$$\hat{\boldsymbol{F}}_h(\boldsymbol{\lambda}) = -\hat{\boldsymbol{F}}_h(1 - \boldsymbol{\lambda}) \tag{7.15}$$

and in particular, $\hat{\boldsymbol{F}}_h(\boldsymbol{\lambda}^*) = \mathbf{0}$ holds with $\boldsymbol{\lambda}^* = 1/2$.

Proof. For $N = 4$, we have

$$\sigma = \begin{pmatrix} 1 & 2 & 3 & 4 \\ 4 & 1 & 2 & 3 \end{pmatrix} \tag{7.16}$$

and so write for any $\boldsymbol{\theta} = (\theta^1, \theta^2, \theta^3, \theta^4) \in \mathbb{T}^4_{\text{ordered}}$

$$\sigma\boldsymbol{\theta} = (\theta^{\sigma(1)}, \theta^{\sigma(2)}, \theta^{\sigma(3)}, \theta^{\sigma(4)}) = (\theta^4, \theta^1, \theta^2, \theta^3) \in \mathbb{T}^4_{\text{ordered}}.$$

For definiteness, in this proof we write all solutions of ODEs explicitly with their initial condition.

For fixed $\boldsymbol{\theta} = \boldsymbol{\theta}(\boldsymbol{\lambda}) \in \mathcal{C}_{\boldsymbol{\lambda}}$, let

$$\boldsymbol{\phi}_{\boldsymbol{\lambda}}(t, \boldsymbol{\theta}) = \Big(\phi^1_{\boldsymbol{\lambda}}(t, \boldsymbol{\theta}), \phi^2_{\boldsymbol{\lambda}}(t, \boldsymbol{\theta}), \phi^3_{\boldsymbol{\lambda}}(t, \boldsymbol{\theta}), \phi^4_{\boldsymbol{\lambda}}(t, \boldsymbol{\theta})\Big)$$

denote the solution of the unperturbed system (6.3) with initial condition $\boldsymbol{\phi}_{\boldsymbol{\lambda}}(0, \boldsymbol{\theta}) = \boldsymbol{\theta}$. As above, we set

$$\sigma\boldsymbol{\phi}_{\boldsymbol{\lambda}}(t, \sigma\boldsymbol{\theta}) \coloneqq \Big(\phi^4_{\boldsymbol{\lambda}}(t, \boldsymbol{\theta}), \phi^1_{\boldsymbol{\lambda}}(t, \boldsymbol{\theta}), \phi^2_{\boldsymbol{\lambda}}(t, \boldsymbol{\theta}), \phi^3_{\boldsymbol{\lambda}}(t, \boldsymbol{\theta})\Big)$$

for the cyclic permutation of $\boldsymbol{\phi}_{\boldsymbol{\lambda}}(t, \boldsymbol{\theta})$ which again is a solution of (6.3) since the functions f and g in it depend only on Z which in turn is invariant under permutations of angles. The periodic orbit of this new solution does in general not lie in the same level set $\mathcal{L}_{\boldsymbol{\lambda}}(\boldsymbol{\Lambda})$ as $\mathcal{C}_{\boldsymbol{\lambda}}$ because permutations of the components of any $\boldsymbol{\theta}$ transform the cross-ratios $\boldsymbol{\Lambda}(\boldsymbol{\theta})$. Indeed, for $\boldsymbol{\theta} \in \mathcal{L}_{\boldsymbol{\lambda}}(\boldsymbol{\Lambda})$, we have $\sigma\boldsymbol{\theta} \in \mathcal{L}_{1-\boldsymbol{\lambda}}(\boldsymbol{\Lambda})$ because

$$\begin{aligned}
\boldsymbol{\Lambda}(\sigma\boldsymbol{\theta}) &= \Lambda_{1,2,3,4}(\sigma\boldsymbol{\theta}) \\
&= \frac{\left(\mathrm{e}^{i\theta^{\sigma(1)}} - \mathrm{e}^{i\theta^{\sigma(4)}}\right)\left(\mathrm{e}^{i\theta^{\sigma(2)}} - \mathrm{e}^{i\theta^{\sigma(3)}}\right)}{\left(\mathrm{e}^{i\theta^{\sigma(2)}} - \mathrm{e}^{i\theta^{\sigma(4)}}\right)\left(\mathrm{e}^{i\theta^{\sigma(1)}} - \mathrm{e}^{i\theta^{\sigma(3)}}\right)} \\
&= \frac{\left(\mathrm{e}^{i\theta^4} - \mathrm{e}^{i\theta^3}\right)\left(\mathrm{e}^{i\theta^1} - \mathrm{e}^{i\theta^2}\right)}{\left(\mathrm{e}^{i\theta^1} - \mathrm{e}^{i\theta^3}\right)\left(\mathrm{e}^{i\theta^4} - \mathrm{e}^{i\theta^2}\right)} \\
&= \Lambda_{4,1,2,3}(\boldsymbol{\theta}) \equiv 1 - \Lambda_{1,2,3,4}(\boldsymbol{\theta}) \\
&= 1 - \boldsymbol{\Lambda}(\boldsymbol{\theta}).
\end{aligned} \tag{7.17}$$

Since $\sigma\boldsymbol{\phi}_{\boldsymbol{\lambda}}(0,\sigma\boldsymbol{\theta}) = \sigma\boldsymbol{\theta} = \boldsymbol{\phi}_{1-\boldsymbol{\lambda}}(0,\sigma\boldsymbol{\theta})$, we have

$$\sigma\boldsymbol{\phi}_{\boldsymbol{\lambda}}(t,\boldsymbol{\theta}) = \boldsymbol{\phi}_{1-\boldsymbol{\lambda}}(t,\sigma\boldsymbol{\theta}) \tag{7.18}$$

by uniqueness of solutions for ODEs and it follows that the periodic orbit of $\sigma\boldsymbol{\phi}_{\boldsymbol{\lambda}}$ is $\mathcal{C}_{1-\boldsymbol{\lambda}}$. Note that from this we also read

$$T(\boldsymbol{\lambda}) = T(1-\boldsymbol{\lambda}) \tag{7.19}$$

so that the periodic orbits in $\mathcal{L}_{\boldsymbol{\lambda}}(\boldsymbol{\Lambda})$ and $\mathcal{L}_{1-\boldsymbol{\lambda}}(\boldsymbol{\Lambda})$ have the same period. From (7.17), we also read

$$\begin{aligned}
(\mathrm{D}\Lambda_{1,2,3,4}\cdot\boldsymbol{h})(\sigma\boldsymbol{\theta}) &= \mathrm{D}_{\vartheta^1}\Lambda_{1,2,3,4}(\boldsymbol{\vartheta})\cdot h(\vartheta^1) + \mathrm{D}_{\vartheta^2}\Lambda_{1,2,3,4}(\boldsymbol{\vartheta})\cdot h(\vartheta^2) + \\
&\quad + \mathrm{D}_{\vartheta^3}\Lambda_{1,2,3,4}(\boldsymbol{\vartheta})\cdot h(\vartheta^3) + \mathrm{D}_{\vartheta^4}\Lambda_{1,2,3,4}(\boldsymbol{\vartheta})\cdot h(\vartheta^4)\Big|_{\boldsymbol{\vartheta}=\sigma\boldsymbol{\theta}} \\
&= \mathrm{D}_{\theta^4}\Lambda_{4,1,2,3}(\boldsymbol{\theta})\cdot h(\theta^4) + \mathrm{D}_{\theta^1}\Lambda_{4,1,2,3}(\boldsymbol{\theta})\cdot h(\theta^1) + \\
&\quad + \mathrm{D}_{\theta^2}\Lambda_{4,1,2,3}(\boldsymbol{\theta})\cdot h(\theta^2) + \mathrm{D}_{\theta^3}\Lambda_{4,1,2,3}(\boldsymbol{\theta})\cdot h(\theta^3) \\
&= (\mathrm{D}\Lambda_{4,1,2,3}\cdot\boldsymbol{h})(\boldsymbol{\theta})
\end{aligned}$$

and thus find, using (7.17), (7.18), and (7.19),

$$\begin{aligned}
\hat{\boldsymbol{F}}_h(1-\boldsymbol{\lambda}) &= \frac{1}{T(1-\boldsymbol{\lambda})}\int_0^{T(1-\boldsymbol{\lambda})} (\mathrm{D}\Lambda_{1,2,3,4}\cdot\boldsymbol{h})\circ\boldsymbol{\phi}_{1-\boldsymbol{\lambda}}(t,\sigma\boldsymbol{\theta})\,\mathrm{d}t \\
&= \frac{1}{T(\boldsymbol{\lambda})}\int_0^{T(\boldsymbol{\lambda})} (\mathrm{D}\Lambda_{1,2,3,4}\cdot\boldsymbol{h})\circ\sigma\boldsymbol{\phi}_{\boldsymbol{\lambda}}(t,\boldsymbol{\theta})\,\mathrm{d}t \\
&= \frac{1}{T(\boldsymbol{\lambda})}\int_0^{T(\boldsymbol{\lambda})} (\mathrm{D}\Lambda_{4,1,2,3}\cdot\boldsymbol{h})\circ\boldsymbol{\phi}_{\boldsymbol{\lambda}}(t,\boldsymbol{\theta})\,\mathrm{d}t \\
&= -\frac{1}{T(\boldsymbol{\lambda})}\int_0^{T(\boldsymbol{\lambda})} (\mathrm{D}\Lambda_{1,2,3,4}\cdot\boldsymbol{h})\circ\boldsymbol{\phi}_{\boldsymbol{\lambda}}(t,\boldsymbol{\theta})\,\mathrm{d}t \\
&= -\hat{\boldsymbol{F}}_h(\boldsymbol{\lambda})
\end{aligned}$$

from which also

$$\hat{\boldsymbol{F}}_h(1/2) = 0$$

follows. Since $\boldsymbol{\lambda}^* = 1/2$ by (4.6) for $N = 4$, we find that $\hat{\boldsymbol{F}}_h$ indeed vanishes at $\boldsymbol{\lambda}^*$ for any smooth choice of h. □

By virtue of Proposition 7.1, $\hat{\boldsymbol{F}}_h$ is continuously differentiable so that the derivative $\mathrm{D}\hat{\boldsymbol{F}}_h(\boldsymbol{\lambda}^*)$ exists for smooth h. As long as this derivative is not zero, $\boldsymbol{\lambda}^*$ is then a hyperbolic fixed point of (7.4) and thus $\mathcal{C}_{\epsilon,\boldsymbol{\lambda}^*}$ is a hyperbolic orbit for $N = 4$. By means of Corollary 3.12 and because the considered perturbation term in (7.1) respects the equivariance of (6.3) under the action of Γ, we can then conclude that the splay state becomes a robust solution of (7.1).

Remarkably, in the proof of Proposition 7.2, we did not make use of the fact that $\mathcal{C}_{\boldsymbol{\lambda}^*}$ lies in the level set $\mathcal{L}_{\boldsymbol{\lambda}^*}(\boldsymbol{\Lambda})$. This means that in fact for *any* splay state in $\mathbb{T}^4_{\mathrm{ordered}}$, the integral (7.3) vanishes, regardless of whether we are dealing with a WS-integrable system or not. However, for general systems of four coupled identical angular variables, this average

becomes meaningless because it is not guaranteed that the dynamics of $\boldsymbol{\lambda}(t)$ for them is slow and thus it is by far not clear whether the averaging principle is applicable to them in the first place.

The proof of Proposition 7.2 cannot readily be generalized to arbitrary N because we made explicit use of the fact that the level sets in $\mathbb{T}^4_{\text{ordered}}$ can be parameterized by a single cross-ratio $\boldsymbol{\lambda} = \boldsymbol{\Lambda}(\boldsymbol{\theta}) = \Lambda_{1,2,3,4}(\boldsymbol{\theta})$ for every $\boldsymbol{\theta} \in \mathbb{T}^4_{\text{ordered}}$. We cannot expect a similar relation to (7.15) for $N > 4$ from which to conclude that $\hat{\boldsymbol{F}}_h$ vanishes at $\boldsymbol{\lambda}^*$. Instead, we have to explicitly calculate $\hat{\boldsymbol{F}}_h(\boldsymbol{\lambda}^*)$ and show that this always yields zero. It is thus instructional to review the case $N = 4$ and directly compute $\hat{\boldsymbol{F}}_h(\boldsymbol{\lambda}^*)$ for that case. Using the fact that averages over a full period of a periodic function are invariant under shifts in time as well as relation (7.18) and the cross-ratio identity (7.17), this is easily done:

$$\begin{aligned}
\hat{\boldsymbol{F}}_h(\boldsymbol{\lambda}^*) &= \frac{1}{T(\boldsymbol{\lambda}^*)} \int_0^{T(\boldsymbol{\lambda}^*)} (\mathrm{D}\Lambda_{1,2,3,4} \cdot \boldsymbol{h}) \circ \boldsymbol{\phi}_{\boldsymbol{\lambda}^*}(t)\, \mathrm{d}t \\
&= \frac{1}{T(\boldsymbol{\lambda}^*)} \int_0^{T(\boldsymbol{\lambda}^*)} (\mathrm{D}\Lambda_{1,2,3,4} \cdot \boldsymbol{h}) \circ \boldsymbol{\phi}_{\boldsymbol{\lambda}^*}\left(t - \frac{T(\boldsymbol{\lambda}^*)}{4}\right) \mathrm{d}t \\
&= \frac{1}{T(\boldsymbol{\lambda}^*)} \int_0^{T(\boldsymbol{\lambda}^*)} (\mathrm{D}\Lambda_{1,2,3,4} \cdot \boldsymbol{h}) \circ \sigma\boldsymbol{\phi}_{\boldsymbol{\lambda}^*}(t)\, \mathrm{d}t \\
&= \frac{1}{T(\boldsymbol{\lambda}^*)} \int_0^{T(\boldsymbol{\lambda}^*)} (\mathrm{D}\Lambda_{4,1,2,3} \cdot \boldsymbol{h}) \circ \boldsymbol{\phi}_{\boldsymbol{\lambda}^*}(t)\, \mathrm{d}t \\
&= \frac{1}{T(\boldsymbol{\lambda}^*)} \int_0^{T(\boldsymbol{\lambda}^*)} (-\mathrm{D}\Lambda_{1,2,3,4} \cdot \boldsymbol{h}) \circ \boldsymbol{\phi}_{\boldsymbol{\lambda}^*}(t)\, \mathrm{d}t \\
&= -\hat{\boldsymbol{F}}_h(\boldsymbol{\lambda}^*).
\end{aligned}$$

so that $\hat{\boldsymbol{F}}_h(\boldsymbol{\lambda}^*) = 0$ for $N = 4$. Note that again, we did not use the fact that the splay state lies in $\mathcal{L}_{\boldsymbol{\lambda}^*}(\boldsymbol{\Lambda})$. To generalize this calculation for the case of arbitrary $N \geq 4$, we must take into consideration that cyclic permutation of the units θ^j are not compatible with our choice (4.3) for the cross-ratio function $\boldsymbol{\Lambda}$: Computing, e. g.,

$$\begin{aligned}
\Lambda_k(\sigma\boldsymbol{\theta}) &= \Lambda_{1,2,3,k+3}(\sigma\boldsymbol{\theta}) \\
&= \frac{\left(\mathrm{e}^{i\theta^{\sigma(1)}} - \mathrm{e}^{i\theta^{\sigma(k+3)}}\right)\left(\mathrm{e}^{i\theta^{\sigma(2)}} - \mathrm{e}^{i\theta^{\sigma(3)}}\right)}{\left(\mathrm{e}^{i\theta^{\sigma(2)}} - \mathrm{e}^{i\theta^{\sigma(k+3)}}\right)\left(\mathrm{e}^{i\theta^{\sigma(1)}} - \mathrm{e}^{i\theta^{\sigma(3)}}\right)} \\
&= \frac{\left(\mathrm{e}^{i\theta^{N}} - \mathrm{e}^{i\theta^{k+2}}\right)\left(\mathrm{e}^{i\theta^{1}} - \mathrm{e}^{i\theta^{2}}\right)}{\left(\mathrm{e}^{i\theta^{1}} - \mathrm{e}^{i\theta^{k+2}}\right)\left(\mathrm{e}^{i\theta^{N}} - \mathrm{e}^{i\theta^{2}}\right)} \\
&= \Lambda_{N,1,2,k+2}(\boldsymbol{\theta}),
\end{aligned}$$

the result is not a component of $\boldsymbol{\Lambda}(\boldsymbol{\theta})$. From this, we see that the $N-3$ cross-ratios $\Lambda_{1,2,3,k+3}$ are not an ideal choice for handling splay states because these functions privilege the first three coordinates θ^1, θ^2, and θ^3 while we would prefer a choice of cross-ratios to parameterize the level sets $\mathcal{L}_{\boldsymbol{\lambda}}(\boldsymbol{\Lambda})$ for which there exists a simple expression for $\boldsymbol{\Lambda}(\sigma\boldsymbol{\theta})$

in terms of $\mathbf{\Lambda}(\boldsymbol{\theta})$. Luckily, (4.3) is not the only possible way to parameterize the invariant level sets $\mathcal{L}_{\boldsymbol{\lambda}}(\mathbf{\Lambda})$. Indeed, an equivalent choice of $N-3$ functionally independent cross-ratios which is more suitable for handling splay states is given by

$$\begin{aligned}\mathbf{\Lambda}(\boldsymbol{\theta}) &\coloneqq (\Lambda_1(\boldsymbol{\theta}), \dots, \Lambda_{N-3}(\boldsymbol{\theta}))\\ \Lambda_k(\boldsymbol{\theta}) &\coloneqq \Lambda_{k,k+1,k+2,k+3}(\boldsymbol{\theta}) = \frac{\left(\mathrm{e}^{i\theta^k} - \mathrm{e}^{i\theta^{k+3}}\right)\left(\mathrm{e}^{i\theta^{k+1}} - \mathrm{e}^{i\theta^{k+2}}\right)}{\left(\mathrm{e}^{i\theta^k} - \mathrm{e}^{i\theta^{k+2}}\right)\left(\mathrm{e}^{i\theta^{k+1}} - \mathrm{e}^{i\theta^{k+3}}\right)}\end{aligned} \tag{7.20}$$

which was in fact used by the authors of [MMS09] to show that *every* cross-ratio can be expressed in terms of the $N-3$ functionally independent ones above. While our previous choice (4.3) was more suitable for the proof of the existence of $\mathcal{M}$, we work from now on exclusively with the ones, defined above. Evaluating $\mathbf{\Lambda}(\sigma\boldsymbol{\theta})$ then reveals that

$$\begin{aligned}\Lambda_{k+1}(\sigma\boldsymbol{\theta}) &= \Lambda_{k+1,k+2,k+3,k+4}(\sigma\boldsymbol{\theta})\\ &= \frac{\left(\mathrm{e}^{i\theta^{\sigma(k+1)}} - \mathrm{e}^{i\theta^{\sigma(k+4)}}\right)\left(\mathrm{e}^{i\theta^{\sigma(k+2)}} - \mathrm{e}^{i\theta^{\sigma(k+3)}}\right)}{\left(\mathrm{e}^{i\theta^{\sigma(k+1)}} - \mathrm{e}^{i\theta^{\sigma(k+3)}}\right)\left(\mathrm{e}^{i\theta^{\sigma(k+2)}} - \mathrm{e}^{i\theta^{\sigma(k+4)}}\right)}\\ &= \frac{\left(\mathrm{e}^{i\theta^{k}} - \mathrm{e}^{i\theta^{k+3}}\right)\left(\mathrm{e}^{i\theta^{k+1}} - \mathrm{e}^{i\theta^{k+2}}\right)}{\left(\mathrm{e}^{i\theta^{k}} - \mathrm{e}^{i\theta^{k+2}}\right)\left(\mathrm{e}^{i\theta^{k+1}} - \mathrm{e}^{i\theta^{k+3}}\right)}\\ &= \Lambda_{k,k+1,k+2,k+3}(\boldsymbol{\theta})\\ &= \Lambda_k(\boldsymbol{\theta})\end{aligned} \tag{7.21}$$

so that the cross-ratios $\mathbf{\Lambda}(\sigma\boldsymbol{\theta})$ can indeed easily be written in terms of $\mathbf{\Lambda}(\boldsymbol{\theta})$. Let us now consider the point $\boldsymbol{\theta}^*$ in the level set of uniform distributions, defined in (4.5), for which we find

$$\begin{aligned}\sigma\boldsymbol{\theta}^* &= (\theta_N^*, \theta_1^* \dots, \theta_{N-1}^*)\\ &= \left(\theta_1^* - \frac{2\pi}{N}, \theta_2^* - \frac{2\pi}{N}, \dots, \theta_N^* - \frac{2\pi}{N}\right)\end{aligned}$$

which we also write as $\sigma\boldsymbol{\theta}^* \equiv \boldsymbol{\theta}^* - 2\pi/N$. For our new cross-ratios, we then have

$$\Lambda_k(\boldsymbol{\theta}^*) = \Lambda_{k+1}(\sigma\boldsymbol{\theta}^*) = \Lambda_{k+1}\left(\boldsymbol{\theta}^* - \frac{2\pi}{N}\right) = \Lambda_{k+1}(\boldsymbol{\theta}^*)$$

because any shift $\theta_j \mapsto \theta_j + c$ in all components of $\boldsymbol{\theta}$ by some fixed value c corresponds to the Möbius map

$$\mathrm{e}^{i\boldsymbol{\theta}} \mapsto \mathrm{e}^{i\boldsymbol{\theta}+ic} = G_{0,c}\left(\mathrm{e}^{i\boldsymbol{\theta}}\right)$$

which in turn keeps cross-ratios invariant. This results in

$$\boldsymbol{\lambda}^* \coloneqq (\lambda_1^*, \dots, \lambda_1^*)$$

with λ_1^* given by (4.6) for $k = 1$ because (4.3) and (7.20) coincide in their first component. Of course, the averaging Proposition 7.1 is not

affected by which cross-ratios we choose to parameterize the level sets (i. e., equivalence classes) in $\mathbb{T}^N_{\text{ordered}}$ so that in particular, we still find a hyperbolic periodic orbit $\mathcal{C}_{\epsilon,\boldsymbol{\lambda}_0}$ for every hyperbolic fixed point $\boldsymbol{\lambda}_0$ of the averaged system

$$\dot{\boldsymbol{\lambda}} = \hat{\boldsymbol{F}}_h(\boldsymbol{\lambda})$$

where $\hat{\boldsymbol{F}}_h(\boldsymbol{\lambda}) = ((\hat{F}_h)_1(\boldsymbol{\lambda}), \dots, (\hat{F}_h)_{N-3}(\boldsymbol{\lambda}))$ is still given by (7.3) but with the new choice (7.20) for $\boldsymbol{\Lambda}$. With these remarks, we are ready to prove our conjecture $\hat{\boldsymbol{F}}_h(\boldsymbol{\lambda}^*) = \mathbf{0}$ for general $N \geq 4$ (which took the author an embarrassingly long time to prove):

Proposition 7.3 *For any $N \geq 4$ and smooth h,*

$$\hat{\boldsymbol{F}}_h(\boldsymbol{\lambda}^*) = \mathbf{0}.$$

Proof. For any fixed but arbitrarily chosen $\boldsymbol{\theta} \in \mathcal{C}_{\boldsymbol{\lambda}^*}$, let again

$$\boldsymbol{\phi}_{\boldsymbol{\lambda}^*}(t) = \left(\phi^1_{\boldsymbol{\lambda}^*}(t), \dots, \phi^N_{\boldsymbol{\lambda}^*}(t)\right)$$

denote the splay state solution of (6.3) with initial condition $\boldsymbol{\phi}_{\boldsymbol{\lambda}^*}(0) = \boldsymbol{\theta}$. Next, for the cyclic permutation σ, given by (7.12), we recall from (7.14) that

$$\sigma\boldsymbol{\phi}_{\boldsymbol{\lambda}^*}(t) = \boldsymbol{\phi}_{\boldsymbol{\lambda}^*}\left(t - \frac{T(\boldsymbol{\lambda}^*)}{N}\right)$$

and from (7.21), that

$$\Lambda_{k+1}(\sigma\boldsymbol{\theta}) = \Lambda_k(\boldsymbol{\theta})$$

and

$$\mathrm{D}\Lambda_{k+1}(\sigma\boldsymbol{\theta}) = \mathrm{D}\Lambda_k(\boldsymbol{\theta})$$

holds for all $\boldsymbol{\theta} \in \mathbb{T}^N_{\text{ordered}}$. Hence, we can for every $k = 1, \dots, N$ (where we set $N+1 \equiv 1$, $N+2 \equiv 2$, and $N+3 \equiv 3$) and any splay state[4] formally[5] write

$$\begin{aligned}
(\hat{F}_h)_{k+1}(\boldsymbol{\lambda}^*) \coloneqq & \frac{1}{T(\boldsymbol{\lambda}^*)} \int_0^{T(\boldsymbol{\lambda}^*)} (\mathrm{D}\Lambda_{k+1} \cdot \boldsymbol{h}) \circ \boldsymbol{\phi}_{\boldsymbol{\lambda}^*}(t)\, \mathrm{d}t \\
= & \frac{1}{T(\boldsymbol{\lambda}^*)} \int_0^{T(\boldsymbol{\lambda}^*)} (\mathrm{D}\Lambda_{k+1} \cdot \boldsymbol{h}) \circ \boldsymbol{\phi}_{\boldsymbol{\lambda}^*}\left(t - \frac{T(\boldsymbol{\lambda}^*)}{N}\right) \mathrm{d}t \\
= & \frac{1}{T(\boldsymbol{\lambda}^*)} \int_0^{T(\boldsymbol{\lambda}^*)} (\mathrm{D}\Lambda_{k+1} \cdot \boldsymbol{h}) \circ \sigma\boldsymbol{\phi}_{\boldsymbol{\lambda}^*}(t)\, \mathrm{d}t \\
= & \frac{1}{T(\boldsymbol{\lambda}^*)} \int_0^{T(\boldsymbol{\lambda}^*)} (\mathrm{D}\Lambda_k \cdot \boldsymbol{h}) \circ \boldsymbol{\phi}_{\boldsymbol{\lambda}^*}(t)\, \mathrm{d}t \\
= & (\hat{F}_h)_k(\boldsymbol{\lambda}^*)
\end{aligned}$$

4 I. e., any T-periodic state $\boldsymbol{\phi}(t)$ that possesses the spatio-temporal symmetry $\sigma\boldsymbol{\phi}(t) = \boldsymbol{\phi}(t - T/N)$ which characterizes a splay state, cf. (7.14), regardless of whether the orbit of $\boldsymbol{\phi}$ lies in $\mathcal{L}_{\boldsymbol{\lambda}^*}(\boldsymbol{\Lambda})$ or not. In other words, in the calculation below, we only use the fact that $\boldsymbol{\phi}_{\boldsymbol{\lambda}^*}(t)$ is a splay state but not that $\mathcal{C}_{\boldsymbol{\lambda}^*} \subset \mathcal{L}_{\boldsymbol{\lambda}^*}(\boldsymbol{\Lambda})$.

5 Note that we let k range over $\{1, \dots, N\}$ instead of $\{1, \dots, N-3\}$ which will be important in the next step of the argument. The integrals $(\hat{F}_h)_{N-2}(\boldsymbol{\lambda}^*)$, $(\hat{F}_h)_{N-1}(\boldsymbol{\lambda}^*)$, and $(\hat{F}_h)_N(\boldsymbol{\lambda}^*)$, although not describing any component of the vector $\hat{\boldsymbol{F}}_h(\boldsymbol{\lambda}^*)$, are still well-defined.

where in the second line we again used the fact that integrals over a full period of a function are invariant under shifts in t. This means that in particular, the $N-3$ components of $\hat{\boldsymbol{F}}_h(\boldsymbol{\lambda}^*)$ coincide. We also have for any $j \in \{1,\dots,N\}$

$$\begin{aligned}(\hat{F}_h)_j(\boldsymbol{\lambda}^*) &= \frac{1}{N}\sum_{k=1}^{N}(\hat{F}_h)_k(\boldsymbol{\lambda}^*)\\ &= \frac{1}{NT(\boldsymbol{\lambda}^*)}\int_0^{T(\boldsymbol{\lambda}^*)}\left(\sum_{k=1}^{N}\mathrm{D}\Lambda_k\cdot\boldsymbol{h}\right)\circ\boldsymbol{\phi}_{\boldsymbol{\lambda}^*}(t)\,\mathrm{d}t\\ &= \frac{1}{NT(\boldsymbol{\lambda}^*)}\int_0^{T(\boldsymbol{\lambda}^*)}\sum_{k=1}^{N}\Big(\mathrm{D}_{\theta_k}\Lambda_k(\boldsymbol{\theta})\cdot h(\theta_k)+\\ &\qquad + \mathrm{D}_{\theta_{k+1}}\Lambda_k(\boldsymbol{\theta})\cdot h(\theta_{k+1})+\\ &\qquad + \mathrm{D}_{\theta_{k+2}}\Lambda_k(\boldsymbol{\theta})\cdot h(\theta_{k+2})+\\ &\qquad + \mathrm{D}_{\theta_{k+3}}\Lambda_k(\boldsymbol{\theta})\cdot h(\theta_{k+3})\Big)\Big|_{\boldsymbol{\theta}=\boldsymbol{\phi}_{\boldsymbol{\lambda}^*}(t)}\mathrm{d}t\end{aligned}$$

where in the third line, we simply expanded the scalar product from the second line. Next, we observe that for every k, the cross-ratio Λ_k only depends on $\theta_k,\dots,\theta_{k+3}$ according to (7.20) and thus for every θ_k, we have exactly four terms in the sum above that contain a derivative of some cross-ratio with respect to θ_k, namely

$$\begin{aligned}\mathrm{D}_{\theta_k}\Lambda_k(\boldsymbol{\theta})\cdot h(\theta_k) &\equiv \mathrm{D}_{\theta_k}\Lambda_{k,k+1,k+2,k+3}(\boldsymbol{\theta})\cdot h(\theta_k),\\ \mathrm{D}_{\theta_k}\Lambda_{k-1}(\boldsymbol{\theta})\cdot h(\theta_k) &\equiv \mathrm{D}_{\theta_k}\Lambda_{k-1,k,k+1,k+2}(\boldsymbol{\theta})\cdot h(\theta_k),\\ \mathrm{D}_{\theta_k}\Lambda_{k-2}(\boldsymbol{\theta})\cdot h(\theta_k) &\equiv \mathrm{D}_{\theta_k}\Lambda_{k-2,k-1,k,k+1}(\boldsymbol{\theta})\cdot h(\theta_k),\ \text{and}\\ \mathrm{D}_{\theta_k}\Lambda_{k-3}(\boldsymbol{\theta})\cdot h(\theta_k) &\equiv \mathrm{D}_{\theta_k}\Lambda_{k-3,k-2,k-1,k}(\boldsymbol{\theta})\cdot h(\theta_k).\end{aligned}$$

We proceed by rearranging the sum accordingly. Collecting the respective terms for every θ_k yields

$$\begin{aligned}(\hat{F}_h)_j(\boldsymbol{\lambda}^*) = \frac{1}{NT(\boldsymbol{\lambda}^*)}\int_0^{T(\boldsymbol{\lambda}^*)}\sum_{k=1}^{N}\mathrm{D}_{\theta_k}\Big(\Lambda_k(\boldsymbol{\theta})+\Lambda_{k-1}(\boldsymbol{\theta})+\\ +\Lambda_{k-2}(\boldsymbol{\theta})+\Lambda_{k-3}(\boldsymbol{\theta})\Big)\cdot h(\theta_k)\Big|_{\boldsymbol{\theta}=\boldsymbol{\phi}_{\boldsymbol{\lambda}^*}(t)}\mathrm{d}t.\end{aligned} \tag{7.22}$$

We claim that (7.22) vanishes because each term the sum in the integrand vanishes identically. To see this, observe that for any $\boldsymbol{\theta}\in\mathcal{L}_{\boldsymbol{\lambda}^*}(\boldsymbol{\Lambda})$, there exists some $(\alpha,\psi)\in\mathbb{D}\times\mathbb{S}^1$ with

$$\mathrm{e}^{i\boldsymbol{\theta}} = G_{\alpha,\psi}\left(\mathrm{e}^{i\boldsymbol{\theta}^*}\right) = \frac{\alpha+\mathrm{e}^{i\psi}\mathrm{e}^{i\boldsymbol{\theta}^*}}{1+\bar{\alpha}\mathrm{e}^{i\psi}\mathrm{e}^{i\boldsymbol{\theta}^*}}$$

where $\boldsymbol{\theta}^*$ is given by (4.5) so that inserting this in (7.22) yields

$$\begin{aligned}\mathrm{D}_{\theta_k}\Lambda_k(\boldsymbol{\theta}) &\equiv \mathrm{D}_{\theta_k}\Lambda_{k,k+1,k+2,k+3}(\boldsymbol{\theta})\\ &= i\mathrm{e}^{i\theta_k}\frac{\left(\mathrm{e}^{i\theta_{k+3}}-\mathrm{e}^{i\theta_{k+2}}\right)\left(\mathrm{e}^{i\theta_{k+2}}-\mathrm{e}^{i\theta_{k+1}}\right)}{\left(\mathrm{e}^{i\theta_{k+3}}-\mathrm{e}^{i\theta_{k+1}}\right)\left(\mathrm{e}^{i\theta_{k+2}}-\mathrm{e}^{i\theta_k}\right)^2}\end{aligned}$$

$$
\begin{aligned}
&= \frac{i\mathrm{e}^{i\frac{2\pi(k-1)}{N}-i\psi}\left(\mathrm{e}^{i\frac{2\pi k}{N}+i\psi}-\mathrm{e}^{i\frac{2\pi}{N}}\alpha\right)\left(\mathrm{e}^{i\frac{2\pi}{N}}-\mathrm{e}^{i\frac{2\pi k}{N}+i\psi}\bar{\alpha}\right)}{\left(\mathrm{e}^{i\frac{2\pi}{N}}-1\right)\left(1+\mathrm{e}^{i\frac{2\pi}{N}}\right)^3\left(1-|\alpha|^2\right)} \\
&= -i\mathrm{e}^{i\theta_k}\frac{\left(\mathrm{e}^{i\theta_{k-3}}-\mathrm{e}^{i\theta_{k-2}}\right)\left(\mathrm{e}^{i\theta_{k-2}}-\mathrm{e}^{i\theta_{k-1}}\right)}{\left(\mathrm{e}^{i\theta_{k-3}}-\mathrm{e}^{i\theta_{k-1}}\right)\left(\mathrm{e}^{i\theta_{k-2}}-\mathrm{e}^{i\theta_k}\right)^2} \\
&= -\mathrm{D}_{\theta_k}\Lambda_{k-3,k-2,k-1,k}(\boldsymbol{\theta}) \\
&\equiv -\mathrm{D}_{\theta_k}\Lambda_{k-3}(\boldsymbol{\theta})
\end{aligned}
$$

so that the first and last term in each summand in (7.22) cancel out. Similarly, we have

$$
\begin{aligned}
\mathrm{D}_{\theta_k}\Lambda_{k-1}(\boldsymbol{\theta}) &\equiv \mathrm{D}_{\theta_k}\Lambda_{k-1,k,k+1,k+2}(\boldsymbol{\theta}) \\
&= i\mathrm{e}^{i\theta_k}\frac{\left(\mathrm{e}^{i\theta_{k-1}}-\mathrm{e}^{i\theta_{k+2}}\right)\left(\mathrm{e}^{i\theta_{k+1}}-\mathrm{e}^{i\theta_{k+2}}\right)}{\left(\mathrm{e}^{i\theta_{k-1}}-\mathrm{e}^{i\theta_{k+1}}\right)\left(\mathrm{e}^{i\theta_k}-\mathrm{e}^{i\theta_{k+2}}\right)^2} \\
&= \frac{i\left(1+\mathrm{e}^{i\frac{2\pi}{N}}+\mathrm{e}^{i\frac{4\pi}{N}}\right)\left(1-\mathrm{e}^{-i\frac{2\pi(k-1)}{N}-i\psi}\alpha\right)\left(\mathrm{e}^{i\frac{2\pi}{N}}-\mathrm{e}^{i\frac{2\pi k}{N}+i\psi}\bar{\alpha}\right)}{\left(1-\mathrm{e}^{i\frac{2\pi}{N}}\right)\left(1+\mathrm{e}^{i\frac{2\pi}{N}}\right)^3\left(1-|\alpha|^2\right)} \\
&= -i\mathrm{e}^{i\theta_k}\frac{\left(\mathrm{e}^{i\theta_{k-1}}-\mathrm{e}^{i\theta_{k-2}}\right)\left(\mathrm{e}^{i\theta_{k+1}}-\mathrm{e}^{i\theta_{k-2}}\right)}{\left(\mathrm{e}^{i\theta_{k-1}}-\mathrm{e}^{i\theta_{k+1}}\right)\left(\mathrm{e}^{i\theta_k}-\mathrm{e}^{i\theta_{k-2}}\right)^2} \\
&= -\mathrm{D}_{\theta_k}\Lambda_{k-2,k-1,k,k+1}(\boldsymbol{\theta}) \\
&\equiv -\mathrm{D}_{\theta_k}\Lambda_{k-2}(\boldsymbol{\theta})
\end{aligned}
$$

so that the second and third term equally cancel in each summand and hence, the integrand and therefore the integral for all components of $\hat{\boldsymbol{F}}_h(\boldsymbol{\lambda}^*)$ vanishes identically. This finishes the proof. □

Similar to Proposition 7.2, as long as the derivative $\mathrm{D}\hat{\boldsymbol{F}}_h(\boldsymbol{\lambda}^*)$ has no eigenvalues with zero real part, $\boldsymbol{\lambda}^*$ is a hyperbolic fixed point of (7.11) so that subsequently, $\mathcal{C}_{\epsilon,\boldsymbol{\lambda}^*}$ becomes a robust orbit and by preserved equivariance, the splay state becomes a robust solution of the system (7.1). That this is in practice really the case will be exemplified for the generalized Active Rotator model, further below.

With this, we end our considerations on splay states. Next, we discuss an interesting consequence of Proposition 7.1 concerning arbitrary orbits $\mathcal{C}_{\boldsymbol{\lambda}} \subset \mathcal{M}$, which also becomes handy, later on.

7.3.3 *Controlling Periodic Orbits*

According to Proposition 7.3, each smooth choice of h in (7.2) renders the splay state robust if $\mathrm{D}\hat{\boldsymbol{F}}_h(\boldsymbol{\lambda}^*)$ has no eigenvalues on the imaginary line. Further, as discussed in Chapter 5, at least for the generalized AR-model (2.6), we know that periodic two-cluster states are also robust.

This evokes the question whether there exist any other orbits $\mathcal{C}_{\boldsymbol{\lambda}} \subset \mathcal{M}$ that can be made robust, i. e., hyperbolic, for a suitable perturbation function h. More precisely: fixing $\boldsymbol{\lambda}_0 \in W$ such that $\mathcal{C}_{\boldsymbol{\lambda}_0} \subset \mathcal{M}$ exists, does there exist a smooth function h of the form (7.1b) such that $\mathcal{C}_{\boldsymbol{\lambda}_0}$ becomes a hyperbolic orbit for (7.1a)?

To answer this question, we note first that the average (7.3) is linear in h, i. e.,

$$\hat{\boldsymbol{F}}_{a_1 h_1 + a_2 h_2} = a_1 \hat{\boldsymbol{F}}_{h_1} + a_2 \hat{\boldsymbol{F}}_{h_2}. \tag{7.23}$$

Choose now any set of $N-2$ linearly independent smooth perturbation functions $h_1, \ldots, h_{N-2} \in H$ where

$$H = \left\{ h \in C^\infty(\mathbb{S}^1, \mathbb{R}) \; ; \; h(\phi) = \sum_{n=2}^{\infty} a_n \sin n\phi + b_n \cos n\phi \right\}$$

is the infinite-dimensional space of smooth functions from $\mathbb{S}^1$ to $\mathbb{R}$ of the form (7.1b). Since the $N-2$ vectors $\hat{\boldsymbol{F}}_{h_j}(\boldsymbol{\lambda}_0) \in \mathbb{R}^{N-3}$ are elements of an $(N-3)$-dimensional vector space, there exist a set of nontrivial coefficients $c_1, \ldots, c_{N-2} \in \mathbb{R}$ for which

$$\sum_{j=1}^{N-2} c_j \hat{\boldsymbol{F}}_{h_j}(\boldsymbol{\lambda}_0) = \mathbf{0}$$

holds. Setting

$$h = \sum_{j=1}^{N-2} c_j h_j,$$

we then find with (7.23) that

$$\hat{\boldsymbol{F}}_h(\boldsymbol{\lambda}_0) = \hat{\boldsymbol{F}}_{\sum_{j=1}^{N-2} c_j h_j}(\boldsymbol{\lambda}_0) = \sum_{j=1}^{N-2} c_j \hat{\boldsymbol{F}}_{h_j}(\boldsymbol{\lambda}_0) = \mathbf{0}.$$

Again, as long as $\mathrm{D}\hat{\boldsymbol{F}}_h(\boldsymbol{\lambda}_0)$ has no eigenvalues on the imaginary line, $\boldsymbol{\lambda}_0$ is a hyperbolic fixed point of the averaged system (7.4) and thus corresponds to a robust periodic orbit $\mathcal{C}_{\epsilon,\boldsymbol{\lambda}_0} \in \mathcal{M}_\epsilon$ for the perturbed system (7.1) by virtue of Proposition 7.1. Further, $\mathcal{C}_{\epsilon,\boldsymbol{\lambda}_0}$ is $\mathcal{O}(\epsilon)$-close to $\mathcal{C}_{\boldsymbol{\lambda}_0}$ such that $\|\boldsymbol{\Lambda}(\boldsymbol{\theta}) - \boldsymbol{\lambda}_0\| = \mathcal{O}(\epsilon)$ for all $\boldsymbol{\theta} \in \mathcal{C}_{\epsilon,\boldsymbol{\lambda}_0}$. Summarizing and intuitively speaking, we can therefore always construct a perturbation h in such a way, that a given periodic orbit $\mathcal{C}_{\boldsymbol{\lambda}_0} \subset \mathcal{M}$ becomes a robust orbit $\mathcal{C}_{\epsilon,\boldsymbol{\lambda}_0}$ under this perturbation.

Note that the construction procedure above generally only yields a hyperbolic orbit but cannot guarantee that this orbit is exponentially stable. Whether the proposed construction can be refined to make the orbit also exponentially stable is an open question. However, it stands to reason that constructing stable limit cycles could actually be achievable: We know that any orbit has at least two exponentially stable directions from the fact that $\mathcal{C}_{\epsilon,\boldsymbol{\lambda}_0} \subset \mathcal{M}_\epsilon$ which is a NAIM. We also have an infinite-dimensional space of possible perturbation function at disposal

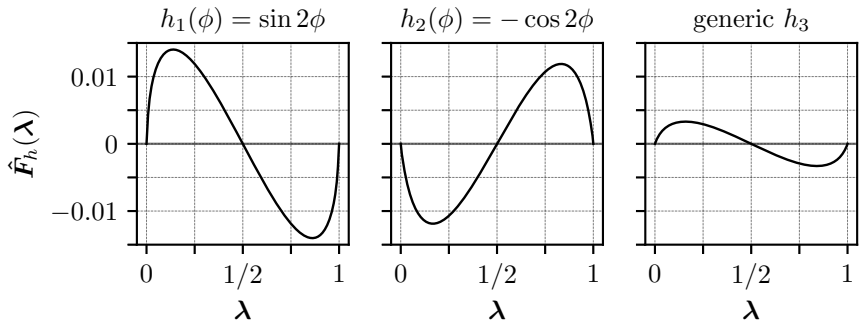

Figure 19: Averaged perturbation $\hat{\boldsymbol{F}}_h$ for $h_1(\phi) = \sin 2\phi$, $h_2(\phi) = -\cos 2\phi$, and the generic perturbation (7.24c) for a system of $N = 4$ units. System parameters in (2.5) are fixed as $\omega = 0.8$ and $\kappa = -0.7$. For all three choices of h, splay states and two-cluster states are of opposite stability.

to choose a finite set $\{h_j\,;\, j = 1, \ldots, N-2\}$ of linearly independent perturbation functions so that it seems reasonable to assume that there is enough variety to choose from in order to achieve our goal of making $\mathcal{C}_{\epsilon,\boldsymbol{\lambda}_0}$ exponentially stable.

We proceed by applying the general results above to our model (2.6) of coupled generalized Active Rotators.

7.4 APPLICATION: ENSEMBLES OF ACTIVE ROTATORS

We now want to discuss the implications from the general results above to our model (2.6) of generalized Active Rotators. We start with an in-depth analysis of the simplest nontrivial case of just $N = 4$ units before we discuss numerical results for larger ensembles.

7.4.1 *A Case Study for $N = 4$ Units*

AVERAGING We begin our discussion by computing the averaged vector field $\hat{\boldsymbol{F}}_h$ for three different choices of perturbation functions h for the classic AR-model (2.5) with fixed parameters $\omega = 0.8$ and $\kappa = -0.7$. Since, we are dealing with four units, we have only a single independent cross-ratio $\boldsymbol{\lambda} = \Lambda_{1,2,3,4}(\boldsymbol{\theta})$ which ranges between zero and one: $\boldsymbol{\lambda} \in V \equiv (0, 1)$. We choose the three functions

$$h_1(\phi) = \sin 2\phi \tag{7.24a}$$

$$h_2(\phi) = -\cos 2\phi \tag{7.24b}$$

$$h_3(\phi) = \frac{1}{\sin\phi - 2} + \frac{1}{\sqrt{3}} + \left(\frac{4}{\sqrt{3}} - 2\right)\sin\phi \tag{7.24c}$$

where h_1 and h_3 are the same functions that we considered in Chapter 5 on periodic two-cluster states. Numerical results for the respective averages are shown in Figure 19.

As expected from Proposition 7.2, we find for all three choices of h that (i) the function $\hat{\boldsymbol{F}}_h$ indeed fulfills relation (7.15) and (ii) splay states are robust solutions for sufficiently small $|\epsilon| \neq 0$ because of

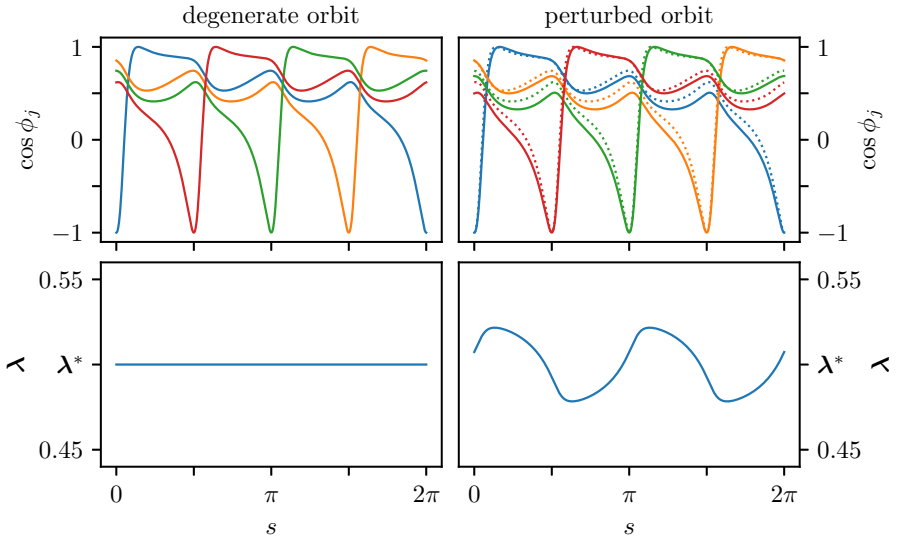

Figure 20: Splay state for the WS-integrable model (2.5) (left) and the perturbed model (2.6) (right) with $h(\phi) = \sin 2\phi$ for $N = 4$ units. Parameters are fixed at $\omega = 0.8$, $\kappa = -0.7$, and $\epsilon = 0.05$. For comparison, the (normalized) time series for the degenerate orbit is also plotted in the top right panel (dotted lines). The splay state is robust under small changes in ϵ. It is stable for $\epsilon > 0$ and unstable for $\epsilon < 0$. The cross-ratio $\boldsymbol{\lambda}(s)$ along the orbit oscillates around $\boldsymbol{\lambda}^*$ with an amplitude of order $\mathcal{O}(\epsilon)$.

$\mathrm{D}\hat{\boldsymbol{F}}_h(\boldsymbol{\lambda}^*) \neq 0$. Moreover, we can directly read from the plots that for the choices h_1 and h_3, splay states must be stable for positive ϵ and unstable otherwise while for h_2, it is exactly the other way around. In Figure 20, we plot the (normalized) times series for the splay state solution for h_1. The upper left panel shows the WS-case $\epsilon = 0$ while the upper right panel depicts the stable splay state for $\epsilon = 0.05$ (together with the time series of the degenerate orbit as dotted lines for comparison). Indeed, we find that the robust orbit $\mathcal{C}_{\epsilon,\boldsymbol{\lambda}^*}$ stays a splay state and that its cross-ratio $\boldsymbol{\lambda}(t) = \boldsymbol{\Lambda} \circ \boldsymbol{\phi}_{\epsilon,\boldsymbol{\lambda}^*}(t)$ now oscillates around the value $\boldsymbol{\lambda}^* = 1/2$, (lower right panel) while for the WS-case, $\boldsymbol{\lambda}(t) = \boldsymbol{\lambda}^*$ is a conserved quantity (lower left panel). Note that this means in particular that the perturbed orbit $\mathcal{C}_{\epsilon,\boldsymbol{\lambda}^*}$ does not lie entirely in the level set $\mathcal{L}_{\boldsymbol{\lambda}^*}(\boldsymbol{\Lambda})$ anymore but intersects it instead. Note also that the amplitude of the oscillation in $\boldsymbol{\lambda}$ is indeed of order $\mathcal{O}(\epsilon)$.

Strictly speaking, $\boldsymbol{\lambda}^*$ is the only zero for all three examples in Figure 19. However, we can see from the plots that

$$\lim_{\boldsymbol{\lambda}\to 0} \hat{\boldsymbol{F}}_h(\boldsymbol{\lambda}) = \lim_{\boldsymbol{\lambda}\to 1} \hat{\boldsymbol{F}}_h(\boldsymbol{\lambda}) = 0$$

in all three cases. Let us therefore formally include the two points $\boldsymbol{\lambda} = 0$ and $\boldsymbol{\lambda} = 1$ into our considerations even though for these two values, we must have at least two of the four units coinciding according to (7.20) so that any state $\boldsymbol{\theta}$ with $\boldsymbol{\Lambda}(\boldsymbol{\theta}) = 0$ or 1 is not an element of $\mathbb{T}^N_{\mathrm{ordered}}$. What is the nature of the dynamics for these limit cases? To answer this question, we might look what the dynamics along the periodic orbits $\mathcal{C}_{\boldsymbol{\lambda}}$ look like for $\boldsymbol{\lambda} \approx 0$ and $\boldsymbol{\lambda} \approx 1$, respectively, in the WS-case $\epsilon = 0$.

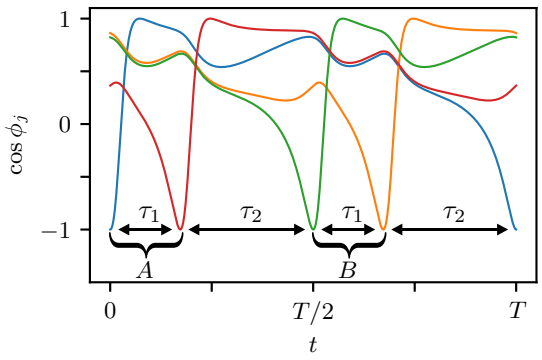

Figure 21: Broken-symmetry state for $N = 4$ ARs for (2.5) with $\omega = 0.8$, $\kappa = -0.7$. The ensemble splits in two groups A and B such that the inter-spike interval τ_1 between two units in the same group is smaller than the inter-spike interval τ_2 between two consecutive units which belong to different groups.

In general, we observe that the dynamics along any orbit $\mathcal{C}_{\boldsymbol{\lambda}}$ with $\boldsymbol{\lambda} \neq \boldsymbol{\lambda}^*$ looks qualitatively like the one, depicted in Figure 21: The ensemble splits in two groups A and B of two consecutive units each, such that the rear units (in Figure 21 represented by a red line for group A and a yellow line for group B) cross, e. g., the point[6] $\phi = \pi$ in the state space $\mathbb{S}^1$ with a time-delay of τ_1 after the front element in the respective groups (here, represented by a blue line for group A and a green line for group B) while for two consecutive units, belonging to different groups, this time-delay is $\tau_2 > \tau_1$. Intuitively speaking, groups therefore consist of two units each, which are more "tightly bound" together but do not yet form a proper cluster (i. e., they do not coincide), they form an "almost-cluster". All these states are of lower spatio-temporal symmetry than the splay state $\boldsymbol{\phi}_{\boldsymbol{\lambda}^*}(t)$. Specifically, one reads from Figure 21 that they obey the relation

$$\begin{aligned}
\sigma^2\boldsymbol{\phi}_{\boldsymbol{\lambda}}(t) &:= \left(\phi_{\boldsymbol{\lambda}}^{\sigma^2(1)}(t), \phi_{\boldsymbol{\lambda}}^{\sigma^2(2)}(t), \phi_{\boldsymbol{\lambda}}^{\sigma^2(3)}(t), \phi_{\boldsymbol{\lambda}}^{\sigma^2(4)}(t)\right) \\
&= \left(\phi_{\boldsymbol{\lambda}}^{3}(t), \phi_{\boldsymbol{\lambda}}^{4}(t), \phi_{\boldsymbol{\lambda}}^{1}(t), \phi_{\boldsymbol{\lambda}}^{2}(t)\right) \\
&= \left(\phi_{\boldsymbol{\lambda}}^{1}\left(t - \frac{T(\boldsymbol{\lambda})}{2}\right), \ldots, \phi_{\boldsymbol{\lambda}}^{4}\left(t - \frac{T(\boldsymbol{\lambda})}{2}\right)\right) \\
&= \boldsymbol{\phi}_{\boldsymbol{\lambda}}\left(t - \frac{T(\boldsymbol{\lambda})}{2}\right)
\end{aligned}$$

with σ from (7.16). We therefore refer to them in what follows as "broken-symmetry states" because in contrast to the splay state and its spatio-temporal symmetry (7.14), the spatio-temporal symmetry of the broken-symmetry states does not fully reflect the equivariance of (2.6) under the action of the cyclic permutation group on $\mathbb{T}^N_{\text{ordered}}$. Note that broken-symmetry states are also of lower symmetry than symmetric two-cluster states since they are not invariant under permutations of units belonging to the same group.

6 Of course, the choice of $\phi = \pi$ is arbitrary and works for any other point in the state space in the same way.

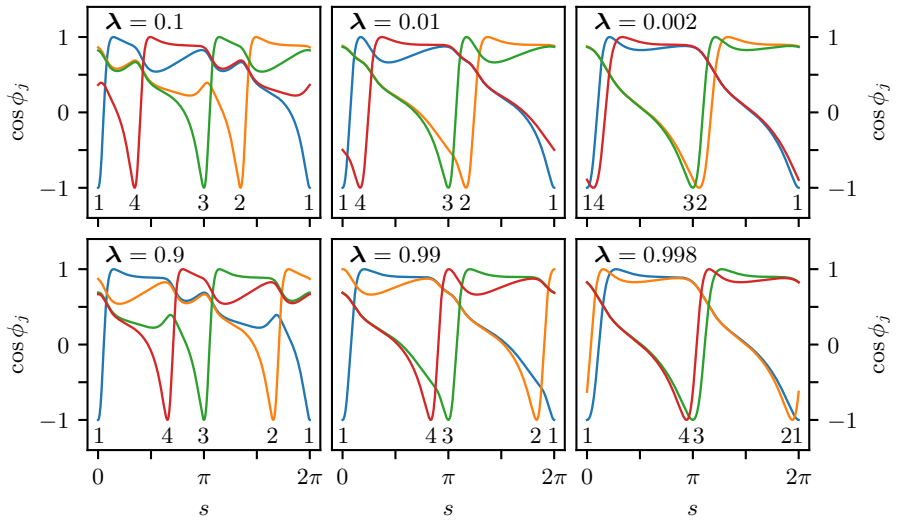

Figure 22: Broken-symmetry states for $N = 4$ ARs for (2.5) with $\omega = 0.8$ and $\kappa = -0.7$ for different values of $\boldsymbol{\lambda}$. The closer $\boldsymbol{\lambda}$ is chosen to 0 or 1, the more pronounced is the grouping of units. Note that for $\boldsymbol{\lambda}$ close to zero, units 1 and 4 form one group while units 3 and 2 form another. For $\boldsymbol{\lambda}$ close to one, units 1 and 2, and 3 and 4 form groups, respectively. The limit cases $\boldsymbol{\lambda} \to 0$ and $\boldsymbol{\lambda} \to 1$, correspond to symmetric periodic two-cluster states.

Choosing $\boldsymbol{\lambda}$ close to $\boldsymbol{\lambda}^*$ yields broken-symmetry states that are almost indistinguishable from splays because there, the time intervals τ_1 and τ_2 are of comparable length: $\tau_1 \simeq \tau_2$. However, as can be seen in Figure 22 in the top row, if we choose $\boldsymbol{\lambda} \approx 0$, we find that the units 1 and 4 as well as the units 2 and 3 form tighter and tighter groups so that in the limit case $\boldsymbol{\lambda} \to 0$, we end up with a symmetric periodic two-cluster state with clusters $A = \{1, 4\}$ and $B = \{2, 3\}$, as familiar from Chapter 5. On the other hand, for $\boldsymbol{\lambda} \approx 1$, the units 1 and 2 on one hand and 3 and 4 on the other form two respective groups until, in the limit case $\boldsymbol{\lambda} \to 1$, we end up with a symmetric periodic two-cluster state with clusters $A = \{1, 2\}$ and $B = \{3, 4\}$, see the bottom row in the same figure. In this sense, we can treat the two points $\boldsymbol{\lambda} = 0$ and $\boldsymbol{\lambda} = 1$ in Figure 19 formally as fixed points, corresponding to two periodic two-cluster states of different cluster compositions. Under this identification, we can conclude that splay states and symmetric periodic two-cluster states in the three given examples of Figure 19 are mutual exclusively stable, i. e., if the splay state is stable, the periodic two-cluster states are unstable and vice versa. Subsequently, a "nonlocal transfer of stability" between these states occurs if we continuously vary ϵ: Three periodic orbits, although well-separated in phase space, go nevertheless through a common stability changing bifurcation at $\epsilon = 0$. The reason for this is of course the NAIM $\mathcal{M}$. While it exists for a whole range of values of ϵ around zero, the dynamics on $\mathcal{M}$ are degenerate at $\epsilon = 0$. Depending on the sign of ϵ, any state $\boldsymbol{\phi}(t) \in \mathcal{M}_\epsilon$ then spirals either towards or away from the splay state orbit $\mathcal{C}_{\epsilon,\boldsymbol{\lambda}^*}$ or the symmetric periodic two-cluster state orbits $\mathcal{C}_{\epsilon,0}$ and $\mathcal{C}_{\epsilon,1}$.

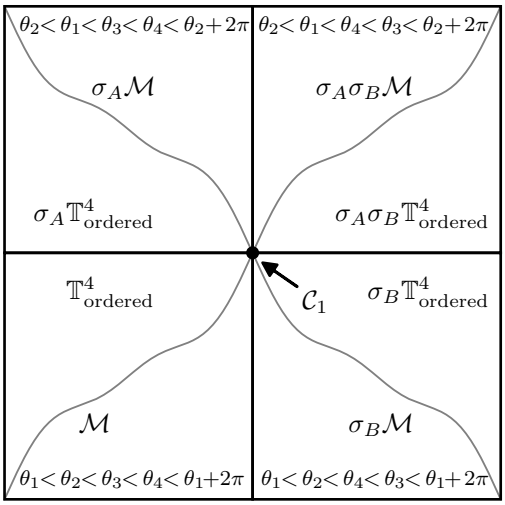

Figure 23: Schematic depiction of how copies of $\mathcal{M}$ coincide in $\mathbb{T}^4$ along their boundaries. Each square represents a copy of the ordered torus $\mathbb{T}^4_{\text{ordered}}$ under the action of the two permutations $\sigma_A : (\theta_1, \theta_2, \theta_3, \theta_4) \mapsto (\theta_2, \theta_1, \theta_3, \theta_4)$ and $\sigma_B : (\theta_1, \theta_2, \theta_3, \theta_4) \mapsto (\theta_1, \theta_2, \theta_4, \theta_3)$. The resulting cyclic orders are also shown. The four copies of $\mathcal{M}$ coincide in the two-cluster orbit $\mathcal{C}_1$ with clusters $A = \{1, 2\}$ and $B = \{3, 4\}$.

GLOBAL STRUCTURE OF $\mathcal{M}$ We want to briefly discuss the relation between the NAIM $\mathcal{M} \subset \mathbb{T}^4_{\text{ordered}}$ and its copies with different cyclic orders. As mentioned above, $\mathcal{M} \subset \mathbb{T}^4_{\text{ordered}}$ contains a periodic orbit $\mathcal{C}_{\boldsymbol{\lambda}}$ for every $\boldsymbol{\lambda} \in (0, 1)$ while its boundary is given by the symmetric periodic two-cluster orbits $\mathcal{C}_0$ and $\mathcal{C}_1$. Hence, we always have four copies of $\mathcal{M}$ whose boundaries coincide along either $\mathcal{C}_0$ or $\mathcal{C}_1$. Each of these copies is the result of a pairwise permutations of some consecutive units, e. g., $\sigma_A : (\theta_1, \theta_2, \theta_3, \theta_4) \mapsto (\theta_2, \theta_1, \theta_3, \theta_4)$, see Figure 23 where the four copies of the closure $\overline{\mathcal{M}}$ coincide along the orbit $\mathcal{C}_1$. Hence, globally, the family $\mathcal{M}$ does not form a manifold any longer but is self-intersecting. Arguably, this corresponds to the fact that the symmetric periodic two-cluster states have in general $N - 2$ instead of $N - 3$ neutrally stable directions.

EXISTENCE AND STABILITY OF SPLAY STATES FOR $|\epsilon| \gg 0$ Let us further investigate the existence and stability of the splay state. In particular, we are now interested in the regime of existence for splay states for values of ϵ that are not necessarily small, in other words, when the system is not close to being WS-integrable. For simplicity, we restrict our attention to the choice $h_1(\phi) = \sin 2\phi$ from (7.24).

In Figure 24 and Figure 25, we show numerical results on the existence and stability of the splay state in dependence of κ and ϵ for fixed $\omega = 0.8$ and $\omega = 0.6$, respectively. Analogous to the diagrams in Chapter 5, a white shading indicates that no splay state exists. In the blue shaded area, it exists and is stable and in the red shaded area, it is unstable. As for the symmetric periodic two-cluster states, we observe a switch in stability at $\epsilon = 0$, as we expected from the considerations

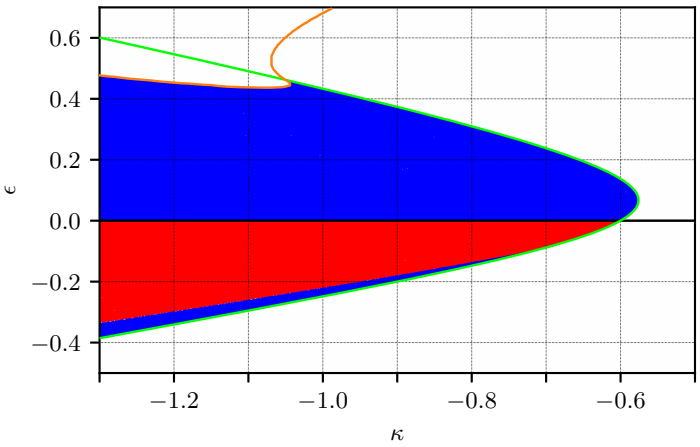

Figure 24: Stability diagram for the splay state for $N = 4$ generalized ARs, obeying (2.6) with $h(\phi) = \sin 2\phi$ and $\omega = 0.8$. A white shading indicates that no splay state exists. In the red shaded region, a splay state exists and is unstable while in the blue shaded region, it is stable. The green line depicts the THB of Δ^s at κ_0, according to (5.5). To the upper left of the orange line, stable solitary state fixed points exist.

in Section 7.3.1 and Figure 19. We also find that the emergence of the splay state coincides with the THB of the synchronous fixed point Δ^s (green line, given by (5.5), cf. Chapter 5) as long as ϵ is smaller than some $\epsilon_{\max}(\omega, \kappa) > 0$ (from the figures, we read $0.5 > \epsilon_{\max}(0.8, \kappa) > 0.4$ and $0.4 > \epsilon_{\max}(0.6, \kappa) > 0.2$). This result falls in line with our expectations since for $\epsilon = 0$, as we established in Theorem 6.8, the splay state is one of the solutions whose orbits lie in $\mathcal{M}$, which in turn emerges in the THB at $\kappa_0 = -\sqrt{1-\omega^2}$. Remarkably, for $\epsilon > \epsilon_{\max}(\omega, \kappa)$, the splay state does not emerge in the THB of Δ^s, any longer. The explanation for this lies in the nature of the orange lines, plotted in the two figures. These lines delimit the upper left corners of the diagrams in which additional stable fixed points exist, that are not synchronous: They are stable two-cluster fixed points where one cluster consists of three units and the other cluster consists of a singleton. Such states are known in the literature as "solitary states" [MPR14; Mik+19; TR19; Ber+20] and play a vital role in WS-theory: It can be shown that WS-integrable systems can only exhibit four different types of attractors, two of which are stationary and periodic solitary states [EM14]. For our system, these fixed points emerge in a saddle-node bifurcation along the upper right branch of the orange line and become unstable in a transcritical bifurcation along the lower left branch of that line in which the larger cluster becomes unstable against splitting perturbations. Loosely speaking, these fixed points take over the role of Δ^s in the emergence of periodic solutions if Δ^s is rendered unstable through its THB. Although a peculiar observation in its own right, a thorough investigation of the solitary state fixed points and their connections to the emergence of splay states is beyond the scope of this thesis because it lies outside the parameter regime, in which Theorem 6.8 and Proposition 7.1 can be applied.

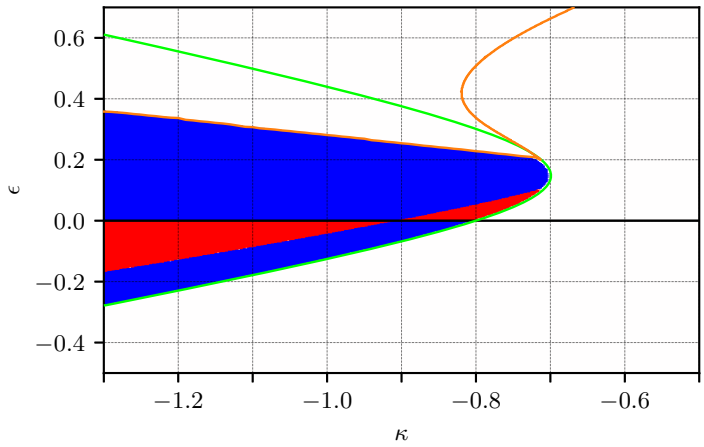

Figure 25: Stability diagram for the splay state for $N = 4$ generalized ARs, obeying (2.6) with $h(\phi) = \sin 2\phi$ and fixed $\omega = 0.6$. The regime of existence for stable solitary state fixed points in the top left corner is delimited by an orange line.

We also note the change in stability of the splay state in the regime to the left of the THB. For $\omega = 0.8$, this happens only for $\epsilon < 0$ where we observe a narrow band, close to the THB in parameter space in which the splay state is stable. The width of this band shrinks to zero for $\epsilon \to 0$. For $\omega = 0.6$, this is not the case and instead we see that the splay state for $\epsilon < 0$ and $\kappa \lesssim \kappa_0$ is stable and only becomes unstable for stronger repulsion while for $\epsilon \gtrsim 0$ and $\kappa \lesssim \kappa_0$, it is unstable and becomes stable for sufficiently strong repulsion. In both case, the responsible bifurcation is a pitchfork of the splay state with two broken-symmetry states. For $\epsilon < 0$, this pitchfork is subcritical (two unstable broken-symmetry states exist to the right of the bifurcation line) while for $\epsilon > 0$, it is supercritical (the broken-symmetry states are stable). This is again in accordance with our expectations from WS-theory since these states lie in the manifold $\mathcal{M}_\epsilon$ and thus, one of their three Floquet multipliers leaves the complex unit circle at $\epsilon = 0$. Finally, comparing Figure 24 with Figure 13, we note that indeed, splay states and symmetric periodic two-cluster states are mutually exclusively stable for $\epsilon \approx 0$, i. e., if the splay state is stable, the two-cluster states are unstable and vice versa, in accordance with the Plot in Panel (a) of Figure 19 for the averaged vector field $\hat{\boldsymbol{F}}_h$. That this is not the case for $\omega = 0.6$ and for κ close to κ_0 is due to the broken-symmetry states as will become clear in the next section. Before we come to this, and as final remark, we note that for $\omega = 0.6$, $-0.8335 \lesssim \kappa < -0.8$, and $\epsilon = 0$, the continuum $\mathcal{M}$ exists while the symmetric periodic two-cluster orbits $\mathcal{C}_0$ and $\mathcal{C}_1$ do not, compare Figure 12 in Chapter 5. In this regime, the points $\boldsymbol{\lambda} = 0, 1$ cannot be identified with periodic two-cluster states anymore since these state do not exist, yet. We will come back to this problem in Section 7.4.2. For now, let us continue by discussing broken-symmetry states in more detail.

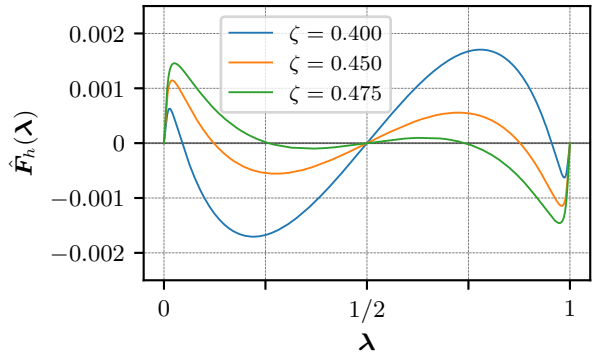

Figure 26: Averaged perturbation $\hat{\boldsymbol{F}}_h$ for $h(\phi) = \zeta \sin 2\phi - (1-\zeta)\cos 2\phi$ for $N = 4$ units. System parameters are fixed at $\omega = 0.8$ and $\kappa = -0.7$ as in Figure 19. Our Proposition 7.1 indicates the presence of robust broken-symmetry states for suitable choices of ζ.

ROBUST BROKEN-SYMMETRY STATES From Section 7.3.3, we know that for four Active Rotators, only two linearly independent perturbation functions are needed, so that for a suitable linear combination $c_1 h_1 + c_2 h_2$ of these two functions, any given periodic orbit $\mathcal{C}_{\boldsymbol{\lambda}} \subset \mathcal{M}$ can be rendered hyperbolic and therefore robust in which case we write $\mathcal{C}_{\epsilon,\boldsymbol{\lambda}}$. In what follows, let us fix $\omega = 0.8$ and $\kappa = -0.7$ and consider the perturbation function

$$h(\phi) = \zeta \sin 2\phi - (1-\zeta)\cos 2\phi \tag{7.25}$$

for (2.6), which is a linear combination of the two linearly independent functions h_1 and h_2 from (7.24). The parameter $\zeta \in [0,1]$ lets h vary smoothly between h_1 and h_2.

In Figure 26, we show plots for $\hat{\boldsymbol{F}}_h$ for three different values of ζ for which we find additional zeros $0 < \boldsymbol{\lambda}_1 < 1/2 < \boldsymbol{\lambda}_2 < 1$ with $\boldsymbol{\lambda}_2 = 1 - \boldsymbol{\lambda}_2$ so that we expect periodic broken-symmetry states $\boldsymbol{\phi}_{\epsilon,\boldsymbol{\lambda}_1}(t)$ and $\boldsymbol{\phi}_{\epsilon,\boldsymbol{\lambda}_2}(t)$ in addition to the generic splay state and periodic two-cluster states. From the slope of $\hat{\boldsymbol{F}}_h$ at the zeros, we further infer that the broken-symmetry states are stable for $\epsilon > 0$ and unstable, otherwise. This is corroborated by numerical results: Fixing $\zeta = 0.45$ in Figure 27 so that $\boldsymbol{\lambda}_1 \simeq 0.121$, we show the (normalized) time-series of the degenerate orbit (left) and the corresponding perturbed state (right) together with their respective cross-ratios $\boldsymbol{\lambda}(t)$. As in Figure 20, in the top right panel, we also show for comparison the time series for the unperturbed orbit as dotted lines. Again, we see that (i) the perturbed orbit indeed yields a broken-symmetry state and (ii) the cross-ratio $\boldsymbol{\lambda}(t)$ ceases to be a conserved quantity but oscillates around a value that is close to $\boldsymbol{\lambda}_1$.

Varying the value of ζ in Figure 26, we see that the loci of the nontrivial zeros move from the two-cluster values $\boldsymbol{\lambda} = 0, 1$ to the splay state value $\boldsymbol{\lambda}^* = 1/2$ for increasing ζ. But for $\zeta = 0$ and $\zeta = 1$, there are no nontrivial zeros present as we saw in Figure 19. Instead, $\boldsymbol{\lambda}_1$ and $\boldsymbol{\lambda}_2$ emerge in a supercritical pitchfork bifurcation of the periodic two-cluster states at $\zeta \simeq 0.320$ and vanish in a supercritical pitchfork of the splay state at $\zeta \simeq 0.485$. Hence, varying ζ for otherwise fixed

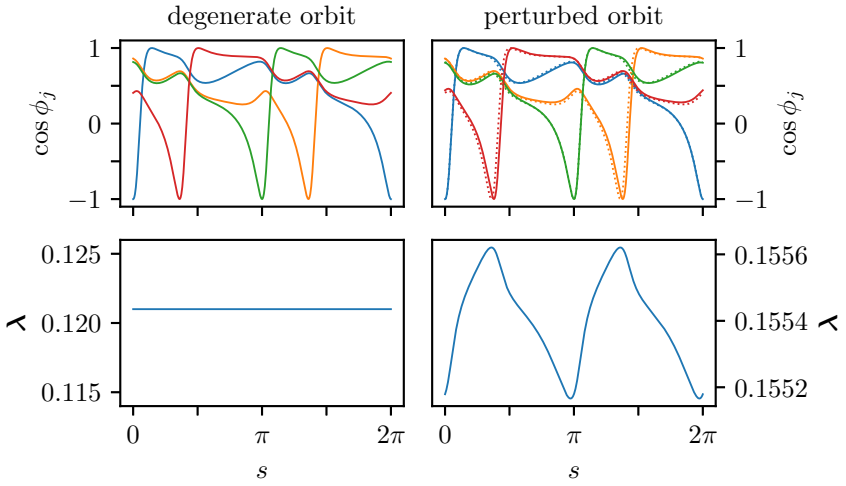

Figure 27: Broken-symmetry state for the WS-integrable model (2.5) and the perturbed model (2.6) with $h(\phi) = \zeta \sin 2\phi - (1-\zeta)\cos 2\phi$ and $\zeta = 0.45$ for $N = 4$ units. System parameters are fixed at $\omega = 0.8$, $\kappa = -0.7$, and $\epsilon = 0.002$. The stable broken-symmetry state is robust under small changes in ϵ.

system parameters ω, κ, and ϵ results in a "local transfer of stability" instead of the nonlocal one that we saw for varying $\epsilon = 0$: Changing the bifurcation parameter ζ results in changes of stability for the splay state and the two-cluster states that do not occur simultaneously but for different values of ζ. If we interpret varying ζ for fixed $\epsilon \neq 0$ as moving along a path in the two-dimensional space

$$H_2 = \operatorname{span}(h_1, h_2)$$

of linear combinations $c_1 h_1 + c_2 h_2$, this path avoids the point $\mathbf{0} \in H_2$, which corresponds to the perturbation function

$$h : \phi \mapsto 0$$

for which (2.6) simply becomes the WS-integrable model (2.5). Thus, in a sense, varying ζ in (7.25) can "unfold" the nonlocal bifurcation of (2.6) at $\epsilon = 0$.[7] The result is schematically illustrated in Panel (a) of Figure 28: Along the x-axis, we vary ζ in (7.25) while the y-axis shall represent the fixed point coordinate $\boldsymbol{\phi}_{\mathcal{P}}^{\mathrm{fix}}$ of some suitable Poincaré map $\mathcal{P}$. Solid lines depict stable fixed points of $\mathcal{P}$ (i. e., periodic orbits of (2.6)) and dashed lines depict unstable ones. Fixing $\epsilon > 0$ and all other system parameters in (2.6) and varying ζ in (7.25), the symmetric periodic two-cluster states (orange lines) become unstable in supercritical pitchforks for $\zeta = \zeta_1 \simeq 0.32$ in which two stable broken-symmetry states (black lines) emerge. Note that the two additional branches of the pitchforks above the top and below the bottom two-cluster states can be interpreted as broken-symmetry states of different cyclic order: The two-cluster state with, e. g., clusters $\phi_1(t) = \phi_2(t)$ and

7 Within the picture of following paths in H_2, varying ϵ corresponds to following a straight line in H_2 that goes through $\mathbf{0}$.

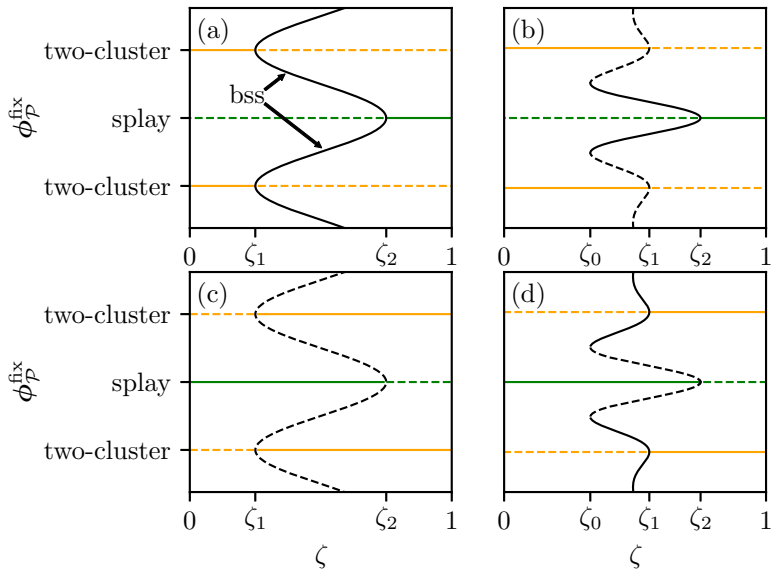

Figure 28: Schematic depiction of the unfolding of the nonlocal stability transfer to the simplest possible local transfer scenarios. In Panels (a) and (c), the transfer occurs through broken-symmetry states (bss) which emerge in pitchfork bifurcations. Panels (b) and (d) represent slightly more complicated scenarios: The broken-symmetry states emerge in a saddle-node bifurcation of periodic orbits and then vanish in consecutive pitchforks with two-cluster states and the splay state, thus changing their respective stability.

$\phi_3(t) = \phi_4(t)$ and therefore $\boldsymbol{\lambda}(t) = 0$ gives, due to symmetry, rise to a broken-symmetry state with $\phi_1(t) < \phi_2(t) < \phi_3(t) < \phi_4(t) < \phi_1(t)+2\pi$ and one with $\phi_2(t) < \phi_1(t) < \phi_4(t) < \phi_1(t) < \phi_2(t) + 2\pi$ because both of these solutions yield the same cross-ratio $\boldsymbol{\lambda}(t) \approx 0$.[8] Since the latter one is not in cyclic order and thus does not exist in $\mathbb{T}^N_{\mathrm{ordered}}$, we can discard it here. It lives in a copy of $\mathbb{T}^N_{\mathrm{ordered}} \subset \mathbb{T}^N$ of different cyclic order. Now, increasing ζ further, the time intervals τ_1 and τ_2 become more and more alike and thus, the broken-symmetry states appear more and more like a splay state until at $\zeta = \zeta_2 \simeq 0.485$, the two broken-symmetry states vanish in another supercritical pitchfork, this time with the unstable splay state, rendering it stable. For $\epsilon < 0$, the stability of all involved orbits is inverted and thus, the scenario looks like in Panel (c) where the pitchforks are now subcritical. These two possible scenarios, which result in a now local transfer of stability, are arguably the simplest unfoldings of the degenerate nonlocal bifurcation at $\epsilon = 0$. However, more complicated versions are possible. In Panels (b) and (d) of the same figure, we depict, as examples, scenarios that involve the emergence of broken-symmetry states through a saddle-node bifurcation at some ζ_0, followed by two pitchforks of the two-cluster states at $\zeta_1 > \zeta_0$ and the splay state at $\zeta_2 > \zeta_1$. Note that here, the two pitchforks are of opposite criticality.

Such more complicated scenarios can be achieved by carefully tuning the system parameters, see Figure 29. There, for $\omega = 0.6$ and $\kappa = -1.3$,

8 This is due to the transformation laws for cross-ratios under permutations [Ric11].

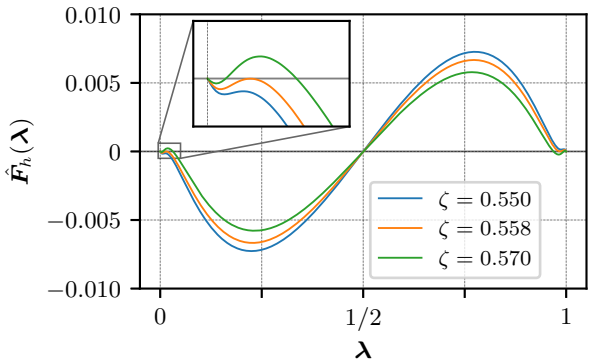

Figure 29: Averaged perturbation $\hat{\boldsymbol{F}}_h(\boldsymbol{\lambda})$ for $h(\phi) = \zeta \sin 2\phi - (1-\zeta)\cos 2\phi$ for $N = 4$ units. System parameters are fixed at $\omega = 0.6$ and $\kappa = -1.3$. Proposition 7.1 dictates that additionally to the robust splay and two-cluster states, two pairs of broken-symmetry states must emerge via two periodic orbit saddle-node bifurcation at $\zeta_0 \simeq 0.558$ (inset). The resulting broken-symmetry states vanish afterwards in respective pitchfork bifurcations with the two-cluster state and the splay state for suitable values of ζ.

we observe two saddle-node bifurcations for the averaged dynamics at $\zeta_0 \simeq 0.558$ in the vicinity of $\boldsymbol{\lambda} = 0$ and $\boldsymbol{\lambda} = 1$ through which a stable and an unstable broken-symmetry fixed point/periodic orbit emerge, respectively. For $\epsilon > 0$, the two unstable broken-symmetry states then render the symmetric periodic two-cluster states unstable in a subcritical pitchfork at $\zeta_1 \simeq 0.589$ while the stable ones render the splay state stable in a supercritical pitchfork at $\zeta_2 \simeq 0.661$. Hence, this bifurcation scenario corresponds to the schematic depiction in Panel (b) of Figure 28. Changing the sign of ϵ results in a scenario, similar to the one, depicted in Panel (d).

In the next section, we investigate the transfer of stability between the splay state and two-cluster states in dependence of κ and ζ. This also allows us to compare the predictions made by the averaging principle with the actual dynamics of the generalized AR-model (2.6).

7.4.2 *Transfer of Stability for $N = 4$ Units*

We want to investigate the transfer of stability between splay states and symmetric periodic two-cluster states in dependence of the coupling strength κ and the parameter ζ which determines the form of the perturbation function h via (7.25). For this, we fix the parameters $\omega = 0.6$ and $\epsilon = 0.05$ and numerically determine the splay state, the symmetric periodic two-cluster states, and any other occurring periodic solutions that might exist together with their respective stabilities. As established in the previous section, varying ζ can be interpreted as following a path in the two-dimensional space of perturbation functions, spanned by h_1 and h_2 of (7.24). Due to the form of h, this path avoids the point $\mathbf{0}$, corresponding to the WS-integrable model (2.5), so that we can investigate the transfer of stability in a generic setting. It further allows us to compare our predictions from the averaging principle for

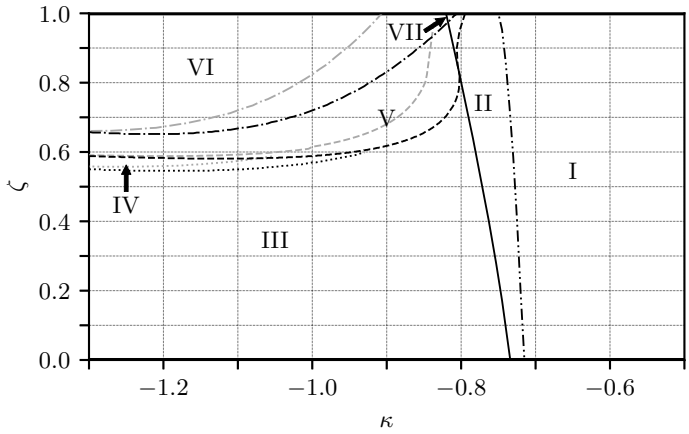

Figure 30: Existence and stability of the splay state, the symmetric periodic two-cluster states, and the broken-symmetry states for (2.6) with $h(\phi)$ from (7.25). System parameters are fixed at $\omega = 0.6$, $\epsilon = 0.05$, and $N = 4$. **Region I**: No periodic orbits exist. **Black dash-double-dotted line**: THB of Δ^s. The resulting splay state is unstable in **Regions II-V** and stable in **Region VI** and **VII**. **Black solid line**: Symmetric periodic two-cluster states emerge through double-SNIC and are stable in **Region III and IV** and unstable in **Regions V** and **VI**. **Black dotted line**: saddle-node bifurcations of stable and unstable broken-symmetry states. **Black dashed line** between **Regions IV** and **V**: subcritical pitchfork of two-cluster state with unstable broken-symmetry states; between **Regions III** and **V**, the dashed line marks a supercritical pitchfork in which stable broken-symmetry states branch off of the two-cluster states. **Black dash-dotted line**: supercritical pitchfork of the splay state and two stable broken-symmetry states. Gray lines indicate corresponding predictions from applying Proposition 7.1.

any occurring limit cycle bifurcations with the actual dynamics for a fixed, fairly large value of ϵ. The results are shown in Figure 30.

Let us begin by discussing the results on the existence and stability of the splay state and the two-cluster states for the actual dynamics in the diagram. In Region I, no periodic orbits exist whatsoever so that the only attractor is the synchronous fixed point Δ^s. The black dash-double-dotted line denotes the THB of Δ^s through which the splay state, together with the manifold $\mathcal{M}_\epsilon$, emerges. It is unstable in Regions II-V and stable in Regions VI and VII. The black solid line denotes the double-SNIC through which the two-cluster states emerge. These states are stable in Regions III and IV and unstable above the black dashed line in the Regions V and VI. From this we see that for fixed coupling strength κ, repulsive enough such that both the splay state and the two-cluster states exist, a local transfer of stability occurs if we increase $\zeta \in [0, 1]$: We always start with an unstable splay state and two stable two-cluster state for small ζ, the latter of which become unstable for some $\zeta_1(\kappa)$. Further increasing ζ eventually renders the splay state stable for some $\zeta_2(\kappa)$ which corresponds to the depicted unfoldings in Panels (a) and (b) of Figure 28.

Two-cluster heteroclinic cycle.

Note that the black dashed line which indicated the stability change of the *periodic* two-cluster state to the left of the double-SNIC can be

extended into Region II. In this region, we observe two types of two-cluster fixed points (the Σ^i and the Ξ^i that emerge in the THB of Δ^{s}, see Chapter 5) which vanish pairwise in the double-SNIC. These fixed points differ essentially in their respective composition of cluster, i. e., whether $A = \{1, 2\}$ and $B = \{3, 4\}$ or $A = \{4, 1\}$ and $B = \{2, 3\}$ and so on. For definiteness, let us assume that

$$A = \{1, 2\}, \quad B = \{3, 4\}.$$

Then, the two-cluster fixed points are of the form

$$\begin{aligned} \Xi^1 &= (\Xi_{\mathrm{s}}, \Xi_{\mathrm{s}}, \Xi_{\mathrm{u}}, \Xi_{\mathrm{u}}), & \Sigma^1 &= (\Sigma_{\mathrm{s}}, \Sigma_{\mathrm{s}}, \Sigma_{\mathrm{u}}, \Sigma_{\mathrm{u}}) \\ \Xi^2 &= (\Xi_{\mathrm{u}}, \Xi_{\mathrm{u}}, \Xi_{\mathrm{s}}, \Xi_{\mathrm{s}}), & \Sigma^2 &= (\Sigma_{\mathrm{u}}, \Sigma_{\mathrm{u}}, \Sigma_{\mathrm{s}}, \Sigma_{\mathrm{s}}). \end{aligned}$$

A stability analysis reveals that the Jacobian of the vector field at the Ξ^i has two negative non-splitting eigenvalues

$$\begin{aligned} \lambda^1_{\text{non-splitting}} &= \lambda^1_{\text{non-splitting}}(\Xi^1) = \lambda^1_{\text{non-splitting}}(\Xi^2) < 0 \\ \lambda^2_{\text{non-splitting}} &= \lambda^2_{\text{non-splitting}}(\Xi^1) = \lambda^2_{\text{non-splitting}}(\Xi^2) < 0 \end{aligned}$$

as well as one positive and one negative splitting eigenvalue

$$\begin{aligned} \lambda^-_{\text{splitting}} &= \lambda^-_{\text{splitting}}(\Xi^1) = \lambda^-_{\text{splitting}}(\Xi^2) < 0 \\ \lambda^+_{\text{splitting}} &= \lambda^+_{\text{splitting}}(\Xi^2) = \lambda^+_{\text{splitting}}(\Xi^2) > 0. \end{aligned}$$

In the diction of Chapter 3, the first two eigenvalues above correspond to *non-splitting* perturbations, which leave both clusters whole ($\lambda^1_{\text{non-splitting}}$ and $\lambda^2_{\text{non-splitting}}$ correspond to eigenvectors of the form $(a, a, b, b)^T$) and thus indicate that the Ξ^i are stable against such non-splitting perturbations (which is in line with Chapter 5 since this means that they are stable in $\mathbb{T}_{1/2}$). The eigenvalues $\lambda^{\pm}_{\text{splitting}}(\Xi^i)$ corresponds to *splitting* perturbation, i. e., perturbations which keep one cluster fixed and split the other. Since these eigenvalues differ in their sign, we can conclude that the Ξ^i are stable with respect to splitting perturbations of *one* cluster but are unstable with respect to perturbations that split the *other* cluster. In particular, for Ξ^1, the cluster $A = \{1, 2\}$ is stable and the cluster $B = \{3, 4\}$ is unstable against splitting perturbation while for Ξ^2, we find the opposite: cluster A is unstable and cluster B is stable.[9]

Numerically interpolating the unstable manifolds of the Ξ^i reveals that they form a heteroclinic cycle. Figure 31 depicts how the angular coordinates $\phi_j(\ell)$ along these heteroclinic orbits depend on the arc length $\ell \in [0, L]$ where $L \simeq 7.2$ is the total length of each of the two heteroclinic orbits. Panel (a) shows $\phi_j(\ell)$ along the heteroclinic orbit that starts at Ξ^1 and ends at Ξ^2 while Panel (b) depicts the situation for the heteroclinic orbit from Ξ^2 to Ξ^1. In particular, we see in Panel (a)

9 The eigenvalue $\lambda^-_{\text{splitting}}(\Xi^1) < 0$ corresponds to the eigenvector $(+1, -1, 0, 0)^T$ and the eigenvalue $\lambda^+_{\text{splitting}}(\Xi^1)$ corresponds to the eigenvector $(0, 0, +1, -1)^T$. For Ξ^2, it is the other way around.

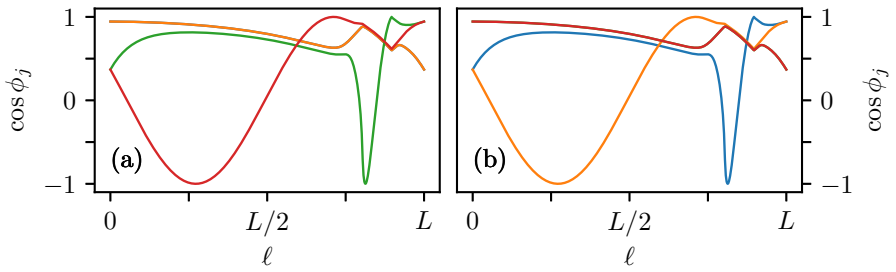

Figure 31: Angular coordinates $\phi_j(\ell)$ along the heteroclinic cycle between Ξ^1 and Ξ^2. The parameter ℓ parameterizes the two branches of the cycle by the arc length $\ell \in [0, L]$ with $L \simeq 7.2$. Along each heteroclinic orbit, one cluster splits and merges again while both clusters switch positions.

how the units 1 and 2 of cluster A (orange and blue line) stay together while cluster B splits along the orbit in the two distinct units 3 and 4 (red and green line) and that at $\ell = L$, the two clusters have switched positions, i. e.,

$$\phi_1(L) = \phi_2(L) = \phi_3(0) = \phi_4(0) = \Xi_\mathrm{u}$$
$$\phi_3(L) = \phi_4(L) = \phi_1(0) = \phi_2(0) = \Xi_\mathrm{s}.$$

In Panel (b), it is the other way around. This heteroclinic cycle is robust in Region II as a result of the permutation symmetry of the system (2.6). Analogous to the discussion in Chapter 5, its asymptotic stability is determined by the quantity

$$\lambda^+_\mathrm{splitting} + \lambda^-_\mathrm{splitting}.$$

If this quantity is greater than zero then, perturbing the system's state away from the cycle, the distance between two units that formed a cluster before grows stronger along one heteroclinic orbit than it shrinks along the other and thus the perturbation grows exponentially and the heteroclinic cycle is asymptotically unstable. If the quantity is smaller than zero, the cycle is stable [And+73; Fie20]. The extended black dashed line in Region II marks where in the κ-ζ-plane we have

$$\lambda^+_\mathrm{splitting} + \lambda^-_\mathrm{splitting} = 0$$

and thus where the stability-changing bifurcation of the cycle occurs. The broken-symmetry states emerge exactly in this bifurcation and exist to the left of the dashed line in Region II so that in this regime, we have to identify $\boldsymbol{\lambda} = 0$ and $\boldsymbol{\lambda} = 1$ with heteroclinic cycles instead of the proper periodic two-cluster state.

Pitchfork bifurcations.

Next, we discuss the observed bifurcations that result in the stabilization and destabilization of the splay state and the periodic two-cluster states. For this, we note first that at the black dotted line, two saddle-node bifurcations occur in which a stable and an unstable broken-symmetry state emerge, respectively. This corresponds to what we have already observed for the averaged dynamics in Figure 29 in the previous section. Along the border between the Regions IV and

V, marked by the left branch of the black dashed line, the unstable broken-symmetry states vanish in subcritical pitchfork bifurcations with the two-cluster states, rendering them unstable. Further increasing ζ lets the stable broken-symmetry states vanish in another, this time supercritical, pitchfork bifurcation (black dash-dotted line) with the splay state which is subsequently stabilized in Region VI and VII. At $(\kappa, \zeta) \simeq (-0.93, 0.6)$, we find a point of codimension 2 in which the saddle-node bifurcations and the subcritical pitchforks coincide. Branching off to the right of this point, the black dashed line now marks two *supercritical* pitchforks between the two-cluster states and the broken-symmetry states at the border between Regions III and V. Overall, the transfer of stability between two-cluster states and the splay state is now a local one. To the right of the codimension 2 point, the transfer corresponds to Panel (a) in Figure 28, to the left, it corresponds to Panel (b). As already noted, in Region II, broken-symmetry states cannot bifurcate from the periodic two-cluster states along the black dashed line but instead emerge in the stability changing bifurcation of the heteroclinic cycle.

Predictions from the averaging principle.

Gray lines in the diagram indicate the corresponding predictions from applying the averaging Proposition 7.1 to determine all stability-changing bifurcations. We immediately see that the predicted bifurcation lines fit better, the more repulsive we choose the coupling strength κ. We note that for $\kappa \gtrsim -0.85$, the predicted additional nontrivial zeros, indicating the presence of a broken-symmetry states, lie so close to $\boldsymbol{\lambda} = 0, 1$ that it becomes impossible to resolve them within numerical accuracy. This explains the abrupt almost vertical slope of the gray dashed line for $\zeta > 0.8$ which is a numerical artifact. We expect that if one was able to determine the nontrivial zeros with higher resolution, the resulting curve would look smoother.

Since the predictions from the averaging principle must coincide with the actual bifurcation diagram in the limit $|\epsilon| \to 0$, we conduct a second stability analysis but this time for $\epsilon = 0.001$. The results are shown in Figure 32. Annotations and line styles are the same as in Figure 30. Indeed, we now find the prediction from applying Proposition 7.1 and the results from the actual dynamics in nearly perfect agreement with each other. The only (slight) exception occurs again for $\kappa \gtrsim -0.85$ and $\zeta \gtrsim 0.8$ but as already mentioned above, it is reasonable to assume that this discrepancy is due to finite resolution and accuracy of the numerical integration, involved, in other words, a numerical artifact. In particular, from Figure 32, we may conclude that our formal identification of symmetric periodic two-cluster states (if they exist) with the zeros of $\hat{\boldsymbol{F}}_h$ at $\boldsymbol{\lambda} = 0, 1$ is correct for small $|\epsilon|$.

With the above observations, we end our discussion of the "local" transfer of stability between splay state and two-cluster states for $N = 4$ and moreover conclude our investigation of systems of four Active Rotators. In the next section, we discuss splay states for larger ensembles.

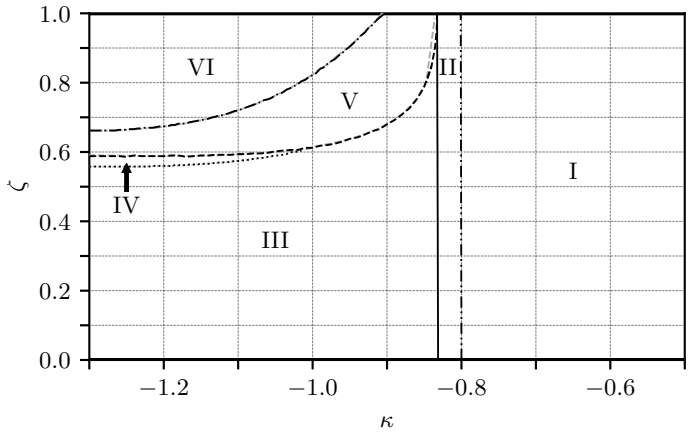

e

Figure 32: Existence and stability of the splay state, the symmetric periodic two-cluster states, and the broken-symmetry states for (2.6) with $h(\phi)$ from (7.25) with $\omega = 0.6$, $\epsilon = 0.001$, and $N = 4$. Black and gray lines correspond to the ones from Figure 30.

7.4.3 *Persistence and Stability of Splay States for $N > 4$ Units*

Leaving the case of $N = 4$ ARs behind, let us discuss how the picture changes if one considers larger ensembles. Two problems arise for the numerical study of splay states in this case: (i) Since for larger values of N, the number of clustered periodic solutions grows rapidly (e. g., in form of clustered splay states), it becomes more and more difficult to find and study pure splay states numerically, at least for the not integrable case $\epsilon \neq 0$. (ii) In Chapter 5, we were in the advantageous situation that periodic two-cluster states have at most three distinct nontrivial Floquet multipliers μ^A, μ^B, and $\mu^{\text{non-splitting}}$, the first two of which determine the splitting stability for the clusters A and B while the latter characterizes the stability against non-splitting perturbations. This occurrence of Floquet multipliers with high multiplicity, however, does not hold anymore for splay states. For increasing N, we are instead confronted with a growing number of distinct Floquet multipliers for which to our best knowledge no closed form exists. Of course, as long as $|\epsilon|$ is sufficiently small, the averaging principle in Proposition 7.1 allows us to determine the stability of the splay state but this tool becomes less and less powerful (at least quantitatively) for $|\epsilon| \gg 0$. Moreover, inquiring the stability of splay states from the averaging principle requires us to find some expression for the derivative $\mathrm{D}\hat{\boldsymbol{F}}_h(\boldsymbol{\lambda}^*)$ at the splay state cross-ratio value $\boldsymbol{\lambda}^*$ which in general can only be approximated by numerically computing $\mathrm{D}\hat{\boldsymbol{F}}_h$ around $\boldsymbol{\lambda}^*$ which poses no real advantage over determining the stability of $\mathcal{C}_{\epsilon,\boldsymbol{\lambda}^*}$ directly by the numerical method, discussed in Chapter 3. In any case, one has to expect that in contrast to the periodic two-cluster states, the stability of splay states depends explicitly on the number N of ARs. We nevertheless want to briefly discuss how our results for $N = 4$ units may generalize for larger N. For this, we restrict our attention to the cases of $N \in \{5, 6, 7, 8\}$ Active Rotators for the above mentioned rea-

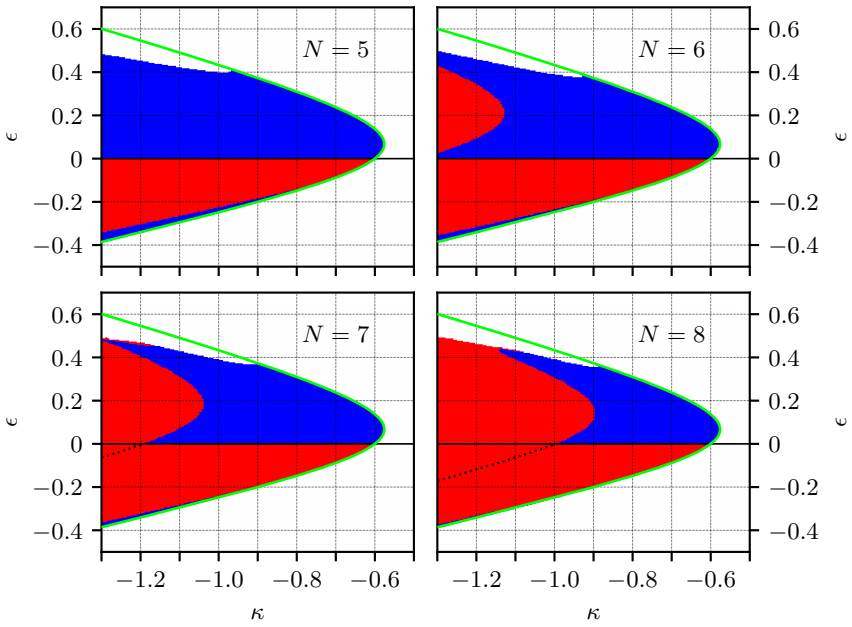

Figure 33: Stability diagram for the splay state for ensemble sizes $N = 5$ to $N = 8$. We fix $\omega = 0.8$ and choose $h(\phi) = \sin 2\phi$. A black dotted line indicates the presence of a subcritical Neimark-Sacker bifurcation for $N = 7$ or a subcritical pitchfork bifurcation of periodic orbits for $N = 8$.

sons. The results are depicted in Figure 33 where we fix $\omega = 0.8$ and consider the perturbation function

$$h_1(\phi) = \sin 2\phi. \tag{7.24a}$$

We note first that, as expected, at least for $\epsilon \approx 0$, the splay state emerges again via the THB of the synchronous fixed point Δ^s (green line). On the other hand, we still find that for $\epsilon \gtrsim 0.4$ and $\kappa \lesssim -0.9$, the role of Δ^s in the creation of the splay state is assumed instead by N stable solitary state fixed points which now each consist of one cluster of $N - 1$ units and a singleton. Since the loci and stability of these steady states directly depend on N (because the relative sizes of, e. g., the clusters $A = \{1\}$ and $B = \{2, \ldots, N\}$ change for varying N), the border between the stable regime of the splay state (blue area) and the regime of the stable solitary state fixed points also varies slightly with increasing N. Next, we note that, at least in the considered parameter regime for κ and ϵ, the stability diagram for the case $N = 5$ looks overall the same as the one in Figure 24 for $N = 4$. In particular, we observe again a change in stability at $\epsilon = 0$ so that for small negative values of ϵ, the splay state is unstable (red area). We also note (for all N) the narrow region of stability close to the THB for $\epsilon < 0$ which we already observed for four ARs. But for larger values of N, we see that the splay state is not necessarily stable for all positive values of ϵ, anymore. This is not in contradiction to the averaging principle: Numerical results show that, e. g., for $N = 6$ and $N = 8$ and fixed $\epsilon > 0$, starting with κ close to the THB and then decreasing κ results in one of the (real)

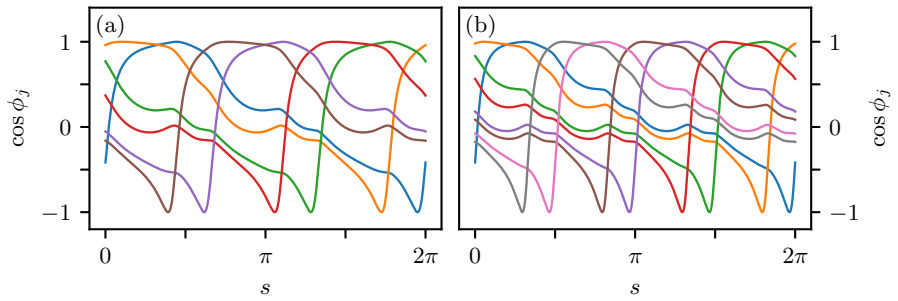

Figure 34: Time series for broken-symmetry states for $N = 6$ (Panel a) and $N = 8$ (Panel b) ARs. System parameters are fixed at $\omega = 0.8$, $\epsilon = 0.4$, $\kappa = -1.25$ and $\omega = 0.8$, $\epsilon = 0.35$, $\kappa = -1.04$, respectively.

Floquet multipliers of the splay state to leave the unit circle, rendering the splay state unstable in this direction. Thus, for $\epsilon > 0$, this results in the border between the stable (blue) and the unstable (red) regime. Choosing $\epsilon < 0$ and gradually decreasing κ yields instead a splay state for which, for moderately repulsive coupling, all but two nontrivial Floquet multipliers lie outside the unit circle. Along the black dotted line, one of these multipliers moves into the unit circle, rendering the splay state stable in the corresponding direction and we see that this line is the continuation of the red-blue border for positive ϵ. Hence, the number of stable and unstable directions of the splay state *in* $\mathcal{M}_\epsilon$ switches at $\epsilon = 0$ in accordance to point four of Proposition 7.1.

Remarkably, if we choose (κ, ϵ) close to the right of the line along which the stability of the splay states changes, we again find unstable broken-symmetry states which eventually coalesce with the splay state at that line and do not exist to its left, rendering the splay state unstable in one direction. Hence, the bifurcation at hand for $N = 6$ and $N = 8$ is a subcritical pitchfork bifurcation of periodic orbits, similar to the one that we observed for $N = 4$. In Figure 34, we show the (normalized) time series of the involved broken-symmetry states. Now, the ensemble splits in $N/2$ groups of two consecutive units, each, which are more tightly placed together than with their other neighbors. The closer (κ, ϵ) is to the dotted bifurcation curve, the more evenly spaced the units in the broken-symmetry states become until the state coalesces with the splay state $\boldsymbol{\phi}_{\boldsymbol{\lambda}^*}(t)$ at the bifurcation. This leads us to the conjecture that broken-symmetry states are not just an artifact from some hidden symmetry for the case of $N = 4$ units but that they play in fact a vital role for general *even* N where they can generally be characterized as periodic solutions $\boldsymbol{\phi}_{\epsilon,\boldsymbol{\lambda}^{\mathrm{bss}}}(t)$ of (2.6) for which

$$\sigma^2 \boldsymbol{\phi}_{\epsilon,\boldsymbol{\lambda}^{\mathrm{bss}}}(t) = \boldsymbol{\phi}_{\epsilon,\boldsymbol{\lambda}^{\mathrm{bss}}}\left(t - \frac{2T(\boldsymbol{\lambda}^{\mathrm{bss}})}{N}\right)$$

holds where $T(\boldsymbol{\lambda}^{\mathrm{bss}})$ denotes the period of $\boldsymbol{\phi}_{\epsilon,\boldsymbol{\lambda}^{\mathrm{bss}}}$. Due to the spatio-temporal symmetry above, the corresponding cross-ratios $\boldsymbol{\lambda}^{\mathrm{bss}}$ for the WS-case $\epsilon = 0$ are of alternating form

$$\boldsymbol{\lambda}^{\mathrm{bss}} = (\lambda_1, \lambda_2, \lambda_1, \ldots, \lambda_2, \lambda_1)$$

in the cross-ratio coordinates (7.20).

Uneven N and the Neimark-Sacker bifurcation.

Broken-symmetry states can only occur for even N since they are essentially characterized by the ensemble to split up in $N/2$ more or less tightly bound groups. So, how can we explain the change in stability for fixed $\epsilon > 0$ and gradually decreasing κ for $N = 7$? Here, in contrast to the cases $N = 6$ and $N = 8$, we find a pair of complex conjugate Floquet multipliers which leave the unit circle for sufficiently negative κ, indicating that at the blue-red border, at least for $N = 7$, the splay state goes through a Neimark-Sacker bifurcation, also known as a secondary Hopf bifurcation [Kuz13]. Again, we find that the border between the stable (blue) and the unstable (red) regime for positive ϵ can be extended for $\epsilon < 0$ (black dotted line) where then two of the four unstable Floquet multipliers[10] become stable for sufficiently strong repulsion. Neimark-Sacker bifurcations, depending on whether they are sub- or supercritical, generally go along with the bifurcation of an unstable or stable invariant two-dimensional torus from the periodic orbit. Since we found no indications of a *stable* invariant torus in our numerical experiments, we conclude that in the case at hand, the bifurcation is in fact subcritical and that the torus must occur to the right of the bifurcation curve. In a sense, it replaces the broken-symmetry states in their role of rendering the splay state unstable for even N an the subcritical Neimark-Sacker bifurcation replaces the subcritical pitchfork of periodic orbits.

We end this chapter with the construction of a robust hyperbolic orbit for an ensemble of $N = 10$ ARs in order to illustrate the proposed procedure in Section 7.3.3.

7.4.4 *Constructing a Robust Periodic Orbit for $N = 10$ Units*

We want to illustrate the method, presented in Section 7.3.3, to control a given periodic orbit $\mathcal{C}_{\boldsymbol{\lambda}} \subset \mathcal{M}$ for some fixed $\boldsymbol{\lambda}$ for the case of $N = 10$ Active Rotators. To this end, we fix the system parameters $\omega = 0.8$ and $\kappa = -0.8$ and choose

$$\begin{aligned}\boldsymbol{\lambda}_0 &= (\lambda_1, \ldots, \lambda_7) \\ &= (0.973, 0.907, 0.862, 0.832, 0.631, 0.248, 0.162)\end{aligned}$$

for the cross-ratios. We show a (normalized) time series for the ϕ_j along $\mathcal{C}_{\boldsymbol{\lambda}_0}$ in Panel (a) of Figure 35 where, as always, different colors indicate different units. For the eight linearly independent perturbation functions $h_1, \ldots, h_8$ that we need for controlling $\mathcal{C}_{\boldsymbol{\lambda}_0}$, we choose

$$\begin{aligned}h_{2j-1}(\phi) &= \sin(j+1)\phi \\ h_{2j}(\phi) &= \cos(j+1)\phi,\end{aligned}$$

10 Remember, that the splay state always possesses at least two stable Floquet multipliers that it inherits from $\mathcal{M}_\epsilon$. Hence, close to the right of the dotted line, the splay possesses four unstable Floquet multipliers.

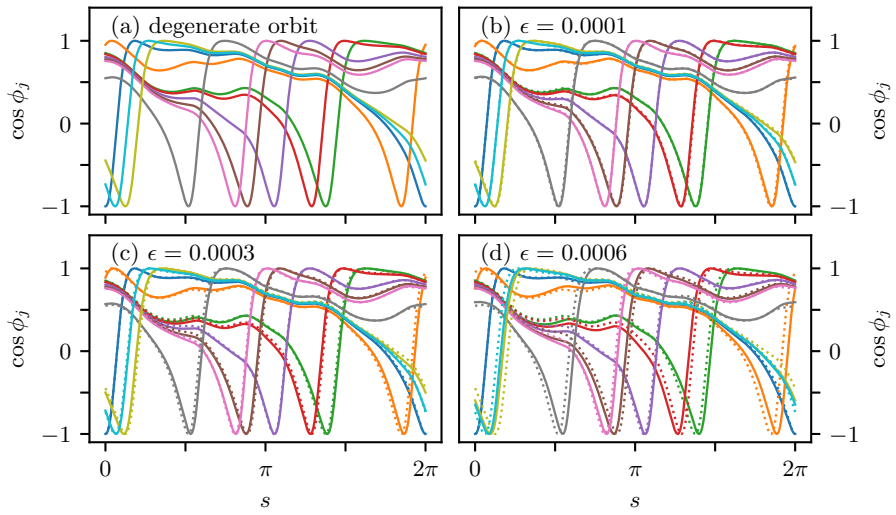

Figure 35: (Normalized) time series for the controlled orbit $\mathcal{C}_{\epsilon,\boldsymbol{\lambda}_0}$ for different values of ϵ. Panel (a) shows the degenerate orbit of the WS-integrable model (2.5). Panel (b) to (d) show the corresponding time series for increasing values of ϵ in (2.6) with h from (7.26) and (7.27). For comparison, we also show the unperturbed time series as dotted lines.

with $j = 1, \ldots, 4$. In other words, we choose the $h_1, \ldots, h_8$ to be the first eight higher Fourier modes so that our desired perturbation function h is of the form

$$h(\phi) = \sum_{j=1}^{4} c_{2j-1} \sin(j+1)\phi + c_{2j} \cos(j+1)\phi. \tag{7.26}$$

In order to make $\mathcal{C}_{\boldsymbol{\lambda}_0}$ robust, we now need to find suitable coefficients $c_1, \ldots, c_8$ to let $\hat{\boldsymbol{F}}_h(\boldsymbol{\lambda}_0) = \mathbf{0}$, i. e., we need to compute the $\hat{\boldsymbol{F}}_{h_k}(\boldsymbol{\lambda}_0)$ via (7.3) and then solve

$$\mathbf{0} = \sum_{j=1}^{4} c_{2j-1} \hat{\boldsymbol{F}}_{h_{2j-1}}(\boldsymbol{\lambda}_0) + c_{2j} \hat{\boldsymbol{F}}_{h_{2j}}(\boldsymbol{\lambda}_0)$$

for the $c_1, \ldots, c_8$. In doing so, we can always set, e. g., $c_8 = 1$ because for each h that fulfills the above equation, any multiple $C \cdot h$ is another solution. We then find

$$\begin{aligned} (c_1, c_3, c_5, c_7) &\simeq (44.27,\ -26.78,\ -9.88,\ 5.01) \\ (c_2, c_4, c_6, c_8) &\simeq (18.33,\ 28.17,\ -17.07,\ 1) \end{aligned} \tag{7.27}$$

such that for sufficiently small $|\epsilon|$, we expect $\mathcal{C}_{\epsilon,\boldsymbol{\lambda}_0}$ to be a hyperbolic orbit of (2.6) with h given by (7.26) and (7.27).

Let us compare this prediction with the numerical results. In Panel (a) of Figure 35, we show the (normalized) time series along the original orbit $\mathcal{C}_{\boldsymbol{\lambda}_0}$ while Panels (b)-(d) show the normalized time series along $\mathcal{C}_{\epsilon,\boldsymbol{\lambda}_0}$ for three different values of ϵ (solid lines) together with the time series for $\mathcal{C}_{\boldsymbol{\lambda}_0}$ (dotted lines) for comparison. For $\epsilon = 0.0001$, both time series nearly coincide but increasing ϵ leads to larger and larger deviations between the two orbits $\mathcal{C}_{\boldsymbol{\lambda}_0}$ and $\mathcal{C}_{\epsilon,\boldsymbol{\lambda}_0}$ and thus the time series.

Increasing ϵ further would let units two and three (teal and olive green lines) eventually form a cluster. Larger values of $|\epsilon|$ result in more and more clustering of the units, i. e., the orbit goes through various bifurcations. At this point, the original orbit $\mathcal{C}_{\boldsymbol{\lambda}_0}$ cannot be further controlled with our choice of h, it ceases to exist.

Computing $\mathrm{D}\hat{\boldsymbol{F}}_h(\boldsymbol{\lambda}_0)$ to determine the stability of $\mathcal{C}_{\epsilon,\boldsymbol{\lambda}_0}$ results in the eigenvalues

$$\begin{aligned}(\lambda_1, \lambda_2, \lambda_3) &\simeq (0.43, -0.79, -0.13)\\ \lambda_{4,5} &\simeq -0.17 \pm 0.13i\\ \lambda_{6,7} &\simeq -0.08 \pm 0.1i\end{aligned}$$

so that we expect the $\mathcal{C}_{\epsilon,\boldsymbol{\lambda}_0}$ to have one real unstable Floquet multiplier, two real stable ones and two pairs of stable complex conjugate multipliers in addition to the two real stable multipliers, inherited by the NAIM $\mathcal{M}_\epsilon$. And indeed, this matches the results from numerical stability analysis where, e. g., for $\epsilon = 0.0006$ in Panel (d) of Figure 35, we have

$$\begin{aligned}(\mu_1, \mu_2, \mu_3) &\simeq (1.005, 0.9998, 0.9997)\\ \mu_{4,5} &\simeq 0.997 \pm 0.002i\\ \mu_{6,7} &\simeq 0.9986 \pm 0.0006i\\ (\mu_8, \mu_9) &\simeq (-4 \cdot 10^{-4}, -1.6 \cdot 10^{-7})\end{aligned}$$

where the last two multipliers are the ones that are inherited from $\mathcal{M}_\epsilon$. Note that the first seven multipliers still have absolute values very close to one since the perturbation parameter ϵ is so small. Overall, the above example illustrates nevertheless that controlling arbitrary orbits in $\mathcal{M}$ is possible.

7.5 CONCLUSION

In Chapter 6, we saw that WS-integrable systems can, under certain conditions, give rise to a NAIM $\mathcal{M}$, foliated by periodic orbits which are neutrally stable in $\mathcal{M}$. This told us that, in some sense, $\mathcal{M}$ is the true fundamental invariant geometric object that we should study because of its robustness and not the individual periodic orbits it is composed of. In this chapter, we put the manifold $\mathcal{M}$ in a broader context of dynamical systems which are close to being WS-integrable. For this, we developed a systematic method to determine which orbits of the continuum survive the transition to nonintegrable systems. The method is based on the averaging principle for periodic orbits. We restricted our attention to the case of on-site perturbations but the results readily generalize to perturbations of the coupling term, as well: In our proof of Proposition 7.1, we only used the fact that the perturbation function is smooth, not that it acts diagonally on $\mathbb{T}^N$. Chapter 5 and the present chapter enable us now to view $\mathcal{M}$ in a broader context of generally nonintegrable systems. The WS-integrable case then corresponds to a

global bifurcation of the dynamics on $\mathcal{M}$. This case is distinguished from general dynamics exactly by its degenerate behavior.

The proposed method to determine robust orbits is really a direct application of the averaging principle for periodic orbits to the dynamics *on* the perturbed manifold $\mathcal{M}_\epsilon$ because only on this manifold are the necessary conditions for applying averaging theory fulfilled. However, this fact does not pose a limitation on the method since $\mathcal{M}_\epsilon$ is a NAIM and therefore, the *asymptotic* dynamics for initial conditions in a neighborhood $U(\mathcal{M}_\epsilon)$ of $\mathcal{M}_\epsilon$ take place entirely on $\mathcal{M}_\epsilon$. In other words, the dynamics on $\mathcal{M}_\epsilon$ serve as a *local model* in the sense of [HI12], i. e., there exists a local continuous mapping $h : U(\mathcal{M}_\epsilon) \to \mathcal{M}_\epsilon$ that maps solutions of the full system to those of the system, restricted to $\mathcal{M}_\epsilon$, cf. Theorems 4.2 and 4.3 in [HI12]. The result is a dimensional reduction of the problem by two. Applying the averaging principle then means to average those components of a given perturbation function that make the cross-ratios nonconstant over a full period of a given periodic orbit in $\mathcal{M}$ of the unperturbed system. If this average vanishes and the eigenvalues of $\mathrm{D}\hat{\boldsymbol{F}}_h$ do not lie on the imaginary line, the orbit is robust.

We note that the proof of Proposition 7.1 relies on the fact that there exists an asymptotic phase-like function S in a neighborhood $U(\mathcal{M})$ of $\mathcal{M}$ which is C^1 and together with the cross-ratio function $\boldsymbol{\Lambda}$ serves as a set of coordinates on $\mathcal{M}_\epsilon$ and relates the dynamics on this manifold to the dynamics on the unperturbed manifold $\mathcal{M}$. The existence of an asymptotic phase for NAIMs and even continuous families of periodic orbits has been studied, e. g., in [Fen77] and [Aul82]. While the asymptotic phase for NAIMs is generally only guaranteed to be continuous, we are in the advantageous position that $\mathcal{M}$ is composed of periodic orbits so that there exists no exponential expansion or contraction on $\mathcal{M}$ from which it follows in particular that S is as smooth as the vector field and so is sufficiently smooth for our purposes [Fen74].

Surprisingly enough, we found that it is in general important to average over the periodic orbits of the *full* WS-integrable system since the averaged vector field in $\boldsymbol{\lambda}$-direction for the truncated system vanishes identically which in turn makes the averaging principle sterile. To show this in Appendix D, we used the fact that for constant $\alpha(t) = \alpha_0$ and $\dot{\psi}(t) = \Omega$, the Fourier series of the function $\psi \mapsto (\mathrm{D}\boldsymbol{\Lambda} \cdot \boldsymbol{h}) \circ \boldsymbol{m}(\alpha_0, \psi, \boldsymbol{\lambda})$ has a vanishing zeroth order Fourier mode for arbitrary α_0, $\boldsymbol{\lambda}$ and smooth h. Once $\alpha(\psi, \boldsymbol{\lambda})$ and $\dot{\psi}(\psi, \boldsymbol{\lambda})$ become nonconstant in ψ, the calculations become highly nontrivial and in particular depend on the specific form of the common fields f and g. We conjecture that both the nonvanishing of $\hat{\boldsymbol{F}}_h$ and the hyperbolicity of the derivative $\mathrm{D}\hat{\boldsymbol{F}}_h(\boldsymbol{\lambda}^*)$ are generic properties for systems of the type (6.3) but were not able yet to prove this. However, as we saw that both properties hold for the case of the generalized AR-model, it would be quite a surprise if this was not a generic feature of systems of the type (6.3).

The result of removing WS-integrability from a system by breaking its symmetry is that instead of infinitely many somewhat parallel lying obits, we are confronted with a slowly spiraling motion along $\mathcal{M}_\epsilon$ and that generally only few orbits survive the introduction of the perturba-

tion term. In particular, we showed that $\hat{\boldsymbol{F}}_h(\boldsymbol{\lambda}^*) = \mathbf{0}$ which indicates that splay states are generally robust solutions for systems of type (7.1) which further emphasizes their special role within the continuum of periodic orbits (and in WS-theory, for that matter). Given the conjecture of hyperbolicity above holds true, we further showed how one can control any given periodic orbit of the continuum, i. e., make it hyperbolic, by constructing a suitable perturbation function. It is not clear whether it also possible to construct the perturbation function in such a way that the orbit becomes exponentially stable. This is certainly the case for $N = 4$ units where we only have a single cross-ratio and therefore $\hat{\boldsymbol{F}}_h$ is one-dimensional so that changing the sign of the perturbation parameter ϵ switches the stability of *any* orbit. However, for larger values of N, things become more difficult because we have multiple components of the averaged vector field which are generally all interrelated. Hence, changing the perturbation function h has an effect on the values of *all* components of $\hat{\boldsymbol{F}}_h$ which poses a nontrivial problem of constructing h in such a way that the spectrum of $\mathrm{D}\hat{\boldsymbol{F}}_h(\boldsymbol{\lambda}_0)$ has negative real part. On the other hand, we have an infinite-dimensional space of perturbation functions at our disposal to do the trick. This infinitude of valid perturbation functions supplies us with a tantalizing variety to find a function that actually makes a given orbit exponentially stable. In any case, this remains a subject for future research.

In the first part of this chapter, all results presented were rigorous and applied to the general class (6.3) of WS-integrable models that only depend on the Kuramoto order parameter. In the second part, we applied the averaging principle to the generalized Active Rotator model which served two purposes: To analyze the asymptotic dynamics of the model but also to discuss the possibilities and limitations of the averaging principle. Particularly, we focused on the simplest nontrivial case of $N = 4$ ARs for which the continuum of orbits in the integrable case consists of what we call broken-symmetry states, which are hybrids between splay states and symmetric periodic two-cluster states: They consist of two groups of two more tightly bound units, each. Varying the cross-ratio controls how tight this grouping is where the two extreme cases yield either a splay state of a true two-cluster state. The proposed method to control periodic orbits in $\mathcal{M}$ allowed us to study how the nonlocal change in stability for splay states and two-cluster states that we observe if we change the sign of the bifurcation parameter ϵ, gets replaced by a more generic *local* transfer of stability between these two types of solutions by means of broken-symmetry states.

We stress that broken-symmetry states show a striking resemblance to so-called "generalized splay states", which were studied in [Ber+21]. Such generalized splay states are defined as phase-locked states for which the Kuramoto-Daido parameter[11] vanishes. While our broken-symmetry states feature compatible dynamics to 2-splay states in the diction of [Ber+21], they seemingly do not fit the definition of a gener-

11 This parameter $Z_k(\boldsymbol{\phi}) = \frac{1}{N}\sum_{j=1}^{N} \mathrm{e}^{ik\phi_j}$ is a generalization of the Kuramoto order parameter [Dai96].

alized splay therein because the Kuramoto-Daido parameter does not vanish for them. However, this is solely due to the fact that the components of $\boldsymbol{\phi}_{\boldsymbol{\lambda}}(t)$ are not proper phase-variables because they do not grow linearly in time. A suitable coordinate change to such phase variables exists and would result in the vanishing of this order parameter.

We continued by conducting a numerical stability analysis for the splay state for large values of ϵ and observed that this solution (and therefore the NAIM $\mathcal{M}_\epsilon$ with it) always emerge in a THB, either of the synchronous fixed point Δ^{s} or a stationary solitary state. This result, which is in agreement with a similar but rigorous result for the WS-integrable case in Chapter 6, illustrates how periodic ensemble dynamics of class I excitable units can emerge under sufficiently strong repulsive coupling besides the already known periodic two-cluster states. It also illustrates how periodic two-cluster states, although clustered splay states themselves, fundamentally differ from all other (clustered) splay states which emerge for the critical coupling κ_0 in the THB. The underlying reason for this is (i) that in $\mathbb{T}_{1/2}$, the transcritical character of the bifurcation at κ_0 is replaced by a pitchfork and (ii) two-cluster dynamics are not subject to WS-theory.

The fact that splay states can at all exist for the systems at hand is of course an immediate consequence of the fact that we are dealing with identical units. If the units would be distinguishable, e. g., by replacing the internal angular velocity parameter ω by site-dependent parameters ω_j, the resulting solution would not be a splay state but instead the time intervals between two consecutive units, crossing a given point in the state space, would not be equal. We already stated that our results are fundamentally limited by the fact that, e. g., the existence of the diffeomorphism $\boldsymbol{m}$ is only guaranteed for identical units since only then the ordered torus $\mathbb{T}^N_{\mathrm{ordered}}$ is invariant. But at least for weakly heterogeneous ensembles and for sufficiently short times, a given state will stay in $\mathbb{T}^N_{\mathrm{ordered}}$ and it might be possible to apply our results to such systems for short times. In this case, since the splay state is generally hyperbolic, it would survive in form of an "imperfect" splay: the time intervals between consecutive units to "spike" would be distinguishable albeit this effect would be small if the differences in, say, the ω_j are small. The same holds true for any other orbit that becomes hyperbolic through symmetry-breaking perturbations. Making the units distinguishable results in making the inter-spike-intervals between consecutive units also more heterogeneous.

A special role in this regard is played by *clustered* splay states. Just as the pure splay state, these solutions are hyperbolic. Making the number of units per cluster unequal results in imperfect clustered splay states. If N is large, the relative differences in cluster size are small and thus these imperfect clustered splays are hyperbolic and of the same stability type as the true clustered splays. Indeed, for randomly chosen initial conditions and large N, it is much more likely that the state converges to an imperfect clustered splay state than to any true (clustered) splay.

As a final result for $N = 4$ units, we investigated the transfer of stability between splay states and two-cluster states under continuous

changes of the perturbation function h. This also served as a comparison between the predictions from the averaging principle and the actual dynamics of the generalized AR-model. Specifically, we found that in the simplest case, the transfer happens via the emergence or disappearance of broken-symmetry states through pitchfork bifurcations of the splay and the symmetric periodic two-cluster states. More complicated scenarios are possible and were, as a matter of fact, observed in the form of additional saddle-node bifurcations of broken-symmetry states, in agreement with the predictions from the averaging principle. Since averaging is a perturbation method and therefore becomes less reliable the larger the perturbation term is, the agreement between averaging theory and numerical results becomes better, the smaller we choose $|\epsilon|$. However, we saw that even for fairly large $|\epsilon|$, the predictions from averaging theory became also quantitatively better, the larger we chose $-\kappa$. Why this is, is not entirely clear to us. An explanation might be that with increasing $|\kappa|$, the repulsive coupling term eventually dominates the on-site dynamics and therefore, in particular, the perturbation term. The result is that the ARs "feel" the perturbation less which has the same effect as making $|\epsilon|$ smaller for fixed κ so that as a consequence, averaging theory and actual dynamics are in better agreement.

Since the splay state is robust for any N, we went on by investigating its stability for larger values of N. Because the Floquet multipliers of the splay state, in contrast to periodic two-cluster states, are not degenerate, the picture here becomes more complex. In particular, for large N, we are not guaranteed anymore to see a switch from exponential stability to exponential instability at $\epsilon = 0$, as for $N = 4$. But at least for moderate values of N and close to the THB of Δ^{s}, we still observed this behavior. For even N, any stability changing bifurcations of the splay state again involved a broken-symmetry state where now the ensemble splits in $N/2$ groups of two units, each. This leads to the conjecture that such states are still a general feature for class I excitable units for even N. Since for odd N, broken-symmetry states cannot exist, they are also not responsible for any change in stability of the splay state in this case. Hence, for $N = 7$, the subcritical pitchfork of the splay state is replaced by a subcritical Neimark-Sacker bifurcation.

If both, the splay state and the periodic two-cluster states, are unstable, the question arises what asymptotic dynamics occur instead. These dynamics are more complex than for the case $N = 4$: In our numerical experiments, we observed, e. g., stable clustered splays or even stable heteroclinic cycles of clustered periodic orbits, to name a few types of asymptotically stable solutions. What all of these solutions have in common is that they do not exist in $\mathbb{T}^N_{\mathrm{ordered}}$ but rather somewhere in its boundary $\partial\mathbb{T}^N_{\mathrm{ordered}}$ which makes them, to some degree, inaccessible to the averaging principle. This brings us to another limitation of the method: It only works as long as we can use the cross-ratios as coordinates together with the Möbius group parameters and this only works rigorously in $\mathbb{T}^N_{\mathrm{ordered}}$. On its boundary $\partial\mathbb{T}^N_{\mathrm{ordered}}$, cross-ratios may or may not become ill-defined because they may be of the form $0/0$. For $N = 4$, this was not a problem as long as we restricted our attention

to *symmetric* two-cluster states but for larger N, two cluster states or clustered splay states may have no well-defined cross-ratios any longer. However, at least to some degree, we can still use the averaging principle to study clustered splay states as long as we are only interested in their stability against *non-splitting* perturbations since we can effectively describe such states and perturbations by applying the averaging principle to the reduced dynamics of the cluster coordinates.

Finally, as a proof of concept for the proposed method of controlling any given orbit in $\mathcal{M}$ by constructing a suitable perturbation function, we illustrated this procedure for an ensemble of $N = 10$ Active Rotators, in good agreement with the numerical stability analysis for the resulting orbits. It is worth noting that while for $N = 4$, the controlled broken-symmetry states are robust even for fairly large values of ϵ, for $N = 10$, one has to be careful with how large to choose $|\epsilon|$. In the example at hand, the orbit went through a first bifurcation already for $\epsilon \simeq 0.0006$ so that for larger values of ϵ, averaging theory already does not describe the actual dynamics any longer. Of course, this has to be brought into perspective by noting that the coefficients (7.27) for this particular h are quite large such that, if we had normalized h first, the prediction from the averaging principle would be valid for almost two more orders of magnitude. Nevertheless, it becomes more and more cumbersome to control orbits for large N and $|\epsilon|$. It is also important to note that averaging theory cannot explain the narrow region of stability of splay states for negative ϵ and close to the THB in Figure 33. It turns out that in this regime again broken-symmetry states exist (emerging in the THB), a fact that is not captured by the averaging principle since these states emerge only for *large* values of $-\epsilon$. At the end of the day, the averaging principle is an appropriate tool to study *small* deviations away from the WS-case.

With this, we end this chapter and also Part II of this thesis. In the next part, we leave the angular dynamics and in particular the Active Rotator models behind us and investigate ensembles of higher-dimensional class I excitable elements in the form of the Morris-Lecar neuron model. This will also serve to study whether and how the previous results on Active Rotators generalize for general excitable elements.

Part III

ENSEMBLES OF MORRIS-LECAR NEURONS

We generalize from one situation to another not because we cannot tell the difference between the two situations but because we judge that they are likely to belong to a set of situations having the same consequence.

— Roger N. Shepard [She87]

8

COUPLED MORRIS-LECAR NEURONS

ABSTRACT

The results on the existence and stability of periodic states for ensembles of excitable elements, presented so far, exclusively dealt with ensembles of angular variables, i. e., with one-dimensional excitable units. To view and assess these results in the broader context of general class I excitable elements is the purpose of this chapter. For this, we conduct numerical simulations for ensembles of voltage-coupled Morris-Lecar neurons [ML81]. The Morris-Lecar model, introduced in 1981 by Morris and Lecar, is a two-dimensional neural model which was originally designed to describe the neurophysiological properties of barnacle giant muscle fibers. Its physiological meaning is of no real importance for this work. We chose it mainly because its parameters can be tuned in such a way that the single neuron exhibits class I excitability [EK90; Tsu+02; Tsu+06].

After introducing the model itself in Section 8.1, we discuss the observed bifurcation scenarios leading to either splay states in Section 8.2.1 or periodic two-cluster states in Section 8.2.2. While many of the effects for coupled Morris-Lecar neurons are also present in ensembles of generalized Active Rotators and can be understood within the framework that we developed in the previous part of this thesis, other effects cannot occur in ensembles of one-dimensional elements and are thus due to the Morris-Lecar models' higher dimensionality. We proceed by discussing how the local transfer of stability, investigated in Section 7.4.2 for Active Rotators, translates to coupled Morris-Lecar neurons. The content of this chapter is based on the publications [RZ21a] and [RZ21b].

8.1 THE MODEL

The Morris-Lecar model is a two-dimensional conductance based model and describes the time evolution of the membrane voltage V of a neuron and a recovery variable w, modeling the normalized conductance for K^+ ions through the cell membrane. Additionally, it assumes that the conductance of the membrane for Ca^{2+} ions responds instantaneously to changes in the membrane voltage. In particular, this instantaneous response causes the upstroke for any spike while the finite time response of the K^+ conductance is responsible for the downstroke. A commonly

studied setup in the context of the ensemble dynamics for N Morris-Lecar neurons consists of an all-to-all pairwise coupling via mutual voltage differences, see for example [PM06; WLL08; DKN13; Tan+14; KSN16]. For the case of identical units, the dynamical equations then read

$$\begin{aligned} C\,\dot{V}_j = & -g_{\mathrm{Ca}}\, n_\infty(V_j)\cdot(V_j - V_{\mathrm{Ca}}) - g_{\mathrm{K}}\, w_j \cdot (V_j - V_{\mathrm{K}}) \\ & - g_{\mathrm{L}}\cdot(V_j - V_{\mathrm{L}}) + I_{\mathrm{app}} + \frac{\kappa}{N}\sum_{k=1}^{N}(V_k - V_j) \end{aligned} \tag{8.1a}$$

$$\dot{w}_j = \nu(V_j)\cdot(w_\infty(V_j) - w_j)\,. \tag{8.1b}$$

Here, $j = 1, \ldots, N$ denotes the jth neuron with membrane voltage V_j and recovery variable w_j. The functions

$$n_\infty(V) = \frac{1}{2}\left(1 + \tanh\frac{V - V_{\mathrm{a}}}{V_{\mathrm{b}}}\right)$$
$$w_\infty(V) = \frac{1}{2}\left(1 + \tanh\frac{V - V_{\mathrm{c}}}{V_{\mathrm{d}}}\right)$$

quantify the proportion of open ion channels for Ca^{2+} and K^+ ions in dependence of V, whereas

$$\nu(V) = \nu_0 \cosh\frac{V - V_{\mathrm{c}}}{V_{\mathrm{e}}}$$

denotes the voltage-dependent inverse recovery time for the K^+ channels. The coefficients g_{Ca}, and g_{K} denote the maximum conductivity for Ca^{2+} and K^+ ions through the membrane while the term $-g_{\mathrm{L}}(V_j - V_{\mathrm{L}})$ represents a leak current I_{L}. In particular, the first term on the right hand side of (8.1a) describes the instantaneous dependence on the Ca^{2+} conductance of V_j, while the second term together with (8.1b) describes the finite-time response of the K^+ conductance. The quantities V_{Ca}, V_{K}, and V_{L} denote the reversal potentials for each of the ion channels and the leak current, i. e., the potentials at which the respective currents through the membrane change direction. Finally, V_{a}, V_{b}, V_{c}, V_{d}, and V_{e} are auxiliary constants while I_{app} represents an external applied current and C is the membrane capacitance.

Since the neurons are coupled exclusively via their respective voltage variables, the notion of repulsive coupling from Chapter 2 does not fully apply to this setup but has to be generalized. Throughout this chapter, the coupling between any two units does not depend on the distance between them in state space $\mathbb{R}^2$ but only on their distance in V-direction. Aside from this caveat, the coupling still has the effect that two units with voltages V_j and V_k experience a tendency to increase the voltage difference $V_j - V_k$ for $\kappa < 0$ so that we speak of *repulsive* coupling while there exists a tendency to decrease this difference if $\kappa > 0$ in which case we speak of *attractive* coupling.

One might argue that in order to compare the ensemble dynamics of coupled Morris-Lecar neurons with those of the Active Rotator models from Part II, a more appropriate setup would consider a coupling

PARAMETER	ERMENTROUT	TSUMOTO
C	1	1
ν_0	0.33	1/3
I_{app}	0.0332	395/1200
g_{K}	2	8
g_{Ca}	1	4
g_{L}	0.5	2
V_{K}	-0.7	-2/3
V_{Ca}	1	1
V_{L}	-0.4	-1/2
V_{a}	-0.01	-0.01
V_{b}	0.15	0.15
V_{c}	0.1	0.1
V_{d}	0.145	0.145
V_{e}	0.145	0.29

Table 1: System parameters for the model (8.1), in accordance with Ermentrout and Kopell [EK90] and Tsumoto et al. [Tsu+02], yielding class I excitable neurons. The parameter I_{app} is free in [Tsu+02] and fixed in [EK90]. We choose the shown values to bring the single neuron closer to its SNIC.

term that depends on the actual distance of the Morris-Lecar neurons in state space instead of just the voltage difference. The motivation for the coupling term at hand is the following: While coupling between neurons usually involves more complicated mechanism like chemical synaptic transmission of signals [DA05], two neurons can also be connected by so-called *gap junctions*, which act as direct electric connections between them and play an important role in fast signal transfers and in synchronization effects between many types of cells, e. g., in the heart [JW94]. On the other hand, the recovery variable w is a rather elusive quantity and takes in practice no part in the coupling of neurons. It is an entirely internal property of a neuron that is completely concealed from other neurons. While the model (8.1) is not readily applicable for the description of real world neural networks, it serves nevertheless as a more realistic description of neural interactions and, as we will see below, its dynamics are to some extend compatible with those of Active Rotators.

The Morris-Lecar model, describing a *single* neuron, features a variety of intrinsic dynamics, depending on the choice of system parameters. Following [EK90; Tsu+02], the parameters used by us are listed in Table 1, for which each unit is close to a SNIC.[1] The two choices differ

1 The parameters from [Tsu+02] are rescaled by measuring V in units of V_{Ca} and time in such units that $C = 1$ and $\nu_0 = 1/3$.

essentially in two ways. The first difference is more conceptual in that the constant V_e, used in $\nu(V)$ is chosen twice as large in [Tsu+02] as in [EK90] which results in a significantly larger recovery time for the former case. However, we found that this does not introduce any considerable qualitative differences in the dynamics for the two parameter sets. The second difference lies in the fact that the values for the conductances g_K, g_{Ca}, and g_L in [Tsu+02] are four times higher than those in [EK90] and we will see below that this has significant consequences. We finally note that while the two sets differ, at first glance, significantly in the external current I_{app} as well, an expansion of (8.1a) as a power series

$$\dot{V}_j = a_0 + a_1 V_j + \mathcal{O}(V_j^2) + \mathcal{O}(w_j) \tag{8.2}$$

in V_j and w_j yields the coefficients

$$\begin{aligned} a_0 &= I_{app} + g_L V_L - \frac{1}{2} g_{Ca} V_{Ca} \left(-1 + \tanh \frac{V_a}{V_b} \right) \\ a_1 &= -g_L + \frac{1}{2} g_{Ca} \left(-1 + \tanh \frac{V_a}{V_b} + \frac{V_{Ca}}{V_b} \left(1 - \tanh^2 \frac{V_a}{V_b} \right) \right) \end{aligned}$$

and reveals that the ratio a_0/a_1 is approximately 0.16 for both choices. Since all auxiliary functions in (8.1) depend only on voltage ratios and (8.1a) is otherwise linear in V, rescaling $V_j \to V_j/a_1$ renders (8.2) as

$$\dot{V}_j = \tilde{a}_0 + V_j + \mathcal{O}(V_j^2) + \mathcal{O}(w_j)$$

with $\tilde{a}_0 = a_0/a_1 \simeq 0.16$. Under this rescaling, I_{app} is completely absorbed into $\tilde{a}_0$ which is approximately the same for both parameter choices. Hence, the two setups only differ significantly in the $\mathcal{O}(V_j^2)$- and $\mathcal{O}(w_j)$-terms which in turn depend on the membrane conductances. Comparing this setup to the generalized AR-model (2.6), this suggests to treat varying the coefficients g_K, g_{Ca}, and g_L for the Morris-Lecar model (8.1) in a similar way to varying ϵh in (2.6), e. g., by varying the parameters ζ in (7.25). We thus expect that a simultaneous rescaling of g_{Ca}, g_L, and g_K results in a similar outcome as varying ζ in (7.25) for (2.6). Hence, whenever we vary conductances, we do so using the parameters from [EK90] and substituting

$$\begin{aligned} g_K &\to (1+\zeta)\, g_K \\ g_{Ca} &\to (1+\zeta)\, g_{Ca} \\ g_L &\to (1+\zeta)\, g_L \end{aligned} \tag{8.3}$$

in (8.1) with scaling parameter $\zeta \in [0,1]$ while adjusting I_{app} such that

$$\tilde{a}_0 = \frac{\frac{1}{1+\zeta} I_{app} + g_L V_L - \frac{1}{2} g_{Ca} V_{Ca} \left(\tanh \frac{V_a}{V_b} - 1 \right)}{-g_L + \frac{1}{2} g_{Ca} \left(\tanh \frac{V_a}{V_b} - 1 + \frac{V_{Ca}}{V_b} \left(1 - \tanh \frac{V_a}{V_b} \right) \tanh \frac{V_a}{V_b} \right)} = \text{const.} \tag{8.4}$$

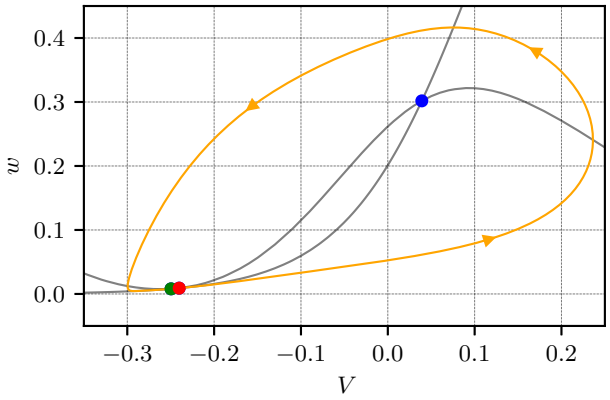

Figure 36: Phase plot for a single Morris-Lecar neuron with system parameters according to [EK90]. The system possesses a stable fixed point (green dot) and a saddle (red dot) as well as an unstable spiral (blue dot). The unstable manifold of the saddle (orange line) ends in the stable fixed point so that the system is close to a SNIC. Gray lines indicate V- and w- nullclines.

to keep the zeroth order term in the rescaled expansion $\dot{V}_j = \tilde{a}_0 + V_j + \mathcal{O}(V_j^2) + \mathcal{O}(w_j)$ constant. Specifically, we fix $\tilde{a}_0 = 0.160367$ in what follows. Varying ζ in the unit interval $[0, 1]$ then corresponds to a path in parameters space of (8.1), leading from the parameters in [EK90] for $\zeta = 0$ to roughly those of [Tsu+02] at $\zeta = 1$

Our aim is thus to investigate the bifurcation scenarios and the stability of periodic states for the model (8.1) in dependence on the parameters κ and ζ.

GENERAL REMARKS Before we discuss the limit cycle creating bifurcations that occur for (8.1), a word is at hand regarding the steady states of the system.

A single Morris-Lecar neuron possesses, for the parameter choices in [EK90] and [Tsu+02], three hyperbolic fixed points, as depicted in Figure 36 for the parameters from [EK90]: A saddle $(V^{\mathrm{u}}, w^{\mathrm{u}})$ (red dot) is connected via its unstable manifold (orange lines) with the stable fixed point $(V^{\mathrm{s}}, w^{\mathrm{s}})$ (green dot) so that the system is close to a SNIC and thus class I excitable. Additionally, the system possesses an unstable spiral (blue dot) which is not of interest in this context and will be neglected henceforth. Gray lines in Figure 36 indicate the V- and w-nullclines.

For the system (8.1) of N Morris-Lecar neurons, this again gives rise to a synchronous fixed point

$$\Delta^{\mathrm{s}} = (\underbrace{V^{\mathrm{s}}, \ldots, V^{\mathrm{s}}}_{N \text{ entries}}, \underbrace{w^{\mathrm{s}}, \ldots, w^{\mathrm{s}}}_{N \text{ entries}})$$

as the unique attractor of the system at $\kappa = 0$ as well as an unstable synchronous fixed point

$$\Delta^{\mathrm{u}} = (\underbrace{V^{\mathrm{u}}, \ldots, V^{\mathrm{u}}}_{N \text{ entries}}, \underbrace{w^{\mathrm{u}}, \ldots, w^{\mathrm{u}}}_{N \text{ entries}}).$$

The phase space of (8.1) can be taken to be $\mathbb{R}^{2N}$. The state space is given by $\mathbb{R}^2$ such that we may view the system as N units $(V_j, w_j) \in \mathbb{R}^2$. As for systems of Active Rotators, the neurons being identical yields invariant two-cluster subspaces of the form

$$\mathbb{T}_p \coloneqq \left\{ (\boldsymbol{V}, \boldsymbol{w}) \in \mathbb{R}^{2N} \; ; \; \begin{array}{c} V_1 = \cdots = V_{pN},\ V_{pN+1} = \cdots = V_N, \\ w_1 = \cdots = w_{pN},\ w_{pN+1} = \cdots = w_N \end{array} \right\}$$

where without loss of generality we index the neurons in such a way that the first $m_A = pN$ neurons belong to cluster $A = \{1, \ldots, pN\}$ and the remaining $m_B = (1-p)N$ neurons belong to cluster $B = \{pN+1, \ldots, N\}$. For $p \in (0,1)$ and $\kappa = 0$, we find two saddles

$$\begin{aligned} \Sigma^1 &= (\underbrace{V^{\mathrm{s}}, \ldots, V^{\mathrm{s}}}_{m_A \text{ entries}}, \underbrace{V^{\mathrm{u}}, \ldots, V^{\mathrm{u}}}_{m_B \text{ entries}}, \underbrace{w^{\mathrm{s}}, \ldots, w^{\mathrm{s}}}_{m_A \text{ entries}}, \underbrace{w^{\mathrm{u}}, \ldots, w^{\mathrm{u}}}_{m_B \text{ entries}}) \\ \Sigma^2 &= (\underbrace{V^{\mathrm{u}}, \ldots, V^{\mathrm{u}}}_{m_A \text{ entries}}, \underbrace{V^{\mathrm{s}}, \ldots, V^{\mathrm{s}}}_{m_B \text{ entries}}, \underbrace{w^{\mathrm{u}}, \ldots, w^{\mathrm{u}}}_{m_A \text{ entries}}, \underbrace{w^{\mathrm{s}}, \ldots, w^{\mathrm{s}}}_{m_B \text{ entries}}). \end{aligned}$$

Analogously to Chapter 5, a reduced model for the two-cluster states can be introduced as

$$\begin{aligned} C\,\dot{V}_A =& -g_{\mathrm{Ca}}\, n_\infty(V_A) \cdot (V_A - V_{\mathrm{Ca}}) - g_{\mathrm{K}}\, w_A \cdot (V_A - V_{\mathrm{K}}) \\ & - g_{\mathrm{L}} \cdot (V_A - V_{\mathrm{L}}) + I_{\mathrm{app}} + (1-p)\,\kappa \cdot (V_B - V_A) \\ \dot{w}_A =& \nu(V_A) \cdot (w_\infty(V_A) - w_A) \\ C\,\dot{V}_B =& -g_{\mathrm{Ca}}\, n_\infty(V_B) \cdot (V_B - V_{\mathrm{Ca}}) - g_{\mathrm{K}}\, w_B \cdot (V_B - V_{\mathrm{K}}) \\ & - g_{\mathrm{L}} \cdot (V_B - V_{\mathrm{L}}) + I_{\mathrm{app}} + p\,\kappa \cdot (V_A - V_B) \\ \dot{w}_B =& \nu(V_B) \cdot (w_\infty(V_B) - w_B) \end{aligned} \tag{8.5}$$

where

$$\begin{aligned} V_A &= V_1 = \cdots = V_{pN} \\ V_B &= V_{pN+1} = \cdots = V_N \end{aligned}$$

and one may identify the reduced fixed points $\Delta^{\mathrm{s}} = (V^{\mathrm{s}}, V^{\mathrm{s}}, w^{\mathrm{s}}, w^{\mathrm{s}})$, $\Delta^{\mathrm{u}} = (V^{\mathrm{u}}, V^{\mathrm{u}}, w^{\mathrm{u}}, w^{\mathrm{u}})$, as well as the saddles $\Sigma^1 = (V^{\mathrm{s}}, V^{\mathrm{u}}, w^{\mathrm{s}}, w^{\mathrm{u}})$ and $\Sigma^2 = (V^{\mathrm{u}}, V^{\mathrm{s}}, w^{\mathrm{u}}, w^{\mathrm{s}})$ of the reduced model at $\kappa = 0$ with their counterparts for the full system.

8.2 LIMIT CYCLE BIFURCATIONS

8.2.1 *The Transcritical Homoclinic Bifurcation*

The THB from [ZT16] for ensembles of one-dimensional units readily translates to systems of two-dimensional elements. Consider a system of general two-dimensional identical units (x_j, y_j), $j = 1, \ldots, N$, under pairwise, possibly nonlinear, all-to-all coupling in their mutual x-differences. Assume that every single unit possesses a sink at $(V, w) = (0,0)$, giving rise to a sink of the system at the origin $\mathbf{0} \coloneqq (0, \ldots, 0) \in$

$\mathbb{R}^{2N}$ for sufficiently small $|\kappa|$. The dynamics in the vicinity of $\mathbf{0}$ can be written in a Taylor expansion as

$$\dot{x}_j = ax_j + by_j + R_1(x_j, y_j) + \frac{\kappa}{N}\sum_{k=1}^{N}\left[(x_k - x_j) + R_2(x_k - x_j)\right]$$
$$\dot{y}_j = cx_j + dy_j + R_3(x_j, y_j)$$

where $R_1(x, y)$ and $R_3(x, y)$ denote the nonlinearities in the on-site dynamics and $R_2(x_k - x_j)$ denotes any nonlinear terms in the coupling between units k and j. The $(2N \times 2N)$-dimensional Jacobian of the right hand side of this equation, evaluated at $\mathbf{0}$, possesses two negative eigenvalues which correspond to the stability of the synchronous fixed point against non-splitting perturbations. These eigenvalues are given by

$$\lambda_{1,2} = \frac{1}{2}\left(a + d \pm \sqrt{(a-d)^2 + 4bc}\right)$$

and are exactly the eigenvalues of the Jacobian for the single unit at $(V, w) = (0, 0)$. In particular, this implies $ad - bc < 0$ and $a + d < 0$ due to the assumed single unit's stability. Further, there exist two degenerate eigenvalues

$$\lambda_{\pm} = \frac{1}{2}\left(a + d - \kappa \pm \sqrt{(a-d-\kappa)^2 + 4bc}\right)$$

of multiplicity $N - 1$, each. These eigenvalues correspond to splitting perturbations of the synchronous fixed point and vanish in a transcritical bifurcation for the critical coupling strength

$$\kappa_0 = \frac{ad - bc}{d}.$$

In particular, for Morris-Lecar neurons, we have

$$a = -\frac{g_{\mathrm{Ca}}(V^{\mathrm{s}} - V_{\mathrm{Ca}})M'(V^{\mathrm{s}}) + g_{\mathrm{Ca}}M(V^{\mathrm{s}}) + g_{\mathrm{K}}w^{\mathrm{s}} + g_{\mathrm{L}}}{C}$$
$$b = -\frac{g_{\mathrm{K}}(V^{\mathrm{s}} - V_{\mathrm{K}})}{C}$$
$$c = \nu'(V^{\mathrm{s}})(W(V^{\mathrm{s}}) - w^{\mathrm{s}}) + \nu(V^{\mathrm{s}})W'(V^{\mathrm{s}})$$
$$d = -\nu(V^{\mathrm{s}}).$$

Numerical results confirm the homoclinic character of the transcritical bifurcation: At κ_0, a multitude of homoclinic orbits forms where along each orbit one or several of the N units leave $(V^{\mathrm{s}}, w^{\mathrm{s}})$ and return from the opposite side as we observed for the AR-model. For $\kappa < \kappa_0$, these homoclinic orbits turn into periodic orbits which look similar to those, discussed for Active Rotators in Chapter 7: The neurons for the most part stay close to the point $(V^{\mathrm{s}}, w^{\mathrm{s}})$ in state space while from time to time and in consecutive order each of the neurons departs from the rest for a short time, tracing a macroscopic contour before returning to the rest of the group, in a regular fashion, which results in a splay state.

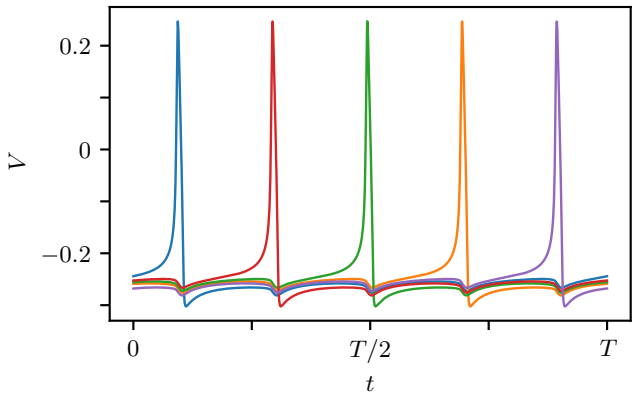

Figure 37: Splay state of period $T \simeq 237.3$ for an ensemble of $N = 5$ Morris-Lecar neurons, obeying (8.1), with system parameters according to [EK90] and $\kappa = -0.07$. Different colors represent different neurons. As for systems of Active Rotators, single units depart from the rest of the ensemble during short spike-like periods while the other units stay close to $(V^{\mathrm{s}}, w^{\mathrm{s}})$ in state space.

In Figure 37, we show the voltage time series of such a splay state for an ensemble of $N = 5$ units where we use system parameters according to [EK90] and set $\kappa = -0.07$. For the parameters from [EK90], the splay states are stable and are unstable for parameters from [Tsu+02]. We discuss stability in more detail in Section 8.3. The existence of splay states and their emergence through a THB is in direct correspondence to the results from Chapter 6 and Chapter 7 where we discussed how splay states emerge generally through a THB for ensembles of classic as well as generalized Active Rotators.

Before we further investigate the stability of splay states, we discuss the emergence of periodic two-cluster states.

8.2.2 *Double-Heteroclinic Bifurcations*

Looking for bifurcation scenarios which lead to periodic two-cluster states, we again consider the invariant subspaces $\mathbb{T}_p$ and the two-cluster dynamics, governed by the reduced equations (8.5). For simplicity, we restrict our attention to the symmetric case $p = 1/2$. In $\mathbb{T}_{1/2}$, one observes again a pitchfork bifurcation instead of the transcritical one for $p \neq 1/2$. Since this pitchfork was always subcritical in our numerical studies, no double-SNICs were observed. Instead, double-heteroclinic bifurcations are found for parameters from [Tsu+02]. A typical scenario is depicted in the panels (a)-(c) from Figure 36. (Here, we fixed $I_{\mathrm{app}} = 7/20$ for a better graphical resolution.) where we show projections on the space, spanned by cluster voltages V_A and V_B. As in the figures from Chapter 5 for Active Rotators, we increase the strength $|\kappa|$ of the repulsive coupling from the left to the right. Depicted are the synchronous fixed points Δ^{s} (green dot) and Δ^{u} (red dot) together with the saddles Σ^1 and Σ^2 (black dots) and their respective unstable manifolds (orange lines). The projection of the diagonal space

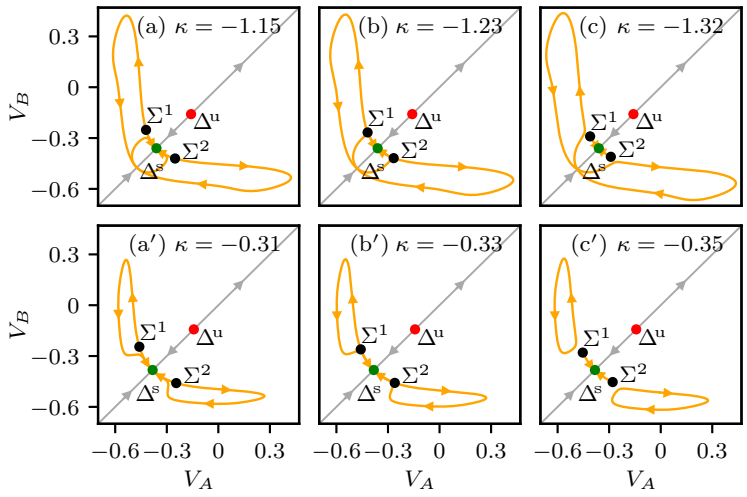

Figure 38: Bifurcation scenarios resulting in symmetric periodic two-cluster states. Depicted are the synchronous states of rest Δ^s and Δ^u and the saddles Σ^1 and Σ^2 together with their unstable manifolds (orange lines). Gray arrows indicate the flow on the space of total synchrony. System parameters are taken from [Tsu+02] with $I_{app} = 7/30$ in the top row and from [EK90] with $I_{app} = 0$ in the bottom row for better graphical resolution. From the left to the right, the repulsive coupling strength $|\kappa|$ is gradually increased. For [Tsu+02], this results in a double-heteroclinic bifurcation at $\kappa \simeq -1.23$ in Panel (b) and for [EK90] in two simultaneous homoclinic bifurcations at $\kappa \simeq -0.33$ in Panel (b′). Panels (c) and (c′) show the emerging periodic two-cluster states as closed orange curves.

$\Delta := \{(V_j, w_j) = (V_k, w_k)\ ;\ j,k = 1,\dots,N\}$ of total synchrony is depicted as a gray line. Arrows indicate the direction of the flow. For clarity, we do not show the stable manifolds of the saddles. In case of the parameters from [Tsu+02] and for moderate coupling strength in Panel (a), the two branches of the unstable manifolds for each Σ^i again end in the synchronous fixed point Δ^s, one branch coming close to the respective opposite saddle, first. Panel (b) shows the heteroclinic orbits, connecting Σ^1 and Σ^2 at the double-heteroclinic bifurcation while in Panel (c), a single periodic orbit has formed in which *both* clusters spike in anti-phase. This scenario is a direct analog to the double-heteroclinic bifurcation for (generalized) Active Rotators that was discussed in Chapter 5. Letting p deviate slightly from the value $1/2$ unfolds the bifurcation so that we again have first a heteroclinic bifurcation, followed by a homoclinic one, equally in correspondence to the (generalized) AR-model. Similar bifurcations can be observed for parameters from [EK90], for sufficiently large I_{app}.

Remarkably, choosing parameters from [EK90], but with I_{app} below the critical value $I_0 \simeq 0.0326$ yields a rather different scenario, as depicted in the bottom row (panels (a′)-(c′)) of Figure 38, where we set $I_{app} = 0$. Here, the unstable manifolds of the saddles still connect each Σ^i with Δ^s for moderate coupling in Panel (a′) but now, they do not approach the respective opposite saddle first. As a result, in Panel (b′), we see instead two simultaneous *homoclinic* orbits, one for each

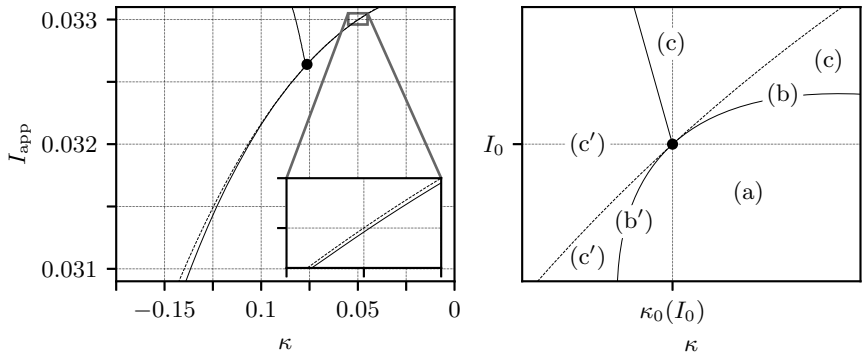

Figure 39: Bifurcation diagram around the codimension 2 point $(I_0, \kappa_0(I_0)) \simeq (0.0326, -0.0763)$ with parameters from [EK90]. The left panel shows numerical results, the right one a schematic depiction to highlight distinct regimes. Labels (a)-(c) and (a′)-(c′) mark regions in which the phase plots look like in the corresponding panels in Figure 38. A dashed black line indicates the THB of Δ^{s}. The lower branch of the solid black line to its right indicates the double-homoclinic bifurcation that yields "Chimera-like" states while the upper branch of this solid line indicates the double-heteroclinic bifurcation in which periodic two-cluster states emerge. At the codimension 2 point (black dot) all three bifurcations coincide. The solid line which branches off the point to the top left indicates the transition between periodic two-cluster state and "Chimera-like" state. The inset illustrates that the double-heteroclinic bifurcation and the THB are separate phenomena.

saddle. From these two simultaneous homoclinic bifurcations two periodic orbits emerge in Panel (c′) in which one cluster spikes while the other one stays close to $(V^{\text{s}}, w^{\text{s}})$ in state space, displaying only "subthreshold" oscillations. This in some loose sense (see the remarks in the introduction) "Chimera-like" splitting into two populations with different spiking properties constitutes a new type of dynamics that cannot occur in ensembles of (generalized) Active Rotators. Its closest analogs in the angular model would either consist of one cluster coordinate, say ϕ_A, staying relatively still at one place on the circle while the other cluster coordinate, say ϕ_B, periodically traverses the full circle or both clusters performing "librations" on the circle where they do not traverse the circle as a whole but stay in bounded subsets. Both behaviors are forbidden for identical angular variables, as noted in Chapter 2.

Numerical results and a schematic depiction of the transition between double-heteroclinic and double-homoclinic bifurcation are shown in the left and right panel of Figure 39, respectively. Here, a dashed line depicts the THB of the synchronous fixed point Δ^{s} while the solid black line to its right depicts either the double-heteroclinic bifurcation (upper branch) or the double-homoclinic bifurcation (lower branch). The inset shows that THB and double-heteroclinic bifurcation are indeed two separate bifurcations, occurring for distinct sets of system parameters. In the schematic diagram to the right, this distinction is highlighted by separating the curves further. The labels (a)-(c) and (a′)-(c′) correspond to the respective panels in Figure 38, where the corresponding typical phase plots for each region are shown. To the left of the THB-

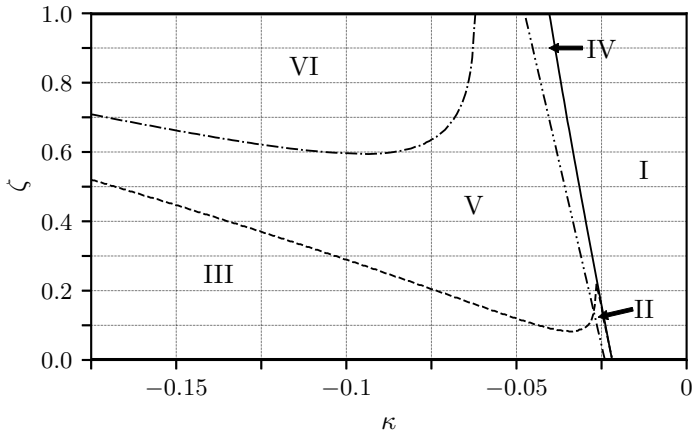

Figure 40: Existence and stability of the splay state, symmetric periodic two-cluster states, and broken-symmetry states for four Morris-Lecar neurons with system parameters from [EK90] but with $V_e = 0.2$ and $\nu_0 = 1/3$. **Region I**: no periodic solutions exist. **Solid line**: Periodic two-cluster states emerge in a double-heteroclinic bifurcation and are unstable in **Regions II and III** and stable otherwise. **Dash-double-dotted line**: THB of Δ^s in which a stable splay state emerges. Along the **dashed line** between Region III and V, subcritical pitchforks of the two-cluster states occur in which broken-symmetry states emerge and exist in Region V. **Dash-dotted line**: subcritical pitchfork of the splay state and broken-symmetry states which renders the splay state unstable in Region VI.

line, additional splay states exist for the full system. The transition between double-heteroclinic and double-homoclinic bifurcation constitutes a codimension 2 point at $(I_0, \kappa_0(I_0)) \simeq (0.0326, -0.0763)$ (black dot) at which they coincide with the THB. From this point, another line branches off to the upper left. Along this line, a homoclinic bifurcation occurs in which the two "Chimera-like" periodic orbits from Panel (c′) merge and form the orbit in Panel (c). Bifurcations of this kind were discussed before, e. g., in [ZL84; ZL89].

We note that as for the two-cluster dynamics of (generalized) Active Rotators that were discussed in Chapter 5, making the clusters slightly unequal in size results in an unfolding of the process but does not considerably change the resulting periodic orbits for the "Chimera-like" states.

8.3 TRANSFER OF STABILITY

As established above, varying the scaling of conductances in (8.1) according to (8.3) bears some resemblance to varying the parameter ζ in (7.25) for the generalized AR-model (2.6). Since we have to expect that varying ζ in (8.3) generically avoids any point of (partial) integrability (if such a point exists at all for the model) we expect a similar nonlocal transfer of stability in ensembles of Morris-Lecar neurons as we observed for Active Rotators in Chapter 7 by means of broken-symmetry states. To compare our results, we again focus on the case of $N = 4$

units. This also circumvents the computational problem of avoiding the possibly many existing clustered solutions for larger N in our search for pure splay states.

Defining a suitable domain in the coupling strength κ and scaling parameter ζ is readily done. Since we found stable splay states and unstable periodic two-cluster states for parameters from [EK90] and unstable splay states and stable periodic two-cluster states for parameters from [Tsu+02], we want the model to be close to the former set of parameters for $\zeta = 0$ and close to the latter set of parameters for $\zeta = 1$. In our studies, it turned out to be sufficient to let κ vary between $\kappa = 0$ and $\kappa = -0.175$ and scale ζ according to (8.3) to achieve this. As mentioned above, we also need to adjust the applied current I_{app} according to (8.4). Since the parameter sets in [EK90] and [Tsu+02] also differ significantly in V_{e} and somewhat in ν_0, we further choose as a compromise $V_{\text{e}} = 0.2$ and $\nu_0 = 1/3$ with the desired outcome that a single neuron behaves qualitatively like the model in [EK90] for $\zeta = 0$ and like the model in [Tsu+02] for $\zeta = 1$. The results are shown in Figure 40.

In Region I, no periodic orbits exist. At the left boundary (solid line) of this region, periodic two-cluster states emerge in a double-heteroclinic bifurcation which is unstable in Regions II and III and stable in Regions IV, V, and VI.[2] The dash-double-dotted line marks the THB of Δ^{s}. The splay state and broken-symmetry states exist only to the left of this line and emerge in this bifurcation. The border between Regions III and V (dashed line) marks a subcritical pitchfork in which the periodic two-cluster states are stabilized and unstable broken-symmetry states emerge. Increasing ζ lets these states either vanish in the THB or in a second subcritical pitchfork, this time with the splay state which is stable in Regions III and V and is rendered unstable in Region VI through the pitchfork.

Characterizing broken-symmetry states for four Morris-Lecar neurons.

The broken-symmetry states indeed feature the same characteristic grouping of units as we have already observed for the Active Rotator models. This is illustrated in Figure 41 where the ensemble splits in two groups, say, $A = \{1, 2\}$ (blue and red lines) and $B = \{3, 4\}$ (green and orange lines), such that we have (with $N + 1 \equiv 1$)

$$\begin{aligned} (V_j, w_j)(t) &= (V_{j+1}, w_{j+1})(t + \tau_1) && \text{if } j = 1, 3 \\ (V_j, w_j)(t) &= (V_{j+1}, w_{j+1})(t + \tau_2) && \text{if } j = 2, 4 \end{aligned}$$

with $\tau_1 < \tau_2$ and $\tau_1 + \tau_2 = T/2$. Hence, the ensemble splits in two groups of two units, each, where the inter-spike interval τ_1 for two units in the same group is smaller than the inter-spike interval τ_2 for two consecutive units from opposite groups, as for the Active Rotator model.

2 Note that in the diagram, the Regions I, II, and IV seem to meet at $\simeq (-0.025, 0.2)$. This is in fact a graphical artifact from the finite resolution in κ and ϵ. As for the Active Rotator model, numerical evidence suggests that Region II forms a increasingly narrow band between Regions I and IV so that periodic two-cluster states are always unstable sufficiently close to the double-heteroclinic bifurcation because they inherit their (splitting) instability from the Σ^i.

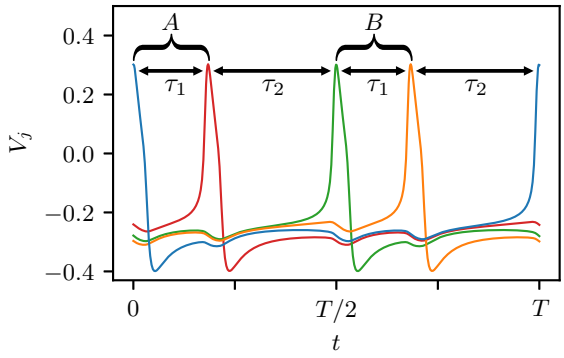

Figure 41: Exemplary voltage time series for a broken-symmetry state of four Morris-Lecar neurons with period $T \simeq 60.3$ for parameters $\zeta = 0.6$ and $\kappa = -0.152$ in Figure 40.

To summarize, in contrast to Figure 30 of Chapter 7, this time we have a regime (Region V) in which *both*, two-cluster states and the splay state, are stable while in Regions III and VI, either the splay state or the periodic two-cluster states are unstable. Comparing with Figure 28, we see that the results match Panel (c) of that figure so that the transfer of stability between splay and periodic two-cluster states is indeed nonlocal and is qualitatively captured by the generalized Active Rotator model.

8.4 CONCLUSION

As for Active Rotators, (clustered) splay states and periodic two-cluster states in ensembles of repulsively coupled Morris-Lecar neurons are not the only possible periodic solutions. In fact, they are not even the only potentially stable limit cycles. Variations again include imperfect clustered splays where the clusters are of unequal size and thus the splay nature is only approximate. Asymmetric periodic two-cluster states can also be observed. This is not surprising, considering that both, splay states and symmetric two-cluster states, are hyperbolic so that unequal cluster sizes in a reduced description in terms of cluster coordinates can be treated by considering weakly heterogeneous ensemble of units, as for Active Rotators. However, the two-dimensional nature of the Morris-Lecar model allows for additional states that are not compatible with systems of one-dimensional units like the AR-models (2.5) and (2.6). As mentioned in Section 8.2.2, one can observe periodic two-cluster states in which one cluster spikes while the other one always stays close to $(V^{\mathrm{s}}, w^{\mathrm{s}})$ in state space in subthreshould oscillations which in the generalized AR-model would correspond to, e. g., a *libration* in which the two clusters oscillate within two small segments of $\mathbb{S}^1$ rather than traversing the entirety of $\mathbb{S}^1$. Such behavior is forbidden for ARs by the gradient nature of (2.6). Another (stable) periodic state which we did not mention here consists of two singletons, spiking in anti-phase while the remainder of the ensemble forms a cluster which stays close

to $(V^{\mathrm{s}}, w^{\mathrm{s}})$. In this case, the two spiking units act as "shepherds" that keep the "flock" of the remaining $N-2$ units in place. Again, one could call such solutions "Chimera-like" states in the broader sense of [ZP17] since again, an ensemble of identical elements splits in two groups which show qualitatively different behavior: The two "shepherds" spike while the rest of the ensemble stays in a subthreshold regime in the lingo of neuroscience. We note that we only observed such states for up to an ensemble size of $N = 10$ units. The existence of such more exotic periodic solutions illustrates the limitation of the angular models (2.5) and (2.6) when it comes to classifying the plethora of possible periodic states in ensembles of general class I excitable units. Studying such more exotic (stable) periodic solutions in depth is beyond the scope of this thesis where we focused on splay states and two-cluster states.

The main result of this chapter is the discussion of the local transfer of stability for Morris-Lecar neurons between splay states and two-cluster states with focus on the case of $N = 4$ units which closely resembles the results for Active Rotators in Chapter 7. This remarkable results implies that the generalized Active Rotator model (2.6) with a controllable perturbation term as in (7.25) is able to serve at least as a qualitative description of this transfer of stability for ensembles of higher-dimensional class I excitable elements. In particular, splay states and periodic two-cluster states interchange (in)stability via broken-symmetry states which, in the simplest case, emerge or vanish in pitchfork bifurcations. At least for $N = 4$, these broken-symmetry states look exactly like those for the angular model: the four units form two groups of two units each so that inter-spike intervals between consecutively spiking neurons differ with respect to whether the two units belong to the same cluster or not. This is reasonable since in order to act as "mediators" between splays and two-cluster states, the broken-symmetry states must vary continuously in their shape between these two rather different types of solutions.

Finally, we note again that in this chapter, we only considered ensembles of four units which was mostly due to the computational problem of having to avoid clustered solutions in our search for pure splay states. In any case, we assume that a more in-depth investigation of larger ensembles would be a worthwhile future endeavor, not least to look out for broken-symmetry states and their role in the (de)stabilization of splays and two-cluster states in these cases.

With this, we end our discussion of coupled Morris-Lecar neurons and Part III of this thesis.

Part IV

CONCLUSION

Every conclusion drawn from our observation is, as a rule, premature, for behind the phenomena which we see clearly are other phenomena that we see indistinctly, and perhaps behind these latter, yet others which we do not see at all.

— Gustave Le Bon [LeB60]

9

CONCLUSION

Hic et ubique.

Synchronization phenomena and, in general, complex collective dynamics of oscillatory systems are so ubiquitous in nature [Buc38; Wal69; Ric+96; Yan+14] and technology [WS94; Str+05; FNP08] that their study has become its own field within the general theory of nonlinear dynamics [PRK03] and neuroscience [Izh10; HI12]. However, not every element that can potentially display periodic activity is necessarily doing so by itself but often has to receive a certain stimulus to switch from a state of rest to a state of (periodic) activity. Arguably *the* prime example for such an occurrence are neurons, which generally only produce some kind of nervous signal, if sufficiently stimulated; a property known in the field as *excitability*.

The main objective of this thesis was the study of the collective dynamics of identical class I excitable elements. Class I excitability of neurons translates to them being close to a Saddle-Node Bifurcation on an Invariant Circle (SNIC) as a dynamical system [Izh10]. Uncoupled, such elements give rise to a stable synchronous state of rest and, while attractive coupling between them tends to simply further increase the stability of this state of rest, nontrivial dynamics can only be expected if at least some of the units are coupled sufficiently repulsively, resulting in a destabilization of the synchronous fixed point [TZT08; DKN13; TZ14; ZT16]. In order to investigate the emerging dynamics for excitable elements, we focused in Parts I and II of this thesis on ensembles of Active Rotators which can be regarded in some sense as a dimensionally reduced description of more complex higher-dimensional excitable units, restricting attention to the dynamics on the invariant circle of the single class I excitable element. More precisely, they serve as a *local model* in the sense of [HI12] for higher-dimensional units.

The classic Active Rotator model, introduced by Shinomoto and Kuramoto in [SK86b] as a toy model for collective activity in, e. g., excitable media, in its simplest form (i. e., identical elements with no noise) falls into the class of Watanabe-Strogatz integrable systems. For this reason, its dynamics is highly degenerate and so cannot serve as an accurate description for the collective dynamics of general excitable elements. The question thus arises what we can learn from the classic model about systems that might be close to being WS-integrable and thus might be accessible to perturbation methods, applied to the model from Shinomoto and Kuramoto. For this, we focused on the case of on-site perturbations, in other words, perturbations that generalize the

single Active Rotator from obeying the Adler equation to cases that involve higher order Fourier modes in the dynamics of each Rotator.

Anticipating one of our main results, we showed rigorously for all WS-integrable systems where the involved common fields are functions of the Kuramoto order parameter, under which conditions they do not just give rise to a continuous family of periodic orbits but that the union of these orbits is equipped with the additional geometric structure of a Normally Attracting Invariant Manifold (NAIM). While this result may at first seem to be only of purely mathematical interest, its consequences are far-reaching. NAIMs are robust under sufficiently small perturbations and so persist if we, e. g., introduce higher Fourier modes in the on-site dynamics, i. e., if we generalize the notion of the Active Rotator to account for more complicated angular dynamics of each individual element. Since in particular, such terms make the full system nonintegrable, the manifold is indeed not just an artifact of WS-integrability but a general feature of such systems and in particular, for ensembles of generalized Active Rotators.

Different coupling terms. Adding higher order Fourier modes to the on-site dynamics of the classic model is only one way to generalize it. Other maybe more popular generalizations involve changes in the *coupling term*, see [EK09; LZL12; Lai18; FOW21] and one might argue that these scenarios are more relevant for practical purposes: At least for coupled oscillators and weak coupling, there always exists a local model in terms of phase oscillators so that, with qualifications, one can restrict one's attention to this case and focus on the effects of different coupling terms which may mimic, e. g., the synaptic coupling between neurons, a coupling that works considerably different from the arguably simplistic sinusoidal coupling term that we were dealing with. However, the existence of the NAIM is not restricted to the special case of Active Rotator models under sinusoidal coupling that we studied. Since NAIMs are robust under *any* small perturbation, introducing such perturbations in the coupling term still results in the persistence of this manifold. Adding, e. g., higher order Fourier modes to the sinusoidal coupling term is thus not fundamentally different from perturbing the on-site dynamics as long as the amplitudes of these modes are sufficiently small. We therefore expect no fundamentally different outcome for such systems of more complicated coupling terms. In particular, our results on the existence of splay states hold in general because their proofs did not rely on the fact that the perturbation term is on-site.

WS-variables. In order to develop suitable methods to investigate systems of generalized Active Rotators that are close to being WS-integrable, we started in Chapter 4 by establishing a set of coordinates on the ordered torus (to which we could without loss of generality restrict our attention for the case at hand of identical elements) in terms of Möbius group parameters and cross-ratios. This was done by proving the existence of a diffeomorphism between that ordered torus and the product space, defined by the ranges of the respective group parameters and cross-ratios. A common approach to apply WS-theory is based on embedding the phase space $\mathbb{T}^N$ in a higher-dimensional product space $\mathbb{D} \times \mathbb{S}^1 \times \mathbb{T}^N$

with variables $(\alpha, \psi, \theta_1, \ldots, \theta_N)$ where $\theta_j = \text{const.}$ for all $j = 1, \ldots, N$. This introduces three additional degrees of freedom in the description of a given system which has to be accounted for by a suitable choice of, e. g., initial conditions for the WS-equations [WS94]. On the other hand, we chose an approach which establishes a unique correspondence between angular variables on the one hand and WS-variables on the other. In particular, by doing so, we did not have to deal with the "gauge" freedom that is present for the usual approach. Describing arbitrary systems of coupled ODEs for angular variables in terms of WS-variables is than easily done by virtue of the found diffeomorphism which is at least not as straight forward for the common embedding approach.

Splays and two-cluster states as prominent periodic solutions.

Since in particular for large ensembles of coupled Rotators, one has to expect an abundance of possible periodic solutions, it is a necessity to choose a sensible subset of periodic orbits to focus on which should be distinct enough in order to cover a wide range of possible asymptotic dynamics for the system at hand. Numerical experiments reveal that two types of periodic solutions play a prominent role as possible stable limit cycles for ensembles of identical Active Rotators: periodic two-cluster states and (clustered) splay states.

Periodic two-cluster states.

Periodic two-cluster states, although themselves clustered splay states, stand out from other clustered splays (i. e., those that are composed of at least three clusters) since their dynamics can generally not be captured through WS-theory. In Chapter 5, we therefore studied such solutions from a more heuristic point of view in the setting for generalized Active Rotators. We discussed the two basic bifurcation scenarios that yield periodic two-cluster solutions in a reduced description of cluster coordinates. We found that they emerge either through two heteroclinic bifurcations or two SNICs, which occur simultaneously in the case of symmetric solutions where both clusters are of equal size, and in consecutive order in the case of asymmetric states. An important result is that periodic two-cluster states do not emerge in the THB of the synchronous state of rest while *how* they emerge is still related to this fixed point bifurcation. In particular, for the symmetric case, the bifurcation of the synchronous fixed point is accompanied by either a sub- or supercritical pitchfork bifurcation that also includes two two-cluster saddles. We also gave a criterion for the criticality of this bifurcation. Even though criticality of the pitchfork does not immediately determine whether periodic two-cluster states are born in double-heteroclinic bifurcations or double-SNICs, it can be used to rule out the latter.

We then showed that for general WS-integrable systems of identical elements, symmetric two-cluster states must be neutrally stable with respect to splitting perturbations while asymmetric two-cluster states are always composed of one stable and one unstable cluster. This statement, which is closely related to a similar finding for ensembles of Kuramoto oscillators under common noise [Gon+19], supports observations from numerical experiments that symmetric two-cluster states are part of the aforementioned continuous family of periodic orbits if that family exist. Surprisingly enough though, these solutions can exist and are then neutrally stable even when no such family of orbits is present.

On the other hand, the family of orbits may also exist without the presence of the periodic two-cluster states. In this case, the two-cluster states are replaced by a heteroclinic cycle. As another result, we could conclude that the exponential stability of symmetric two-cluster states against splitting perturbations for ensembles of generalized Active Rotators directly depends on the choice of higher order Fourier modes in their on-site dynamics which goes along with a generic change of stability if the signs of these higher order terms change. On the other hand, for asymmetric two-cluster states, we described how the regimes of stability for these states in parameter space are nested in each other so that particularly, in order for a given periodic two-cluster state of fixed cluster size ratio, coupling must be chosen sufficiently repulsive in order to stabilize the state.

The splay state and the continuum.

The second prominent possible type of attractor for ensembles of (generalized) Active Rotators is the (clustered) splay state and its imperfect[1] variations. Previous numerical evidence suggested that this periodic solutions for the WS-integrable case emerges when the synchronous state of rest ceases to be asymptotically stable and that it is just one solution in a whole continuum of orbits [ZT16]. We thus conducted an exhaustive investigation of this continuum in Chapter 6 by means of the tools, introduced and developed in Chapter 3 and Chapter 4. For this, we studied the above-mentioned class of WS-integrable systems for which the common fields in the equations of motion only depend on the Kuramoto order parameter. We were then able to show rigorously that under certain simple conditions, systems of this type possess a continuous family of periodic orbits and moreover, that the union of these orbits is equipped with the desired NAIM-structure. For this, we first showed that the order parameter can be approximated by one of the Möbius group parameters in C^1-norm on those level sets that lie close to the level set of uniform distributions. Using this approximation, studying the continuum can be drastically simplified by truncating higher order terms in the equations of motion, effectively reducing the problem of finding periodic orbits to determining stable fixed point in one of the truncated equations. For this truncated system, we could then show directly that the found periodic orbits form a NAIM. Using the persistence theorem for NAIMs then guarantees the existence of the continuum and subsequently normal hyperbolicity of its union also for the full system. Using a result from the theory of equivariance of ODEs under finite group actions, it could then be shown, that the periodic solution in the level set of uniform distributions must be a splay state. Since the classic Shinomoto-Kuramoto model falls in the studied class of WS-integrable systems, existence and normal hyperbolicity for this model become a simple application of the results above. In particular, we could prove that for the classic model, the continuum indeed emerges exactly when the synchronous fixed point of the system becomes unstable so that the transcritical bifurcation of the synchronous state of rest is indeed also homoclinic in nature, validat-

1 I. e., variations where the individual clusters differ in size.

ing the observations from [ZT16]. As an additional result, it follows that a similar family of periodic orbits emerges for attractive coupling but that this family is normally repelling and thus unstable. Applying the same results to the case where the Shinomoto-Kuramoto elements become oscillating on their own further reveals the existence of yet another family of orbits with the same normal hyperbolicity property which remarkably changes stability when the coupling constant changes its sign but otherwise exists for all coupling strengths. We note that the occurrence of splay states in WS-integrable systems has been shown before for different setups [AGM91; Mir94].

Handling perturbations with the averaging principle.

Introducing higher order Fourier modes in Chapter 7, we could make use of the normal hyperbolicity of the continuum to develop a framework for determining which orbits of the continuum become robust for a given perturbation of the WS-integrable model by means of averaging theory. As already mentioned, we focused on perturbations that leave the units of the ensemble identical and perturb them in their on-site dynamics, even though this is not a necessary condition for applying averaging methods in general. For this, we could build on the results of the preceding chapter by restricting attention to the dynamics on the NAIM. While the periodic orbits that composed this NAIM in the WS-integrable case are neutrally stable and are therefore not readily robust, the manifold itself is, so that it makes sense to study the dynamics on it even when the system becomes nonintegrable. Then, for all initial states sufficiently close by, the corresponding trajectories will essentially travel along this manifold after a short initial episode of exponentially fast convergence to it. The objective is then to determine which orbits "survive" the introduction of perturbation terms. To achieve this, we used a classic result from averaging theory which allows to compute, based on the degenerate dynamics of the integrable model, the time-averaged dynamics of the now slowly varying cross-ratios for any initial state on the NAIM. Determining the averaged vector field is done by integrating the projection of the perturbation normal to the level sets of constant cross-ratios along a given orbit of the continuum. If the integral vanishes, there exists (with qualifications) a corresponding orbit with cross-ratios close to those of the orbit over which was averaged. This orbit for the perturbed vector field can then be viewed as the robust survivor of the continuum in the new perturbed system. We stress again that this approach relies heavily on the fact that the continuum in the WS-case forms a NAIM. If this was not the case, the introduction of perturbations might very well leave no remnants of the continuum behind to which restricting the dynamics and averaging would make sense. We also stress that the criterion only works if the found fixed point of the averaged dynamics is hyperbolic. Whether this is the case depends on the specific setup but we conjecture that it is the case for generic systems and on-site perturbation functions h.

Robust splay states.

Assuming that the conjecture above holds, we proceeded by showing that the splay state, which always exists for the investigated class of systems (cf. [Mir94] for a related result on the existence of splay states), persists for smooth h. Hence, splay states are in particular general

features in ensembles of identical generalized Active Rotators. Their stability directly depends on the form of h. This also implies that such states generally change their stability if the sign of the perturbation parameter changes which is corroborated by numerical results on the stability of splay states. However, in contrast to two-cluster states, the stability of splay states also depends on the size of the ensemble. While we saw for four Rotators that splay states can be made asymptotically stable by changing the sign of the perturbation parameter ϵ, the picture becomes more complicated for larger ensembles. Remarkably, we could observe how for even ensemble sizes, the stabilization or destabilization of splay states involves what we call broken-symmetry states which are generally hybrids between splay states and clustered splay states and are essentially what is known as *generalized splay states* in the literature in disguise [Ber+21]. Even though for systems of just four Active Rotators, broken-symmetry states can be asymptotically stable, they suffer from the same problem as splay states for larger ensembles: Their Floquet multipliers are not degenerate and thus, their stability depends explicitly on the ensemble size. Nevertheless, they stand out from the rest of the continuum by their spatio-temporal symmetry as a third vital class of periodic solutions, on par with the splay state and periodic two-cluster states.

Broken-symmetry states.

Another consequence[2] from the averaging principle is that one can always control a given periodic orbit (i. e., make it hyperbolic and thus robust) by choosing a suitable perturbation term. While making the orbit hyperbolic is easily done, it stands to question whether one can choose h to also make it exponentially stable. Although this seems reasonable, given the fact that we have an infinite-dimensional space of possible perturbation terms from which we only need to choose a finite linear combination in order to do the trick, this is by far not a trivial statement and remains an open problem. In any case, this is not just a gimmick without practical implications. We made excessive use of it in our subsequent study of four Active Rotators because it allows to "unfold" the "nonlocal transfer of stability" between the splay state and the periodic two-cluster states that is present in the classic Active Rotator model. Studying this unfolded general interplay that now involves the splay state, broken-symmetry states, and two-cluster states did not just serve as a proof of concept for the averaging method (which is in good agreement with the numerical results) but also illuminates how general systems of repulsively coupled class I excitable elements interact.

Controlling orbits and the transfer of stability between splay states and two-cluster states.

We already noticed that continuous families of periodic solutions are a common occurrence in WS-integrable systems since continuously varying cross-ratios lets one not just move continuously through the invariant level sets of the cross-ratio function but also varies the vector field from level set to level set. Remarkably enough, families of neutrally stable periodic solutions have been observed and investigated for systems of random Janus oscillator networks [Per+20] which features

Families of periodic orbits and clustering in other settings.

2 Again assuming the conjecture on generic hyperbolicity.

what the authors therein call "breathing standing wave solutions". One major difference in their work is that the single units of the ensemble are distinguishable so that the system cannot be described within the Watanabe-Strogatz framework but instead with the Ott-Antonsen ansatz. This remarkable result illustrates that families of periodic solutions are not just a phenomenon in WS-theory. However, the nature of the periodic solutions in [Per+20] is of a rather different kind since they occur as solutions to equations that describe the system's order parameter rather than the single angular variables so that it is not clear whether, e. g., the method of averaging could be used in order to investigate random networks of Janus oscillator.

Clustering in ensembles of phase oscillators is a common phenomenon in numerous setups and with various types of coupling , cf. [HMM93; Oku93; Ash+07; LY12], to name a few and is, e. g., necessary for the existence of Chimera states [SK15]. However, a crucial difference between Kuramoto-type phase oscillators and Active Rotators lies in the fact that the former show homogeneous evolution in $\mathbb{S}^1$ while for the latter, the angular velocity $\dot{\phi}$ is intrinsically coordinate-dependent. As a result, in case of global coupling, the symmetry of the ensemble of identical phase oscillators is higher than that of ensembles of identical ARs. While both systems are equivariant under permutations, the dynamics of the former is additionally invariant with respect to shifts of all angles by an arbitrary constant, while the latter model lacks this equivariance. This might explain why we did not observe persistent heteroclinic networks (apart from those in the two-cluster subspace) in our numerical studies, while they are characteristic for angular oscillators with higher-order Fourier terms [HMM93; Ash+07; ABM08]. Instead, as demonstrated in Chapter 5 and Chapter 7, introducing such terms leads to the birth of collective oscillations via the formation of structurally unstable hetero- or homoclinic connections. The splitting stability of the resulting periodic states is directly linked to these higher order terms.

Limitations.

A word of caution is at hand about the limitation of our results, so far. Another common generalization of the classic identical Active Rotator model (which was already studied by Shinomoto and Kuramoto) is to consider heterogeneous ensembles, i. e., ensembles of nonidentical elements. There exist results on weakly heterogeneous perturbations to WS-integrable systems [PR08; PR11; VRP16] not to mention the Ott-Antonsen ansatz as an alternative approach to handle heterogeneous ensembles of angular variables [OA08; Gol+18; Gol19; Tyu+18; Tyu+19]. We, on the other hand, are to some extent confined to studying perturbations that leave the units identical. If the ensemble becomes heterogeneous, the dynamics is generally not any longer confined to the ordered torus. But this ordered torus is crucial to establishing the WS-variables as equivalent coordinates to the angular coordinates in which the dynamics are usually written. While the NAIM should still persist *locally* even when the units become distinguishable, it becomes in this case important to know *how far* the NAIM extends in the phase space and what can be said about its boundary and at least for $N = 4$ units,

we saw that multiple copies of $\mathcal{M}$ can be joined along clustered periodic orbits such that the global NAIM intersects itself. How the manifold in the ordered torus and its various copies in the other subspaces of fixed cyclic order are connected along their boundaries for general N is yet not fully understood. In any case, we believe that looking for NAIMs and applying the averaging principle could also be important techniques for the study of (weakly) nonidentical Active Rotators because in this case, any state with initial condition in the ordered torus should at least for some amount of time stay there.

Noise.

Another question that we did not address in this work is what happens to the continuum if we consider noisy systems. Noise affects the continuum since the cross-ratios are no longer conserved quantities and hence, the system jumps between the $\mathcal{C}_{\boldsymbol{\lambda}} = \mathcal{M} \cap \mathcal{L}_{\boldsymbol{\lambda}}(\boldsymbol{\Lambda})$. However, at least as long as the noise is not too strong, it should not dramatically effect the dynamics on the NAIM for short times: For the classic model, instead of being restricted to one of the infinitely many orbits of the manifold, the state of the system will randomly move between level sets and thus orbits. But since the vector field changes only slightly between neighboring level sets, the dynamics will look rather similar. Only over long times should a considerable change in the dynamics of the state be noticeable. For the generalized model, and again under weak noise, the splay state and periodic two-cluster state stay potential attractors as hyperbolic orbits in which case weak noise will lead to random fluctuations of the state around these orbits. Both, the case of nonidentical elements and that of noisy systems, pose limitations with respect to observing the continuum and NAIM in experimental setups. Already the original work by Watanabe and Strogatz on Josephson junctions dealt with the highly idealized model of identical junctions in the overdamped limit. Since one has to expect both, noise and heterogeneity, in practice, it is not clear in what respect the degenerate dynamics that were discussed here can be observed in experiments. For this, a more general approach is necessary that also incorporates, e. g., the results from [VRP16].

The connection between Active Rotators and Morris-Lecar neurons.

Phase oscillators emerge in the study of coupled general oscillators via phase reduction under the assumption of weak coupling between units. Since class I excitable elements are characterized by the existence of an invariant circle, the (generalized) Active Rotator model suggests itself as a similar reduction for such elements by restricting attention to the dynamics on the invariant circle, i. e., it serves as a local model for higher-dimensional excitable systems. Of course, any ensemble of general higher-dimensional class I excitable units will be far from being WS-integrable but on the other hand, the results from Chapter 7 (in particular on the transfer of stability) suggest that the found dynamics are robust features of ensembles of Active Rotators even for fairly large perturbations away from the integrable case so that it is reasonable to expect compatible dynamics in higher-dimensional systems. To further investigate the general dynamics of excitable elements, in Part III of this thesis, we studied ensembles of Morris-Lecar neurons, repulsively coupled via their mutual membrane voltage differences. Even though

this membrane coupling is not an exact equivalent of the repulsive coupling between ARs because it acts only in the voltage variable, this setup looks sufficiently similar to the angular model to test how our results from Part II generalize to somewhat more realistic models.[3]

Indeed, regarding periodic two-cluster states, we found that these solutions emerge in double-heteroclinic bifurcations that we already observed for the angular model. As mentioned before, this is not surprising given that these clustered solutions can be written in terms of cluster coordinates such that we are effectively dealing with two coupled excitable elements for which it was rigorously shown before that double-heteroclinic bifurcations yield periodic solutions under weak coupling if both neurons are close to their respective SNIC [BM13]. While we did not observe any double-SNICs, this can be explained by the fact that the occurring pitchfork bifurcations of two-cluster saddles and the synchronous fixed point were always subcritical so that SNICs simply cannot occur. Whether the pitchforks can be made supercritical so that one might observe a double-SNIC is hard to say. The dynamics of a single Morris-Lecar neuron depends intimately on a plethora of parameters so that it is an art to tune these parameters to yield the desired behavior [Tsu+06]. On the other hand, we observed, again for a minimal example of four units to avoid clustering in the numerical experiments, splay states which emerge in a THB of the synchronous state of rest. Moreover, we observed a local transfer of stability between periodic two-cluster states and splay states by means of broken-symmetry states, akin to what we found in Chapter 7 for Active Rotators. This finding is in so far remarkable as that it indicates that such transfers are indeed general features and not artifacts of the nature of the Active Rotator model.[4] It is therefore not far fetched to conjecture that broken-symmetry states equally exist for larger even numbered ensembles of Morris-Lecar neurons, just as we observed them for the Active Rotator model.

Generalizations and outlook.

In our proof for the existence of the NAIM, we made use of the fact that the Kuramoto order parameter can under certain conditions be approximated by one of the group parameters of the group of Möbius transformations. The order parameter naturally occurs for systems of coupled Active Rotators due to the first order sinusoidal coupling term. However, since the effects of higher order coupling terms in oscillatory systems are an ongoing subject of interest from a theoretical [Dai92; SOR11; GP19; Li+19; XS21] as well as from an experimental perspective [KZH05; Gol+11; Gol+13], it might be worthwhile to further investigate the implications of more complicated types of coupling than the purely sinusoidal one beyond our perturbative results. We note that splay states and corresponding continua of periodic orbits have for ex-

3 We stress that the voltage-coupled Morris-Lecar neurons are still by far not a realistic model for actual neural networks because this is not how neurons are connected in reality. However, at least to some extend it might be considered more realistic than the AR-model by virtue of the fact that the Morris-Lecar neuron is modeled after some types of real neurons.

4 They are, however, the direct result of dealing with identical elements.

ample been observed and investigated in ensembles of pulse-coupled theta neurons, which are equivalent to Active Rotators [Lai18]. This finding can be understood in terms of the WS-framework, since this system is also WS-integrable. It has also been shown that integrability can under certain circumstances (e. g., pure higher order harmonic coupling, see [GP19]) be extended to systems that involve different types of coupling than the simple sinusoidal one. One might thus ask what happens if we consider systems for which the common fields in the equations of motion depend on the higher order generalizations of the Kuramoto parameter, known as Kuramoto-Daido parameters. Whether the arguments, presented here, also work for these more general cases is a matter of future research so that for now we can only speculate: Most of the methods and arguments that we presented in this work are fairly general and should work in different settings, as well. In particular, the averaging method should be readily applicable because it does not actually depend on the specific type of dynamics of the system. As longs as there exists a NAIM of periodic orbits, the averaging principle could be applied fruitfully to the dynamics on that manifold. The problem then really lies in whether one can show that the continuous family of periodic orbits for WS-integrable systems yields a NAIM in the first place. Here, our argument depended heavily on the approximation, mentioned above. Whether a similar approximation holds for general Kuramoto-Daido parameters is an intriguing question for future work. Even bolder would be the ambition to investigate under which conditions the continuous families of periodic orbits, which are a common occurrence within the context of WS-integrability, are equipped with the structure of a normally hyperbolic or even attracting invariant manifold. Whenever this is the case, perturbing the equations of motion could in general be dealt with by investigating the dynamics on that manifold, for example by means of the averaging principle.

Finally, it is also tantalizing to speculate whether or not such a manifold is present for models like the coupled Morris-Lecar neurons. But this model is far from being integrable so to assume the existence of such a structure for this model is bold, to say the least. If it does not exist, it means that the NAIM for the case of ARs is not really essential to understand the dynamics of repulsively coupled class I excitable units, however useful it is for the systematic study of coupled Active Rotators. On the other hand, there, the NAIM emerged together with the splay state in the transcritical homoclinic bifurcation of the synchronous state of rest just as the splay state for the Morris-Lecar neurons emerged in a THB. The question is then how exactly the network of homoclinic orbits at this bifurcation and the NAIM are related. If one could figure out what made the THB for coupled Active Rotators in that respect so special, one might also hold the answer to whether or not a NAIM exists for more complicated systems of repulsively coupled excitable elements.

Part V

APPENDIX

Do not worry about your difficulties in Mathematics. I can assure you mine are still greater.

— Albert Einstein [Ein43]

A

THE MÖBIUS GROUP

In this appendix, we discuss the group properties of the Möbius group $\mathcal{G}$. Recall that a group $(G, \circ)$ consists of a set G and a group operation $\circ : G \times G \to G$ such that (i) there exists an identity element $e \in G$ with $e \circ g = g \circ e = g$ for all $g \in G$, (ii), for each $g \in G$, there exists an inverse element g^{-1} such that $g \circ g^{-1} = g^{-1} \circ g = e$, and (iii) the group operation is associative, i. e., $f \circ (g \circ h) = (f \circ g) \circ h$ for all $f, g, h \in G$. When there is no ambiguity with respect to what the group operation looks like, we also write G instead of $(G, \circ)$ to denote the group.

For the definition of (real and complex) Lie groups and the fact that $\mathcal{G}$ is a Lie group, we refer to [Hal15] and [Ols10], respectively.

THE GROUP OPERATION IN $\mathcal{G}$ We start by writing down an explicit formula for the group operation in terms of the group parameters α and ψ of $\mathcal{G}$. Recall the definition (4.2) of a Möbius transformation

$$G_{\alpha,\psi}(w) \coloneqq \frac{\alpha + \mathrm{e}^{i\psi} w}{1 + \bar{\alpha}\mathrm{e}^{i\psi} w} \tag{4.2}$$

with $\alpha \in \mathbb{D}$ and $\psi \in \mathbb{S}^1$ for every $w \in \partial\mathbb{D}$. From this, we demand for every two Möbius maps $G_{\alpha,\psi}$ and $G_{\alpha',\psi'}$ that the composition $G_{\alpha,\psi} \circ G_{\alpha',\psi'}$ can be equally written as $G_{\alpha'',\psi''}$ for some $\alpha'' \in \mathbb{D}$ and $\psi'' \in \mathbb{S}^1$. We compute

$$\begin{aligned}
G_{\alpha,\psi} \circ G_{\alpha',\psi'}(w) &= G_{\alpha,\psi}\left(\frac{\alpha' + \mathrm{e}^{i\psi'} w}{1 + \bar{\alpha}'\mathrm{e}^{i\psi'} w}\right) \\
&= \frac{\alpha + \mathrm{e}^{i\psi}\frac{\alpha' + \mathrm{e}^{i\psi'} w}{1 + \bar{\alpha}'\mathrm{e}^{i\psi'} w}}{1 + \bar{\alpha}\mathrm{e}^{i\psi}\frac{\alpha' + \mathrm{e}^{i\psi'} w}{1 + \bar{\alpha}'\mathrm{e}^{i\psi'} w}} \\
&= \frac{\alpha(1 + \bar{\alpha}'\mathrm{e}^{i\psi'} w) + \mathrm{e}^{i\psi}(\alpha' + \mathrm{e}^{i\psi'} w)}{1 + \bar{\alpha}'\mathrm{e}^{i\psi'} w + \bar{\alpha}\mathrm{e}^{i\psi}(\alpha' + \mathrm{e}^{i\psi'} w)} \\
&= \frac{\alpha + \mathrm{e}^{i\psi}\alpha' + (\alpha\bar{\alpha}'\mathrm{e}^{i\psi'} + \mathrm{e}^{i\psi}\mathrm{e}^{i\psi'})w}{1 + \bar{\alpha}\mathrm{e}^{i\psi}\alpha' + (\bar{\alpha}'\mathrm{e}^{i\psi'} + \bar{\alpha}\mathrm{e}^{i\psi}\mathrm{e}^{i\psi'})w} \\
&= \frac{\frac{\alpha + \mathrm{e}^{i\psi}\alpha'}{1 + \bar{\alpha}\mathrm{e}^{i\psi}\alpha'} + \frac{1 + \alpha\mathrm{e}^{-i\psi}\bar{\alpha}'}{1 + \bar{\alpha}\mathrm{e}^{i\psi}\alpha'}\mathrm{e}^{i\psi}\mathrm{e}^{i\psi'} w}{1 + \frac{\bar{\alpha} + \mathrm{e}^{-i\psi}\bar{\alpha}'}{1 + \alpha\mathrm{e}^{-i\psi}\bar{\alpha}'}\frac{1 + \alpha\mathrm{e}^{-i\psi}\bar{\alpha}'}{1 + \bar{\alpha}\mathrm{e}^{i\psi}\alpha'}\mathrm{e}^{i\psi}\mathrm{e}^{i\psi'} w} \\
&\overset{!}{=} G_{\alpha'',\psi''}(w).
\end{aligned}$$

Extending the domain of $G_{\alpha,\psi}$ from $\partial\mathbb{D}$ to $\mathbb{C}$, we set

$$\alpha'' = G_{\alpha,\psi}(\alpha') \quad \text{and} \quad \mathrm{e}^{i\psi''} = \frac{1+\alpha\mathrm{e}^{-i\psi}\bar{\alpha}'}{1+\bar{\alpha}\mathrm{e}^{i\psi}\alpha'}\mathrm{e}^{i\psi}\mathrm{e}^{i\psi'}. \tag{A.1}$$

Next, we need to verify that $\psi'' \in \mathbb{S}^1$ and $\alpha'' \in \mathbb{D}$. We find

$$|\mathrm{e}^{i\psi''}|^2 = \frac{1+\alpha\mathrm{e}^{-i\psi}\bar{\alpha}'}{1+\bar{\alpha}\mathrm{e}^{i\psi}\alpha'}\,\frac{1+\bar{\alpha}\mathrm{e}^{i\psi}\alpha'}{1+\alpha\mathrm{e}^{-i\psi}\bar{\alpha}'} = 1$$

and

$$|\alpha''|^2 = \frac{\alpha+\mathrm{e}^{i\psi}\alpha'}{1+\bar{\alpha}\mathrm{e}^{i\psi}\alpha'}\,\frac{\bar{\alpha}+\mathrm{e}^{-i\psi}\bar{\alpha}'}{1+\alpha\mathrm{e}^{-i\psi}\bar{\alpha}'} = \frac{|\alpha|^2+|\alpha'|^2+\alpha\mathrm{e}^{-i\psi}\bar{\alpha}'+\bar{\alpha}\mathrm{e}^{i\psi}\alpha'}{1+|\alpha|^2|\alpha'|^2+\alpha\mathrm{e}^{-i\psi}\bar{\alpha}'+\bar{\alpha}\mathrm{e}^{i\psi}\alpha'} < 1$$

because of

$$\begin{aligned} & |\alpha|^2+|\alpha'|^2 < 1+|\alpha|^2|\alpha'|^2 \\ \Leftrightarrow \quad & |\alpha'|^2(1-|\alpha|^2) < 1-|\alpha|^2 \\ \Leftrightarrow \quad & |\alpha'|^2 < 1. \end{aligned}$$

Hence, the composition rules (A.1) are well-defined.

GROUP PROPERTIES OF $\mathcal{G}$ Next, we check the group properties, i. e., we confirm the existence of the identity element, inverse elements, and the associative property of the group operation. The first two can be readily derived from the definition of $G_{\alpha,\psi}$ and the composition rule (A.1). For this, we note first that $G_{\alpha,\psi} = G_{\alpha,1} \circ G_{0,\psi}$ for which we find $G_{\alpha,1}^{-1} = G_{-\alpha,1}$ and $G_{0,\psi}^{-1} = G_{0,-\psi}$. Hence, with the neutral element e being the identity map $\mathrm{id} : w \mapsto w$, we have

$$\begin{aligned} e &= \mathrm{id} = G_{0,0} \\ G_{\alpha,\psi}^{-1} &= (G_{\alpha,1} \circ G_{0,\psi})^{-1} = G_{0,\psi}^{-1} \circ G_{\alpha,1}^{-1} = G_{0,-\psi} \circ G_{-\alpha,1}. \end{aligned}$$

Thus, we have

$$\begin{aligned} e(w) &= w \\ G_{\alpha,\psi}^{-1}(w) &= \mathrm{e}^{-i\psi}\frac{-\alpha+w}{1-\bar{\alpha}w}. \end{aligned}$$

The associative property follows immediately from the associative property for compositions of functions.

B

THE TRANSCRITICAL HOMOCLINIC BIFURCATION OF Δ^{s}

In this appendix, we derive implicit expressions in the system parameters ω, ϵ, and κ_0 for the THB of the synchronous fixed point Δ^{s} to study the dependence of κ_0 on ω and ϵ. At Δ^{s}, we have $\phi_j = \phi_k$ and $\dot{\phi}_j = 0$ for all $j, k \in \{1, \ldots, N\}$ and the Jacobian of the vector field in (2.4) is highly degenerate. It possesses one simple eigenvalue $\lambda_1 = f'(\phi^{\mathrm{s}}) < 0$ which is just the eigenvalue for an isolated Active Rotator at its stable fixed point and is thus non-splitting, and a second eigenvalue $\lambda_2 = f'(\phi^{\mathrm{s}}) - \kappa\, g'(0)$ of multiplicity $(N-1)$ which corresponds to splitting perturbations. The condition for the occurrence of the THB is therefore $\lambda_2 = 0$.

Focusing on the generalized AR-model (2.6), to derive implicit expressions that interrelate the system parameters at the THB, we start by writing down the two resulting equations for $\dot{\phi}_j = 0$ and $\lambda_2 = 0$

$$0 = \omega - \sin\phi + \epsilon\, h(\phi) \tag{B.1a}$$
$$0 = -\cos\phi + \epsilon\, h'(\phi) - \kappa_0 \tag{B.1b}$$

in polynomial form by use of the Weierstraß (tangent half-angle) substitution

$$q \equiv \tan\frac{\phi}{2}, \quad \sin\phi = \frac{2q}{1+q^2}, \quad \cos\phi = \frac{1-q^2}{1+q^2}.$$

To eliminate q in the resulting polynomial expressions for (B.1), we then compute the resultant [GKZ94], with help of *Mathematica 12.1.1.0*. We start with the perturbation $h(\phi) = \sin 2\phi$ in (5.1a).

SECOND SINE MODE PERTURBATION (5.1A) Our considerations above yield for the system $\dot{\phi}_j = \omega - \sin\phi_j + \epsilon \sin 2\phi_j + \frac{\kappa}{N}\sum_{k=1}^{N}\sin(\phi_k - \phi_j)$ with the perturbation function (5.1a) the two defining equations

$$0 = \omega - \sin\phi^{\mathrm{s}} + \epsilon \sin 2\phi^{\mathrm{s}}$$
$$0 = -\cos\phi^{\mathrm{s}} + 2\epsilon\, \cos 2\phi^{\mathrm{s}} - \kappa_0.$$

Employing the Weierstraß transformations then results, after multiplying with $(1+q^2)^2$, in the two polynomial equations

$$0 = \omega(1+q^2)^2 - 2q(1+q^2) + 4\epsilon q(1-q^2) \tag{B.2a}$$
$$0 = (1-q^4) - 2\epsilon\left((1-q^2)^2 - (2q)^2\right) + \kappa_0(1+q^2)^2. \tag{B.2b}$$

Computing the resultant of the right hand sides of these equations and eliminating nonzero prefactors yields

$$\begin{aligned} 0 = &-1 + 12\epsilon^2 - 48\epsilon^4 + 64\epsilon^6 + \kappa_0^2 + 4\epsilon^2\kappa_0^2 - \\ &- 32\epsilon^4\kappa_0^2 - 4\epsilon\kappa_0^3 + 4\epsilon^2\kappa_0^4 + \omega^2 - 80\epsilon^2\omega^2 - \\ &- 128\epsilon^4\omega^2 + 32\epsilon^2\omega^2\kappa_0^2 + 64\epsilon^2\omega^4 \end{aligned} \tag{5.5}$$

which is the desired expression for the THB that we use in Chapter 5 and Chapter 7.

Equation (5.5) cannot be solved explicitly for κ_0. However, it allows for a series expansion of κ_0 in powers of ϵ. Inserting the formal power series $\kappa_0 = \sum_{n=0}^{\infty} a_n \epsilon^n$ with unknown coefficients a_n, and collecting powers of ϵ yields

$$\begin{aligned} 0 = &\Big[a_0^2 + \omega^2 - 1\Big] + \Big[2a_0a_1 - 4a_0^3\Big]\epsilon + \Big[4a_0^4 + 32\omega^2a_0^2 - 12a_1a_0^2 + \\ &+ 4a_0^2 + 2a_2a_0 + 64\omega^4 + a_1^2 - 80\omega^2 + 12\Big]\epsilon^2 + \mathcal{O}(\epsilon^3) \end{aligned}$$

which can be solved successively for the a_n since each prefactor of ϵ must vanish. For a_0, we find two possible solutions $a_0 = \pm\sqrt{1-\omega^2}$. This is due to the fact that (B.1a) and subsequently (5.5) do not discriminate between the fixed points Δ^{s} and Δ^{u}. Since we are exclusively interested in the bifurcation of Δ^{s}, we dismiss the positive solution corresponding to the bifurcation of Δ^{u} and thus find $a_0 = -\sqrt{1-\omega^2}$. The remaining coefficients can than be computed consecutively so that we arrive at the unique expansion

$$\kappa_0 = -\sqrt{1-\omega^2} + 2(1-\omega^2)\epsilon + 2\omega^2\frac{4\omega^2-5}{\sqrt{1-\omega^2}}\epsilon^2 + \mathcal{O}(\epsilon^3). \tag{5.6}$$

GENERIC PERTURBATION (5.1b) Applying the same procedure as above to the perturbation function

$$h(\phi) = \frac{1}{\sin\phi - 2} + \frac{1}{\sqrt{3}} + \left(\frac{4}{\sqrt{3}} - 2\right)\sin\phi \tag{5.1b}$$

leads to the trigonometric expressions

$$\begin{aligned} 0 &= \omega - \sin\phi^{\mathrm{s}} + \epsilon\left(\frac{1}{\sin\phi^{\mathrm{s}} - 2} + \frac{1}{\sqrt{3}} + \frac{4-2\sqrt{3}}{\sqrt{3}}\sin\phi^{\mathrm{s}}\right) \\ 0 &= \cos\phi^{\mathrm{s}}\left(1 + \epsilon\left(\frac{1}{(\sin\phi^{\mathrm{s}} - 2)^2} - \frac{4}{\sqrt{3}} + 2\right)\right) + \kappa_0. \end{aligned}$$

These expressions can again be brought into purely polynomial form

$$\begin{aligned}
0 =& \Big[-(3-2\sqrt{3}) - (24-14\sqrt{3})q + (18-12\sqrt{3})q^2 - \\
& - (24-14\sqrt{3})q^3 - (3-2\sqrt{3})q^4 \Big]\epsilon - \\
& - 12\big[q - q^2 + q^3\big] + 6\big[1 - q + 2q^2 - q^3 + q^4\big]\omega \\
0 =& \Big[-(27-16\sqrt{3}) + (48-32\sqrt{3})q - (51-32\sqrt{3})q^2 + \\
& + (51-32\sqrt{3})q^4 - (48-32\sqrt{3})q^5 + (27-16\sqrt{3})q^6 \Big]\epsilon - \\
& - 12\big[1 - 2q + 2q^2 - 2q^4 + 2q^5 - q^6\big] - \\
& - 12\big[1 - 2t + 4q^2 - 4q^3 + 4q^4 - 2q^5 + q^6\big]\kappa_0
\end{aligned}$$

by using the Weierstraß substitution and eliminating any occurring denominators. Computing the resultant of the right hand sides of these equations to eliminate the variable q, we find

$$\begin{aligned}
0 = & \Big[-1296 - (24192-14688\sqrt{3})\epsilon - (414072-238752\sqrt{3})\epsilon^2 - \\
& - (3923784-2265480\sqrt{3})\epsilon^3 - (23142105-13361088\sqrt{3})\epsilon^4 - \\
& - (86925726-50186592\sqrt{3})\epsilon^5 - (203065782-117240084\sqrt{3})\epsilon^6 - \\
& - (269732688-155730240\sqrt{3})\epsilon^7 - (155967240-90047728\sqrt{3})\epsilon^8 \Big] + \\
& + \Big[1296 + (18360-11232\sqrt{3})\epsilon + (229176-132120\sqrt{3})\epsilon^2 + \\
& + (1474002-851040\sqrt{3})\epsilon^3 + (5318343-3070548\sqrt{3})\epsilon^4 + \\
& + (10200132-5889048\sqrt{3})\epsilon^5 + (8125452-4691232\sqrt{3})\epsilon^6 \Big]\kappa_0^2 + \\
& + \Big[27\epsilon^2 + (108-72\sqrt{3})\epsilon^3 + (252-144\sqrt{3})\epsilon^4 \Big]\kappa_0^4 + \\
& + \Big[2592 + (38880-24624\sqrt{3})\epsilon + (544968-313488\sqrt{3})\epsilon^2 + \\
& + (3987936-2302740\sqrt{3})\epsilon^3 + (17329248-10005000\sqrt{3})\epsilon^4 + \\
& + (44550756-25721394\sqrt{3})\epsilon^5 + (62598048-36141000\sqrt{3})\epsilon^6 + \\
& + (36958320-21337896\sqrt{3})\epsilon^7 \Big]\omega - \\
& - \Big[2592 + (29160-18576\sqrt{3})\epsilon + (289872-166644\sqrt{3})\epsilon^2 + \\
& + (1359612-785088\sqrt{3})\epsilon^3 + (3186288-1839600\sqrt{3})\epsilon^4 + \\
& + (2978352-1719552\sqrt{3})\epsilon^5 \Big]\kappa_0^2\,\omega - \\
& - \Big[648 + (3672-3240\sqrt{3})\epsilon + (2106-288\sqrt{3})\epsilon^2 - \\
& - (324396-186984\sqrt{3})\epsilon^3 - (2296917-1326168\sqrt{3})\epsilon^4 - \\
& - (6437124-3716472)\sqrt{3}\epsilon^5 - (6648996-3838800\sqrt{3})\epsilon^6 \Big]\omega^2 +
\end{aligned} \tag{B.3}$$

(continue on next page)

$$
\begin{aligned}
&+\Big[1944+(16686-11016\sqrt{3})\epsilon+(123660-70740\sqrt{3})\epsilon^2+\\
&\quad+(375624-217008\sqrt{3})\epsilon^3+(429264-247824\sqrt{3})\epsilon^4\Big]\kappa_0^2\,\omega^2-\\
&-\Big[1944+(24192+15444\sqrt{3})\epsilon+(262440-150840\sqrt{3})\epsilon^2+\\
&\quad+(1325304-765288\sqrt{3})\epsilon^3+(3312576-1912512\sqrt{3})\epsilon^4+\\
&\quad+(3277152-1892064\sqrt{3})\epsilon^5\Big]\omega^3-\\
&-\Big[648+(3996-2700\sqrt{3})\epsilon+(19440-11088\sqrt{3})\epsilon^2+\\
&\quad+(28656-16560\sqrt{3})\epsilon^3\Big]\kappa_0^2\,\omega^3+\\
&+\Big[1863+(16362-11016\sqrt{3})\epsilon+(126468-72108\sqrt{3})\epsilon^2+\\
&\quad+(393912-227664\sqrt{3})\epsilon^3+(461376-266352\sqrt{3})\epsilon^4\Big]\omega^4+\\
&+\Big[81+(324-216\sqrt{3})\epsilon+(756-432\sqrt{3})\epsilon^2\Big]\kappa_0^2\,\omega^4-\\
&-\Big[648+(3996-2754\sqrt{3})\epsilon+(19872-11304\sqrt{3})\epsilon^2+\\
&\quad+(29520-17064\sqrt{3})\epsilon^3\Big]\omega^5+\\
&+\Big[81+(324-216\sqrt{3})\epsilon+(756-432\sqrt{3})\epsilon^2\Big]\omega^6.
\end{aligned}
\tag{B.3}
$$

This is the expression that was used to plot the THB (green line) in Figure 14. Due to the scope of this equation, we refrain from calculating a series expansion of κ_0 in ϵ.

C

CHANGE OF PITCHFORK CRITICALITY

In this appendix, we derive an implicit expression in ω and ϵ for the codimension 2 bifurcation in which the pitchfork bifurcation of Δ^{s} in (2.6) with perturbation function $h(\phi) = \sin 2\phi$ changes its criticality. At this point, we have additionally to the condition (5.5) for the critical coupling strength κ_0 the conditions $c_1 = 1$ or $c_1 = 0$ with c_1 given by (5.11).

We start by bringing (5.11) in polynomial form via a Weierstraß substitution which yields

$$\begin{aligned} 0 = &- \Big[2c_1\epsilon + 1\Big]q^8 + \Big[12c_1\epsilon + 4(8\epsilon+1)^2\Big]q^6 + \\ &+ \Big[- 2c_1\epsilon + c_1(2\epsilon+1) + c_1 - 64\epsilon(8\epsilon+1) + 8(8\epsilon+1)\Big]q^4 + \\ &+ \Big[- 12c_1\epsilon + 256\epsilon^2 - 64\epsilon + 4\Big]q^2 + 2c_1\epsilon - c_1. \end{aligned}$$

Computing the resultant of the right hand side of this expression with the one of (B.2a) which determines coordinates if Δ^{s} yields for the critical value $c_1 = 1$

$$\begin{aligned} 0 = &+ 4\Big[1 - 2\omega^2\Big]^2 + \Big[1796\omega^6 - 1924\omega^4 + 545\omega^2 - 48\Big]\epsilon^2 + \\ &+ 4\Big[16384\omega^8 - 22272\omega^6 + 9390\omega^4 - 1393\omega^2 + 48\Big]\epsilon^4 - \\ &- 4\Big[256\omega^4 - 273\omega^2 + 64\Big]\epsilon^6 \end{aligned} \tag{5.12}$$

which is the sought expression in Chapter 5. For the case $c_1 = 0$, we find analogously

$$9\omega + 64\omega\Big[16\omega^2 - 9\Big]\epsilon^2 = 0.$$

However, this second case did not occur in our numerical work. We refrain from computing similar expressions for perturbation type (5.1b) due to its complicated algebraic form.

D

AVERAGING FOR THE TRUNCATED SYSTEM

We want to discuss the limitations of the averaging principle for WS-integrable systems (6.3) from Proposition 7.1 by showing that the function $\hat{\boldsymbol{F}}_h$, defined in (7.3), vanishes identically for any smooth choice of h if one averages over the periodic orbits $\mathcal{C}_{\boldsymbol{\lambda}}^{\text{trunc}} \subset \mathcal{M}^{\text{trunc}}$ of the truncated system (6.13). This serves two purposes: (i) It shows that $\hat{\boldsymbol{F}}_h$ can indeed be trivial and hence, it is not guaranteed that we can use Proposition 7.1 to determine robust periodic orbits for perturbed WS-integrable systems. (ii) It illustrates that to compute $\hat{\boldsymbol{F}}_h$ and its zeros for systems of the type (6.3), we cannot approximate the dynamics on the manifold $\mathcal{M}$ by the dynamics on $\mathcal{M}^{\text{trunc}}$. (For the truncated dynamics, we would have exact expressions which in turn would make computing the integral in (7.3) much easier!) Instead, we have to first determine the periodic orbit $\mathcal{C}_{\boldsymbol{\lambda}}$ of the full system (6.3) and subsequently average $\mathrm{D}\boldsymbol{\Lambda} \cdot \boldsymbol{h}$ over it.

Recall from the proof of Theorem 6.5 that the periodic solutions of (6.13) that formed the NAIM $\mathcal{M}^{\text{trunc}}$ were of the form

$$(\alpha(t), \psi(t), \boldsymbol{\lambda}(t)) = (\alpha, \Omega t, \boldsymbol{\lambda})$$

in WS-variables where $\alpha_0 \in \mathbb{D}$ is a fixed point of (6.13a) and $\Omega \neq 0$ is the angular velocity of the $2\pi/\Omega$-periodic solution $\boldsymbol{\phi}_{\boldsymbol{\lambda}}^{\text{trunc}}(t)$. In general, there exists no further restrictions on α_0 and Ω so that we can consider them arbitrarily fixed. The solution in angular variables with orbit $\mathcal{C}_{\boldsymbol{\lambda}}^{\text{trunc}} \subset \mathcal{M}^{\text{trunc}}$ is then given by

$$\boldsymbol{\phi}_{\boldsymbol{\lambda}}^{\text{trunc}}(t) = \boldsymbol{m}(\alpha_0, \Omega t, \boldsymbol{\lambda}) \tag{D.1}$$

via the diffeomorphism $\boldsymbol{m}$ from Proposition 4.12. From (7.3), we subsequently find with the substitution $\psi = \Omega t$

From now on, we drop the index from α_0 for brevity and just write α.

$$\begin{aligned}
\hat{\boldsymbol{F}}_h(\boldsymbol{\lambda}) &= \frac{\Omega}{2\pi} \int_0^{\frac{2\pi}{\Omega}} (\mathrm{D}\boldsymbol{\Lambda} \cdot \boldsymbol{h}) \circ \boldsymbol{\phi}_{\boldsymbol{\lambda}}^{\text{trunc}}(t)\, \mathrm{d}t \\
&= \frac{\Omega}{2\pi} \int_0^{\frac{2\pi}{\Omega}} (\mathrm{D}\boldsymbol{\Lambda} \cdot \boldsymbol{h}) \circ \boldsymbol{m}(\alpha, \Omega t, \boldsymbol{\lambda})\, \mathrm{d}t \\
&= \frac{1}{2\pi} \int_0^{2\pi} (\mathrm{D}\boldsymbol{\Lambda} \cdot \boldsymbol{h}) \circ \boldsymbol{m}(\alpha, \psi, \boldsymbol{\lambda})\, \mathrm{d}\psi \\
&= \frac{1}{2\pi} \int_0^{2\pi} \mathrm{D}\boldsymbol{\Lambda}(\boldsymbol{\theta}) \cdot \boldsymbol{h}(\boldsymbol{\theta})\Big|_{\mathrm{e}^{i\boldsymbol{\theta}} = G_{\alpha,\psi}(\boldsymbol{z})} \mathrm{d}\psi
\end{aligned} \tag{D.2}$$

where we set $\boldsymbol{z} = \mathrm{e}^{i\boldsymbol{\Theta}(\boldsymbol{\lambda})}$ for brevity. From this, we see that $\hat{\boldsymbol{F}}_h(\boldsymbol{\lambda})$ is in fact the zeroth Fourier mode of the vector-valued function

$$\psi \mapsto \mathrm{D}\boldsymbol{\Lambda}(\boldsymbol{\theta}) \cdot \boldsymbol{h}(\boldsymbol{\theta})\Big|_{\mathrm{e}^{i\boldsymbol{\theta}} = G_{\alpha,\psi}(\boldsymbol{z})}$$

with fixed α and $\boldsymbol{z}$. We claim that this zeroth mode vanishes for any smooth choice for $h : \mathbb{S}^1 \to \mathbb{R}$, independently of $\alpha \in \mathbb{D}$ and $\boldsymbol{z} \in \left\{ \boldsymbol{z} \in \partial\mathbb{D}^N \,;\, z_p \neq z_q \text{ for } p \neq q \right\}$ which then implies that $\hat{\boldsymbol{F}}_h$ vanishes identically for any periodic solution of type (D.1). Because of the linearity of (D.2) in h, in order to prove our claim, it suffices to show that this zeroth mode vanishes for every function

$$H : \psi \mapsto \mathrm{D}\Lambda_{p,q,r,s}(\boldsymbol{\theta}) \cdot \boldsymbol{h}(\boldsymbol{\theta})\Big|_{\mathrm{e}^{i\boldsymbol{\theta}} = G_{\alpha,\psi}(\boldsymbol{z})}$$

where $\Lambda_{p,q,r,s}$ is an arbitrary cross-ratio function with mutually distinct $p, q, r, s \in \{1, \ldots, N\}$ and any smooth $h : \theta \mapsto \sin \nu\theta$ or $h : \theta \mapsto \cos \nu\theta$ with $\nu \in \mathbb{Z}$ and, with the identities

$$\begin{aligned} \sin \nu\theta &= \frac{1}{2i}\left(\mathrm{e}^{i\nu\theta} - \mathrm{e}^{-i\nu\theta}\right) \\ \cos \nu\theta &= \frac{1}{2}\left(\mathrm{e}^{i\nu\theta} + \mathrm{e}^{-i\nu\theta}\right), \end{aligned}$$

this amounts to showing that the zeroth complex Fourier mode of H vanishes for every $h : \theta \mapsto \mathrm{e}^{i\nu\theta}$ with $\nu \in \mathbb{Z}$.

The only nonzero entries of $\mathrm{D}\Lambda_{p,q,r,s}$ are

$$\begin{aligned} \mathrm{D}_{\theta_p}\Lambda_{p,q,r,s}(\boldsymbol{\theta}) &= i\frac{\mathrm{e}^{i\theta_p}\left(\mathrm{e}^{i\theta_r} - \mathrm{e}^{i\theta_q}\right)\left(\mathrm{e}^{i\theta_r} - \mathrm{e}^{i\theta_s}\right)}{\left(\mathrm{e}^{i\theta_p} - \mathrm{e}^{i\theta_r}\right)^2\left(\mathrm{e}^{i\theta_q} - \mathrm{e}^{i\theta_s}\right)} \\ \mathrm{D}_{\theta_q}\Lambda_{p,q,r,s}(\boldsymbol{\theta}) &= i\frac{\mathrm{e}^{i\theta_q}\left(\mathrm{e}^{i\theta_s} - \mathrm{e}^{i\theta_p}\right)\left(\mathrm{e}^{i\theta_s} - \mathrm{e}^{i\theta_r}\right)}{\left(\mathrm{e}^{i\theta_q} - \mathrm{e}^{i\theta_s}\right)^2\left(\mathrm{e}^{i\theta_p} - \mathrm{e}^{i\theta_r}\right)} \\ \mathrm{D}_{\theta_r}\Lambda_{p,q,r,s}(\boldsymbol{\theta}) &= i\frac{\mathrm{e}^{i\theta_r}\left(\mathrm{e}^{i\theta_q} - \mathrm{e}^{i\theta_p}\right)\left(\mathrm{e}^{i\theta_p} - \mathrm{e}^{i\theta_s}\right)}{\left(\mathrm{e}^{i\theta_p} - \mathrm{e}^{i\theta_r}\right)^2\left(\mathrm{e}^{i\theta_q} - \mathrm{e}^{i\theta_s}\right)} \\ \mathrm{D}_{\theta_s}\Lambda_{p,q,r,s}(\boldsymbol{\theta}) &= i\frac{\mathrm{e}^{i\theta_s}\left(\mathrm{e}^{i\theta_p} - \mathrm{e}^{i\theta_q}\right)\left(\mathrm{e}^{i\theta_q} - \mathrm{e}^{i\theta_r}\right)}{\left(\mathrm{e}^{i\theta_q} - \mathrm{e}^{i\theta_s}\right)^2\left(\mathrm{e}^{i\theta_p} - \mathrm{e}^{i\theta_r}\right)}. \end{aligned} \tag{D.3}$$

We further find

$$\begin{aligned} \mathrm{e}^{i\theta_j} &= G_{\alpha,\psi}(z_j) \\ &= \frac{\alpha + \mathrm{e}^{i\psi} z_j}{1 + \bar{\alpha}\mathrm{e}^{i\psi} z_j} \\ &= \alpha + (1 - |\alpha|^2) \sum_{n=1}^{\infty} (-\bar{\alpha})^{n-1} z_j^n \mathrm{e}^{in\psi} \end{aligned} \tag{D.4}$$

where in the last line, we used again the geometric series identity $\sum_{n=0}^{\infty} z^n = 1/(1-z)$ for $|z| < 1$. The last line of (D.4) is simply the Fourier series of the function $\psi \mapsto G_{\alpha,\psi}(z_j)$. Subsequently, we find for the powers of $\mathrm{e}^{i\theta_j}$ and $\mathrm{e}^{-i\theta_j}$ with $\nu \geq 0$ the Fourier series

$$\begin{aligned} \mathrm{e}^{i\nu\theta_j} &= \alpha^\nu + \nu z_j (1 - |\alpha|^2)\alpha^{\nu-1}\mathrm{e}^{i\psi} + \text{ higher modes} \\ \mathrm{e}^{-i\nu\theta_j} &= \bar{\alpha}^\nu + \nu \bar{z}_j (1 - |\alpha|^2)\bar{\alpha}^{\nu-1}\mathrm{e}^{-i\psi} + \text{higher modes} \end{aligned}$$

up to their respective first modes. Inserting (D.4) in (D.3) and collecting powers of $\mathrm{e}^{i\psi}$ yields

$$\begin{aligned}
\mathrm{D}_{\theta_p}\Lambda_{p,q,r,s}(\boldsymbol{\theta}) &= A_{p,q,r,s} + B_{p,q,r,s}\,\mathrm{e}^{-i\psi} + C_{p,q,r,s}\,\mathrm{e}^{i\psi}\\
\mathrm{D}_{\theta_q}\Lambda_{p,q,r,s}(\boldsymbol{\theta}) &= A_{q,p,s,r} + B_{q,p,s,r}\,\mathrm{e}^{-i\psi} + C_{q,p,s,r}\,\mathrm{e}^{i\psi}\\
\mathrm{D}_{\theta_r}\Lambda_{p,q,r,s}(\boldsymbol{\theta}) &= A_{r,s,p,q} + B_{r,s,p,q}\,\mathrm{e}^{-i\psi} + C_{r,s,p,q}\,\mathrm{e}^{i\psi}\\
\mathrm{D}_{\theta_s}\Lambda_{p,q,r,s}(\boldsymbol{\theta}) &= A_{s,r,q,p} + B_{s,r,q,p}\,\mathrm{e}^{-i\psi} + C_{s,r,q,p}\,\mathrm{e}^{i\psi}
\end{aligned}$$

with Fourier coefficients

$$\begin{aligned}
A_{a,b,c,d} &= -i\frac{z_a(z_b-z_c)(z_c-z_d)(1+|\alpha|^2)}{(z_a-z_c)^2(z_b-z_d)(1-|\alpha|^2)}\\
B_{a,b,c,d} &= -i\frac{(z_b-z_c)(z_c-z_d)\alpha}{(z_a-z_c)^2(z_b-z_d)(1-|\alpha|^2)}\\
C_{a,b,c,d} &= -i\frac{z_a^2(z_b-z_c)(z_c-z_d)\bar\alpha}{(z_a-z_c)^2(z_b-z_d)(1-|\alpha|^2)}
\end{aligned}$$

for which the identities

$$\begin{aligned}
A_{p,q,r,s} + A_{q,p,s,r} + A_{r,s,p,q} + A_{s,r,q,p} &= 0\\
B_{p,q,r,s}\,z_p + B_{q,p,s,r}\,z_q + B_{r,s,p,q}\,z_r + B_{s,r,q,p}\,z_s &= 0\\
C_{p,q,r,s}\,\bar z_p + C_{q,p,s,r}\,\bar z_q + C_{r,s,p,q}\,\bar z_r + C_{s,r,q,p}\,\bar z_s &= 0
\end{aligned} \tag{D.5}$$

hold. We are now ready to determine the Fourier expansion of H. Beginning with $h:\theta\mapsto \mathrm{e}^{i\nu\theta}$ and $\nu\geq 0$, we find

$$\begin{aligned}
H(\psi) &= \mathrm{D}\Lambda_{p,q,r,s}(\boldsymbol{\theta})\cdot\boldsymbol{h}(\boldsymbol{\theta})\Big|_{\mathrm{e}^{i\boldsymbol{\theta}}=G_{\alpha,\psi}(\boldsymbol{z})}\\
&= \mathrm{D}_{\theta_p}\Lambda_{p,q,r,s}(\boldsymbol{\theta})\mathrm{e}^{i\nu\theta_p} + \mathrm{D}_{\theta_q}\Lambda_{p,q,r,s}(\boldsymbol{\theta})\mathrm{e}^{i\nu\theta_q} +\\
&\quad + \mathrm{D}_{\theta_r}\Lambda_{p,q,r,s}(\boldsymbol{\theta})\mathrm{e}^{i\nu\theta_r} + \mathrm{D}_{\theta_s}\Lambda_{p,q,r,s}(\boldsymbol{\theta})\mathrm{e}^{i\nu\theta_s}\\
&= (A_{p,q,r,s} + A_{q,p,s,r} + A_{r,s,p,q} + A_{s,r,q,p})\alpha^\nu +\\
&\quad + (B_{p,q,r,s}\,z_p + B_{q,p,s,r}\,z_q +\\
&\qquad + B_{r,s,p,q}\,z_r + B_{s,r,q,p}\,z_s)\nu(1-|\alpha|^2)\alpha^{\nu-1} +\\
&\quad + \text{ higher modes}
\end{aligned}$$

for which the zeroth mode vanishes identically because of the identities (D.5). Similarly, we find for the case $h:\theta\mapsto \mathrm{e}^{-i\nu\theta}$ with $\nu\geq 0$ the expansion

$$\begin{aligned}
H(\psi) &= \mathrm{D}\Lambda_{p,q,r,s}(\boldsymbol{\theta})\cdot\boldsymbol{h}(\boldsymbol{\theta})\Big|_{\mathrm{e}^{i\boldsymbol{\theta}}=G_{\alpha,\psi}(\boldsymbol{z})}\\
&= \mathrm{D}_{\theta_p}\Lambda_{p,q,r,s}(\boldsymbol{\theta})\mathrm{e}^{-i\nu\theta_p} + \mathrm{D}_{\theta_q}\Lambda_{p,q,r,s}(\boldsymbol{\theta})\mathrm{e}^{-i\nu\theta_q} +\\
&\quad + \mathrm{D}_{\theta_r}\Lambda_{p,q,r,s}(\boldsymbol{\theta})\mathrm{e}^{-i\nu\theta_r} + \mathrm{D}_{\theta_s}\Lambda_{p,q,r,s}(\boldsymbol{\theta})\mathrm{e}^{-i\nu\theta_s}\\
&= (A_{p,q,r,s} + A_{q,p,s,r} + A_{r,s,p,q} + A_{s,r,q,p})\bar\alpha^\nu +\\
&\quad + (C_{p,q,r,s}\,\bar z_p + C_{q,p,s,r}\,\bar z_q +\\
&\qquad + C_{r,s,p,q}\,\bar z_r + C_{s,r,q,p}\,\bar z_s)\nu(1-|\alpha|^2)\bar\alpha^{\nu-1} +\\
&\quad + \text{ higher modes}
\end{aligned}$$

which again vanishes because of (D.5). This finishes the proof.

BIBLIOGRAPHY

[AS04] D. M. Abrams and S. H. Strogatz. "Chimera states for coupled oscillators." In: *Physical Review Letters* 93.17 (2004), p. 174102 (cit. on p. 3).

[Ace+05] J. A. Acebrón, L. L. Bonilla, C. J. P. Vicente, F. Ritort, and R. Spigler. "The Kuramoto model: A simple paradigm for synchronization phenomena." In: *Reviews of Modern Physics* 77.1 (2005), p. 137 (cit. on p. 3).

[Adl46] R. Adler. "A Study of locking phenomena in oscillators." In: *Proceedings of the IRE* 34.6 (1946), pp. 351–357 (cit. on p. 16).

[Ahl79] L. V. Ahlfors. *Complex analysis: an introduction to the theory of analytic functions of one complex variable*. 3rd ed. New York: McGraw-Hill, 1979 (cit. on pp. 42, 44, 45).

[AA98] D. J. Aidley and D. J. Ashley. *The physiology of excitable cells*. 4th ed. Cambridge University Press, 1998 (cit. on p. 11).

[And18] P. W. Anderson. *The economy as an evolving complex system*. 1st ed. Vol. 5. Boca Raton: CRC Press, 2018 (cit. on p. 1).

[And+73] A. A. Andronov, E. A. Leontovich, I. I. Gordon, and A. G. Maier. *Theory of bifurcations of dynamic systems on a plane*. Jerusalem: Israel Program of Scientific Translations, 1973 (cit. on pp. 73, 143).

[AGK91] D. G. Aronson, M. Golubitsky, and M. Krupa. "Coupled arrays of Josephson junctions and bifurcation of maps with SN symmetry." In: *Nonlinearity* 4.3 (1991), p. 861 (cit. on p. 5).

[AGM91] D. G. Aronson, M. Golubitsky, and J. Mallet-Paret. "Ponies on a merry-go-round in large arrays of Josephson junctions." In: *Nonlinearity* 4.3 (1991), p. 903 (cit. on pp. 4, 5, 179).

[ABM08] P. Ashwin, O. Burylko, and Y. Maistrenko. "Bifurcation to heteroclinic cycles and sensitivity in three and four coupled phase oscillators." In: *Chaos* 237.4 (2008), pp. 454–466 (cit. on p. 181).

[ACN16] P. Ashwin, S. Coombes, and R. Nicks. "Mathematical frameworks for oscillatory network dynamics in neuroscience." In: *The Journal of Mathematical Neuroscience* 6.1 (2016), pp. 1–92 (cit. on p. 3).

[AKS90] P. Ashwin, G. P. King, and J. W. Swift. “Three identical oscillators with symmetric coupling.” In: *Nonlinearity* 3.3 (1990), p. 585 (cit. on pp. 62, 86).

[Ash+07] P. Ashwin, G. Orosz, J. Wordsworth, and S. Townley. “Dynamics on networks of cluster states for globally coupled phase oscillators.” In: *SIAM Journal on Applied Dynamical Systems* 6.4 (2007), pp. 728–758 (cit. on p. 181).

[AS92] P. Ashwin and J. W. Swift. “The dynamics of weakly coupled identical oscillators.” In: *Journal of Nonlinear Science* 2.1 (1992), pp. 69–108 (cit. on p. 62).

[Aul82] B. Aulbach. “Invariant manifolds with asymptotic phase.” In: *Nonlinear Analysis* 6.8 (1982), pp. 817–827 (cit. on p. 151).

[Bač+18] I. Bačić, S. Yanchuk, M. Wolfrum, and I. Franović. “Noise-induced switching in two adaptively coupled excitable systems.” In: *The European Physical Journal Special Topics* 227.10 (2018), pp. 1077–1090 (cit. on p. 19).

[BM13] C. Baesens and R. S. MacKay. “Interaction of two systems with saddle-node bifurcations on invariant circles: I. foundations and the mutualistic case.” In: *Nonlinearity* 26.12 (2013), p. 3043 (cit. on pp. 59, 72, 73, 83, 183).

[Bai+09] Y. Baibolatov, M. Rosenblum, Z. Z. Zhanabaev, M. Kyzgarina, and A. Pikovsky. “Periodically forced ensemble of nonlinearly coupled oscillators: From partial to full synchrony.” In: *Physical Review E* 80.4 (2009), p. 046211 (cit. on p. 109).

[Ber09] M. Berger. *Geometry I*. 3rd ed. Berlin: Springer, 2009 (cit. on p. 52).

[Ber+20] R. Berner, A. Polanska, E. Schöll, and S. Yanchuk. “Solitary states in adaptive nonlocal oscillator networks.” In: *The European Physical Journal Special Topics* 229.12 (2020), pp. 2183–2203 (cit. on p. 135).

[BSY19] R. Berner, E. Schöll, and S. Yanchuk. “Multiclusters in networks of adaptively coupled phase oscillators.” In: *SIAM Journal on Applied Dynamical Systems* 18.4 (2019), pp. 2227–2266 (cit. on p. 3).

[Ber+21] R. Berner, S. Yanchuk, Y. Maistrenko, and E. Schöll. “Generalized splay states in phase oscillator networks.” In: *Chaos* 31.7 (2021), p. 073128 (cit. on pp. 5, 152, 180).

[Bos21] S. Bosch. *Lineare Algebra*. 6th ed. Berlin: Springer, 2021 (cit. on p. 50).

[BLL21] W. J. Bosl, A. Leviton, and T. Loddenkemper. “Prediction of seizure recurrence. A note of caution.” In: *Frontiers in Neurology* 12 (2021), p. 773 (cit. on p. 2).

[Buc88] J. Buck. "Synchronous rhythmic flashing of fireflies. II." In: *The Quarterly Review of Biology* 63.3 (1988), pp. 265–289 (cit. on p. 2).

[Buc38] J. B. Buck. "Synchronous rhythmic flashing of fireflies." In: *The Quarterly Review of Biology* 13.3 (1938), pp. 301–314 (cit. on pp. 2, 175).

[BG01] P.-L. Buono and M. Golubitsky. "Models of central pattern generators for quadruped locomotion I. Primary gaits." In: *Journal of Mathematical Biology* 42.4 (2001), pp. 291–326 (cit. on pp. 37, 38).

[Can02] B. Cantwell. *Introduction to symmetry analysis*. 1st ed. Cambridge University Press, 2002 (cit. on p. 36).

[Car37] R. D. Carmichael. *Introduction to the theory of groups of finite order*. 1st ed. Boston: Ginn and Company, 1937 (cit. on pp. 38, 121).

[Cha+17] S. Chandra, D. Hathcock, K. Crain, T. M. Antonsen, M. Girvan, and E. Ott. "Modeling the network dynamics of pulse-coupled neurons." In: *Chaos* 27.3 (2017), p. 033102 (cit. on p. 3).

[Che+17] H.-B. Chen, Y.-T. Sun, J. Gao, C. Xu, and Z.-G. Zheng. "Order parameter analysis of synchronization transitions on star networks." In: *Frontiers of Physics* 12.6 (2017), p. 120504 (cit. on p. 5).

[Chi99] C. Chicone. *Ordinary differential equations with applications*. 1st ed. New York: Springer, 1999 (cit. on pp. 26, 33, 39, 98).

[CS99] P. S. Churchland and T. J. Sejnowski. *The computational brain*. 1st ed. Cambridge: MIT press, 1999 (cit. on p. 2).

[CHR82] A. H. Cohen, P. J. Holmes, and R. H. Rand. "The nature of the coupling between segmental oscillators of the lamprey spinal generator for locomotion: A mathematical model." In: *Journal of Mathematical Biology* 13.3 (1982), pp. 345–369 (cit. on p. 21).

[Dai92] H. Daido. "Order function and macroscopic mutual entrainment in uniformly coupled limit-cycle oscillators." In: *Progress of Theoretical Physics* 88.6 (1992), pp. 1213–1218 (cit. on p. 183).

[Dai96] H. Daido. "Onset of cooperative entrainment in limit-cycle oscillators with uniform all-to-all interactions: bifurcation of the order function." In: *Physica D* 91.1 (1996), pp. 24–66 (cit. on p. 152).

[DKN13] H. Daido, A. Kasama, and K. Nishio. "Onset of dynamic activity in globally coupled excitable and oscillatory units." In: *Physical Review E* 88.5 (2013), p. 052907 (cit. on pp. 160, 175).

[DA05] P. Dayan and Laurence F. Abbott. *Theoretical neuroscience: computational and mathematical modeling of neural systems*. 2nd ed. Cambridge: MIT Press, 2005 (cit. on pp. 2, 21, 161).

[DS93] R. Dermietzel and D. C. Spray. "Gap junctions in the brain: where, what type, how many and why?" In: *Trends in Neurosciences* 16.5 (1993), pp. 186–192 (cit. on p. 21).

[Dip+12] M. Dipoppa, M. Krupa, A. Torcini, and B. S. Gutkin. "Splay states in finite pulse-coupled networks of excitable neurons." In: *SIAM Journal on Applied Dynamical Systems* 11.3 (2012), pp. 864–894 (cit. on p. 5).

[DS20] S. Dixit and M. D. Shrimali. "Static and dynamic attractive-repulsive interactions in two coupled nonlinear oscillators." In: *Chaos* 30.3 (2020), p. 033114 (cit. on p. 20).

[DGP17] A. V. Dolmatova, D. S. Goldobin, and A. Pikovsky. "Synchronization of coupled active rotators by common noise." In: *Physical Review E* 96.6 (2017), p. 062204 (cit. on pp. 4, 19).

[DB14] F. Dörfler and F. Bullo. "Synchronization in complex networks of phase oscillators: A survey." In: *Automatica* 50.6 (2014), pp. 1539–1564 (cit. on p. 3).

[Ein43] A. Einstein. *Letter to Barbara Lee Wilson*. 1943 (cit. on p. 185).

[Eld13] J. Eldering. *Normally hyperbolic invariant manifolds: the noncompact case*. 1st ed. Berlin: Springer, 2013 (cit. on p. 34).

[Eld] J. Eldering. Private Communication (cit. on p. 34).

[Eld+21] J. Eldering, J. S. W. Lamb, T. Pereira, and E. R. dos Santos. "Chimera states through invariant manifold theory." In: *Nonlinearity* 34.8 (2021), pp. 5344–5374 (cit. on pp. 4, 6, 36, 91, 96).

[EM14] J. R. Engelbrecht and R. Mirollo. "Classification of attractors for systems of identical coupled Kuramoto oscillators." In: *Chaos* 24.1 (2014), p. 013114 (cit. on pp. 4, 52, 83, 107, 135).

[EK09] G. B. Ermentrout and T.-W. Ko. "Delays and weakly coupled neuronal oscillators." In: *Philosophical Transactions of the Royal Society A* 367.1891 (2009), pp. 1097–1115 (cit. on p. 176).

[EK86] G. B. Ermentrout and N. Kopell. "Parabolic bursting in an excitable system coupled with a slow oscillation." In: *SIAM Journal on Applied Mathematics* 46.2 (1986), pp. 233–253 (cit. on p. 16).

[EK90] G. B. Ermentrout and N. Kopell. "Oscillator death in systems of coupled neural oscillators." In: *SIAM Journal on Applied Mathematics* 50.1 (1990), pp. 125–146 (cit. on pp. 159, 161–163, 166–170).

[Fen74] N. Fenichel. "Asymptotic stability with rate conditions." In: *Indiana University Mathematics Journal* 23.12 (1974), pp. 1109–1137 (cit. on pp. 34, 151).

[Fen77] N. Fenichel. "Asymptotic stability with rate conditions, II." In: *Indiana University Mathematics Journal* 26.1 (1977), pp. 81–93 (cit. on pp. 34, 116, 151).

[FM71] N. Fenichel and J. K. Moser. "Persistence and smoothness of invariant manifolds for flows." In: *Indiana University Mathematics Journal* 21.3 (1971), pp. 193–226 (cit. on pp. 34, 36, 70).

[Fie+21] B. Fiedler, S. W. Haugland, F. P. Kemeth, and K. Krischer. "Global heteroclinic rebel dynamics among large 2-clusters in permutation equivariant systems." In: *SIAM Journal on Applied Dynamical Systems* 20.3 (2021), pp. 1277–1319 (cit. on p. 5).

[Fie20] M. J. Field. *Lectures on bifurcations, dynamics and symmetry.* 1st ed. Boca Raton: CRC Press, 2020 (cit. on pp. 71, 73, 143).

[FNP08] G. Filatrella, A. H. Nielsen, and N. F. Pedersen. "Analysis of a power grid using a Kuramoto-like model." In: *The European Physical Journal B* 61.4 (2008), pp. 485–491 (cit. on p. 175).

[Fra+21] I. Franović, S. Eydam, S. Yanchuk, and R. Berner. "Collective activity bursting in networks of excitable systems adaptively coupled to a pool of resources." In: *preprint arXiv:2112.12104* (2021) (cit. on p. 4).

[FOW21] I. Franović, E. Omel'chenko, and M. Wolfrum. "Bumps, chimera states, and Turing patterns in systems of coupled active rotators." In: *Physical Review E* 104.5 (2021), p. L052201 (cit. on p. 176).

[Fra+20] I. Franović, S. Yanchuk, S. Eydam, I. Bačić, and M. Wolfrum. "Dynamics of a stochastic excitable system with slowly adapting feedback." In: *Chaos* 30.8 (2020), p. 083109 (cit. on p. 19).

[Fri15] P. Fries. "Rhythms for cognition: communication through coherence." In: *Neuron* 88.1 (2015), pp. 220–235 (cit. on p. 1).

[Gal09] R. F. Galán. "The phase oscillator approximation in neuroscience: an analytical framework to study coherent activity in neural networks." In: *Coordinated Activity in the Brain.* New York: Springer, 2009, pp. 65–89 (cit. on p. 3).

[GKZ94] I. M. Gelfand, M. Kapranov, and A. Zelevinsky. *Discriminants, resultants, and multidimensional determinants*. 1st ed. Boston: Birkhäuser, 1994 (cit. on p. 189).

[Gia+12] G. Giacomin, K. Pakdaman, X. Pellegrin, and C. Poquet. "Transitions in active rotator systems: invariant hyperbolic manifold approach." In: *SIAM Journal on Mathematical Analysis* 44.6 (2012), pp. 4165–4194 (cit. on p. 4).

[Gir+16] A. Girón, H. Saiz, F. S. Bacelar, R. F. S. Andrade, and J. Gómez-Gardenes. "Synchronization unveils the organization of ecological networks with positive and negative interactions." In: *Chaos* 26.6 (2016), p. 065302 (cit. on p. 20).

[GJC11] M. Giver, Z. Jabeen, and B. Chakraborty. "Phase and frequency entrainment in locally coupled phase oscillators with repulsive interactions." In: *Physical Review E* 83.4 (2011), p. 046206 (cit. on p. 20).

[Goe95] C. J. Goebel. "Comment on "Constants of motion for superconductor arrays"." In: *Physica D* 80.1 (1995), pp. 18–20 (cit. on p. 52).

[GE02] P. Goel and G. B. Ermentrout. "Synchrony, stability, and firing patterns in pulse-coupled oscillators." In: *Physica D* 163.3-4 (2002), pp. 191–216 (cit. on p. 21).

[Gol19] D. S. Goldobin. "Relationships between the distribution of Watanabe-Strogatz variables and circular cumulants for ensembles of phase elements." In: *Fluctuation and Noise Letters* 18.02 (2019), p. 1940002 (cit. on pp. 5, 181).

[Gol+18] D. S. Goldobin, I. V. Tyulkina, L. S. Klimenko, and A. Pikovsky. "Collective mode reductions for populations of coupled noisy oscillators." In: *Chaos* 28.10 (2018), p. 101101 (cit. on pp. 5, 181).

[Gol+13] E. Goldobin, R. Kleiner, D. Koelle, and R. G. Mints. "Phase retrapping in a pointlike φ Josephson junction: the butterfly effect." In: *Physical Review Letters* 111.5 (2013), p. 057004 (cit. on p. 183).

[Gol+11] E. Goldobin, D. Koelle, R. Kleiner, and R. G. Mints. "Josephson junction with a magnetic-field tunable ground state." In: *Physical Review Letters* 107.22 (2011), p. 227001 (cit. on p. 183).

[Gol+92] D. Golomb, D. Hansel, B. Shraiman, and H. Sompolinsky. "Clustering in globally coupled phase oscillators." In: *Physical Review A* 45.6 (1992), p. 3516 (cit. on p. 4).

[GS00] M. Golubitsky and I. Stewart. *The symmetry perspective: from equilibrium to chaos in phase space and physical space*. revised. Basel: Birkhäuser, 2000 (cit. on pp. 37, 38).

[Gol+98] M. Golubitsky, I. Stewart, P.-L. Buono, and J. J. Collins. "A modular network for legged locomotion." In: *Physica D* 115.1-2 (1998), pp. 56–72 (cit. on p. 37).

[GP19] C. C. Gong and A. Pikovsky. "Low-dimensional dynamics for higher-order harmonic, globally coupled phase-oscillator ensembles." In: *Physical Review E* 100.6 (2019), p. 062210 (cit. on pp. 183, 184).

[Gon+19] C. C. Gong, C. Zheng, R. Toenjes, and A. Pikovsky. "Repulsively coupled Kuramoto-Sakaguchi phase oscillators ensemble subject to common noise." In: *Chaos* 29.3 (2019), p. 033127 (cit. on pp. 77, 83, 177).

[Gro59] D. M. Grobman. "Homeomorphism of systems of differential equations." In: *Doklady Akademii Nauk SSSR* 128.5 (1959), pp. 880–881 (cit. on p. 26).

[GH13] J. Guckenheimer and P. Holmes. *Nonlinear oscillations, dynamical systems, and bifurcations of vector fields*. corrected. Berlin: Springer, 2013 (cit. on pp. 23, 25, 26).

[Hak08] H. Haken. *Brain dynamics: an introduction to models and simulations*. 2nd ed. Berlin: Springer, 2008 (cit. on p. 21).

[Hal15] B. Hall. *Lie groups, Lie algebras, and representations: an elementary introduction*. New York: Springer, 2015 (cit. on p. 187).

[HMM93] D. Hansel, G. Mato, and C. Meunier. "Clustering and slow switching in globally coupled phase oscillators." In: *Physical Review E* 48.5 (1993), p. 3470 (cit. on pp. 5, 181).

[HMM95] D. Hansel, G. Mato, and C. Meunier. "Synchrony in excitatory neural networks." In: *Neural Computation* 7.2 (1995), pp. 307–337 (cit. on p. 21).

[Har60] P. Hartman. "A lemma in the theory of structural stability of differential equations." In: *Proceedings of the American Mathematical Society* 11.4 (1960), pp. 610–620 (cit. on p. 26).

[HK02] R. Hegselmann and U. Krause. "Opinion dynamics and bounded confidence models, analysis, and simulation." In: *Journal of Artificial Societies and Social Simulation* 5.3 (2002) (cit. on p. 1).

[HPS77] M. W. Hirsch, C. C. Pugh, and M. Shub. *Invariant manifolds*. Berlin: Springer, 1977 (cit. on pp. 34, 36, 70).

[Hod48] A. L. Hodgkin. "The local electric changes associated with repetitive action in a non-medullated axon." In: *The Journal of Physiology* 107.2 (1948), pp. 165–181 (cit. on p. 13).

[Hol90] P. Holmes. "Poincaré, celestial mechanics, dynamical-systems theory and 'chaos'." In: *Physics Reports* 193.3 (1990), pp. 137–163 (cit. on p. 1).

[HK15] R. W. Hölzel and K. Krischer. "Stability and long term behavior of a Hebbian network of Kuramoto oscillators." In: *SIAM Journal on Applied Dynamical Systems* 14.1 (2015), pp. 188–201 (cit. on p. 3).

[HS11] H. Hong and S. H. Strogatz. "Conformists and contrarians in a Kuramoto model with identical natural frequencies." In: *Physical Review E* 84.4 (2011), p. 046202 (cit. on p. 2).

[HI12] F. C. Hoppensteadt and E. M. Izhikevich. *Weakly connected neural networks*. Berlin: Springer, 2012 (cit. on pp. 16, 17, 116, 151, 175).

[Hsi91] D. A. Hsieh. "Chaos and nonlinear dynamics: application to financial markets." In: *The Journal of Finance* 46.5 (1991), pp. 1839–1877 (cit. on p. 1).

[IAJ98] N. Ichinose, K. Aihara, and K. Judd. "Extending the concept of isochrons from oscillatory to excitable systems for modeling an excitable neuron." In: *International Journal of Bifurcation and Chaos* 8.12 (1998), pp. 2375–2385 (cit. on p. 16).

[Izh99] E. M. Izhikevich. "Class 1 neural excitability, conventional synapses, weakly connected networks, and mathematical foundations of pulse-coupled models." In: *IEEE Transactions on Neural Networks* 10.3 (1999), pp. 499–507 (cit. on p. 21).

[Izh00] E. M. Izhikevich. "Neural excitability, spiking and bursting." In: *International Journal of Bifurcation and Chaos* 10.06 (2000), pp. 1171–1266 (cit. on p. 14).

[Izh10] E. M. Izhikevich. *Dynamical Systems in Neuroscience*. Cambridge: MIT Press, 2010 (cit. on pp. 1, 11, 12, 175).

[JPP08] J. Javaloyes, M. Perrin, and A. Politi. "Collective atomic recoil laser as a synchronization transition." In: *Physical Review E* 78.1 (2008), p. 011108 (cit. on p. 21).

[Jir+13] P. Jiruska, M. De Curtis, J. G. R. Jefferys, C. A. Schevon, S. J. Schiff, and K. Schindler. "Synchronization and desynchronization in epilepsy: controversies and hypotheses." In: *The Journal of Physiology* 591.4 (2013), pp. 787–797 (cit. on p. 2).

[JW94] D. Johnston and S. M.-S. Wu. *Foundations of cellular neurophysiology*. Cambridge: MIT press, 1994 (cit. on pp. 11, 161).

[Jos62] B. D. Josephson. "Possible new effects in superconductive tunnelling." In: *Physics Letters* 1.7 (1962), pp. 251–253 (cit. on p. 4).

[KH97] A. Katok and B. Hasselblatt. *Introduction to the modern theory of dynamical systems*. Cambridge University Press, 1997 (cit. on p. 25).

[KS09] J. P. Keener and J. Sneyd. *Mathematical physiology I*. 2nd ed. Berlin: Springer, 2009 (cit. on p. 11).

[Kem+21] F. P. Kemeth, B. Fiedler, S. W. Haugland, and K. Krischer. "2-Cluster fixed-point analysis of mean-coupled Stuart-Landau oscillators in the center manifold." In: *Journal of Physics: Complexity* 2.2 (2021), p. 025005 (cit. on p. 5).

[KHK19] F. P. Kemeth, S. W. Haugland, and K. Krischer. "Cluster singularity: The unfolding of clustering behavior in globally coupled Stuart-Landau oscillators." In: *Chaos* 29.2 (2019), p. 023107 (cit. on p. 5).

[Kem+16] F. P. Kemeth, S. W. Haugland, L. Schmidt, I. G. Kevrekidis, and K. Krischer. "A classification scheme for chimera states." In: *Chaos* 26.9 (2016), p. 094815 (cit. on p. 7).

[KZH05] I. Z. Kiss, Y. Zhai, and J. L. Hudson. "Predicting mutual entrainment of oscillators with experiment-based phase models." In: *Physical Review Letters* 94.24 (2005), p. 248301 (cit. on p. 183).

[KZH06] I. Z. Kiss, Y. Zhai, and J. L. Hudson. "Characteristics of cluster formation in a population of globally coupled electrochemical oscillators: An experiment-based phase model approach." In: *Progress of Theoretical Physics Supplement* 161 (2006), pp. 99–106 (cit. on p. 5).

[KF19] V. Klinshov and I. Franović. "Two scenarios for the onset and suppression of collective oscillations in heterogeneous populations of active rotators." In: *Physical Review E* 100.6 (2019), p. 062211 (cit. on pp. 2, 19).

[KSN16] J. A. Kromer, L. Schimansky-Geier, and A. B. Neiman. "Emergence and coherence of oscillations in star networks of stochastic excitable elements." In: *Physical Review E* 93.4 (2016), p. 042406 (cit. on pp. 4, 19, 160).

[Kur75] Y. Kuramoto. "Self-entrainment of a population of coupled non-linear oscillators." In: *International Symposium on Mathematical Problems in Theoretical Physics*. Springer. 1975, pp. 420–422 (cit. on pp. 3, 87).

[Kur84] Y. Kuramoto. *Chemical oscillations, waves, and turbulence*. Berlin: Springer, 1984 (cit. on pp. 3, 19).

[KB02] Y. Kuramoto and D. Battogtokh. "Coexistence of coherence and incoherence in nonlocally coupled phase oscillators." In: *Nonlinear Phenomena in Complex Systems* 5.4 (2002) (cit. on p. 3).

[Kuz13] Y. A. Kuznetsov. *Elements of applied bifurcation theory*. 3rd ed. Berlin: Springer, 2013 (cit. on pp. 14, 25, 26, 33, 70, 74, 148).

[Lai14] C. R. Laing. "Derivation of a neural field model from a network of theta neurons." In: *Physical Review E* 90.1 (2014), p. 010901 (cit. on p. 21).

[Lai15] C. R. Laing. "Exact neural fields incorporating gap junctions." In: *SIAM Journal on Applied Dynamical Systems* 14.4 (2015), pp. 1899–1929 (cit. on p. 21).

[Lai18] C. R. Laing. "The dynamics of networks of identical theta neurons." In: *The Journal of Mathematical Neuroscience* 8.1 (2018), pp. 1–24 (cit. on pp. 21, 176, 184).

[LB20] C. R. Laing and C. Bläsche. "The effects of within-neuron degree correlations in networks of spiking neurons." In: *Biological Cybernetics* 114.3 (2020), pp. 337–347 (cit. on p. 20).

[LeB60] G. Le Bon. *The crowd*. New York: Viking Press, 1960 (cit. on p. 173).

[Lee12] J. M. Lee. *Introduction to smooth manifolds*. 2nd ed. Berlin: Springer, 2012 (cit. on p. 100).

[LK21] S. Lee and K. Krischer. "Attracting Poisson chimeras in two-population networks." In: *Chaos* 31.11 (2021), p. 113101 (cit. on p. 3).

[Li+19] X. Li, J. Zhang, Y. Zou, and S. Guan. "Clustering and Bellerophon state in Kuramoto model with second-order coupling." In: *Chaos* 29.4 (2019), p. 043102 (cit. on p. 183).

[LZL12] X. M. Liang, L. Zhao, and Z. H. Liu. "Signal amplification of active rotators with phase-shifted coupling." In: *The European Physical Journal B* 85.6 (2012), pp. 1–6 (cit. on p. 176).

[Lor07] J. Lorenz. "Continuous opinion dynamics under bounded confidence: A survey." In: *International Journal of Modern Physics C* 18.12 (2007), pp. 1819–1838 (cit. on p. 1).

[LY12] L. Lücken and S. Yanchuk. "Two-cluster bifurcations in systems of globally pulse-coupled oscillators." In: *Chaos* 241.4 (2012), pp. 350–359 (cit. on pp. 5, 57, 181).

[MPR14] Y. Maistrenko, B. Penkovsky, and M. Rosenblum. "Solitary state at the edge of synchrony in ensembles with attractive and repulsive interactions." In: *Physical Review E* 89.6 (2014), p. 060901 (cit. on p. 135).

[MPT05] Y. L. Maistrenko, O. V. Popovych, and P. A. Tass. "Chaotic attractor in the Kuramoto model." In: *International Journal of Bifurcation and Chaos* 15.11 (2005), pp. 3457–3466 (cit. on p. 3).

[MCG20] S. Majhi, S. N. Chowdhury, and D. Ghosh. "Perspective on attractive-repulsive interactions in dynamical networks: Progress and future." In: *Europhysics Letters* 132.2 (2020), p. 20001 (cit. on p. 20).

[Mañ78] R. Mañé. "Persistent manifolds are normally hyperbolic." In: *Transactions of the American Mathematical Society* 246 (1978), pp. 261–283 (cit. on p. 34).

[MPT10] T. V. Martins, M. Pineda, and R. Toral. "Mass media and repulsive interactions in continuous-opinion dynamics." In: *EPL* 91.4 (2010), p. 48003 (cit. on p. 20).

[MMS09] S. A. Marvel, R. E. Mirollo, and S. H. Strogatz. "Identical phase oscillators with global sinusoidal coupling evolve by Möbius group action." In: *Chaos* 19.4 (2009), p. 043104 (cit. on pp. 4, 42, 44, 51, 52, 125).

[MS09] S. A. Marvel and S. H. Strogatz. "Invariant submanifold for series arrays of Josephson junctions." In: *Chaos* 19.1 (2009), p. 013132 (cit. on p. 4).

[MMJ86] D. C. Michaels, E. P. Matyas, and J. Jalife. "Dynamic interactions and mutual synchronization of sinoatrial node pacemaker cells. A mathematical model." In: *Circulation Research* 58.5 (1986), pp. 706–720 (cit. on p. 2).

[Mik+19] M. Mikhaylenko, L. Ramlow, S. Jalan, and A. Zakharova. "Weak multiplexing in neural networks: Switching between chimera and solitary states." In: *Chaos* 29.2 (2019), p. 023122 (cit. on p. 135).

[Mir94] R. E. Mirollo. "Splay-phase orbits for equivariant flows on tori." In: *SIAM Journal on Mathematical Analysis* 25.4 (1994), pp. 1176–1180 (cit. on pp. 4, 5, 179).

[MS90] R. E. Mirollo and S. H. Strogatz. "Synchronization of pulse-coupled biological oscillators." In: *SIAM Journal on Applied Mathematics* 50.6 (1990), pp. 1645–1662 (cit. on p. 21).

[MM03] I. Moerdijk and J. Mrcun. *Introduction to foliations and Lie groupoids*. Cambridge University Press, 2003 (cit. on p. 100).

[MP04] Y. Moreno and A. F. Pacheco. "Synchronization of Kuramoto oscillators in scale-free networks." In: *Europhysics Letters* 68.4 (2004), p. 603 (cit. on p. 3).

[ML81] C. Morris and H. Lecar. "Voltage oscillations in the barnacle giant muscle fiber." In: *Biophysical Journal* 35.1 (1981), pp. 193–213 (cit. on p. 159).

[Myu+15] J. Myung, S. Hong, D. DeWoskin, E. De Schutter, D. B. Forger, and T. Takumi. "GABA-mediated repulsive coupling between circadian clock neurons in the SCN encodes seasonal time." In: *Proceedings of the National Academy of Sciences* 112.29 (2015), E3920–E3929 (cit. on p. 20).

[NW92] S. Nichols and K. Wiesenfeld. "Ubiquitous neutral stability of splay-phase states." In: *Physical Review A* 45.12 (1992), p. 8430 (cit. on pp. 4, 5).

[Oku93] K. Okuda. "Variety and generality of clustering in globally coupled oscillators." In: *Chaos* 63 (1993), pp. 424–436 (cit. on pp. 5, 31, 181).

[Olm15] S. Olmi. "Chimera states in coupled Kuramoto oscillators with inertia." In: *Chaos* 25.12 (2015), p. 123125 (cit. on p. 3).

[Ols10] J. Olsen. *The geometry of Möbius transformations*. University of Rochester, 2010. URL: `http://www.johno.dk/mathematics/moebius.pdf` (cit. on pp. 42, 49, 187).

[Olv00] P. J. Olver. *Applications of Lie groups to differential equations*. 2nd ed. Berlin: Springer, 2000 (cit. on p. 36).

[OA08] E. Ott and T. M. Antonsen. "Low dimensional behavior of large systems of globally coupled oscillators." In: *Chaos* 18.3 (2008), p. 037113 (cit. on pp. 4, 181).

[OA09] E. Ott and T. M. Antonsen. "Long time evolution of phase oscillator systems." In: *Chaos* 19.2 (2009), p. 023117 (cit. on p. 4).

[PM06] D. Pazó and E. Montbrió. "Universal behavior in populations composed of excitable and self-oscillatory elements." In: *Physical Review E* 73.5 (2006), 055202(R) (cit. on p. 160).

[Per+10] P. Perlikowski, S. Yanchuk, O. V. Popovych, and P. A. Tass. "Periodic patterns in a ring of delay-coupled oscillators." In: *Physical Review E* 82.3 (2010), p. 036208 (cit. on p. 5).

[Per+20] T. Peron, D. Eroglu, F. A. Rodrigues, and Y. Moreno. "Collective dynamics of random Janus oscillator networks." In: *Physical Review Research* 2.1 (2020), p. 013255 (cit. on pp. 180, 181).

[PR08] A. Pikovsky and M. Rosenblum. "Partially integrable dynamics of hierarchical populations of coupled oscillators." In: *Physical Review Letters* 101.26 (2008), p. 264103 (cit. on pp. 52, 91, 96, 112, 181).

[PR11] A. Pikovsky and M. Rosenblum. "Dynamics of heterogeneous oscillator ensembles in terms of collective variables." In: *Physica D* 240.9-10 (2011), pp. 872–881 (cit. on pp. 5, 181).

[PR15] A. Pikovsky and M. Rosenblum. "Dynamics of globally coupled oscillators: Progress and perspectives." In: *Chaos* 25.9 (2015), p. 097616 (cit. on p. 4).

[PRK03] A. Pikovsky, M. Rosenblum, and J. Kurths. *Synchronization*. Cambridge University Press, 2003 (cit. on pp. 1, 15, 19, 175).

[PLR06] A. Pluchino, V. Latora, and A. Rapisarda. "Compromise and synchronization in opinion dynamics." In: *The European Physical Journal B* 50.1 (2006), pp. 169–176 (cit. on p. 2).

[Pól77] G. Pólya. *Mathematical methods in science*. Cambridge University Press, 1977 (cit. on pp. 9, 55).

[RS00] R. Remmert and G. Schumacher. *Funktionentheorie*. 5th ed. Berlin: Springer, 2000 (cit. on pp. 49, 105).

[Ric+96] P. Richard, B. M. Bakker, B. Teusink, K. Van Dam, and H. V. Westerhoff. "Acetaldehyde mediates the synchronization of sustained glycolytic oscillations in populations of yeast cells." In: *European Journal of Biochemistry* 235.1-2 (1996), pp. 238–241 (cit. on p. 175).

[Ric11] J. Richter-Gebert. *Perspectives on projective geometry: a guided tour through real and complex geometry*. Berlin: Springer, 2011 (cit. on pp. 120, 139).

[RE89] J. Rinzel and G. B. Ermentrout. "Analysis of neural excitability and oscillations." In: *Methods in neuronal modeling: from ions to networks*. Cambridge: MIT Press, 1989 (cit. on p. 14).

[Roh+12] M. Rohden, A. Sorge, M. Timme, and D. Witthaut. "Self-organized synchronization in decentralized power grids." In: *Physical Review Letters* 109.6 (2012), p. 064101 (cit. on p. 1).

[RZ21a] R. Ronge and M. A. Zaks. "Emergence and stability of periodic two-cluster states for ensembles of excitable units." In: *Physical Review E* 103.1 (2021), p. 012206 (cit. on pp. 57, 83, 159).

[RZ21b] R. Ronge and M. A. Zaks. "Splay states and two-cluster states in ensembles of excitable units." In: *The European Physical Journal Special Topics* 230.14 (2021), pp. 2717–2724 (cit. on pp. 111, 159).

[RZP] R. Ronge, M. A. Zaks, and T. Pereira. "Continua and hyperbolicity of periodic orbits in ensembles of oscillators." (in preparation) (cit. on pp. 41, 85, 111).

[Ros+21] A. Ross, S. N. Kyrychko, K. B. Blyuss, and Y. N. Kyrychko. "Dynamics of coupled Kuramoto oscillators with distributed delays." In: *Chaos* 31.10 (2021), p. 103107 (cit. on p. 3).

[Rud76] W. Rudin. *Principles of mathematical analysis*. 3rd ed. New York: McGraw-Hill, 1976 (cit. on pp. 48, 116).

[SK86a] H. Sakaguchi and Y. Kuramoto. "A soluble active rotater model showing phase transitions via mutual entertainment." In: *Progress of Theoretical Physics* 76.3 (1986), pp. 576–581 (cit. on p. 3).

[SSK88] H. Sakaguchi, S. Shinomoto, and Y. Kuramoto. "Phase transitions and their bifurcation analysis in a large population of active rotators with mean-field coupling." In: *Progress of Theoretical Physics* 79.3 (1988), pp. 600–607 (cit. on p. 4).

[SVM07] J. A Sanders, F. Verhulst, and J. Murdock. *Averaging methods in nonlinear dynamical systems*. 2nd ed. Berlin: Springer, 2007 (cit. on pp. 19, 39, 112).

[Sch65] J. Scherr. “Beaumarchais.” In: *Studien*. Vol. 1. Verlag von Otto Wigand, Leipzig, 1865 (cit. on p. 218).

[SK15] L Schmidt and K Krischer. “Clustering as a prerequisite for chimera states in globally coupled systems.” In: *Physical Review Letters* 114.3 (2015), p. 034101 (cit. on p. 181).

[SK14] L. Schmidt and K. Krischer. “Two-cluster solutions in an ensemble of generic limit-cycle oscillators with periodic self-forcing via the mean-field.” In: *Physical Review E* 90.4 (2014), p. 042911 (cit. on p. 5).

[She87] R. N. Shepard. “Toward a universal law of generalization for psychological science.” In: *Science* 237.4820 (1987), pp. 1317–1323 (cit. on p. 157).

[SK86b] S. Shinomoto and Y. Kuramoto. “Phase transitions in active rotator systems.” In: *Progress of Theoretical Physics* 75.5 (1986), pp. 1105–1110 (cit. on pp. 3, 4, 16, 19, 20, 23, 109, 175).

[Sin93] W. Singer. “Synchronization of cortical activity and its putative role in information processing and learning.” In: *Annual Review of Physiology* 55.1 (1993), pp. 349–374 (cit. on p. 1).

[SOR11] P. S. Skardal, E. Ott, and J. G. Restrepo. “Cluster synchrony in systems of coupled phase oscillators with higher-order coupling.” In: *Physical Review E* 84 (3 2011), p. 036208 (cit. on p. 183).

[Sma76] S. Smale. “A mathematical model of two cells via Turing’s equation.” In: *The Hopf bifurcation and its applications*. Berlin: Springer, 1976, pp. 354–367 (cit. on p. 3).

[Son+14] B. Sonnenschein, T. K. D. M. Peron, F. A. Rodrigues, J. Kurths, and L. Schimansky-Geier. “Cooperative behavior between oscillatory and excitable units: the peculiar role of positive coupling-frequency correlations.” In: *The European Physical Journal B* 87.8 (2014), pp. 1–11 (cit. on pp. 3, 19).

[Son+13] B. Sonnenschein, M. A. Zaks, A. B. Neiman, and L. Schimansky-Geier. “Excitable elements controlled by noise and network structure.” In: *The European Physical Journal Special Topics* 222.10 (2013), pp. 2517–2529 (cit. on p. 19).

[SS10] E. M. Stein and R. Shakarchi. *Complex analysis*. Princeton University Press, 2010 (cit. on p. 42).

[Ste11] I. Stewart. “Phase oscillators with sinusoidal coupling interpreted in terms of projective geometry.” In: *International Journal of Bifurcation and Chaos* 21.06 (2011), pp. 1795–1804 (cit. on p. 52).

[Str00] S. H. Strogatz. "From Kuramoto to Crawford: exploring the onset of synchronization in populations of coupled oscillators." In: *Physica D* 143.1 (2000), pp. 1–20 (cit. on p. 3).

[Str18] S. H. Strogatz. *Nonlinear dynamics and chaos: With applications to physics, biology, chemistry, and engineering.* 2nd ed. Boca Raton: CRC Press, 2018 (cit. on p. 23).

[Str+05] S. H. Strogatz, D. M. Abrams, A. McRobie, B. Eckhardt, and E. Ott. "Crowd synchrony on the Millennium Bridge." In: *Nature* 438.7064 (2005), pp. 43–44 (cit. on pp. 1, 175).

[SM93] S. H. Strogatz and R. E. Mirollo. "Splay states in globally coupled Josephson arrays: Analytical prediction of Floquet multipliers." In: *Physical Review E* 47.1 (1993), p. 220 (cit. on pp. 4, 5).

[Sug+94] T. Sugawara, M. Tachikawa, T. Tsukamoto, and T. Shimizu. "Observation of synchronization in laser chaos." In: *Physical Review Letters* 72.22 (1994), p. 3502 (cit. on p. 1).

[SSW92] J. W. Swift, S. H. Strogatz, and K. Wiesenfeld. "Averaging of globally coupled oscillators." In: *Physica D* 55.3-4 (1992), pp. 239–250 (cit. on p. 4).

[Tan+14] G. Tanaka, K. Morino, H. Daido, and K. Aihara. "Dynamical robustness of coupled heterogeneous oscillators." In: *Physical review E* 89.5 (2014), p. 052906 (cit. on p. 160).

[TR19] E. Teichmann and M. Rosenblum. "Solitary states and partial synchrony in oscillatory ensembles with attractive and repulsive interactions." In: *Chaos* 29.9 (2019), p. 093124 (cit. on pp. 20, 135).

[Tes+07] C. J. Tessone, A. Scire, R. Toral, and P. Colet. "Theory of collective firing induced by noise or diversity in excitable media." In: *Physical Review E* 75.1 (2007), p. 016203 (cit. on p. 19).

[TZT08] C. J. Tessone, D. H. Zanette, and R. Toral. "Global firing induced by network disorder in ensembles of active rotators." In: *The European Physical Journal B* 62.3 (2008), pp. 319–326 (cit. on p. 175).

[TZ14] P. Tomov and M. A. Zaks. "Phase dynamics on small hexagonal lattices with repulsive coupling." In: *International Conference on Nonlinear Dynamics of Electronic Systems*. Springer. Berlin, 2014, pp. 246–253 (cit. on pp. 2, 4, 19, 175).

[Tra09] T. Trappenberg. *Fundamentals of computational neuroscience.* Oxford University Press, 2009 (cit. on p. 2).

[TS92] K. Y. Tsang and I. B. Schwartz. "Interhyperhedral diffusion in Josephson-junction arrays." In: *Physical Review Letters* 68.15 (1992), p. 2265 (cit. on p. 4).

[TW90] K. Y. Tsang and K. Wiesenfeld. "Attractor crowding in Josephson junction arrays." In: *Applied Physics Letters* 56.5 (1990), pp. 495–496 (cit. on p. 5).

[Tsi+05] L. S. Tsimring, N. F. Rulkov, M. L. Larsen, and M. Gabbay. "Repulsive synchronization in an array of phase oscillators." In: *Physical Review Letters* 95.1 (2005), p. 014101 (cit. on p. 20).

[Tsu+06] K. Tsumoto, H. Kitajima, T. Yoshinaga, K. Aihara, and H. Kawakami. "Bifurcations in Morris-Lecar neuron model." In: *Neurocomputing* 69.4-6 (2006), pp. 293–316 (cit. on pp. 159, 183).

[Tsu+02] K. Tsumoto, T. Yoshinaga, K. Aihara, and H. Kawakami. "Bifurcations in Morris-Lecar neuron models." In: *International Symposium on Nonlinear Theory and its Applications* (2002) (cit. on pp. 159, 161–163, 166, 167, 170).

[Tur53] A. M. Turing. "The chemical basis of morphogenesis." In: *Philosophical Transactions of the Royal Society B* 237 (1953), pp. 37–72 (cit. on p. 3).

[Tyu+18] I. V. Tyulkina, D. S. Goldobin, L. S. Klimenko, and A. Pikovsky. "Dynamics of noisy oscillator populations beyond the Ott-Antonsen ansatz." In: *Physical Review Letters* 120.26 (2018), p. 264101 (cit. on pp. 5, 181).

[Tyu+19] I. V. Tyulkina, D. S. Goldobin, L. S. Klimenko, and A. Pikovsky. "Two-bunch solutions for the dynamics of Ott-Antonsen phase ensembles." In: *Radiophysics and Quantum Electronics* 61.8 (2019), pp. 640–649 (cit. on pp. 5, 181).

[US06] P. J. Uhlhaas and W. Singer. "Neural synchrony in brain disorders: relevance for cognitive dysfunctions and pathophysiology." In: *Neuron* 52.1 (2006), pp. 155–168 (cit. on p. 2).

[Vel06] J. L. P. Velazquez. "Brain research: a perspective from the coupled oscillators field." In: *NeuroQuantology* 4.2 (2006), pp. 155–165 (cit. on p. 3).

[VRP16] V. Vlasov, M. Rosenblum, and A. Pikovsky. "Dynamics of weakly inhomogeneous oscillator populations: perturbation theory on top of Watanabe-Strogatz integrability." In: *Journal of Physics A* 49.31 (2016), 31LT02 (cit. on pp. 5, 91, 112, 181, 182).

[VZP15] V. Vlasov, Y. Zou, and T. Pereira. "Explosive synchronization is discontinuous." In: *Physical Review E* 92.1 (2015), p. 012904 (cit. on pp. 3, 91).

[Wal69] T. J. Walker. "Acoustic synchrony: two mechanisms in the snowy tree cricket." In: *Science* 166.3907 (1969), pp. 891–894 (cit. on p. 175).

[WLL08] J. Wang, M. Lu, and H. Li. "Synchronization of coupled equations of Morris-Lecar model." In: *Communications in Nonlinear Science and Numerical Simulation* 13.6 (2008), pp. 1169–1179 (cit. on p. 160).

[WS93] S. Watanabe and S. H. Strogatz. "Integrability of a globally coupled oscillator array." In: *Physical Review Letters* 70.16 (1993), p. 2391 (cit. on p. 4).

[WS94] S. Watanabe and S. H. Strogatz. "Constants of motion for superconducting Josephson arrays." In: *Physica D* 74.3 (1994), pp. 197–253 (cit. on pp. 4, 41, 51–53, 81, 96, 175, 177).

[Wer06] D. Werner. *Funktionalanalysis*. 5th ed. Berlin: Springer, 2006 (cit. on p. 36).

[WH89] K. Wiesenfeld and P. Hadley. "Attractor crowding in oscillator arrays." In: *Physical Review Letters* 62.12 (1989), p. 1335 (cit. on p. 5).

[WS95] K. Wiesenfeld and J. W. Swift. "Averaged equations for Josephson junction series arrays." In: *Physical Review E* 51.2 (1995), p. 1020 (cit. on p. 21).

[Wig94] S Wiggins. *Normally hyperbolic invariant manifolds in dynamical systems*. Berlin: Springer, 1994 (cit. on p. 34).

[Wig03] S. Wiggins. *Introduction to applied nonlinear dynamical systems and chaos*. 2nd ed. Berlin: Springer, 2003 (cit. on pp. 25, 28).

[Win01] A. T. Winfree. *The geometry of biological time*. 2nd ed. Berlin: Springer, 2001 (cit. on pp. 1, 11, 15).

[WYD21] M. Wolfrum, S. Yanchuk, and O. D'Huys. *Multiple self-locking in the Kuramoto-Sakaguchi system with delay*. 2021. URL: `https://www.wias-berlin.de/preprint/2890/wias_preprints_2890.pdf` (cit. on p. 3).

[XS21] C. Xu and P. S. Skardal. "Spectrum of extensive multiclusters in the Kuramoto model with higher-order interactions." In: *Physical Review Research* 3.1 (2021), p. 013013 (cit. on p. 183).

[Yan+14] Y. Yaniv, I. Ahmet, J. Liu, A. E. Lyashkov, T.-R. Guiriba, Y. Okamoto, B. D. Ziman, and E. G. Lakatta. "Synchronization of sinoatrial node pacemaker cell clocks and its autonomic modulation impart complexity to heart beating intervals." In: *Heart Rhythm* 11.7 (2014), pp. 1210–1219 (cit. on p. 175).

[YS99] M. K. S. Yeung and S. H. Strogatz. "Time delay in the Kuramoto model of coupled oscillators." In: *Physical Review Letters* 82.3 (1999), p. 648 (cit. on p. 3).

[ZL84] M. A. Zaks and D. V. Liubimov. "The abnormally rapid convergence of a bifurcation sequence of the doubling type in systems with two saddle equilibriums." In: *Zhurnal Eksperimentalnoi i Teoreticheskoi Fiziki* 87 (1984), pp. 1696–1699 (cit. on p. 169).

[ZL89] M. A. Zaks and D. V. Lyubimov. "Bifurcation sequences in the dissipative systems with saddle equilibria." In: *Banach Center Publications* 1.23 (1989), pp. 367–380 (cit. on p. 169).

[Zak+03] M. A. Zaks, A. B. Neiman, S. Feistel, and L. Schimansky-Geier. "Noise-controlled oscillations and their bifurcations in coupled phase oscillators." In: *Physical Review E* 68.6 (2003), p. 066206 (cit. on p. 19).

[ZP17] M. A. Zaks and A. Pikovsky. "Chimeras and complex cluster states in arrays of spin-torque oscillators." In: *Scientific reports* 7.1 (2017), pp. 1–10 (cit. on pp. 7, 172).

[ZT16] M. A. Zaks and P. Tomov. "Onset of time dependence in ensembles of excitable elements with global repulsive coupling." In: *Physical Review E* 93 (2 2016), 020201(R) (cit. on pp. 4, 5, 19, 20, 22, 62, 85–88, 113, 164, 175, 178, 179).

[Zil+07] R. Zillmer, R. Livi, A. Politi, and A. Torcini. "Stability of the splay state in pulse-coupled networks." In: *Physical Review E* 76.4 (2007), p. 046102 (cit. on p. 5).

[ZZ09] W. Zou and M. Zhan. "Splay states in a ring of coupled oscillators: From local to global coupling." In: *SIAM Journal on Applied Dynamical Systems* 8.3 (2009), pp. 1324–1340 (cit. on p. 5).

SELBSTSTÄNDIGKEITSERKLÄRUNG

Ich erkläre, dass ich die Dissertation selbständig und nur unter Verwendung der von mir gemäß § 7 Abs. 3 der Promotionsordnung der Mathematisch-Naturwissenschaftlichen Fakultät, veröffentlicht im amtlichen Mitteilungsblatt der Humboldt-Universität zu Berlin Nr. 126/ 2014 am 18.11.2014, angegebenen Hilfsmittel angefertigt habe.

Berlin, Mai 2022

Robert Ronge

Aller Anfang ist schwer, ja wohl; aber das rechtzeitige Aufhören ist eine noch schwierigere Kunst.

— Johannes Scherr [Sch65]

COLOPHON

This document was typeset with LaTeX, using a customization of the `classicthesis`–template, developed by André Miede.